

## Preface

### Special Issue on Cognitive Mobility

One of the cornerstones of 21<sup>st</sup> Century global society is our ever-expanding mobility. Its sustainability within the current framework is increasingly questionable. Rapid digital development is giving us new tools to reduce the environmental footprint of our mobility system by increasing its efficiency; it is called cognitive mobility.

The articles of this special edition cover the most relevant areas of cognitive mobility. One of the pillars of understanding better mobility is the use of smarter sensors. The paper “Data acquisition as basic of cognitive approach” shows a tangible example. The measured and collected data is the basis of further evaluations; one is presented in the paper “Investigating the energetics of electric vehicles based on real measurements.” As one of the main aims of the cognitive mobility approach is to develop mobility to be more sustainable, the energy use of vehicles is a key topic. Engines will play a role in the next decades; papers deal with increased efficiency of engines, such as “Cost-efficient training method for artificial neural networks based on engine measurements” or “Research on the Quantification of Exhaust Emission Volumes in an Opted Road Section.” The main energy converter could be an electric “Competition vs. Cooperation: Do Subsidies with Government-Set Eligibility Threshold Values Behave as Focal Points on the Hungarian BEV Market?” or partially at least partially internal combustion engine with liquid fuel “Evaluation of an Oil Refining Tower by Numerical Simulation”. Using cognitive tools for improving the drivetrain is essential as well, as presented in “Integrated Torque Vectoring Control Using Vehicle Yaw Rate and Sideslip Angle for Improving Steering and Stability of All Off-Wheel-Motor Drive Electric Vehicles” or in Energy condition measurement of gear shifting under load in commercial vehicles.

One of the rapidly developing areas of cognitive mobility is the safety and security of the system. Understanding the challenges and research for the solution is a key topic is in authentication “Investigating the safety effect of PKI authentication in automotive systems”, in environment perception “Neural network-based multi-class traffic-sign classification with the German Traffic Sign Recognition Benchmark” and relation with vulnerable participants as well, like in “Assessability of road accidents – a methodology for exploring the effect of accident type and data recording technology“

Handling the more wider aspects with interdisciplinary approach is as well part of cognitive mobility. Sustainability across generations is represented in “Who should communicate to make the world a greener place?”. Environment and pollution questions are appearing in “Adapting to climate change in the digital era

– a new dimension of regional sustainability?” and “Eye tracking study of visual pollution”. Transport management and Covid 19 challenges are touched as well with the cognitive mobility aspect in “Prediction of transport performance development due to the impact of COVID-19 measures in the context of sustainable mobility in railway passenger transport”

It is time to express our special gratitude to Anna Sudár, Marianna Márkus, and Janka Patkó for giving technical background for this special issue. We are grateful to all the writers and co-authors for their dedication to developing contributions for this special issue and sharing their findings with the journal. Last but not least, we would like to thank the editorial board of the journal *Acta Polytechnica Hungarica*, Ms. Anikó Szakál, Prof. Imre J. Rudas, and Prof. Levente Kovács, for their help in publishing this Special Issue.

***Prof. Dr. Máté Zöldy***

Guest editor

***Prof. Dr. Péter Baranyí***

Guest editor

# Research on the Quantification of Exhaust Emission Volumes in an Opted Road Section

**Branislav Šarkan<sup>1</sup>, Jozef Pal'o<sup>1</sup>, Michal Loman<sup>1</sup>,  
Ondrej Stopka<sup>2,\*</sup>, Jacek Caban<sup>3</sup>, Karolina Čeháková<sup>1</sup>,  
Wojciech Gołębiowski<sup>4</sup> and Jan Pečman<sup>2</sup>**

<sup>1</sup> University of Žilina, Faculty of Operation and Economics of Transport and Communications, Department of Road and Urban Transport, Univerzitná 8215/1, 01026 Žilina, Slovakia; branislav.sarkan@fpedas.uniza.sk (B.Š.); jozef.palo@fpedas.uniza.sk (J.P.); loman@stud.uniza.sk (M.L.); cehakova@stud.uniza.sk (K.Č.)

<sup>2</sup> Institute of Technology and Business in České Budějovice, Faculty of Technology, Department of Transport and Logistics, Okružní 517/10, 37001 České Budějovice, Czech Republic; stopka@mail.vstecb.cz (O.S.); pecman@mail.vstecb.cz (J.Pe.)

<sup>3</sup> Lublin University of Technology, Faculty of Mechanical Engineering, Department of Automation, Nadbystrzycka 36, 20618 Lublin, Poland; j.caban@pollub.pl (J.C.)

<sup>4</sup> University of Life Sciences in Lublin, Faculty of Production Engineering, Department of Power Engineering and Transportation, Głęboka 28, 20612 Lublin, Poland; wojciech.golebiowski@up.lublin.pl (W.G.)

\* Correspondence: stopka@mail.vstecb.cz

---

*Abstract: The air quality in the urban zone is influenced by many factors, of which transport plays a significant role. Air quality has an impact on the health of inhabitants, demographic, urbanization processes, as well as a whole mobility, and is currently one of the most important challenges faced by municipal authorities. The article focuses on analyzing the impact of exhaust gases and their emissions produced by motor vehicles on the environment in the opted territory, namely Hasičská Street in the city of Trenčín, Slovakia. Investigated and quantified emissions in the context of vehicles' mobility comply with a number of vehicles registered in Slovakia. The primary task of the research is to determine the amount of produced emissions in the researched area without the use of measuring technology. It is a process of modeling emission coefficients on the basis of which it is possible to reliably determine the level of pollution in the monitored area. The research per se is based upon a traffic survey carried out over the period September-October 2021. Following the analysis, obtained values were classified into certain vehicle categories registered in Slovakia while observing the relevant EU Regulations. The research involved measuring the volume of exhaust emissions produced by vehicles when in motion through the examined transport*

---

*section. We further compared the resulting exhaust emissions with emissions automatically recorded by the national weather station. The levels of individual harmful substances registered by the Slovak Hydrometeorological Institute were naturally higher than the values achieved by the survey itself, as the weather station records emissions from multiple mobility activities. In regard to emissions obtained by the survey, we achieved related values of indicators as follows: CO, HC, NO<sub>x</sub>, and PM. The category of passenger cars topped the list, as automobiles produced 90.17% pollutants of all the recorded vehicles. Bus services capped NO<sub>x</sub> emission production. The highest emission rates were detected between 2 and 3 pm due to the peak traffic in the observed section. The analysis has proved significantly lower emission volumes produced by haulage compared to other vehicle categories.*

*Keywords: road transport; mobility; exhaust emissions; exhaust gases; weather station*

---

## **1 Introduction**

Thanks to its flexibility, road traffic is the most viable way of people' mobility, ranging from the use of light vehicles to heavy utility combustion engine machines. These engines are powered by fossil fuels emitting harmful gas substances and solid particles, putting the road transport sector on the top of the list of global environmental and health threats [1-3]. Apart from greenhouse gases, exhaust emissions involve evaporative and odorous emissions, the latter stemming from tire, brake lining, clutch and roadway wearoff or vehicle corrosion [4-7]. A recent dramatic population growth, rapid economic development, urbanization and the resulting exponential increase in automotive production incurred proportional health risks [8-10]. It is expected that by 2040, the number of automobiles will nearly have doubled up to 2 bil. Another prognosis suggests that the total of road vehicles will have reached 2 or 3 bil by 2050 [11]. It is predicted that the majority of this massive upsurge will take place in Asian countries, especially China and India, given to the rapid economic development, prosperity and tremendous population growth. A considerable increase in GNP in these regions will boost the demand for motor vehicles including those from the "luxurious" section. It is thereby foreseen that emission rates produced by road traffic will be rising on the global scale through the following years [12].

Traffic in general is responsible for more than 25% of greenhouse emissions in the entire EU, being the largest contributor to the climate change. Cutting down on vehicle emissions is thereby vital for reaching zero exhaust fumes by 2050, as stipulated in EU's long-term strategies [13]. Currently, software programs and models are used within large cities to determine the magnitude of exhaust gas emissions. Estimated levels of emissions from road transport can be helpful in assessing the overall air quality in urban areas. A lot of urban projects thereby rely on modeling methods to obtain direct results [14]. Testing automobiles involves vehicle certification. Emission measurements and vehicle testing take place using a

chassis dynamometer, as producers have to prove that their vehicles comply with emission standards (the approval of a specific type) [15, 16]. For that reason, new vehicles are exempt from a regular emission test for a prescribed period. After the expiration of this time limit, all vehicles have to undergo emission inspection to ensure that the vehicle emissions did not exceed the specified limit.

In the Slovak Republic, the issue of air pollution and emission production is effectively tackled by the Slovak Hydrometeorological Institute, which publishes regular reports on the air quality and emission rates in the country (in selected localities). The institute further provides information on the air quality received from the weather stations. According to the study [17], the correct placement of stations monitoring air quality is essential. The institute further provides information on the air quality received from the weather stations. These sites are laid out throughout the Slovak Republic, regularly recording data on the air quality. However, the stations are very unevenly distributed, and it is not possible to cover the entire territory. The results from these measuring stations can only be accepted for the area that is in the immediate vicinity of the measuring station. The measured results inform about the air quality in the specific place [18]. The similar research carried out in the USA revealed a significant growth in the monitored values, heralding that the air quality deterioration is mainly caused by the road traffic [19]. Research involved a data analysis from the national weather station, focusing on the air quality in the monitored road section.

Research is aimed at measuring exhaust emissions by means of a traffic survey. The examination involved quantifying emission rates for individual vehicle categories when in motion. Subsequently, we compared the obtained results with the values provided by the weather station. The final outcomes informed us about emissions produced by a specific vehicle category regarding mobility. The secondary outputs encompassed the comparison of the recorded data. The research revealed that mobility by using road transport largely contributes to the air pollution in the road section under examination. Our main contribution is the identification of emissions from specific categories of vehicles used in an urban area, which can be important for traffic management enterprises to monitor and manage emissions in a given area. It will also make it possible to decide on the development and deployment of alternative communication and mobility systems in the city zone (e.g., car sharing, city bike system, etc.).

The conducted research was aimed at identifying the production of exhaust gas emissions by road transport. The research points to different levels of pollution depending on the category and number of vehicles that were registered during the research. Currently, the Slovak Republic does not have a universal tool for monitoring air quality in urban areas. Within cities or larger agglomerations, there is no study available on how to monitor and evaluate air quality in a specific section. In the near future, it is planned to create measuring points in selected places that will continuously monitor air quality. The results of the study can serve as a tool for decision making on a correct location of measuring devices to permanently monitor

the categorization of vehicles in order to quantify the value of the emissions produced. Based on the results of measurements and current data, specific measures can be introduced (entry ban, restricted entry for selected types of vehicles, alternative mobility approaches and so forth) with the aim of permanently reducing emissions in the urban environment. The research findings further provide support for planning the optimization of air quality management policies toward the creation of sustainable cities. On the territory of the Slovak Republic, there is still no tool for preventing the movement of passenger traffic in the built-up area of cities. To a large extent, the study could be beneficial in building a green policy and permanently reducing emissions due to traffic within cities.

The measured data were compared with the results of the monitoring station of the Slovak Hydrometeorological Institute. Due to the insufficient coverage of the territory, the data results have only an informative character. Based on the information on air quality, it is not possible to implement any steps that would lead to the improvement of the current mobility situation in the territory of the Slovak Republic. The research results represent a universal tool based on which the intensity of air pollution can be predicted without the need of installing specific measurement devices. The research conducted is the only one of its kind that, based on the methodology created, can quantify the amount of air pollution in a given area. Compared to an air quality measuring station, it can provide an approach for improving air quality wherever it is placed.

## 2 Data and Methods

The prerequisite for the correct calculation of exhaust gas emissions was the identification of the number and category of vehicles on the selected section. To obtain data from a specific area, a traffic survey was carried out on the 1<sup>st</sup> class road no. 61, Hasičská Street in Trenčín, Slovak Republic. The conducted traffic survey serves as the primary source of data, based on which the production of exhaust gas emissions from traffic activity was calculated. The survey was conducted to count vehicles in both traffic directions. The results of the traffic survey can be seen in Figure 1.

The survey results (Figure 1) indicate categories and numbers of vehicles passing through the monitored section. The diagram suggests passenger cars constituting the largest number - 25,802 vehicles, while N1 "LORRY" trucks comprised the smallest amount - 135 vehicles. The total contribution of passenger cars to released pollutants amounts 90.17%. The diagram (red curve) shows that the highest number of vehicles, i.e., the heaviest road load, goes through the section between 2 and 3 pm, followed by 7 and 8 am, which is obviously related to the rush hour in this locality.

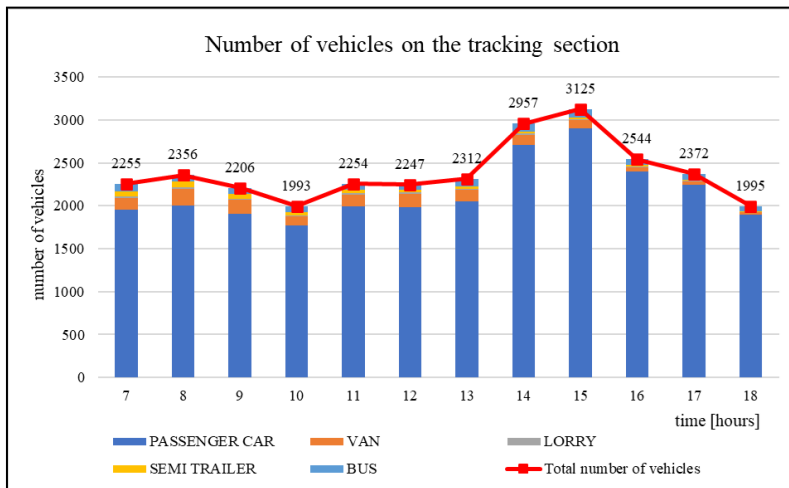


Figure 1

Number of vehicles in the monitored section [authors based on a traffic survey]

On the other hand, the figures fell to a trough between 9 and 11 am and were on a slide again as of 4 pm. We can thereby predict that the monitored section will see increased exhaust emission rates during the rush hour.

In the vicinity of the examined section, it can find the aforementioned weather station (Figure 2) [20]. Based on the data on the concentration of air pollutants received from the hydrometeorological institute and figures obtained by the survey, we can explore the extent to which road traffic is responsible for air pollution within the specific road section.

The survey took place in the time interval of 12 hours on 24.11.2022 from 7am to 7pm on vehicle categories as follows:

- passenger cars,
- N1 category with the maximum permissible load not exceeding 3,5 t (Van),
- N2 category with the maximum permissible load from 3,5 up to 12 t (Lorry),
- N3 category with the maximum permissible load exceeding 12 t (Semi Trailer),
- buses.

Measured emissions were subsequently evaluated and compared to values from the weather station. The survey covered pollutants: CO, HC, NO<sub>x</sub> and PM. These harmful substances were emitted from all the monitored vehicle categories, allowing us to draw a close comparison.



Figure 2

Measured section and location of the weather station (authors according to [www.mapy.cz](http://www.mapy.cz))

Passenger car category included vehicles registered in the territory of the Slovak Republic according to the internal database of the Ministry of the Interior. We further classified the vehicles according to the type of fuel, comprising two categories:

- petrol-powered vehicles, representing 54% of all registered vehicles,
- diesel-powered vehicles, representing 46% of all registered vehicles.

The next step involved the analysis of different categories, followed by a classification according to European emission standards. All categories were assigned emission standards in a range from Euro 3 to Euro 6. Vehicles of Euro 2 standard or less were marked as “older” (see Table 1).

Table 1

Percentage of vehicles registered in Slovakia (internal data of the Ministry of the Interior, Slovakia)

	Petrol %	Diesel %
older	36	19
EURO 3	6	14
EURO 4	22	22
EURO 5	15	27
EURO 6	21	18

The table shows the high proportion of vehicles with the EURO4 emission standard (22% for each type of fuel). In another case, up to 21% of vehicles with the emission standard Euro6 for petrol and 27% of vehicles complying with the emission standard Euro5 - for diesel are registered in the database. In the overall comparison, regardless of fuel, older vehicles represent the highest share of the total number in Slovakia. For this reason, it is possible to claim that the introduction of stricter

measures for entry into selected parts and the overall regulation of emissions is necessary for the territory of Slovakia.

The traffic survey identified the overall traffic intensity and the traffic composition within the monitored section. The proportional distribution of the vehicles allowed calculating exhaust emissions in the examined segment. The survey also involved categories of vans and lorries, including N1 class represented by 91% and N2 represented by 9%. The acquired data were processed according to the database of The Ministry of the Interior of the Slovak Republic. N3 category comprised semi-trailers. All the heavy-weight categories (N1, N2 and N3) were classified according to relevant emission standards like in the event of passenger cars (EURO III, EURO IV, EURO V, EURO VI and older).

Various methods were involved in calculating exhaust vehicle emissions, offering multiple ways of application. The traffic survey, which presents a cornerstone of our research, allowed us to classify the vehicles according to their traits. The database of the Ministry of the Interior of Slovak Republic – the total number of registered vehicles in the territory of Slovak Republic – governed the data processing and dividing registered vehicles into categories according to the fuel type (petrol, diesel).

Based on the classification and identification of the exact number of vehicles of individual categories, it is possible to calculate the number of exhaust gases in the monitored section. Each vehicle type and EURO emission class was assigned an emission classification (exhaust emissions), through which it is possible to determine the total volume of emissions produced in the examined section. Based on the average value of emissions detected in the vehicle type approval process (g/km), we decided on the emissions produced by passenger cars registered in the territory of the Slovak Republic. Emission coefficients for buses are calculated map planner Map&Guide. The scheduler is able to simulate the production of exhaust emissions with high accuracy with respect to the required emission standard. The values (emission coefficients, table 3) that are the result of average values from the map planner enter the research. The average values were determined based on the calculation of several conditions in which the vehicle can move on the road. Measurements of bus emissions were largely based on Guo et al.'s research study on regulated pollutants from diesel and CNG buses using selective catalytic reduction in the EURO 5 DIESEL emission class [21].

The following Figure 3 presents an illustrative scheme and the procedure of the conducted research. The picture shows the individual steps that guided the research.

In Tables 2-4, the values of the emission coefficients are quantified, which are further included in the calculation of the total amount of emissions produced by the respective category of vehicles.

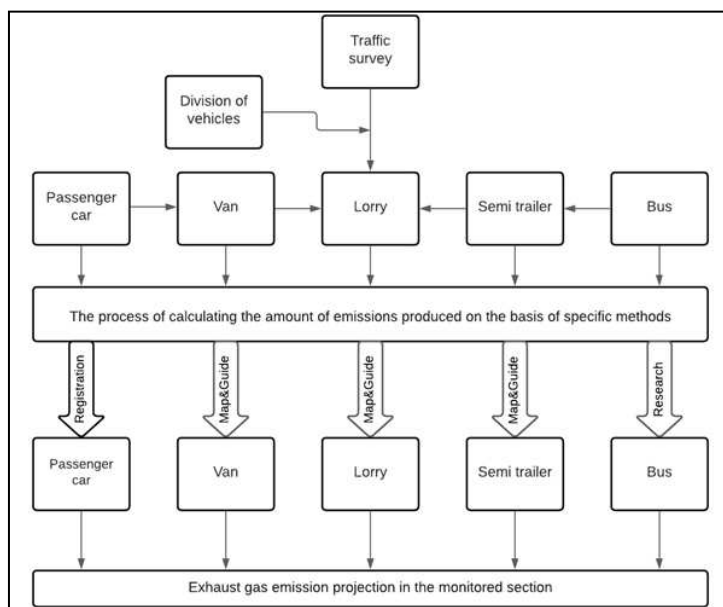


Figure 3  
Scheme and procedure of the research [authors]

Table 2  
Values of emission coefficients for petrol passenger vehicles entered the calculation [data from the Ministry of the Interior on the results of vehicle type approval]

Passenger car – Petrol [g/km]					
	CO	HC	HC+NO <sub>x</sub>	NO <sub>x</sub>	PM
Older	0.5795	0.0803	-	0.0593	0.1005
Euro 3	0.5846	0.0784	-	0.0501	0.0845
Euro 4	0.4163	0.0502	-	0.0261	0.0348
Euro 5	0.3992	0.0453	-	0.0251	0.0038
Euro 6	0.3632	0.0357	-	0.0227	0.0019
Passenger car – Diesel [g/km]					
	CO	HC	HC+NO <sub>x</sub>	NO <sub>x</sub>	PM
Older	0.3077	0.1514	0.4544	0.3594	0.0484
Euro 3	0.2332	0.0356	0.4368	0.4011	0.0407
Euro 4	0.1515	0.0250	0.2369	0.2119	0.0168
Euro 5	0.2323	0.0267	0.1738	0.1471	0.0085
Euro 6	0.1660	0.0280	0.0804	0.0524	0.0030

The data in Table 2 above represent the average values of emission production during type approval of individual emission classes of passenger vehicles. The values are expressed in g/km. The traffic survey took place in 300-meter-long

section. The resulting values are thereby converted to g/300 m (gram over 300-meter-long section).

Table 2 depicts emission values for passenger cars. The tables outline the background to calculating exhaust emissions in the monitored segment. In the following Table 3, it is possible to monitor the data on the production of emissions for vehicles of categories N1, N2, and N3. The values in the table are taken from the Map&Guide planner, which provides a detailed description of emissions production. Each vehicle category was simulated in different states (empty vehicle, loaded vehicle). The resulting value shown in the table represents the average value of several simulations.

Table 3

Emission coefficients for the individual categories of lorries that entered the calculation [data based on the simulation in the route planner]

Van (N1) [g/km]				
	CO	HC	NO <sub>x</sub>	PM
Euro 3	0.0189	0.0126	0.9409	0.0262
Euro 4	0.0127	0.0071	0.5505	0.0010
Euro 5	0.0910	0.0040	0.6956	0.0015
Euro 6	0.0091	0.0040	0.2476	0.0015
Lorry (N2) [g/km]				
	CO	HC	NO <sub>x</sub>	PM
Euro 3	0.4745	0.1345	35.0650	0.0657
Euro 4	0.8183	0.0123	16.4790	0.0204
Euro 5	0.0692	0.0135	0.1402	0.0021
Euro 6	0.0692	0.0135	0.1402	0.0021
Semi Trailer (N3) [g/km]				
	CO	HC	NO <sub>x</sub>	PM
Euro 3	11.3060	0.2895	58.1140	0.1362
Euro 4	12.7810	0.0195	25.8320	0.0360
Euro 5	12.1980	0.0197	17.3330	0.0366
Euro 6	0.1560	0.0255	0.2254	0.0037

Table 3 illustrates emission values for lorries, providing the background for further calculations. The examined vehicles comprised three categories.

In Table 4, the data on the production of emissions entering into the calculation are summarized. Based on the analysis of the emission class of buses that drive through the measuring point, it was found that all vehicles meet the EURO5 emission standard. For this reason, only one emission limit is sufficient, which will participate in the calculations of the total production of emissions from buses.

Table 4  
Emission coefficients for buses that entered the calculation [21]

	Bus - Diesel [g/km]			
	CO	HC	NO <sub>x</sub>	PM
Euro 5	2.17	0.06	2.81	0.0015

Table 4 informs about exhaust emissions representing emission values for buses - EURO 5 DIESEL. The presented figures were taken from the conducted study. The data represents the average value of exhaust gas emissions that were identified based on the measurement in real conditions in the studies of Guo *et al.* [21].

### 3 Results

The conducted survey yielded results to determine values of CO, HC, NO<sub>x</sub> and PM in the monitored section. The bar charts (Figures 4-7) below depict calculated exhaust emissions of passing vehicles. The total amount of illustrated emissions is confined to the road traffic within the monitored section.

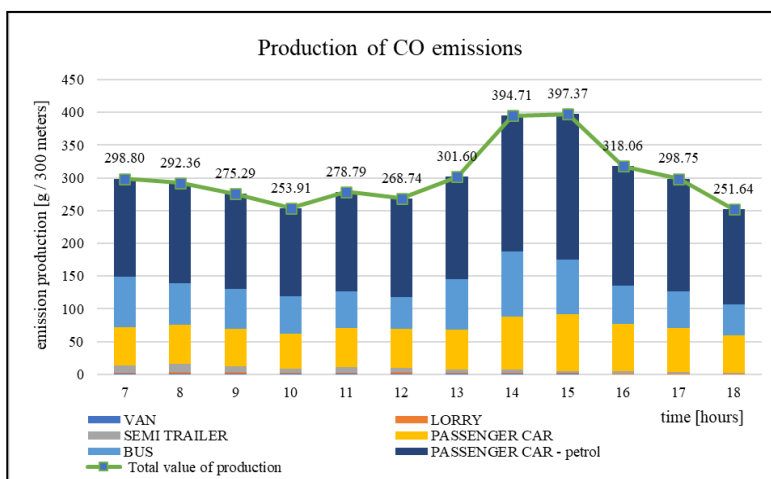


Figure 4  
Production of CO emissions in the monitored section [authors]

Figure 4 portrays CO emissions in the examined section, indicating the peak between 2 pm and 3 pm when exhaust emissions reached 397 g/300 m. The largest amount of CO emissions was produced by petrol-powered vehicles and buses. The chart hits the trough at 6 pm when the traffic is the lightest. Vehicles of N1 category (Van) indicated the lowest emission levels.

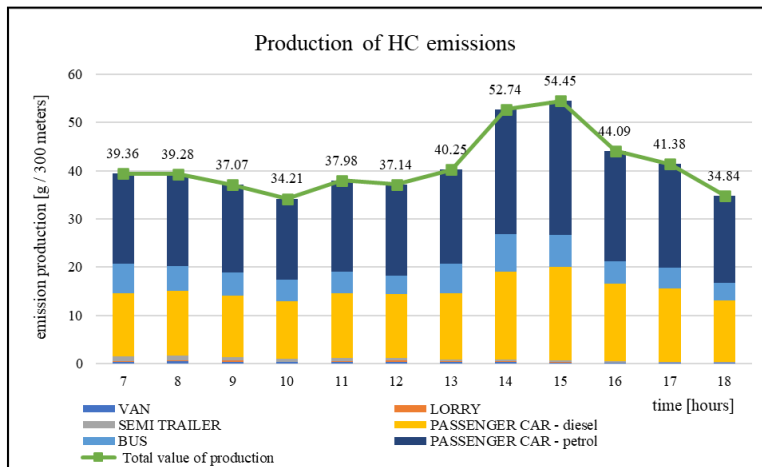


Figure 5

Production of HC emissions in the monitored section [authors]

Figure 5 demonstrates that the production of HC emissions rose to the peak between 2 pm and 3 pm, as in the event of CO. The overall emission value of HC was 54.45 g/300 m at that time. The largest volume of pollutants in the monitored section was produced by passenger cars - 419.86 g/300 m. The lowest emission rates were recorded in N2 category (Lorry), namely 2.02 g/300 m.

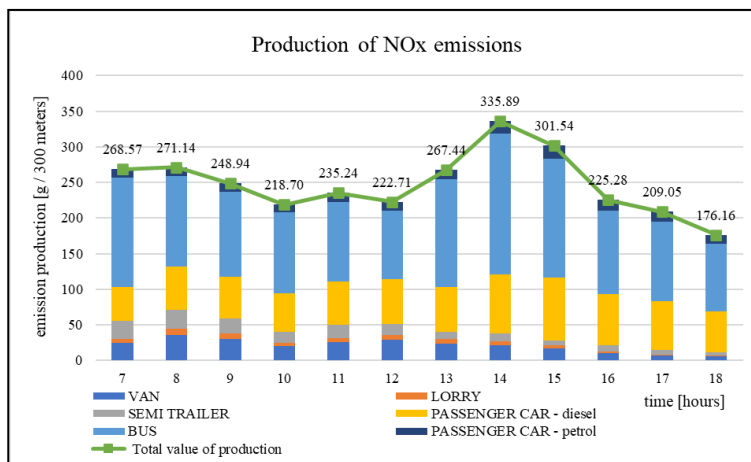


Figure 6

Production of NO<sub>x</sub> emissions in the monitored section [authors]

The same scenario unfolds in the event of NO<sub>x</sub> emissions. The measured exhaust gases topped the highest values at 2 pm - 335.89 g/300 m, indicating buses as the biggest polluters. As contrasted to previous cases, NO<sub>x</sub> rates increased even in other

vehicle categories. The total value of production is thereby even. Vehicles of N2 category (Lorry) showed the smallest numbers - 60.36 g/300 m. To make a crude comparison, the difference between emissions produced by buses and Lorries amounts to 1,501.36 g/300 m. This variation was calculated from the overall pollutants produced throughout a one-day survey.

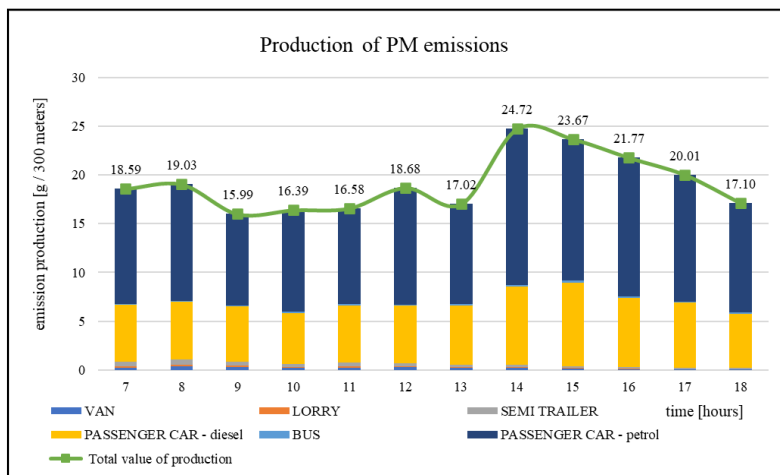


Figure 7

Production of PM emissions in the monitored section [authors]

Figure 7 suggests a situation similar to the previous charts. PM emissions reached the peak 24.72 g/300 m at 2 pm. What strikes the eye is that emission levels are the highest in passenger cars, especially petrol-powered vehicles. The production of other categories is almost negligible. The one-day survey detected the overall PM value 22.54 g/300 m for all vehicle categories, with passenger cars covering 221.04 g/300 m. This value represents 96.5% from the total amount of produced pollutants.

### 3.1 Survey Results Compared to the Weather Station

For a larger contribution to the science, we compared our results with values recorded by the weather station (NMSKO) located near the measured section. We may thereby suppose that results, i.e., recorded data, reflect the road traffic flow. Analyzing the produced statistics, we can estimate the extent to which the road traffic is impactful on the air quality, detecting the amount of released pollutants. Multiple studies [22, 23] argue that although the road traffic is not the only air polluter, its contribution tops the highest numbers.

The first step involved the data analysis from NMSKO. The weather station is operated by the Slovak Hydrometeorological Institute. The obtained information provided us with values recorded by the weather station during the days of our

survey. The statistics on the air quality were updated every hour. We subsequently compared the data on emissions received from the weather station with values achieved by our survey, trying to discover a correlation. Exhaust emissions produced during the survey are expressed in g/300 m and fumes recorded by the weather station are suggested in g/m<sup>3</sup>. Although the presented units cannot be fully compared, we can see a simple correlation between individual figures. The compiled statistics on NO<sub>x</sub>, HC and PM are comparable only if they comply with the research and values recorded by the weather station. The following Table 5 contains the result of comparing in pairs with the final results.

Table 5  
The result of comparison in pairs with the final results

	Weather station [ $\mu\text{g}/\text{m}^3$ ]			Emission calculation [g/300 meters]		
	PM	CO	NO <sub>x</sub>	PM	CO	NO <sub>x</sub>
7	49	949	45	19	299	269
8	39	923	32	19	292	271
9	37	949	43	16	275	249
10	39	969	42	16	254	219
11	44	994	63	17	279	235
12	55	984	58	19	269	223
13	63	979	79	17	302	267
14	72	1020	120	25	395	336
15	67	1120	74	24	397	302
16	63	1003	68	22	318	225
17	64	967	53	20	299	209
18	59	989	49	17	252	176

The data determined by the calculation were compared with the data recorded by the measuring station. The results can be seen in Table 5. The data indicates a clear correlation between the observed values. This equivalence is further demonstrated graphically in Figures 8-10.

Table 6  
Assessment of dependence between monitored data - correlation coefficients

PM	0.7351
CO	0.7109
NO <sub>x</sub>	0.6112

Table 6 shows the values of the correlation coefficients for the monitored values of pollutants. It is an observation of the dependence between the data that was monitored by the air quality station and the data that was obtained by the research. The values of correlation coefficients correspond to direct dependence. For solid PM particles, the value of the correlation coefficient is at the level of 0.7351, which represents a high degree of dependence between the observed data. Similarly, for

CO emissions, the value of the correlation coefficient is at the level of 0.7109. For NO<sub>x</sub> emissions, the value of the correlation coefficient is at the level of 0.6112, which represents a slight dependence. Also, in this case, it is possible to assume that the NO<sub>x</sub> values are influenced by the passage of road transport vehicles. It is possible that the values declared by the measuring station could have been affected by pollution other than just the influence of road traffic.

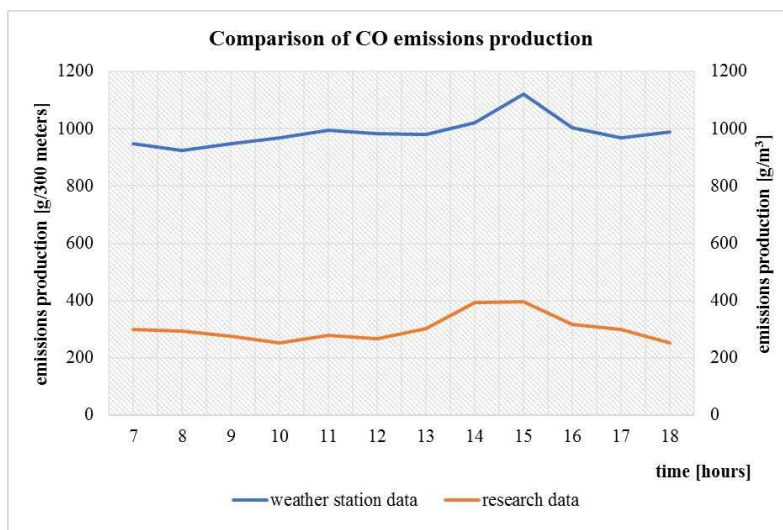


Figure 8

Comparison of CO emissions distribution – weather station vs. research [authors]

Figure 8 portrays the course of CO emissions released to the atmosphere. While the data recorded by the weather station involve emissions from all contributing factors (general value), our research is confined to traffic pollutants. The diagram, however, suggests that both curves reflect similar trends, indicating that road traffic is hugely impactful on the air quality. The weather station curve reaches the peak between 3 pm and 4 pm, whereas the curve tracking our survey tops the values between 2 pm and 3 pm.

Courses describing NO<sub>x</sub> emissions depicted in Figure 10 clearly reflect significant changes in investigated values. In general, we may argue that differences between values recorded by the weather station and figures calculated from the survey have compelling reasons. The survey calculations are derived from data reflecting the average city drive, emission class and fuel type. The produced emissions are expressed in g/300 m. The research only deals with emissions produced by monitored vehicles, whereas the weather station includes all air city pollutants, e.g., chimney fumes, industry, etc. Striking variations in the compared values may also involve changeable weather conditions, daily temperature differences, humidity and heat, traffic collisions and other transport situations affecting the air quality.

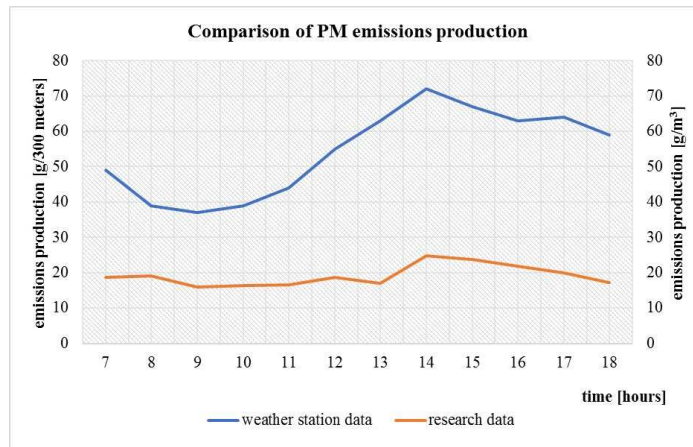


Figure 9

Essential Comparison of PM emissions distribution – weather station vs research [authors]

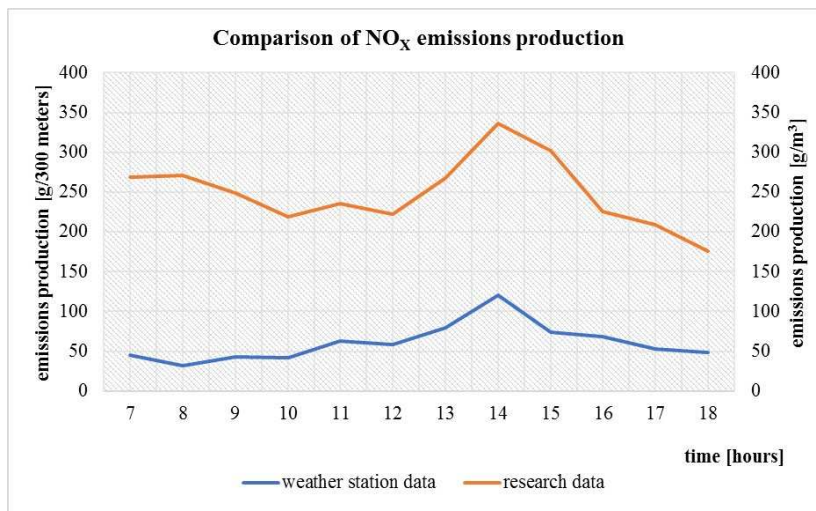


Figure 10

Comparison of NO<sub>x</sub> emissions distribution – weather station vs. research [authors]

## 4 Discussion

Most cities all over the world have recently been witnessing rapid urbanization. Municipalities are making great effort to establish effective transport infrastructure to comply with rapid urban and economic development. The local industrial state

heavily depends on good mobility, i.e., how easy is to move people, products and services using an efficient transport system [24-26]. Abdull, et al., [27] carried out identical research on road traffic emissions in urban areas, specifically a freeway in the city of Kyoto, Japan, involving COPERT PC program for making calculations. The traffic survey revealed the heaviest traffic flow of trucks between 7 am and 9 am, whereas passenger cars hit the peak in the morning rush hour. The overall traffic flow fell to the trough around 12 pm. The number of passing passenger cars did not reach the top again until 5 pm, followed by a steady decline until 6 pm. Truck intensity did not increase again until 2 pm and slumped by 6 pm. Analyzing the traffic speed, the authors found out that more than 75% of vehicles did not go under 46 km/h. The growing traffic volume leads to a slowdown, causing minor traffic disruption. Continuous speedup-slowdown adversely affects the traffic dynamics, hugely increasing released emissions. COPERT IV for the emission analysis revealed that heavy traffic at low speed produced the largest quantity of harmful substances, detecting pollutants as follows: PM, C<sub>6</sub>H<sub>6</sub>, CO, and NO<sub>x</sub>. Trucks produced higher amount of PM and NO<sub>x</sub> compared to passenger cars, as truck engines were working to the maximum due to the disrupted traffic flow. Higher emissions create road dust clouds and cause brake, tire and roadway wear-off. C<sub>6</sub>H<sub>6</sub> (benzene) constituted 1% of the volume of petrol, largely contributing to the increased emissions of passenger cars. CO pollutant also scaled with the use of passenger cars, which constituted the largest number of the examined vehicles [28]. The survey involving buses might have been biased by the COVID-19 pandemic on-set. The impact of the crisis on the bus service and the imposed restrictions were analyzed by Czodörová, et al., [29]. Moreover, Mikulski, et al., [30] investigated the reduction of transport-related air pollution and the impact of the COVID-19 pandemic on the level of NO<sub>x</sub> emissions in one of the big cities in Poland.

Mostafavi, et al., [31] examined pollution in the city of Arak in Iran. The authors explored the impact of industrial harmful substances and road traffic on air pollution rates, focusing on pollutants including: NO<sub>x</sub>, CO and SO<sub>2</sub>. Annual reports on industrial sectors, vehicle data, traffic flow and weather records comprised the conceptual framework of the analysis. The authors compared the obtained results with real statistics recorded by weather stations. Modeling the input data involved 3 types: information on permanent and temporary sources of pollution, local weather records, topographical data (mountain range height, valley depth, wind speed and direction, temperature and humidity). The analysis proved that road traffic is the largest polluter increasing NO<sub>x</sub>, CO and SO<sub>2</sub> levels. To change the unfavorable situation would involve supporting public transport, promoting electric vehicles and bicycles, imposing traffic restrictions within the city center or building highways. Industrial companies largely contributing to the air pollution would have to be relocated to the outskirts [31].

Increased exhaust emissions occur particularly strongly in the initial phase of the combustion engine operation, which has been pointed out in many scientific studies [32-35]. For example, Jayaratne, et al., [36] explored a cold start of engines.

The authors revealed that cold starts of petrol cars produce increased CO emissions, lasting several travelled kilometers. The high pollution levels prevailed throughout the night, when the outermost atmospheric layer is sinking down, pressing the air closer to the Earth. Driving vehicles with fully warmed-up engines showed relatively low CO emissions, leading to higher pollutant rates in the evening hours. Vehicles with fully warmed-up engines going to the city center through the measured section in the morning leave the city with cold engines, thus releasing more emissions [35]. The impact of cold starts on emissions and confirming its theory may be developed in further research.

- The survey revealed that road traffic in the monitored part of Trenčín was not re-sponsible for the air pollution to the extent we had expected. It was also proved that passenger cars are the biggest contributor to emission production given their largest representation in the research. The research conducted investigated that passenger cars had the strongest representation (90%) in our experiment. Other categories comprised 10%, out of which the category Lorry constitutes the smallest number (1%). Although haulage releases fewer emissions than passenger transport, certain restrictions on freight transport must be imposed to ensure safety and avoid traffic disruption. These vehicle categories are primarily responsible for excessive roadway wearoff and an increased noise level within the monitored area. Please only use font type Times Roman CE.
- When it comes to reducing emissions and the number of vehicles in motion (limiting the phenomenon of transport congestion) on the inner roads of metropolises, one of the directions of action is, for example, the vehicle rental system, as noted in the works [37] or in the further perspective of transport development, shared autonomous vehicles SAV [38]. Both of these concepts lead to a completely different perception and use of transport in modern cities. The first of them assumes no ownership of the vehicle and greater efficiency in the use of rental vehicles and limits their number in traffic and in parking lots. The second concept goes even further beyond the advantages mentioned in the first concept, it enables automatic driving, increasing traffic flow and thus the capacity of routes, through communication between vehicles and infrastructure, and real-time traffic monitoring, which reduces travel time [39]. Both solutions serve to reduce fuel consumption and therefore emissions. Moreover, the concept of autonomous vehicles assumes that an electric motor will be used to power these vehicles [40]. This is given that it is easier to control the electric motor than the internal combustion engine in the vehicle [41], and the computing power saved in this way can be used to control the vehicle and its orientation in the field [42].

## Conclusions

The presented research shows the potential of current conventional drive and conventional driving vehicles to reduce emissions and what is translated into the

identification of the overall level of pollution from transport in the urban area. In addition, other directions of reducing emissions in cities were signaled, related not only to the development of electric vehicles, but also autonomous vehicles in the future.

The experimental results of the impact of road traffic mobility on the environment in the 1st class road Hasičská Street No. 61 in the city of Trenčín, Slovakia and complex emission quantification proved that passenger cars are the most distinct category contributing to the air pollution regarding all recorded pollutants, i.e., CO, HC, NO<sub>x</sub> and PM.

Road haulage comprising category N3 – SEMI TRAILER hit the road mostly in the late morning hours, arguably supplying local storehouses and logistic centers or transporting goods. Our survey indicated that category N3 is the largest polluter of all monitored freight tiers regarding CO, HC and PM emissions, despite having the smallest representation in our experiment.

The city of Trenčín and its surroundings concentrate numerous logistic storehouses and centers including CT Park Trenčín – 2 km away, Coop Trenčín Logistics Center – 4.5 km away and Sihot Park Chochoľná logistic center – 10.5 km away from the examined area. We suppose that vehicles of N3 category transport goods to the storehouses or other logistic and distribution centers through the monitored transport territory of Trenčín.

As for the further research, we suggest that subsequent in-depth analysis of the impact of road traffic mobility emissions on the environment should, *inter alia*, involve traffic congestions, types and numbers of vehicles classified according to specific emission standards, including the influence of weather conditions and air pressure on the air pollution in the area.

The results of the research declare that the biggest air polluter in the monitored area is precisely passenger vehicles. This is due to the fact that their number represents 95% of the total number of vehicles passed. It is this phenomenon that results in a large amount of pollutants emitted into the air. In the future, it is necessary to focus on ways to reduce these emissions. One of the possibilities is increasing the share of electric cars and vehicles powered by an alternative drive.

This is primarily about reducing emissions directly in urban areas. So far, low-emission zones in cities have not been introduced in the territory of the Slovak Republic. The results of the research can be taken into account as a tool for monitoring pollution caused by road traffic anywhere within the city. The results clearly point to the fact that even passenger vehicles pose a threat in the process of air pollution.

### **Acknowledgement**

This research was funded by the VEGA project. 1/0426/22 Quantification of the impact of road transport on the environment in urban areas.

This research was also funded by the KEGA project. 041ŽU-4/2022 Implementation of students in the teaching process through the implementation of practical measurements in the form of driving and laboratory tests of road vehicles using multimedia tools.

This research was also funded by the SVV project 02SVV2325, funded by the Ministry of Education, Youth and Sports, Czech Republic.

### References

- [1] Prideaux, B. (2000) The role of the transport system in destination development. *Tourism Management*, Vol. 21, No. 1, pp. 53-63, DOI: 10.1016/S0261-5177(99)00079-5
- [2] Harrison, R. M., Beddows, D. C. (2017) Efficacy of recent emissions controls on road vehicles in Europe and implications for public health. *Scientific Reports*, Vol. 7, 1152 DOI: 10.1038/s41598-017-01135-2
- [3] Öhrström, E., Skånberg, A., Svensson, H., Gidlöf-Gunnarsson, A. (2006) Effects of road traffic noise and the benefit of access to quietness. *Journal of Sound and Vibration*, Vol. 295, Nos. 1-2, pp. 40-59, DOI: 10.1016/j.jsv.2005.11.034
- [4] Pénard-Morand, C., Annesi-Maesano, I. (2004) Air pollution: from sources of emissions to health effects. *Breathe*, Vol. 1, No. 2, pp. 108-119, DOI: 10.1183/18106838.0102.108
- [5] Achour, H., Carton, J., Olabi, A.G. (2011) Estimating vehicle emissions from road transport, case study: Dublin City. *Applied Energy*, Vol. 88, No. 5, pp. 1957-1964, DOI: 10.1016/j.apenergy.2010.12.032
- [6] Panko, J., Kreider, M., Unice, K. (2018) Review of tire wear emissions: a review of tire emission measurement studies: identification of gaps and future needs. *Non-Exhaust Emissions*, pp. 147-160, DOI: 10.1016/B978-0-12-811770-5.00007-8
- [7] Szczucka-Lasota, B., Węgrzyn, T., Łazarz, B., Kamińska, J. A. (2021) Tire pressure remote monitoring system reducing the rubber waste. *Transportation Research Journal Part D Transport and Environment*, Vol. 98, 102987, DOI: 10.1016/j.trd.2021.102987
- [8] Zum Hagen, F. H. F., Mathissen, M., Grabiec, T., Hennicke, T., Rettig, M., Grochowicz, J., Vogt, R., Benter, T. (2019) Study of brake wear particle emissions: impact of braking and cruising conditions. *Environmental Science and Technology*, Vol. 53, No. 9, pp. 5143-5150, DOI: 10.1021/acs.est.8b07142
- [9] Adamec, V., Ličbinský, R., Cholava, R. (2011) Doprava a zdravotné riziká dopravy. *Transactions on Transport Sciences*, Vol. 4, No. 3, 115, DOI: 10.2478/v10158-011-0011-y

- 
- [10] Krzyżanowski, M., Kuna-Dibbert, B., Schneider, J. (Eds.) (2005) Health effects of transport-related air pollution. WHO Regional Office Europe
- [11] McMichael, A. J. (1997) Transport and health: assessing the risks. In *Health at the Crossroads. Transport Policy and Urban Health*. London School of Hygiene and Tropical Medicine Fifth Annual Public Health Forum
- [12] Sustainable transport, <https://www.worldbank.org/en//transport/overview>, accessed on 2021-09-14
- [13] Ooi, G. L. (2008) Cities and sustainability: Southeast Asian and European perspectives. *Asia Europe Journal*, Vol. 6, No. 2, pp. 193-204, DOI: 10.1007/s10308-008-0176-0
- [14] Greenhouse gas emission intensity of fuels and biofuels for road transport in Europe, from <https://www.eea.europa.eu/data-and-maps/indicators/greenhouse-gas-emissions-intensity-of/assessment>, accessed on 2021-09-15
- [15] Harantová, V., Hájnik, A., Kalašová, A. (2020) Comparison of the flow rate and speed of vehicles on a representative road section before and after the implementation of measures in connection with COVID-19. *Sustainability*, Vol. 12, No. 17, 7216, DOI: 10.3390/su12177216
- [16] Pavlovic, J., Marotta, A., Ciuffo, B. (2016) CO<sub>2</sub> emissions and energy demands of vehicles tested under the NEDC and the new WLTP type approval test procedures. *Applied Energy*, Vol. 177, pp. 661-670, DOI: 10.1016/j.apenergy.2016.05.110
- [17] Sun, C., Li, V. O., Lam, J. C., & Leslie, I. (2019) Optimal citizen-centric sensor placement for air quality monitoring: A case study of city of Cambridge, the United Kingdom. *IEEE Access*, 7, 47390-47400
- [18] Slovak Hydrometeorological Institute, available online from [https://www.shmu.sk/sk/?page=1&id=oko\\_imis](https://www.shmu.sk/sk/?page=1&id=oko_imis) accessed on 2021-09-07
- [19] Hitchcock, G., Conlan, B., Kay, D., Brannigan, C., Newman, D. (2014) *Air quality and road transport: impacts and solutions*. London
- [20] Slovak Hydrometeorological Institute 2 - air pollution, from <https://www.shmu.sk/sk/?page=2049&id=1093>, assessed on 2021.09.14
- [21] Guo, J., Ge, Y., Hao, L., Tan, J., Li, J., Feng, X. (2014) On-road measurement of regulated pollutants from diesel and CNG buses with urea selective catalytic reduction systems. *Atmospheric Environment*, Vol. 99, pp. 1-9, DOI: 10.1016/j.atmosenv.2014.07.032
- [22] Landrigan, P. J. (2017) Air pollution and health. *The Lancet Public Health*, Vol. 2, No. 1, pp. e4-e5, DOI: 10.1016/S2468-2667(16)30023-8
- [23] Jaskiewicz, M., Lisiecki, J., Lisiecki, S., Pokropinski, E., Wieckowski, D. (2015) Facility for performance testing of power transmission units.

- Scientific Journals of the Maritime University of Szczecin, Vol. 114, No. 42, pp. 14-25
- [24] Kwok, R. C., Yeh, A. G. (2004) The use of modal accessibility gap as an indicator for sustainable transport development. *Environment and Planning A: Economy and Space*, Vol. 36, No. 5, pp. 921-936, DOI: 10.1068/a3673
- [25] Stanley, J. K., Hensher, D. A., & Loader, C. (2011) Road transport and climate change: Stepping off the greenhouse gas. *Transportation Research Part A: Policy and Practice*, 45(10), 1020-1030
- [26] Kazancoglu, Y., Ozbiltekin-Pala, M., & Ozkan-Ozen, Y. D. (2021) Prediction and evaluation of greenhouse gas emissions for sustainable road transport within Europe. *Sustainable Cities and Society*, 70, 102924
- [27] Abdull, N., Minoru Y., Yoko S. (2020) Traffic characteristics and pollutant emission from road transport in urban area. *Air Qual Atmos Health*, Vol. 13, pp. 731-738, DOI: 0.1007/s11869-020-00830-w
- [28] Skrúcaný, T., Kendra, M., Čechovič, T., Majerník, F., Pečman, J. (2021) Assessing the Energy Intensity and Greenhouse Gas Emissions of the Traffic Services in a Selected Region. *LOGI – Scientific Journal on Transport and Logistics*, Vol. 12. No. 1, pp. 25-35, DOI: 10.2478/logi-2021-0003
- [29] Czódorová, R., Dočkalik, M., Gnap, J. (2021) Impact of COVID-19 on bus and urban public transport in SR. *Transportation Research Procedia*, Vol. 55, pp. 418-425, DOI: 10.1016/j.trpro.2021.07.005
- [30] Mikulski, M., Drożdziel, P., Tarkowski, S. (2021) Reduction of transport-related air pollution. A case study based on the impact of the COVID-19 pandemic on the level of NO<sub>x</sub> emissions in the city of Krakow. *Open Engineering*, Vol. 11, No. 1, pp. 790-796, DOI: 10.1515/eng-2021-0077
- [31] Mostafavi, S. A., Safikhani, H., Salehfard, S. (2021) Air pollution distribution in Arak city considering the effects of neighboring pollutant industries and urban traffics. *International Journal of Energy and Environmental Engineering*, Vol. 12, No. 2, pp. 307-333, DOI: 10.1007/s40095-020-00379-5
- [32] Ambrozik, A., Ambrozik, T., Kurczyński, D., Łagowski, P., Trzensik, E. (2014) Cylinder pressure patterns in the SI engine fuelled by methane and by methane and hydrogen blends. *Solid State Phenomena*, Vol. 210, pp. 40-49, DOI: 10.4028/www.scientific.net/SSP.210.40
- [33] Cui, Y., Peng, H., Deng, K., Shi, L. (2014) The effects of unburned hydrocarbon recirculation on ignition and combustion during diesel engine cold starts. *Energy*, Vol. 64, pp. 323-329, DOI: 10.1016/j.energy.2013.10.083

- 
- [34] Figlus, T., Konieczny, Ł., Burdzik, R., Czech, P. (2015) The effect of damage to the fuel injector on changes of the vibroactivity of the diesel engine during its starting. *Vibroengineering Procedia*, Vol. 6, pp. 180-184
- [35] Giechaskiel, B., Zardini, A. A., Clairotte, M. (2019) Exhaust gas condensation during engine cold start and application of the dry-wet correction factor. *Applied Sciences*, Vol. 9, No. 11, 2263, DOI: 10.3390/app9112263
- [36] Jayaratne, R., Thai, P., Christensen, B., Liu, X., Zing, I., Lamont, R., Dunbabin, M., Dawkins, L., Bertrand, L., Morawska, L. (2021) The effect of cold-start emissions on the diurnal variation of carbon monoxide concentration in a city centre. *Atmospheric Environment*, Vol. 245, 118035, DOI: 10.1016/j.atmosenv.2020.118035
- [37] Koller, T., Tóth-Nagy, C. Perger, J. (2022) Implementation of vehicle simulation model in a modern dynamometer test environment. *Cognitive Sustainability*, Vol. 1, No. 4, DOI: 10.55343/cogsust.29
- [38] Zöldy, M. (2019) Improving heavy duty vehicles fuel consumption with density and friction modifier. *International Journal of Automotive Technology*, Vol. 20, No. 5, pp. 971-978, DOI: 10.1007/s12239-019-0091-y
- [39] Salisu, U. O., Oyesiku, O. O. (2020) Traffic Survey Analysis: Implications for Road Transport Planning in Nigeria. *LOGI – Scientific Journal on Transport and Logistics*, Vol. 11, No. 2, pp. 12-22, DOI: 10.2478/logi-2020-0011
- [40] Faryński, J. J., Żardecki, D. P., Dębowski, A. (2021) Study of the problem and the idea of operation of four-wheel-steering cars. *The Archives of Automotive Engineering – Archiwum Motoryzacji*, Vol. 94, No. 4, pp. 39-59, DOI: 10.14669/AM.VOL94.ART4
- [41] Tucki, K., Orynycz, O., Wasiak, A., Świć, A., Mruk, R., & Botwińska, K. (2020) Estimation of carbon dioxide emissions from a diesel engine powered by lignocellulose derived fuel for better management of fuel production. *Energies*, Vol. 13, No. 3, Art. no. 561, DOI: 10.3390/en13030561
- [42] Zöldy, M., Baranyi, P. (2023) Definition, Background and Research Perspectives Behind “The Cognitive Mobility Concept”. *Infocommunications Journal, Special Issue: Internet of Digital & Cognitive realities*, Vol. 2023, pp. 35-40, DOI: 10.36244/ICJ.2023.SI-IODCR.6

# Assessability of Road Accidents – a Methodology for Exploring the Effect of Accident Type and Data Recording Technology

Vida Gábor<sup>1</sup>, Wenzsky Nóra<sup>2</sup>, Török Árpád<sup>1</sup>

<sup>1</sup> Department of Automotive Technologies, Faculty of Transportation Engineering and Vehicle Engineering, Budapest University of Technology and Economics  
Stoczek utca 6, 1111 Budapest, Hungary  
e-mail: vida.gabor@kjk.bme.hu, torok.arpad@kjk.bme.hu

<sup>2</sup> Centre of Modern Languages, Faculty of Economic and Social Sciences, Budapest University of Technology and Economics  
Egry József utca 1, 1111 Budapest, Hungary  
e-mail: wenzsky.nora@gtk.bme.hu

---

*Abstract: Road accidents are reconstructed by forensic experts to reveal the causes of accidents and help authorities determine liability. However, how well an accident is assessable depends on various factors. The database-independent methodology proposed here makes it possible to explore the relationship between assessability, accident type and data recording technology. A combination of statistical tests (Mann–Whitney U Test, Wilcoxon Signed-rank Test, Kruskal–Wallis Test with Bonferroni Correction) are to be applied to a database of road accidents. As a result of these tests, it can be determined how the assessability of various accident types can be improved by the development in data recording technologies. This widely applicable, novel tool of the Cognitive Mobility realm is in practice a methodology for exploring the assessability of various types of road accidents. It can help decision-makers determine the development directions of new technologies.*

*Keywords: accident reconstruction; assessability; statistical methods; data recording technology; forensic expert*

---

## 1 Introduction

Road accident reconstruction, as its name implies, is a process that goes in the opposite direction as designing and construction. While designers calculate what could happen if forces are exerted on a structure built from the given materials, forensic experts determine what processes may have taken place, what forces may have been exerted if the given accident happened. In order to be able to reconstruct an accident, and thus determine causes and liability, basically as much data should be obtained about the case as possible. The range of data used for the reconstruction

process is wide. Being static, some data are easy to obtain, such as information on the terrain of the accident site, the make of the vehicles included or the traffic rules valid at the given section of the road. Other data must be recorded after the whole process, e.g. the position of the vehicles, skid marks, injuries and the damage caused.

However, the success of accident reconstruction does not solely depend on the amount of data collected. The assessability of an accident, i.e. how well the process can be reconstructed and how much liability can be determined, depends on various other factors as well, including accident type (e.g. head-on collision vs. leaving the track), data quality (e.g. accuracy) and data recording technology (e.g. yaw marks photographed vs. speed data recorded by the vehicle's tachograph). If it is known how these different factors affect level of assessability, data recording technologies can be developed in a way that could make accident reconstruction more precise not only for all accident types, but for a specific accident type if necessary. Moreover, based on such a quantification methodology, it may be determined what data recording technology is required for a certain accident type to be assessed at the highest possible level. Conversely, if we know the applied data recording technology, we can predict the level of assessability for each accident type.

With the emergence of highly or fully automated vehicles, i.e. a cognitive multimodal transport system [1], new types of accidents are expected to occur. In order to be able to reconstruct and assess these yet unknown accident types, probably new data recording technologies need to be developed. The model presented here is freely expandable, i.e. emerging accident recording technologies and accident types can also be added to it. This way, the effectiveness of the new technologies can also be measured. Also, the methodology can be customized to the needs of users – maybe for a certain database, more accident categories should be established or more levels of data recording technologies are to be explored.

In order to be able to develop and operate efficient, safe and environmentally friendly mobility systems and vehicle networks, it is indispensable to identify the factors that influence the operation of the various networks. As a result, the role of unconscious, irrational factors in the decision making process about mobility networks may be minimized. The aim of this article is to show how it is possible to identify the data that should be collected to help identify the causal links that lead to accidents in the best way.

This study presents a novel methodology based on various statistical methods for quantifying how accident type and data recording technology affect the assessability of road accidents. Section 2 clarifies basic concepts and reviews the relevant literature. In Section 3, the methodological steps are described in detail: the statistical methods to explore the possible differences between accident types and data recording technologies are presented. Section 4 concludes the article. The methodology presented here was developed based on a database of real road accidents [2].

## 2 Background

The basic concepts used in this study are defined as follows.

- The **assessability of an accident** is the degree to which the causes of the accident and liability can be determined based on the available data. Four categories of assessability are set up here (Table 1).

Table 1  
Accident assessability levels

<i>Accident process</i> \ <i>Accident cause Liability</i>	<i>Not determinable</i>	<i>Determinable</i>
<i>Not or partly determinable</i>	<i>Level 1</i>	<i>Level 3</i>
<i>Fully determinable</i>	<i>Level 2</i>	<i>Level 4</i>

- **Traditional data recording technology** ( $T_0$ ) is the technology to be applied by the police in the case of a road accident or a traffic crime. For example, in Hungary the technology is defined by the relevant Police Decree [3].
- **EDR data recording technology** ( $T_1$ ) is defined as traditional data recording technology complemented by accident data recorded in the Event Data Recorder modules of the vehicles participating in the given accident, as defined by the regulatory framework [4].
- **EDR+ data recording technology** ( $T_2$ ) is defined as EDR data recording technology complemented by data recorded in highly automated or fully automated vehicles. These extra data may include GPS coordinates, GPS time, video recordings of the accident environment, elements/objects in the traffic environment and their distance from the ego vehicle (Figure 1).
- **Accident type** is the category of a given accident process, determined by the most prominent property of the accident with regard to accident causes and liability. The seven categories (denoted  $A_1$ – $A_7$ ) used in this study were set up based on the following properties: relative position of the collided vehicles (e.g., rear-end) or the conflict type (e.g., lane changing) or the traffic environment (e.g., at traffic lights) [2].



Figure 1

Data recording technologies applied in this study

In order to be able to explore relationships between data recording technologies, accident type and assessability, a database must be compiled. The statistical calculations are to be carried out on this database, which is illustrated in Table 2. Column 1 is the registry number of the accident; Column 1 encodes the accident type. Columns 3-5 show assessability levels according to Table 1 above. The methodology presented below was tested against a public database of real-life road accidents [2]. As the overwhelming majority of these accidents were recorded by traditional methods, and EDR data were only available in a low number of cases, Columns 4 and 5 give the assessability for the case if data provided by the relevant modern data recording technology were present.

Table 2  
Database structure

No.	Accident type [A <sub>1-i</sub> ]	Data recording technology		
		T <sub>0</sub>	T <sub>1</sub>	T <sub>2</sub>
		Assessability [1–4]		
1	1	1	1	4
2	3	3	4	4
3	2	2	4	4
...				
n	6	3	3	4

Statistical methods have been applied successfully to analyze objectively measurable characteristics of road accidents or of accident participants. For example, Shaadan *et al.* [5] used the Mann–Whitney Test to reveal the correlations between the gender of accident participants and the number of serious or fatal accidents, and also between the age of participants and the severity of accidents.

The topic of the present study is closer to those research projects that examine the physical parameters of road accidents. The Mann–Whitney Test and the Chi-square Test was applied by Baker [6] in an analysis of correlations between the dynamics of the crash and the severity of brain damage caused by the accident. Ayazi *et al.*

[7] applied the Chi-square Test to reveal the correlations between accident causes and types, environmental factors (e.g., road and visibility conditions) and accident severity.

Concerning the latest technology, accidents by self-driving cars were simulated by [8]. The collision reconfiguration system applying three different decision-making strategies was tested: the degree of seriousness of accidents was analyzed using the Kruskal–Wallis Test.

However, to the best of our knowledge, assessability of road accidents has not been analyzed with the help of statistical methods. It is self-evident that assessability, thus the success of reconstruction basically depends on the amount of accident data. In general, the higher the amount of available data is, the higher level of assessability can be reached. However, according to our hypothesis, assessability levels also depend on accident type and the applied data recording technology. In order to reveal the differences between these categories, statistical methods are to be utilized. The methodology and the various statistical tests used here are described in detail in Section 3.

### 3 Methodology

The system presented here is a step-by-step method for revealing, by means of statistical analyses, how factors, namely accident type and data recording technology, affect the assessability of road accidents. In general, the type of statistical tests that can be applied to a given dataset depends on the characteristics of the sets, primarily on the distribution of data. It must be checked whether the data in the samples are distributed according to normal distribution (e.g., using the Saphiro–Wilk Test [9]).

If the examined sample has a normal distribution, the means of the examined groups can be compared using the analysis of variance (ANOVA) [10]. This method can actually be defined as a generalization of the t-test for comparing more than two samples. It is important to emphasize that the application of ANOVA requires the distribution of the analyzed samples to be normal regarding the investigated variable. When applying the ANOVA method, the variance of the sample is given by the following formula:

$$s^2 = \frac{1}{n-1} \sum_i (x_i - \bar{x})^2 \quad (1)$$

where

$s^2$  – mean square;

$n$  – number of elements in the sample;

$x_i$  – variable value of the  $i^{\text{th}}$  element;

$\bar{x}$  – mean value of the investigated variable.

Based on the introduced formula, the analysis of variance identifies three different variance metrics:

- (1) a total variance which can be derived from the deviations between the grand mean and the variable values of the elements;
- (2) an error variance, which can be derived from the deviations between the variable values of the elements and their appropriate treatment means, and
- (3) a treatment variance.

Table 3  
Comprehensive overview of the methodology

No.	Data recording technology	Samples		Tested entities	Samples Independent (I) Connected (C)	Comparison	Statistical test
		1	2				
1.	$T_0$	$A_i$	a) comp. set ( $UA_i$ ) b) total set (U)	Assessability of accident types according to data recording technology	I	pairwise	Mann-Whitney U Test
2.	$T_1$	$A_i$	a) comp. set ( $UA_i$ ) b) total set (U)				
3.	$T_2$	$A_i$	a) comp. set ( $UA_i$ ) b) total set (U)				
4.	$T_0 - T_1$	$A_i T_0$	$A_i T_1$	Change in assessability according to type of change	C	pairwise	Wilcoxon Signed Rank Test
5.	$T_0 - T_2$	$A_i T_0$	$A_i T_2$				
6.	$T_0$ $T_1$ $T_2$	a) $A_i T_0$ b) $A_i T_1$ c) $A_i T_2$	a) $A_j T_0$ b) $A_j T_1$ c) $A_j T_2$	Assessability ranks within data recording technology	I	groupwise	Kruskal-Wallis Test Bonferroni Correction
7.	$T_0$ $T_1$ $T_2$	a) $A_i T_0$ b) $A_i T_1$ c) $A_i T_2$	a) $A_j T_0$ b) $A_j T_1$ c) $A_j T_2$				
8.	$T_0$ $T_1$ $T_2$	a) $A_i T_0 - T_1 \Delta$ b) $A_i T_0 - T_2 \Delta$ c) $A_i T_1 - T_2 \Delta$	a) $A_j T_0 - T_1 \Delta$ b) $A_j T_0 - T_2 \Delta$ c) $A_j T_1 - T_2 \Delta$	Assessability change of accident types according to type of change	I	groupwise	Kruskal-Wallis Test Bonferroni Correction
9.	$T_0$ $T_1$ $T_2$	a) $A_i T_0 - T_1 \Delta$ b) $A_i T_0 - T_2 \Delta$ c) $A_i T_1 - T_2 \Delta$	a) $A_j T_0 - T_2 \Delta$ b) $A_j T_0 - T_2 \Delta$ c) $A_j T_1 - T_2 \Delta$				
$T_0, T_1, T_2$ – data recording technologies $A_i, A_j$ – assessability of accidents in a given accident type $\Delta$ – change in assessability of accidents for a given accident type							

However, it must be emphasized that in the case of non-normally distributed variables, non-parametric statistical methods must be applied.

Based on our experiences and the performed investigations, the distributions of the variables characterizing road accidents are not normal. Therefore, non-parametric statistical methods are applied in further research phases. Accordingly, the methods presented here were selected because the example dataset did not have a normal distribution. Furthermore, the assessability values examined here are independent of each other, as the assessability of a given accident does not depend on the assessability of another accident.

In this analysis,  $T_0$ ,  $T_1$  and  $T_2$  denote the data recording technologies.  $T_0$  is the baseline technology (in our database, traditional).  $T_1$  marks a higher level of development: it includes all techniques in  $T_0$ , and some more advanced ones (in our database, this category corresponds to EDR).  $T_2$  denotes the highest level (in our case, EDR+), which means that in addition to all previous techniques ( $T_0$  and  $T_1$ ), further data recording techniques are available. Accidents were put into 7 categories (denoted  $A_1$ – $A_7$ ), and assessability had four levels (marked 1–4, 4 being the highest level).

### 3.1 Comparison of Accident Types

In the first round of analyses, pairwise comparisons are to be made in order to explore whether there are any accident types whose assessability is significantly different from that of other accident types. For this analysis, the Mann–Whitney U Test was applied [11, 12], which compares two samples (Sample 1 and Sample 2), which are the values of the same parameter – in this case, assessability. The test calculates the probability of a randomly selected value  $X$  from Sample 1 being greater than value  $Y$  randomly selected from Sample 2. The calculation is based on Equations (2-4).

$$U_1 = n_1 n_2 + \frac{n_1(n_1 + 1)}{2} - R_1 \quad (2)$$

$$U_2 = n_1 n_2 + \frac{n_2(n_2 + 1)}{2} - R_2 \quad (3)$$

$$Z = \frac{U - \frac{n_1 n_2}{2}}{\sqrt{\frac{n_1 n_2 (n_1 + n_2 + 1)}{12}}} \quad (4)$$

where,

$n_1$  – number of elements in Sample 1;

$n_2$  – number of elements in Sample 2;

$R_1$  – sum of the ranks in Sample 1;

$R_2$  – sum of the ranks in Sample 2;

$U_1$  – test function value for Sample 1;

$U_2$  – test function value for Sample 2;

$Z$  – value of function approaching the normal distribution.

For our database, for each test in this group, the significance level of the Mann–Whitney U Test was set to  $\alpha = 0.05$ . Our hypotheses were identified according to the following consideration. In the case of randomly selected values  $X_{\text{Sample1}}$  and  $X_{\text{Sample2}}$  from two different populations, the probability of  $X_{\text{Sample1}}$  being larger or equal to  $X_{\text{Sample2}}$  is larger than the probability of  $X_{\text{Sample2}}$  being larger than  $X_{\text{Sample1}}$ :

H0:  $X_{\text{Sample1}} \geq X_{\text{Sample2}}$

H1:  $X_{\text{Sample1}} < X_{\text{Sample2}}$

This means the test investigates the probability of Type I error (i.e., of rejecting a correct H0) related to the compared assessability values. If the chance of rejecting a correct null hypothesis is too high, we cannot accept H1. Accordingly, if  $p$  is lower than  $\alpha = 0.05$ , the probability of Type I error is tolerably low, so the null hypothesis (H0) can be rejected, and H1 is accepted, i.e., the assessability of accidents in the examined type is significantly worse than that of the bigger set (Sample 2). Such a result entails that with the given data recording technology, the examined accident type cannot be assessed as well as the other accidents.

There are two runs within each test type: in the first run, assessability values of a given accident type (Sample 1) are compared to such values of the complementary set. The aim of this is to see whether the level of assessability of the tested accident type is different from that of the other types. In the second run, Sample 1 is compared to the total set.

### 3.1.1 Test 1 – Baseline

The aim of the first test is to see for each accident category whether there is a significant difference in assessability levels compared to all other accident categories and to the average of the total sample, with data recording  $T_0$ .

In this test, Sample 1 is composed of the assessability values for a given accident type (Figure 2), for example  $A_1$ . In the first run, the assessability values of the given accident type are compared to the assessability values of the complementary set (Sample 2), i.e., those of all the other accident types (in our case,  $A_2$ – $A_7$ ). In the next run, Sample 2 is larger than in the first run: it is the total, unified set, i.e., in our case assessability values for all accident types ( $A_1$ – $A_7$ ).

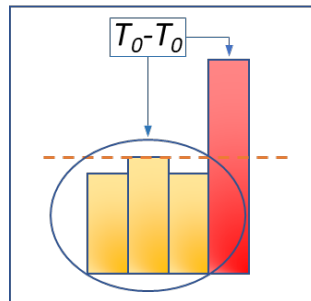


Figure 2

Test 1 – assessability of Sample 1 (red) compared to that of Sample 2 (yellow), data recorded by  $T_0$

### 3.1.2 Test 2 – Higher Level Data Recording ( $T_1$ )

Test 2 aims to reveal whether there is a significant difference in assessability for a given accident category with data recorded by a higher-level technology, namely  $T_1$  compared to other accident types (Figure 3). Therefore, Sample 1 is the assessability of a given accident type with  $T_1$  data recording. Results are calculated for a comparison with the baseline category and also for the same data recording category.

Consequently, in Test 2a, assessability values in Sample 1 are compared to the average assessability of the complementary set and the total set with the baseline level data recording technology  $T_0$ . In Test 2b, however, values in Sample 1 are compared to values in the complementary and the total set if data are recorded by  $T_1$ .

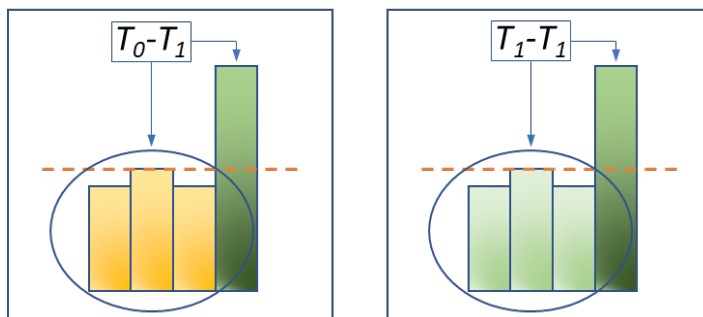


Figure 3

Test 2 – assessability of Sample 1 (dark green,  $T_1$ ) compared to that of Sample 2 (yellow) – data recorded by  $T_0$  (Test 2a, left); and to Sample 2 (light green) data recorded by  $T_1$  (Test 2b, right)

### 3.1.3 Test 3 – Highest Level Data Recording ( $T_2$ )

Similarly, to Test 2, the aim of Test 3 is to reveal whether there is a significant difference in assessability for a given accident category with data recorded by the highest-level technology, namely  $T_2$ , compared to other accident types (Figure 4). Therefore, Sample 1 is the assessability of a given accident type with  $T_2$  data recording. Results are calculated for a comparison with the baseline category  $T_0$  and also for the same data recording category,  $T_2$ .

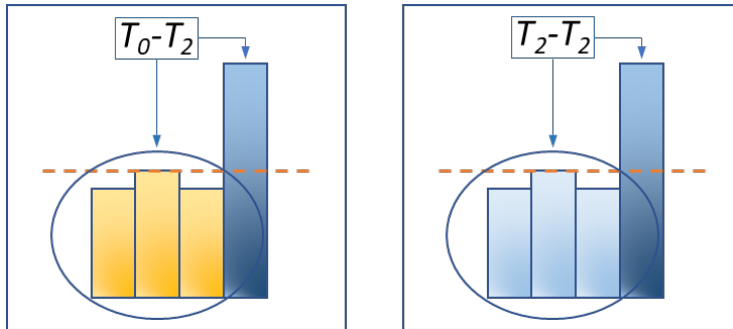


Figure 4

Test 3 – assessability of Sample 1 (dark blue,  $T_2$ ) compared to that of Sample 2 (yellow) – data recorded by  $T_0$  (Test 3a, left); and to Sample 2 (light blue) data recorded by  $T_2$  (Test 3b, right)

As a result of, Tests 1-3, it can be seen which accident types have a significantly lower assessability than the others for each data recording category.

## 3.2 Comparison of Data Recording Technologies

The second round of analyses focuses on data recording technologies. The aim is to test whether the development of data recording technologies (from  $T_0$  to  $T_2$ ) can actually improve the assessability of the different accident groups. To see this, the assessability levels according to data recording technology within an accident type were compared (Figure 5).

The Wilcoxon Signed-rank Test [13] was applied to compare the connected groups which had a non-normal distribution. In each group, the accidents were the same, and an assessability value was assigned to each accident according to data recording technology. The tested hypotheses are as follows.

$H_0$ : The median difference is zero.

$H_1$ : The median difference is not zero,  $\alpha = 0.05$ .

Pairwise differences in assessability are ranked according to their absolute value, and ranks are assigned. In the next step, positive or negative signs are assigned to these ranks, depending on whether the original difference was positive or negative.

Then, test ranks ( $R_i$ ) of corresponding pairs ( $Y_i - X_i$ ) are summed separately, i.e. positive values ( $W^+$ ) (5) and negative values ( $W^-$ ) (6), and the negative sum is subtracted from the positive sum (7).

$$W^+ = \sum_{Y_i - X_i > 0} R_i \quad (5)$$

$$W^- = \sum_{Y_i - X_i < 0} R_i \quad (6)$$

$$W = W^+ - W^- \quad (7)$$

After identifying test statistics ( $W$ ), we have to compare it to the critical value depending on sample size and significance level.

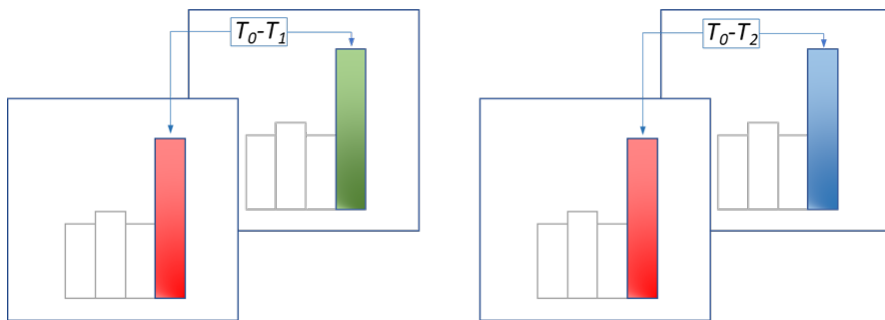


Figure 5

Assessability of a given accident group (Sample 1: red,  $T_0$ ) according to data recording technology.

Test 4 (left) – data recording technology  $T_1$  (green); Test 5 (right) – data recording technology  $T_2$  (blue)

### 3.2.1 Test 4 – Baseline ( $T_0$ ) vs. $T_1$

In this test, for each data recording technology, assessability values for each accident are compared: Sample 1 corresponds to values assigned for  $T_0$  and Sample 2 to  $T_1$  data recording technology. The test reveals whether there is a significant change in assessability with the introduction of  $T_1$  technology for the given accident type.

### 3.2.2 Test 5 – Baseline ( $T_0$ ) vs. $T_2$

The aim of this test is to reveal how the introduction of the highest level of data recording technologies affect assessability compared to the baseline. Thus, for each data recording technology, assessability values for each accident are compared:

Sample 1 corresponds to values assigned for  $T_0$  and Sample 2 to  $T_2$  data recording technology.

### 3.3 Ranking by Assessability

The previous tests can prove whether there is a difference in assessability levels for different accident types with different data recording technologies. However, the above tests cannot rank the accident types according to assessability. To reveal the ranking between accident types, assessability levels for different accident types were compared within each data recording technology. For this, a 2-step analysis was carried out. In Test 6, the Kruskal–Wallis Test with Bonferroni Correction was applied to compare multiple independent groups (i.e., assessability levels for accident types  $A_1$ – $A_7$  within categories  $T_0$ ,  $T_1$  and  $T_2$ ). In Test 7, those pairs in which stochastic dominance is proven by Test 6 were compared with the Mann–Whitney Test.

#### 3.3.1 Test 6 – Comparison of All Possible Pairs

In this test, Sample 1 is made up of the values for assessability for a given accident type, for a certain data recording technology (e.g.,  $A_2$ ,  $T_1$ ). Sample 2 is composed of values for assessability for another accident type, for the same data recording technology (e.g.,  $A_3$ ,  $T_1$ ). All possible pairs are tested for each data recording technology (for  $T_0$ ,  $T_1$ , and  $T_2$ , respectively, see Figure 6). Thus, non-normally distributed independent group samples are compared using the Kruskal–Wallis Test [14].

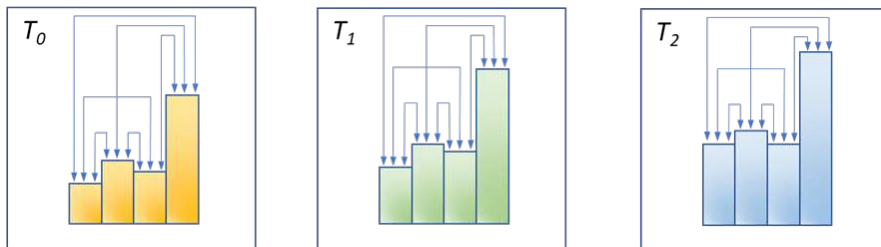


Figure 6

Test 6: assessability of accident groups according to data recording technology: Test 6a:  $T_0$  (yellow); Test 6b:  $T_1$  (green); Test 6c:  $T_2$  (blue)

For this test, the following hypotheses are formed.

$H_0$ : the medians of Samples are equal

$H_1$ : some of the medians of the Samples are not equal

The following formula is used for calculating the statistical test results.

$$H = (N - 1) \frac{\sum_{i=1}^g n_i (\bar{r}_i - \bar{r})^2}{\sum_{i=1}^g \sum_{j=1}^{n_i} (r_{ij} - \bar{r})^2} \quad (8)$$

where

$n_i$  – is the number of elements in the  $i^{\text{th}}$  sample;

$r_{ij}$  – is the rank (among all elements) of the  $j^{\text{th}}$  element in the  $i^{\text{th}}$  sample;

$N$  – is the number of elements across all groups;

$\bar{r}_i$  – is the average rank of the  $i^{\text{th}}$  sample;

$\bar{r}$  – is the average rank of all samples in the unified sample;

$g$  – is the number of samples.

In order to minimize Type I Error, i.e. rejecting the null hypothesis although it is actually true, the Bonferroni Correction was applied. The aim of this correction is to diminish the unfavorable effect of the Type I Error, which increases when comparing groups [15]. The basic principle is that the significance level ( $\alpha$ ) is lowered proportionally to the number of hypothesis tests ( $m$ ). Consequently, the null hypothesis is dropped if for the value  $p_i$  of the  $i^{\text{th}}$  hypothesis test proves to be true.

The following inequity (9) supports the applicability of the Bonferroni correction [16]. In this formula,  $m_0$  marks the number of true null hypotheses.

$$EF = P \left\{ \bigcup_{i=1}^{m_0} \left( p_i \leq \frac{\alpha}{m} \right) \right\} \leq \sum_{i=1}^{m_0} \left\{ P \left( p_i \leq \frac{\alpha}{m} \right) \right\} = m_0 \frac{\alpha}{m} \leq \alpha \quad (9)$$

Test 6 shows for which pairs the assessability difference can be regarded as stochastically dominant within a given data recording technology group. For example, if for the accident type pair  $A_3$ – $A_5$  the Kruskal–Wallis Test has a significant  $p$ -value for the  $T_1$  data recording technology, it means that the level of assessability for either  $A_3$  or  $A_5$  is significantly higher than for the other member of the pair. However, this test does not determine for which group the values are higher.

### 3.3.2 Test 7 – Pairwise Comparison

To determine for which member of the pair the assessability change is more significant, a pairwise comparison is required. The comparison is to be made by the Mann–Whitney U Test for each pair (c.f. Section 3.1, Tests 1-3). Only those pairs are to be tested, in which the Test 6 indicated stochastic dominance (Figure 7).

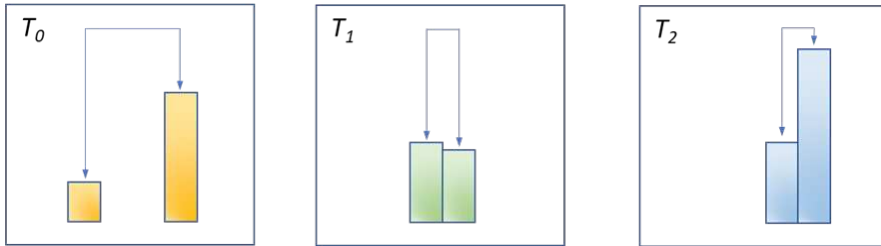


Figure 7

Comparison of accident groups with stochastic dominance from Test 6: Test 7a:  $T_0$  (yellow); Test 7b:  $T_1$  (green); Test 7c:  $T_2$  (blue)

In this test, Sample 1 is composed of the assessability values for a given accident type for a given data recording technology, for example  $A_1$  ( $T_1$ ). Sample 2 is the set of assessability values for another accident type for the same data recording technology, for example  $A_3$  ( $T_1$ ).

As a result of, Tests 6 and 7, it can be determined for the significantly differing pairs which one has a significantly higher assessability value than the other member of the pair. Thus, a partial ordering can be set up.

### 3.4 Change in Assessability

In order to see to what extent assessability changes with the introduction of more and more developed data recording technologies, the values for assessability change for each accident type ( $A_1$ – $A_7$ ) are to be compared to those of each other group with the same method that is followed by Tests 6 and 7. The only difference is that the dependent variable is the change in assessability for a given accident type between two data recording technologies.

#### 3.4.1 Test 8 – Comparison of All Possible Pairs

In this test, Sample 1 is made up of the values for assessability change for a given accident type, for a certain development in data recording technology (e.g.  $A_2$ , development  $T_0$ – $T_1$ ). Sample 2 is composed of values for assessability change for another accident type, for the same development in data recording technology (e.g.,  $A_3$ , development  $T_0$ – $T_1$ ). All possible pairs are tested for each type of development (i.e.,  $T_0 - T_1$ ,  $T_0 - T_2$ ,  $T_1 - T_2$ , see Figure 8). As there are four assessability levels (1-4), the values examined here range from 0 (no change) to 3 (maximum change from 1 to 4).

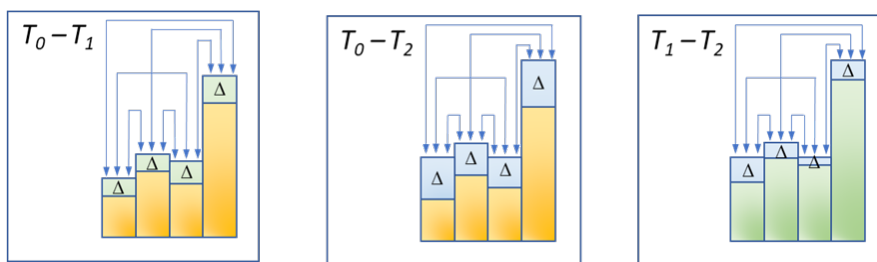


Figure 8

Test 8: comparison of assessability change ( $\Delta$ ): Test 8a:  $T_0-T_1$  (yellow–green); Test 8b:  $T_0-T_1$  (yellow–blue); Test 8c:  $T_1-T_2$  (green–blue)

Test 8 shows for which pairs the assessability change can be regarded as stochastically dominant for a certain type of change in data recording technology (i.e., a)  $T_0 - T_1$ , b)  $T_0 - T_2$  or c)  $T_1 - T_2$ ). For example, if for the accident type pair A3–A5 the Test 8 has a significant  $p$ -value for the  $T_1 - T_2$  development in data recording, it implies that the assessability change for either A3 or A5 is significantly higher than for the other member of the pair. However, this test does not determine for which group the values are higher.

### 3.4.2 Test 9 – Pairwise Comparison

To determine for which member of the pair the assessability change is more significant, a pairwise comparison is required. The comparison is to be made by the Mann–Whitney U Test for each pair (c.f. Section 3.1, Tests 1-3). Only those pairs are to be tested, in which the Test 8 indicated stochastic dominance (Figure 9).

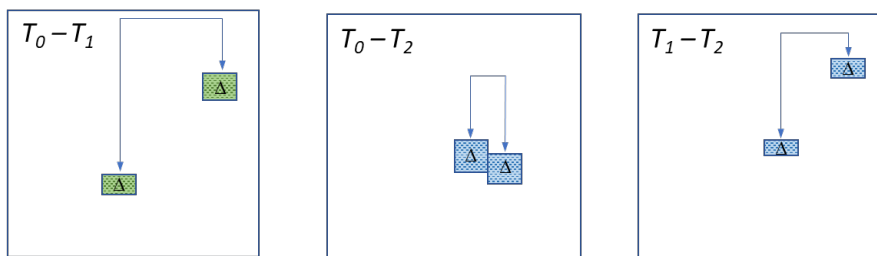


Figure 9

Test 9: comparison of significant assessability change ( $\Delta$ ): Test 9a:  $T_0-T_1$ ; Test 9b:  $T_0-T_1$ ; Test 9c:  $T_1-T_2$

In this test, Sample 1 is composed of the assessability change values for a given accident type for a given data recording technology change, for example  $A_1+T_1-T_2$ . Sample 2 is made up of assessability change values for another accident type for the same data recording technology change, for example  $A_3+T_1-T_2$ .

The result of the test shows for which accident type which development of data recording technology resulted in a significant improvement in assessability.

## Conclusions

This study presented a detailed methodology composed of various statistical tests for exploring how the development of data recording technologies and accident type influence the assessability of road accidents. The series of tests can be run on any database composed of real or simulated road accidents, in which the independent variables are accident type and data recording technology, and the dependent variable is the level of assessability for each accident.

The analysis described here is a combination of statistical methods that can be applied to samples with non-normal distribution: the Mann–Whitney U Test, the Wilcoxon Signed-rank Test and the Kruskal–Wallis Test with Bonferroni Correction. As a result of, these tests, it can be determined which data recording technologies improve the assessability of accidents the best and to what extent the assessability of which accident types improves due to a change in assessability. Such results can be utilized by the automotive industry to set the direction of development for data recording technology.

This methodology was tested against a database of real road accidents in Hungary [2]. However, the list of accident types and data recording technologies can be extended without a modification of the model. Thus, the methodology proposed here can be applied to databases other than the test database. Consequently, the effects of future developments in data recording and the emergence of new or different accident types can also be tested by this methodology.

## References

- [1] Zöldy, M. and Baranyi, P. “The Cognitive Mobility Concept.” *Infocommunications Journal*, Special Issue: Internet of Digital & Cognitive realities, 2023, 35-40, <https://doi.org/10.36244/ICJ.2023.SI-IODCR.6>
- [2] Vida, G. and Török, Á. “The impact of accident data recording technology on liability issues.” *Mendeley Data*, V1. 2022, <https://data.mendeley.com/datasets/hw6ft7jzcb/1> (Downloaded: 14 January 2022)
- [3] 32/2016. (XII. 16.) ORFK Instruction 32/2016 (XII. 16.) amending ORFK Instruction 60/2010 (OT 34.) on the rules of police procedure in the event of traffic accidents and traffic offences, and ORFK Instruction 26/2013 (VI. 28.) on the police use of technical means for documenting traffic offences [ORFK utasítás a közlekedési balesetek és a közlekedés körében elkövetett bűncselekmények esetén követendő rendőri eljárás szabályairól szóló 60/2010. (OT 34.) ORFK utasítás, valamint a közlekedési jogsértést dokumentáló technikai eszközök rendőrségi alkalmazásáról szóló 26/2013. (VI. 28.) ORFK utasítás módosításáról] <https://net.jogtar.hu/jogszabaly?docid=A16U0032.ORF&txtreferer=00000001.TXT> (Downloaded: 14 February 2023)

- [4] LLI Electronic Code of Federal Regulations (e-CFR). Title 49 – Transportation. Subtitle B – Other Regulations Relating to Transportation. Chapter V – National Highway Traffic Safety Administration, Department of Transportation. Part 563 – Event Data Recorders. § 563.5 Definitions. <https://www.law.cornell.edu/cfr/text/49/563.5> (Downloaded: 14 February 2023)
- [5] Shaadan, N., Azhar Suhaimi, M. I. K., Hazmir, M. I. and Hazmir, E. N. “Road accidents analytics with data visualization: a case study in Shah Alam Malaysia.” *Journal of Physics, Conference Series* 1988. 012043. 1988/2021. doi:10.1088/1742-6596/1988/1/012043
- [6] Baker, C. E., Martin, P., Wilson, M. H., Ghajari, M. and Sharp, D. J. “The relationship between road traffic collision dynamics and traumatic brain injury pathology.” *Brain Communications*, 4(2), feac033. 2022, doi: 10.1093/braincomms/feac033
- [7] Ayazi, E., Khorsand, R. and Sheikholeslami, A. “Investigating the effectiveness of geometric and human factors on the severity of urban crashes.” *Materials Science and Engineering*, 671, 012102. 2020, doi:10.1088/1757-899X/671/1/012102
- [8] Parseh, M. and Asplund, F. “New needs to consider during accident analysis: Implications of autonomous vehicles with collision reconfiguration systems.” *Accident Analysis & Prevention*, 173, 106704. 2022, doi: 10.1016/j.aap.2022.106704
- [9] Shapiro, S. S. and Wilk, M. B. (1965). “An analysis of variance test for normality.” *Biometrika*, 52(3), 591-611, <https://sci2s.ugr.es/keel/pdf/algorithm/articulo/shapiro1965.pdf> (Downloaded: 10 December 2022)
- [10] Fisher, R. (1925) *Statistical Methods For Research Workers*. Cosmo, Edinburgh
- [11] Mann, H. and Whitney, D. “Controlling the false discovery rate: a practical and powerful approach to multiple testing.” *Annals of Mathematical Statistics*, 18(1), 50-60, 1947, doi: 10.1214/aoms/1177730491
- [12] Nachar, N. “The Mann–Whitney U: A test for assessing whether two independent samples come from the same distribution.” *Tutorials in quantitative Methods for Psychology*, 4(1), 13-20, 2008, doi: 0.20982/tqmp.04.1.p013
- [13] Wilcoxon, F. (1992) “Individual comparisons by ranking methods.” In Kotz, S. and Johnson, N. L. (eds): *Breakthroughs in Statistics*. Springer, New York, NY. pp. 196-202, doi: 10.1007/978-1-4612-4380-9\_16
- [14] Kruskal, W. H. and Wallis, W. A. “Use of ranks in one-criterion variance analysis.” *Journal of the American Statistical Association*, 47(260), 583-621, 1952

- [15] Bonferroni, C. E. *Statistical theory of classification and calculation of the probability* [Teoria statistica delle classi e calcolo delle probabilità]. Pubblicazioni del R. Istituto superiore di scienze economiche e commerciali di Firenze, Florence R. Istituto superiore di scienze economiche e commerciali, Seeber, Firenze. 1936
- [16] Boole, G. (1847) *The Mathematical Analysis of Logic*. Philosophical Library

# Eye Tracking Study of Visual Pollution in the City of Zilina

**Radovan Madleňák, Lucia Madleňáková, Margita Majerčáková, Roman Chinoracký**

University of Zilina, Univerzitna 8215/1, 01026 Zilina, Slovakia; e-mail:  
radovan.madlenak@uniza.sk; lucia.madlenakova@uniza.sk;  
margita.majercakova@uniza.sk; roman.chinoracky@uniza.sk

---

*Abstract: This paper examines the issue of visual pollution in the city of Žilina, focusing specifically on outdoor advertising. A quantitative study was conducted to investigate the density of outdoor advertising on major roads in the town, as well as the topics of the advertisements. The research data collected provides pertinent information for policymakers and marketing firms to consider when forming policies concerning transportation, the environment, and outdoor advertising. This study is essential to comprehend the effects of visual pollution on the cognitive mobility of drivers navigating city roads. The findings of this study suggest that outdoor advertising has a pretty limited impact on how drivers perceive their environment and interact with it. Consequently, the results of this research can be used to create more effective policies related to outdoor advertising and traffic safety.*

*Keywords: visual pollution; eye tracking study; outdoor advertising; road safety*

---

## 1 Introduction

The turn of the third millennium has seen mobility become a fundamental pillar of our society. The rapid advancements in technology have enabled us to enhance our cognitive capacity in a variety of fields; mobility is one of the most significantly impacted. Mobility has become a multifaceted concept in our understanding; its relevance in transportation has also manifested in the digital realm and other areas. Consequently, the potential of mobility has become increasingly visible in its ability to bring about positive changes in our society, as highlighted by [1].

The concept of mobility is inherently related to the notion of taking initiative. Decisions are integral to mobility, as they determine whether an activity is mobile or not and can be taken multiple times throughout. The type of device or vehicle used, and the quality of such, heavily influences the decision making process, resource requirements, and ultimate outcome of the mobility. Furthermore, in addition to the infrastructure needed, mobility also necessitates a variety of

resources such as money, time, and energy. The human-machine interface plays a vital role and offers a broad spectrum of options, including smartphones, smart maps, web-tracking interfaces, and simulation software, as noted by [2].

Decision making is extremely important not only for increasingly automated vehicles, but also for driver support. Intensive research is under way in this area to investigate the implications of cognitive memory for decision making in traffic. One excellent example is continuous, dynamic route re-design through the inclusion of cognitive variables, which has been found to significantly reduce error rates. This suggests that vehicles are capable of learning from cognitive variables, opening the possibility of unsupervised learning to make sensible traffic decisions. According to [2], it is worth mentioning that the cognitive process involved in vehicle-related decision making bears resemblance to that of the human mind, where event classification is linked to patterns that have been previously processed.

The decision making of drivers in real-world conditions is often impacted by a range of external stimuli. These can include the physical environment and the objects which populate it. According to research [3], analyzing and detecting patterns of driver behavior under real-world conditions can provide valuable data for autonomous vehicle decision making, by understanding the interplay between humans, machines, and the environment.

A specific example of objects found in the vicinity of the vehicle are outdoor advertising objects. This illustrates the importance of external stimuli when determining driver behavior and could have important implications for autonomous vehicle decision making. Outdoor advertising, alternatively termed out-of-home (OOH) advertising is a form of media, which is intended to reach consumers who are away from their dwellings. This includes billboards, signs, placards, and other forms of advertising which are situated in public spaces such as thoroughfares, sidewalks, and public transit systems. From an outlook of road safety, outdoor advertising contributes to visual pollution and can have a negative impact on the safety of drivers and pedestrians. Recent research of Abdullah and Sipos [4], Pečeliūnas *et al.* [5] and Čubranić-Dobrodolac *et al.* have focused on analyzing drivers' behavior and predicting the likelihood of traffic accidents using statistical models. Their research shows that the abundance of outdoor advertising has the potential to cause distraction and cognitive impairment, which can increase the risk of accidents. Therefore, it is important to consider the effect of outdoor advertising on road safety when designing and implementing an advertising campaign.

The term "visual pollution" was initially used by William H. Whyte in his 1980 publication *The Social Life of Small Urban Spaces* [7] to describe the adverse impacts of the visual environment on human perception. Outdoor advertising is a major contributor to this phenomenon, as it can be seen from a distance and often covers large public areas, making it difficult to ignore. The use of bright colors, shapes, and fonts in outdoor advertising can be overwhelming and distracting, thus disrupting the natural aesthetic of a landscape or urban skyline. The presence of outdoor advertising in elevated areas can lead to an increase in light pollution.

The presence of aesthetically displeasing objects and structures along transportation routes constitutes visual pollution in transportation. This includes, but is not limited to billboards and other forms of advertising, litter, derelict vehicles, and other signs of urban decline. Madlenak and Madlenakova [8] conducted a study on visual pollution in road infrastructure, highlighting the negative impact of excessive advertising and visual clutter. Toros [9] analyzed the issue of visual pollution caused by advertising signboards in Ankara, emphasizing the need for regulations and guidelines to manage outdoor advertising. Liu and Liu [10] conducted a positioning analysis of urban outdoor advertising and suggested the importance of location in maximizing the effectiveness of advertising. These studies provide insight into the impact of outdoor advertising on visual pollution and the need for regulations and strategic placement of ads. Visual pollution in transport can have deleterious consequences on the mental health and well-being of individuals and on the quality of life within a community. Mohamed *et al.* [11] studied the effects of visual pollution on the people of Saudi Arabia, highlighting its manifestations and negative consequences. Lopez and Custodio [12] discussed the legal framework for addressing "forgotten" pollution, including noise, smells, and visual impacts, in Mexico. Latypova *et al.* [13] conducted a study on visual garbage from a visual ecology perspective, providing insights into its impact on the environment. Moreover, visual pollution can be a source of distraction for drivers and could be a contributory factor to traffic accidents.

Visual pollution in transportation plays a detrimental role in the environment and people's ability to enjoy the area, as it is both distracting and an eyesore. Visual pollution has a negative impact on the environment and the enjoyment of public spaces. Allahyari *et al.* [14] evaluated visual pollution in urban squares using SWOT, AHP, and QSPM techniques. Chmielewski [15] proposed a 3D Isovist and Voxel approach for the assessment of visual impact of advertisement billboards, while Chmielewski [16] used tangential view landscape metrics to measure visual pollution. Chmielewski *et al.* [17] conducted intervisibility analysis and public surveys to measure the visual pollution caused by outdoor advertisements in urban streets. Such pollution can also reduce air quality, obstruct views, and distract drivers, thus leading to dangerous road conditions. Codato [18] discusses the troubled relationship between visual pollution and noise, highlighting the negative effects of these pollutants on the environment and society. Correa and Mejia [19] examine the impact of visual pollution on the population, emphasizing how it can reduce air quality and obstruct views. Madlenak and Hudak [12] focus on the visual pollution of road infrastructure in Slovakia and highlight the negative impact of visual pollution on drivers, leading to dangerous road conditions. The studies collectively suggest that visual pollution can lead to harmful consequences for both the environment and society. As argued by Rodrigue, Comtois, and Slack [21], reducing visual pollution in transport systems is crucial to promote a safe environment, enhance the aesthetic quality of the area, and prevent road accidents. It is imperative to prioritize strategies that reduce visual pollution in transport infrastructure. Rodrigue, Comtois, and Slack [22] describe that transport systems

are vital components of modern societies, consisting of networks of infrastructure and vehicles that enable the movement of people and goods between different locations. These systems encompass a wide range of modes (in city and rural condition), including roads, railways, waterways, airports, and various types of public transportation such as buses and taxis as it is described in Gaal, Horváth, Török, and Csete's article [23]. The efficient functioning of transport systems is crucial for economic development, social integration, and environmental sustainability. However, the negative impact of transport systems, such as visual pollution, noise pollution, and carbon emissions, cannot be overlooked.

Visual pollution is known to have detrimental effects on transport systems by reducing visibility, increasing the probability of accidents, and creating a hostile environment for pedestrians and cyclists. It can also result in a decrease in the aesthetic value of the surroundings, thus reducing the attractiveness of public transport and pedestrian-friendly modes of transport, and negatively affecting the tourism industry. Stoma *et al.* [24] have suggested that autonomous vehicles may provide a solution to the issue of visual pollution in transport by reducing the risk of accidents and potentially creating a more pleasing environment for pedestrians and cyclists. This development could lead to increased safety and improved quality of life for all commuters, which would result in a more efficient transportation system. In addition, visual pollution may obscure road signs, leading to confusion and further risks to safety.

Visual pollution can also increase noise levels, as it can reflect sound waves and amplify noise in the area. This can be especially problematic in urban areas, where noise pollution is already high. Additionally, visual pollution can reduce the amount of sunlight that is allowed to reach a given area, which can lead to decreased air circulation and higher temperatures, making it less comfortable for people to travel in the area.

Visual pollution can have diverse effects on the surrounding environment and the economy. Apart from its negative impact on the aesthetic and functional aspects of transportation, it may reduce property values, and in turn, influence businesses and individuals. Chuang *et al.* [25] revealed that visual pollution may decrease the value of a place and lower the effectiveness of advertising. Additionally, visual pollution may induce littering and various forms of environmental degradation, leading to the deterioration of the area's natural resources.

Visual pollution refers to the presence of intrusive or distracting visual stimuli in the environment, which can negatively affect individuals' well-being and cognitive processes. Tarkowski *et al.* [26] investigated the potential influence of driver distraction on the extension of reaction time. Through their research, the authors found that visual distractions, particularly those related to smartphones, can significantly increase drivers' reaction time. This increase in reaction time poses a higher risk of accidents, as delayed responses can lead to compromised driving performance and reduced overall safety. Salisu and Oyesiku [27] conducted a traffic

survey analysis in Nigeria to identify traffic patterns and inform road transport planning. Their study revealed that traffic congestion and inadequate infrastructure are major challenges that impede the efficient movement of people and goods in Nigeria. The presence of visual pollution, such as poorly designed road signage or excessive billboards, can contribute to traffic congestion by diverting drivers' attention and increasing cognitive load.

Ližbetin and Stopka [28] proposed a roundabout solution for a particular traffic operation to reduce congestion and increase safety. The study demonstrated that the implementation of a well-designed roundabout can effectively alleviate traffic delays and increase the capacity of the intersection. By reducing visual clutter, such as confusing signage or excessive road markings, drivers can navigate intersections more easily, enhancing their driving experience and minimizing the potential for accidents. Słomiński and Sobaszek [29] developed a dynamic autonomous identification and intelligent lighting system for moving objects with discomfort glare limitation. Their research aimed to minimize discomfort glare, which can occur when drivers are exposed to bright lights or reflections. The study showed that the implemented system effectively reduced discomfort glare while improving visibility of moving objects. By mitigating visual pollution caused by excessive or poorly directed lighting, drivers can maintain better focus and reaction time, contributing to safer driving conditions.

Wang *et al.* [30] investigated the effect of particulate iron on tracking indoor PM<sub>2.5</sub> of outdoor origin in a case study conducted in Nanjing, China. Their findings revealed that particulate iron can serve as an important tracer for indoor PM<sub>2.5</sub> originating from outdoor sources. This knowledge can inform indoor air quality management, allowing for the development of strategies to reduce visual pollution caused by outdoor particulate matter, which may obscure visibility and affect drivers' respiratory health. Rybicka *et al.* [31] applied an emission standard methodology to compare a specific railway line with parallel road transport. Their research demonstrated that railway transport emits fewer pollutants compared to road transport, suggesting that it can be an effective alternative for reducing emissions. By reducing the visual pollution associated with vehicle emissions, such as smog or exhaust fumes, railway transport can contribute to improved air quality and a more pleasant driving environment. Frej *et al.* [32] discussed the importance of alternative drive vehicles in road transport, specifically in Poland and the European Union. The authors highlighted the potential benefits of alternative drive vehicles, including reduced emissions and increased energy efficiency. Policy incentives were identified as crucial in promoting the adoption of these vehicles, which can contribute to a decrease in visual pollution caused by conventional vehicles, such as smoke or noise pollution.

In conclusion, the reviewed literature demonstrates that visual pollution can have significant implications for drivers. Factors such as distractions, traffic congestion, poorly designed infrastructure, discomfort glare, and vehicle emissions all contribute to visual pollution and can negatively impact driver performance, safety,

and overall driving experience. Strategies aimed at reducing visual pollution, such as improved road design, intelligent lighting systems, and the adoption of alternative drive vehicles, are essential for creating a safer and more sustainable transportation environment.

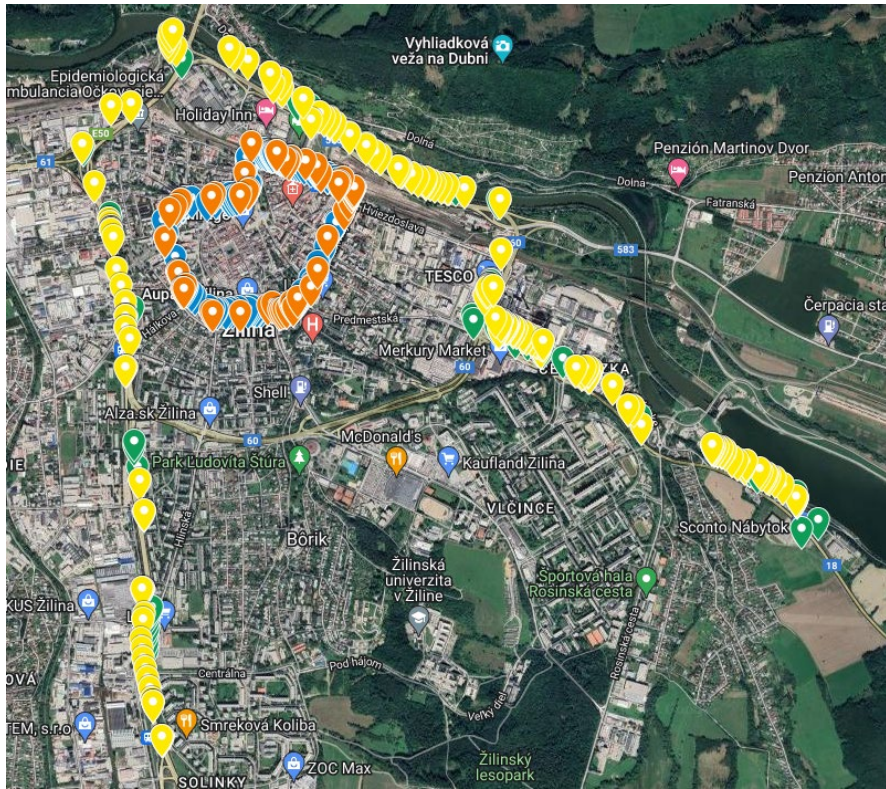
## 2 Methodology

The city of Žilina, located in Northern Slovakia, was chosen as the site for a comprehensive research project which aimed to assess the influence of visual smog on drivers in the city. Visual pollution, in the form of large-format outdoor advertising, was the primary focus of the study. To this end, two routes within the city limits of Žilina were selected for an empirical analysis. The study adopted a scientific approach, utilizing eye-tracking technology to measure the effects of visual smog on drivers. The results of the study are expected to provide valuable insights into the impact of visual pollution on drivers in Žilina, as well as in other cities with similar characteristics.

The individual routes and the advertisements that are placed on them are meticulously processed and registered in the developed Google Maps application (see Figure 1). This interactive mapping application serves as a comprehensive repository of all registered advertisements, including their geographic location, distribution, and other pertinent indicators. The collected data encompasses the proprietor of the advertising medium, the type of medium and the content of the advertisement. For large-scale advertising, the data recorded also includes the advertiser, the precise advertisement (e.g., logo, product, service) and a visual representation of the advertisement.

Following the analysis of visual pollution, the impact of outdoor advertising on car drivers was measured using HMI equipment - SMI's eye-tracking glasses. The same type of equipment was used in a study by Pavlenko and Shamanina [33] on eye tracking in the study of cognitive processes. This technology allowed for the quantification of the effects of outdoor advertising on car driver behavior as demonstrated in the study conducted by Bozomitu, Pășărică, Tărniceriu, and Rotariu [34] in the development of an eye tracking-based human-computer interface for real-time applications.

The SMI ETG 2W head-mounted eye-tracking glasses, in conjunction with the iViewETG version 2.8 software, were chosen as the primary tool for data acquisition. This specific device was designed to monitor the real-time visual behavior of subjects and capture relevant data. It consists of three high-speed cameras, two of which are infrared cameras utilized to track and record the movement and positioning of the subjects' pupils in both eyes.



Routes and outdoor advertising placement in selected routes in Zilina

The third camera is a high-definition scene camera with a resolution of  $1280 \times 960$  p @24 fps, capturing the surrounding environment. The use of this equipment has been previously employed by the authors [35] in a study on experimental testing of vehicle-driver interaction through eye-tracking technology in laboratory conditions.

Additionally, a notebook was connected to the glasses to facilitate data recording (see Fig. 2). The SMI ETG 2W is capable of providing a highly accurate and reliable eye tracking data set with a sampling frequency of 60 Hz that is extended throughout the entire field of view. This eye tracking system has been specifically designed to ensure a tracking range of  $80^\circ$  horizontal and  $60^\circ$  vertical with a gaze tracking accuracy that does not vary over distance, achieving an impressive  $0.5^\circ$  accuracy.

The SensoMotoric Instruments (SMI) BeGaze software version 3.7.59 was utilized for a comprehensive analysis of the data collected by the SMI ETG 2W.

The 11 drivers, composed of 6 females and 5 males aged between twenty-one and thirty-seven years, completed test drives across two measurement days. To ensure the accuracy of the research, five measurements were taken on Route 1 (the inner

circle – orange marks) and six measurements were taken on Route 2 (the bypass route – yellow marks). The test drives were conducted under various conditions, such as weather and traffic, to produce a comprehensive overview of the results. These conditions included clear, cloudy, and rainy weather, as well as both with and without traffic.



Figure 2

Measurement using an eye tracker in Zilina

### 3 Results

In the eye-tracking research, the primary objective was to evaluate the influence of visual smog on the attentional processes of motor vehicle drivers while driving. To do this, we analyzed a variety of physiological variables, including the number of fixations, saccades, and blinks as it was stated in study Przepiorka *et al.* [36]. This provided us with a comprehensive understanding of how cognitive processes are used by drivers while they are behind the wheel. Additionally, this study also sought to investigate the ability of drivers to notice an advertising area close to the road in order to discover the effects of visual smog on their attention as it was mentioned in the study Kainz *et al.* [37]. The term 'saccade', derived from the French verb for 'jerk', was used for the first time to describe eye movements by Javal in the 1880s. It is used to designate the rapid, conjugate (with both eyes performing the same action) movements we make when re-orienting our foveal region to a new spatial

location; the average rate of saccades is three per second. Saccades are normally identified as 'ballistic' movements, implying that the trajectory cannot be altered once initiated. Additionally, it is often asserted that during saccades, we become 'effectively blind'. Saccades, characterized by rapid eye movements, are commonly preceded and followed by fixations, which represent periods of relative stillness during which visual information is processed. The differentiation between fixations and saccades involves complex rules and algorithms employed by researchers and eye-tracking software (Feng *et al.* [38]; Hu *et al.* [39] and Xuguang & Jianping, [40]). The duration of fixations usually ranges from 200 to 300 milliseconds but can be either shorter or longer. Additionally, the average fixation duration is contingent upon the context in which it is observed; for example, fixations tend to be of shorter duration when reading than when viewing scenes. During the analysis stage, fixations are of particular interest to researchers, especially if gaze is being used as a proxy for 'attention'.

Blinks, although not actual movements of the eye itself, play a crucial role in effective eye tracking due to several reasons. One of these reasons, as mentioned in the study by Snegireva *et al.*, [41], is that gaze cannot be monitored if the eye is not visible. In their validity study utilizing eye tracking in male youth and adult athletes of selected contact sports, the authors found that blink duration is increased in concussed youth athletes. Blinks can disrupt fixations, leading to the appearance of two separate fixations within the same area in the eye-tracking data. Although this may not pose a significant issue in many scenarios, the length and position of the fixations are crucial factors to consider.

### 3.1 Route 1 – Inner Circle

Route 1 of the city of Žilina is an ideal choice to conduct analysis due to its location in the center of the city and its length of approximately 3,300 meters. The route is known to experience heavy traffic during peak hours, such as the morning and afternoon rush hours. Furthermore, three flat sections exist along the route, providing adequate visibility for drivers. Not only this, but there is no need to be vigilant of intersections without traffic signals as the route follows the main road. In total, seven traffic lights can be found along this route.

From the perspective of the driver, it is imperative to exercise heightened caution when traversing Route 1, due to the presence of various intersections, crossings, and bus stops that can significantly impede the flow of traffic. Moreover, the conditions of Route 1 vary according to the day of the week and time of day; thus, the driver must be prepared to adjust to the conditions accordingly. All in all, Route 1 serves as a potential driving route that requires one to be constantly adjusting to changing conditions.

The main thoroughfare of Route 1 boasts a total of one hundred and thirty-nine advertising displays that are visible to motorists. The strategic positioning of the

advertising carriers along this route is beneficial to both the proprietors of the carriers and the companies advertising their wares, as a significant number of cars, pedestrians and cyclists traverse the route on a daily basis.

Despite being located in a highly populated urban area, Route 1 has been found to have a significantly higher than average concentration of billboards and bigboards. This is especially evident when surveying strategic locations such as buildings and intersections, where drivers can more easily perceive the advertisements due to their conspicuous placement. As much as 20% of all the advertisements recorded in this area are in the form of billboards and bigboards.

Table 1  
Route 1 – Physiological characteristics of the drivers

	Number of fixations [per minute]	Number of saccades [per minute]	Number of blinks [per minute]	Drive durations [min.]
Driver 1	171	156	13	9:19
Driver 2	82	49	7	9:34
Driver 3	96	88	5	10:08
Driver 4	163	146	15	9:39
Driver 5	166	156	6	9:38
Average	135,6	119	9,2	9:40

Data in the table represents a comparison of driving characteristics between five different drivers on the route 1. Driver 1 has the highest number of fixations and saccadic movements, and the highest number of blinks per minute. Driver 2 has the lowest number of fixations and saccadic movements, and the lowest number of blinks per minute. Driver 3 and Driver 5 have similar numbers of fixations and saccadic movements, but Driver 5 has fewer blinks. Driver 4 has the second highest numbers of fixations and saccadic movements, and the second highest number of blinks. All five drivers have similar driving durations.

Conceptually, Driver 1 obtained the most beneficial outcomes. Nevertheless, it is essential to be aware that an excessive amount of fixations or saccades can induce feelings of anxiety or unease whilst driving. The average number of fixations per minute for the drivers that took part in the study was 135.6, with the average value of saccades being 119, equaling approximately two fixations and saccades for each driver per second.

### 3.2 Route 2 – Outer Bypass

Route 2 was the second route under consideration for analysis. The outer loop route was determined to be more advantageous as it provided longer and more even stretches of roadway, frequently with two lanes in each direction. Moreover, the route was composed of three extended straight stretches, which cumulatively accounted for approximately 80 % of the total length of the route.

From the driver's point of view, the number of pedestrian crossings and intersections is roughly the same. In comparison to Route 1, the driver is not required to pay as much attention while driving. On Route 2, the most important points are where the lanes diverge or converge into one. There are long stretches of flat road which give the driver the opportunity to drive in a more leisurely manner. The positioning of the billboards is strategically advantageous, and with only a few exceptions, they are clearly visible. Drivers who encounter billboards located on the opposite side of the road may, however, experience a slight decrease in visibility.

Analysis of Route 2 yielded the highest number of advertisements of the four routes studied, totaling up to 166. The majority of these advertisements were brand-related, with billboards and bigboards making up the second and third-most numerous categories, respectively.

Driver 1 has the highest number of fixations (183 per minute), the second highest number of saccadic movements (167 per minute) and the second lowest number of blinks (15 per minute). Driver 2 has the second lowest number of fixations (142 per minute), the second lowest number of saccadic movements (115 per minute) and the highest number of blinks (21 per minute). Driver 3 has the third highest number of fixations (150 per minute), the third highest number of saccadic movements (128 per minute) and the second highest number of blinks (21 per minute). Driver 4 has the second highest number of fixations (178 per minute), the fourth highest number of saccadic movements (155 per minute) and the third highest number of blinks (22 per minute). Driver 5 has the fourth highest number of fixations (159 per minute), the fifth highest number of saccadic movements (148 per minute) and the fourth highest number of blinks (23 per minute). Driver 6 has the lowest number of fixations (132 per minute), the lowest number of saccadic movements (109 per minute) and the second lowest number of blinks (18 per minute).

Table 2  
Route 2 – Physiological characteristics of the drivers

	Number of fixations [per minute]	Number of saccades [per minute]	Number of blinks [per minute]	Drive durations [min.]
Driver 1	183	167	15	19:47
Driver 2	142	115	21	26:48
Driver 3	150	128	21	23:55
Driver 4	178	155	22	21:52
Driver 5	159	148	23	21:19
Driver 6	132	109	18	21:42
Average	157,3	137	20	22:34

Driver 1 demonstrated the most noteworthy results on the subsequent course, yet this may be an indication of his uneasiness during the run. On average, the members of the driving group exhibited 157.3 fixations per minute and 137 saccadic movements. This yields to a greater mean of fixations and saccadic movements per second of the drivers during the course in comparison to route 1.

### 3.3 Visibility of Outdoor Advertising by Driver

The most essential information obtained from the measurement was the fixation of drivers' eyes on the external ads (see Fig. 3). An eye-tracker was utilized to assess gazes directed at large-format promotional surfaces located within the driver's visual range.



Figure 3

Driver fixation for large format advertising on Route 2

Table 3

Route 1 – Visibility of Outdoor ads formats by drivers

Route 1	Number of Outdoor ads	Outdoor ads seen	Ads seen to total ads ratio
Driver 1	25	3	12%
Driver 2	25	0	0%
Driver 3	25	2	8%
Driver 4	25	0	0%
Driver 5	25	1	4%

An aggregate of 25 large-format advertisements were evaluated on Route 1 and 137 on Route 2. Drivers on these two routes rarely focused their attention on the ads. Route 1 had only 6 fixations in total, equating to 5% of the total possible ad views (See Table 3). Route 2 was more compelling, with 108 fixations observed, making up 13% of the overall ad views (see Table 4).

The final stage of the research sought to ascertain whether drivers are consciously aware of visual smog (outdoor advertising) while driving. The objective was to determine whether drivers perceive outdoor advertising while driving.

Table 4  
Route 2 – Visibility of Outdoor ads formats by drivers

Route 2	Number of Outdoor ads	Outdoor ads seen	Ads seen to total ads ratio
Driver 1	137	24	18%
Driver 2	137	9	7%
Driver 3	137	7	5%
Driver 4	137	22	16%
Driver 5	137	26	19%
Driver 6	137	20	15%

Advertising spaces included billboards and bigboards, but also banners, tarpaulins and other signs located near the road. Out of the eleven participants in the survey, nine reported being aware of various forms of visual smog while driving, indicating that up to 82% of respondents are consciously aware of outdoor advertising (see Fig. 4).

This finding is in contrast with the results of the eye-tracking experiment, which demonstrated that out of 959 outdoor advertising spaces, only 114 (11.9%) were observed by drivers. This discrepancy between the conscious and subconscious perceptions of outdoor advertising spaces near the road is noteworthy. In this case, conscious perception is based on the responses from the questionnaire survey, while subconscious perception is inferred from the eye-tracking data.

It is important to note that the outcome of the experiment could be affected by the amount of traffic during the measurement, as well as by the general conditions of the road in question.

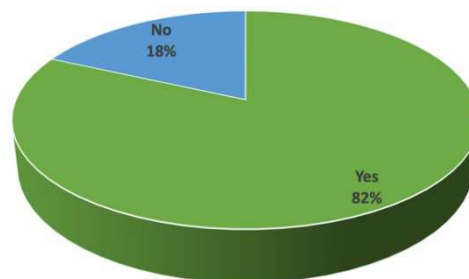


Figure 4  
Overall perception of outdoor advertising during the driving

The findings of this research have far-reaching implications for the effectiveness of outdoor advertising. It can be argued that the discrepancy between the conscious and subconscious perception of outdoor advertising spaces near the road could be due to the fact that drivers are often preoccupied with other tasks and may not be able to devote their full attention to outdoor advertising. Therefore, it is possible that outdoor advertising needs to be more eye-catching, or placed in more visible

locations, in order to be more effective. Additionally, further research should be conducted to determine whether the conscious perception of visual smog is affected by factors such as the driver's age or the type of vehicle being driven. By doing so, it may be possible to develop more effective strategies for targeting outdoor advertising.

### **Discussion**

The study aimed to investigate the influence of visual smog, specifically outdoor advertising, on the attentional processes of motor vehicle drivers, with a focus on the role of cognitive mobility. Cognitive Mobility is an inclusive approach that considers both artificial and natural cognitive features of the driver in understanding mobility comprehensively. In order to assess this influence, the researchers analyzed physiological variables such as fixations, saccades, and blinks to understand how drivers allocate their attention while driving.

To conduct the investigation, eye-tracking research was performed on two routes, Route 1 and Route 2, to examine the drivers' perception of outdoor advertising. Route 1, situated in the city center with heavy traffic and numerous intersections, exhibited a higher concentration of billboards and bigboards compared to Route 2, which offered longer and more evenly distributed stretches of roadway. Among all the drivers, drivers on Route 1 displayed the highest number of fixations, saccades, and blinks per minute, indicating heightened cognitive processing. It is worth noting that excessive fixations and saccades may induce feelings of anxiety or unease while driving. On Route 2, drivers exhibited a higher mean of fixations and saccades per second in comparison to Route 1. This route had a greater number of advertisements, and drivers demonstrated higher fixation rates on the ads compared to Route 1. The overall fixation rates on outdoor ads remained relatively low on both routes. Interestingly, a discrepancy emerged between conscious perception, as reported by respondents, and subconscious perception, as indicated by eye-tracking data, of outdoor advertising. While 82% of the respondents reported being aware of visual smog, the eye-tracking experiment revealed that only 11.9% of outdoor advertising spaces were observed by drivers. This finding suggests that drivers may not fully attend to outdoor advertising due to the presence of other tasks and distractions while driving.

The results imply that outdoor advertising may need to be more eye-catching or positioned in more visible locations to be effective. It is crucial to consider factors such as driver age and vehicle type in understanding the conscious perception of visual smog. Based on the results of this study, there is a need to develop basic recommendations for decision-makers on the placement of advertisements with a focus on ensuring the safety of both drivers and pedestrians on the roads, which will be the subject of our further research. Additionally, future research should delve into these factors and develop more effective strategies for targeting outdoor advertising.

## Conclusions

In conclusion, this study highlights the ineffectiveness of placing outdoor advertising, also known as visual smog, in downtown areas for targeting motorists. Empirical evidence indicates that these advertisements have an insignificant impact on their target audience, providing a rational basis for advertising agencies to reconsider the practice of creating large-scale visual smog in densely populated urban areas. Moreover, the findings suggest that outdoor advertising does not significantly influence the decision making process of drivers. Therefore, it is crucial to consider the concept of cognitive mobility, which emphasizes the importance of drivers' cognitive capabilities in response to changing environmental and situational factors. Understanding and integrating cognitive mobility into the design and implementation of outdoor advertising campaigns can lead to more effective and impactful strategies in targeting drivers.

## Acknowledgement

This publication was created as a part of research project: The Operational Program Integrated Infrastructure 2014–2020 for the project: Innovative solutions for propulsion, energy, and safety components of means of transport, with ITMS project code 313011V334, co-financed from the resources of the European Regional Development Fund.

## References

- [1] Zoldy M., Baranyi P. Definition, Background and Research Perspectives Behind ‘The Cognitive Mobility Concept, *Infocommunications Journal*, Special Issue: Internet of Digital & Cognitive realities, 2023, pp. 35-40, <https://doi.org/10.36244/ICJ.2023.SI-IODCR.6>
- [2] Zoldy M., Baranyi P. Cognitive Mobility–CogMob. In 12<sup>th</sup> IEEE International Conference on Cognitive Infocommunications (CogInfoCom 2021) Proceedings IEEE, 2021, pp. 921-925
- [3] Zoldy M., Szalmane Csete M., Kolozsi P. P., Bordas P., and Torok A. “Cognitive Sustainability”. 2022. *Cognitive Sustainability*, Vol. 1, No. 1, Dec. 2022, doi:10.55343/cogsust.7
- [4] Abdullah P., Sipos T. Drivers’ Behavior and Traffic Accident Analysis Using Decision Tree Method. *Sustainability* 2022; 14(18)
- [5] Pečeliūnas R., Žuraulis V., Drożdziel P., Pukalskas S. Prediction of road accident risk for vehicle fleet based on statistically processed tire wear model. *Promet Traffic Traffico* 2022;34(4):619-630
- [6] Čubranić-Dobrodolac M., Švadlenka L., Čičević S., Dobrodolac M. Modelling driver propensity for traffic accidents: a comparison of multiple regression analysis and fuzzy approach. *Int J Injury Cont Saf Promot* 2020; 27(2):156-167

- [7] Whyte W.H. *The Social Life of Small Urban Spaces*. 8th ed. Project for Public Spaces; New York, NY: 1980
- [8] Madlenak R., Madlenakova L. *Visual pollution of the road infrastructure*. 1st ed. EDIS; Žilina: 2022
- [9] Toros S. *Visual Pollution in Ankara: An Analysis on Advertising Signboards*. *Türkiye İletişim Araştırmaları Dergisi - Turkish review of communication studies*. 2021; pp. 242-260, <https://doi.org/10.17829/turcom.934456>
- [10] Liu B., Liu F. *Positioning Analysis of Urban Outdoor Advertising*. In: Yue X, McAleer M, eds. *Northeast Normal University - China. International Conference on Economics and Management Innovations (ICEMI 2017)*, Vol. (1) Issue (1) 2017; pp. 415-416, <https://doi.org/10.26480/icemi.01.2017.415.416>
- [11] Mohamed M., Ibrahim A., Dodo Y., Bashir F. *Visual pollution manifestations negative impacts on the people of Saudi Arabia*. *International Journal of Advanced and Applied Sciences*. 2021;8:94-101, <https://doi.org/10.21833/ijaas.2021.09.013>
- [12] Lopez T., Custodio M. *Noise, Smells, And Visual Impacts: A Flimsy Legal Framework For "Forgotten" Pollution In Mexico*. *Actualidad Juridica Ambiental*. 2022; pp. 39-57
- [13] Latypova A., Lenkevich A., Kolesnikova D., Ocheretyany K. *Study of Visual Garbage as Visual Ecology Perspective*. *Galactica Media-Journal of Media Studies - Galaktika Media-Zhurnal Media ISSLEDOVANIJ*. 2022;4:153-172, <https://doi.org/10.46539/gmd.v4i2.283>
- [14] Allahyari H., Nasehi S., Salehi E., Zebardast L. *Evaluation of visual pollution in urban squares, using SWOT, AHP, and QSPM techniques (Case study: Tehran squares of Enghelab and Vanak)*. *Pollution*. 2017;3:655-667, <https://doi.org/10.22059/poll.2017.62780>
- [15] Chmielewski S. *Towards Managing Visual Pollution: A 3D Isovist and Voxel Approach to Advertisement Billboard Visual Impact Assessment*. *International Journal of Geo-Information*. 2021;10, <https://doi.org/10.3390/ijgi10100656>
- [16] Chmielewski S. *Chaos in Motion: Measuring Visual Pollution with Tangential View Landscape Metrics*. *LAND*. 2020;9, <https://doi.org/10.3390/land9120515>
- [17] Chmielewski S., Lee D., Tompalski P., Chmielewski T., Wezyk P. *Measuring visual pollution by outdoor advertisements in an urban street using intervisibility analysis and public surveys*. *International Journal of Geographical Information Science*. 2016; 30:801-818, <https://doi.org/10.1080/13658816.2015.1104316>

- [18] Codato M. Visual pollution and noise: A troubled relationship between environment and society. *Revista Eletronica em Gestao Educacao e Tecnologia Ambiental*. 2014; 18:1312-1317, <https://doi.org/10.5902/2236117014516>
- [19] Correa V., Mejia A. Visual Pollution Indicators and its Effects on Population. *ENFOQUE UTE*. 2015;6:115-132
- [20] Madlenak, R., Hudak, M. The Research of Visual Pollution of Road Infrastructure in Slovakia. In: Mikulski J, ed. *University of Zilina. Challenge of transport telematics, TST 2016*. 2016; 415-425, [https://doi.org/10.1007/978-3-319-49646-7\\_35](https://doi.org/10.1007/978-3-319-49646-7_35)
- [21] Flad H. Country clutter: Visual pollution and the rural roadscape. *Annals of the American Academy of Political and Social Science*. 1997; 553:117-129
- [22] Rodrigue J.-P., Comtois C., Slack B. *The Geography of Transport Systems*. 2<sup>nd</sup> ed. Routledge; London; New York: 2009
- [23] Gaal G., Horvath E., Torok A., Csete M. Analysis of public transport performance in Budapest, Hungary. *Period Polytech Soc Manage Sci* 2015; 23(1):68-7
- [24] Stoma M., Dudziak A., Caban J., Drożdziel P. The future of autonomous vehicles in the opinion of automotive market users. *Energies* 2021;14(16)
- [25] Chuang MH., Chen CL., Ma JP. Eye tracking analysis of readers' psychological interaction with marketing copy referencing life values. *Commun Comput Info Sci* 2015; 528:87-92, [https://doi.org/10.1007/978-3-319-21380-4\\_16](https://doi.org/10.1007/978-3-319-21380-4_16)
- [26] Tarkowski S., Caban J., Dzienkowski M., Nieoczym A., Zarajczyk J. Driver's distraction and its potential influence on the extension of reaction time. *The Archives of Automotive Engineering – Archiwum Motoryzacji*, 2022, 98(4), 65-78, <https://doi.org/10.14669/AM/157645>
- [27] Salisu U.O., Oyesiku O.O. Traffic Survey Analysis: Implications for Road Transport Planning in Nigeria. *LOGI – Scientific Journal on Transport and Logistics*, 2020, 11(2), 12-22, <https://doi.org/10.2478/logi-2020-0011>
- [28] Lizbetin J., Stopka O. Proposal of a Roundabout Solution within a Particular Traffic Operation. *Open Engineering*, 2016, 6(1), 441-445, <https://doi.org/10.1515/eng-2016-0066>
- [29] Slominski S., Sobaszek M. Dynamic autonomous identification and intelligent lighting of moving objects with discomfort glare limitation. *Energies*, 2021, 14(21) <https://doi.org/10.3390/en14217243>
- [30] Wang Z., Liu C., Hua Q., Zheng X., Ji W., Zhang X. Effect of particulate iron on tracking indoor PM<sub>2.5</sub> of outdoor origin: A case study in Nanjing, China. *Indoor and Built Environment*, 2020, 30(5), 711-723, <https://doi.org/10.1177/1420326X19899145>

- [31] Rybicka I., Stopka O., Luptak V., Chovancova M., Drozdziel P. Application of the methodology related to the emission standard to specific railway line in comparison with parallel road transport: A case study. In: MATEC Web of Conferences, Vol. 244, 3<sup>rd</sup> Innovative Technologies in Engineering Production, ITEP 2018, Bojnice, Slovakia, 11-13 September 2018, Code 143364, <https://doi.org/10.1051/mateconf/201824403002>
- [32] Frej D., Grabski P., Szumska E. M. The Importance of Alternative Drive Vehicles in Road Transport in Poland and the European Union. *LOGI – Scientific Journal on Transport and Logistics*, 2021, 12(1), 67-77, <https://doi.org/10.2478/logi-2021-0007>
- [33] Pavlenko V., Shamanina T. Eye Tracking in the Study of Cognitive Processes. *CEUR Workshop Proceedings*; 2022, Volume 3171, pp. 1617-1628
- [34] Bozomitu R. G., Pasarica A., Tarniceriu D., Rotariu C. Development of an eye tracking-based human-computer interface for real-time applications. *Sensors* 2019;19(16), <https://doi.org/10.3390/s19163630>
- [35] Madlenak R., Benus J., Madlenakova L. Experimental Testing of the Vehicle-driver Interaction by Eye-tracking Technology in Laboratory Conditions. *Transport Means - Proceedings of the International Conference*; 2021, pp. 359-364
- [36] Przepiorka A. M., Hill T., Blachnio A. P., Sullman M. J. M., Taylor J. E., Mamcarz P. Psychometric properties of the Driving Behaviour Scale (DBS) among Polish drivers. *Transp Res Part F Traffic Psychol Behav* 2020; 73:29-37, <https://doi.org/10.1016/j.trf.2020.06.008>
- [37] Kainz O., Gera M., Petija R., Michalo M., Cymbalak D., Jakab F., Vapenik R. Enhancing Attention through the Eye Tracking. *ICETA 2020 - 18th IEEE International Conference on Emerging eLearning Technologies and Applications, Proceedings*; 2020, pp. 266-271, <https://doi.org/10.1109/ICETA51985.2020.9379229>
- [38] Feng T., Zhao Z., Tian X. Drivers' Visual Characteristics of Urban Expressway Based on Eye Tracker. *Lect Notes Electr Eng* 2023; 944:325-339, [https://doi.org/10.1007/978-981-19-5615-7\\_23](https://doi.org/10.1007/978-981-19-5615-7_23)
- [39] Hu H., Cheng M., Gao F., Sheng Y., Zheng R. Driver's preview modeling based on visual characteristics through actual vehicle tests. *Sensors* 2020;20(21):1-23, <https://doi.org/10.3390/s20216237>
- [40] Xuguang Z., Jianping G. Research on the fixation transition behavior of drivers on expressway in foggy environment. *Saf Sci* 2019;119:70-75, <https://doi.org/10.1016/j.ssci.2018.08.020>
- [41] Snegireva N., Derman W., Patricios J., Welman K. Blink duration is increased in concussed youth athletes: A validity study using eye tracking in male youth and adult athletes of selected contact sports. *Physiol Meas* 2022;43(7) <https://doi.org/10.1088/1361-6579/ac799b>

# Energy Condition of Gear Shifting under Load in Commercial Vehicles

**Attila Szegedi**

Department for Vehicle and Agriculture Machines, University of Nyíregyháza, Kótaji út 9-11, 4400 Nyíregyháza, Hungary; szegedi.attila@nye.hu

**Imre Zsombok**

Department Automotive Technologies, Budapest University of Technology and Economics (BME), Stoczek utca 6, 1111 Budapest, Hungary, imre.zsombok@auto.bme.hu

---

*Abstract: In the fight against global warming, all increase in energy efficiency contributes to reaching the target numbers. This is especially true for agriculture, where a huge number of large vehicles work. Currently, used modern tractors are equipped with powershift transmissions, which allow for shifting underload. In the case of tractors, owing to the large traction force and low speed of tractors, kinetic energy loss during shifting is high, which reduces efficiency. The traction test presented here aimed to analyse the shifting process of a tractor from an energetic perspective. It was a challenging task to select the appropriate measuring devices and to create a measurement system for this purpose, due to the extremely short (0.3-0.5 s) shifting time. In order to be able to analyse the parameter changes and the cause-and-effect relationships between speed and engine revolution, and between traction force and slip in the shifting process. Two scenarios were examined: fixed speed and fixed traction force. Data characterizing shifting while high traction force is exerted was analysed by methods of mathematical statistics. The unit changes of traction force and slip and the required time were analysed. Traction force increased after shifting (+ 5 kN), which indicates that extra traction force is needed to make up for speed lost during shifting, and because of which slip is considerably increased, typically by more than 10%. After shifting, traction force vacillates at a frequency around 2 Hz, similarly to the vacillation of engine revolution. When changing down, the process starts with a decrease in slip. After almost 0.15 s, traction force plummets by 15 kN at the beginning of shifting. At the same time, slip also decreases, for a short time it can also exhibit negative values. The analysis proved that slip continuously causes considerable losses to various degrees during shifting. In order to minimize these losses, recommendations are given both for driving technique and for the parameter settings of the controlling software.*

*Keywords: transmission; gear shifting; agricultural vehicles*

---

# 1 Introduction

Efficient energy consumption is a crucial factor in the development and operation of agricultural engines. According to studies, the correct specification of fuels can influence the fuel consumption and emission of commercial vehicles [1]. However, irrespective of the applied fuel mixture, the aim is to maximize the efficiency of energy conversion in the powertrain [2].

Furthermore, the need is growing to improve the utilization rate, the energy consumption [3] and the compliance to environmental expectations of tractors. Consequently, besides the constant development of engines and the addition of various biofuels [4], it is also a requirement to increase the energy-efficiency of tractor powertrains. Efficiency and emission are interconnected: other publications surveyed the air pollutant emission of agricultural engines [5]. They proved that the optimal load of the engine exercises a significant effect on decreasing the particle matter (PM) emission of diesel engines (smoke value) [6]. In the case of agricultural heavy-duty vehicles, the optimal load can be achieved by ensuring optimal transmission. Battery electricity is under research as well as energy provider for agriculture, but it has several barriers [7].

During the operation of a tractor, the choice of the setup of the power-shift gear and the actual transmission rate (both for automatic and manual transmission) influence engine load. As a result, during development and operation, the powertrain of tractors must be examined as one system from the engine to the soil. Results in the field of energetics and operation can only be reached if the modifications and developments of the various elements of the transmission system are coordinated. This development direction follows one of the major trends of the mobility: i.e. the increasing artificial and human cognitive level [8]. A design method for a new power-cycling hydro-mechanical continuously variable transmission (PCHMCVT) system is proposed to solve it [9].

After the creation of powershift and continuously variable transmissions (CVT), the aim was to create the simplest possible transmission technologies while keeping the possibility of shifting underload [10]. While earlier the main goals of development were optimizing the utilization of engine power and the enhancement of driver comfort, today the major aim is to minimize power loss. After examining the characteristics of tractor CVT systems through precise simulations, it was proved that tractor CVT systems can be used in a wider range of fields, and they ensure the lowest specific fuel consumption owing to the optimal load of the engine [11]. A deeper analysis [12] proved that for the power-split infinitely variable transmission (IVT) systems applied in tractors, the best power transmission efficiency ( $\eta = 0.90\text{--}0.94$ ) is witnessed if the infinitely variable member's transmission is in the range of  $i = 0.85\text{--}2.4$ . The structural build-up of mass-produced power-shift CVT systems and the relevant transmission ranges were compared in mass-produced tractors [13]. The power dissipation was explored by

preliminary calculations and real-life tests, which gave important information for the evaluation of power loss of different constructions.

Although hydrostatic transmission offers the best regulation possibilities for vehicles moving in the fields, its efficiency is lower than that of mechanical transmission [14, 15]. Therefore, hydrostatic transmission is primarily used in slow harvesters or as the IVT member of power-split powershift systems in agricultural engineering. In a study on power dissipation of tractors [16], it was revealed that especially at higher speed, significant power loss is due to the viscosity of the lubricant and the operation of the transmission's own hydraulic system, besides the friction of the parts of the mechanical transmission system. It is also mentioned that even the unloaded powershift transmission's own hydraulic system increases the frictional and inertial resistance, which are altogether responsible for 52% of losses in the powertrain. Furthermore, 40% of losses arise from oil splashes and the dynamic viscosity of the oil. According to the results of powershift transmission tests, a 10% decrease in the amount of oil in the system resulted in a 13% decrease in frictional resistance. Indirect tests showed that more than half of the losses in the hydraulic system arose in the final reduction and the resistance in the brake plates that are submerged in oil.

For the operation and control of clutches, it is important to know the processes present in the operating system. Model calculations based on simulations [17] proved that during the optimization of the control of pneumatic clutches, pneumatic control might result in a 100 ms delay. They examined the release and the closure of the pneumatic clutch in several scenarios (e.g. dynamic acceleration, normal operation), taking into consideration the operation of the control valve and the filling and emptying of the operating cylinders.

Research [18] presents results on agricultural vehicle tractive performance on an asphalt road. Under typical working circumstances, the tractor tractive efficiency depends on its rolling efficiency when the tractive force is smaller, and depends on its slip efficiency when the tractive force is larger. As the variation range of slip coefficient turns to be minor, and the variation trend of slip coefficient becomes understandable when the gearbox of the tractor is switched from low gear to high.

Considerable losses emerge at the soil–wheel interaction as well [19]. During their survey of rolling resistance, special emphasis was given to the determination of work necessary for the deformation of the soil [20].

When analysing the shifting processes, it is important to determine the kinetic energy losses of the machine group, as it influences the quality of work through the lowering of work speed. Earlier studies [21, 22] revealed that the machine group that had slowed down during gear shifting, had to be accelerated again, which increased unit energy consumption. In order to increase shifting comfort and to optimize performance transmission during gear shifting, a number of new criteria and solutions have arisen in the design of transmissions [23, 24]. It was proven [25] that the actual speed of the tractor must be taken into consideration for the

programming of the shift duration to ensure the continuity of performance transmission during shifting.

Besides classic field tests for agricultural heavy-duty vehicles and models and simulations, road acceleration tests also emerged [26]. By applying different constructions of power-shift transmissions, the traction performance of tractors was determined [27] in public road traction tests. They also determined the efficiency of the powertrain and the losses due to running resistances with the help of engine mapping curves. One of the three tractors examined had a powershift transmission, while the other two were equipped with CVT powershift transmissions, and their performance was comparable. The best efficiency was 85%, achieved by one of the CVT transmissions, while the other two types produced 64 and 65%.

The changes in the torque characteristics of powershift transmissions of tractors were examined in detail [28], especially concerning the soil-dependent periodicity of the motor torque load, which influences the tractor wheel slip. With the slip growing, the shifting process is accompanied by the kinetic energy loss of the tractor+trailer combination, i.e. by a decrease in work speed. To eliminate this loss, if the engine's revolution gets out of the sensitivity range, the resulting torque change might result in shifting. It is only possible to fulfil this requirement if the total inertia torque is minimally decreased, i.e. during a partial torque transmission it is advisable to change the transmission rate, i.e. to shift gears. A detailed model and simulation of partial power shift transmission is presented as well [29]. During the research it was observed that the engine load and fuel consumption were directly proportional to the engine load levels. However, it was statistically proved that there was no significant difference between the simulation and measured engine torque and fuel consumption at each load level.

The present study describes a series of field measurements conducted on a tractor+trailer combination with respect to the changes of traction and energetic characteristics during shifting and explores the connections between the influencing factors. The above references proved that for slow energy-consuming processes with high traction power, the traditional choosing of optimal work speed can only rarely be achieved. When the machine group slows down during gear shifting, the arising energy loss must be compensated for, which increases the unit energy need of the work process. This study explores how much energy loss arises in the case of powershift transmissions which can be operated underload. The hydraulic control of the transmission of the examined current tractor works with constant durations, and constant pre-calibrated cross-section through a pulse-width modulation (PWM) directional control valve (DCV). The aim of the research is to explore how optimal these parameters are while changing the traction force load and the work speed. The present article discusses the field traction tests of tractors, including the measurement techniques, the test results and their analysis.



20-25%, while soil cohesion was medium. One month after cultivation, the soil compaction was also medium. The examined area is utilized as a plough land, it is plain, and the length of the measurement was more than 500 meters, which is ideal from the testing perspective.

## 2.1 Tractor Characteristics

A CLAAS ARION 420 tractor was used in the experiment. It had a powershift transmission system with 16 gears, with 4 power shift gears (1–2–3–4) in 4 power shift ranges (A–B–C–D). Shifting between ranges (A–B–C–D) is only possible when unloaded, while gear shifting (1–2–3–4) is possible when loaded. The traction force of the tested tractor running in the field ranged from 10 to 25 kN in the 5 to 18 km/h speed range.

The major technical parameters of the tested tractor are given in Table 1.

Table 1  
Technical specifications of CLAAS Arion 420

Name	Data
Type	CLAAS ARION 420 DPS
Vehicle identification number (VIN)	A2114DA/12103714 LZZ009
Year of production	2015
Engine identification number (EIN)	CD4045L216148
Displacement	4525 cm <sup>3</sup>
Producer	John Deere
Performance	88 kW/2200 f/min
Weight	4900 kg
Back tires	520/70 R38

## 2.2 Trailer Characteristics

In order to determine the traction characteristics of the tractor, a special brake cart developed by NAIK-MGI was used, in which different load parameters could be set. A similar attachment was used by the Italian CREA-ING laboratory in 2015 [32]. The data characterizing the tractor–brake cart group were determined by force measurements (see Figure 2). The measurement system depicted in Figure 2 was operated, and the data was collected by the data collector computer installed into the brake cart. The major characteristics of the brake cart are given in Table 2.

Table 2  
Technical specifications of the A–MAZ brake cart

Technical parameter	Value
Engine performance	400 kW
Braking/traction performance	250 kW
Maximal braking/traction force	150 kN
Operational speed range	0–35 km/h

During field tests, the change in the adhesive force is modelled by extra loading of the brake cart. The regulating algorithm offers two possibilities (freely chosen by the operator):

- (i) measurements at constant speed (regulated for speed);
- (ii) measurements at constant traction force (regulated for traction force).

The connection of the brake cart and the build-up of the measurement system are shown in Figure 2. Traction force was measured by a strain gauge inside the towing bar, which sent the data to the data collector system.

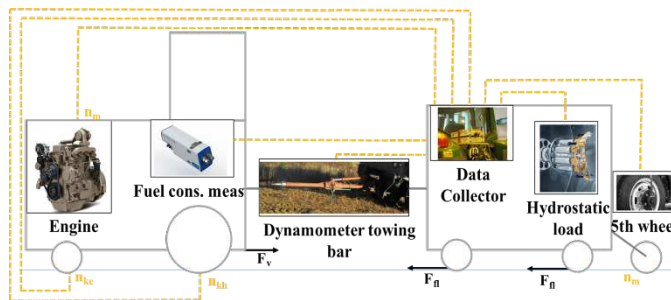


Figure 2  
Sketch of the measurement system

The following traction characteristics were recorded by the measurement system shown in Figure 2. The peripheral speed  $v_k$  [m/s] of the tractor's driven wheel can be calculated from the revolution  $n_k$  measured by the revolution meter in the wheel, and the rolling radius  $r_g$  (1).

$$v_k = 2 \cdot \pi \cdot r_g \cdot \frac{n_k}{60} \quad v_k = 2 \cdot \pi \cdot r_g \cdot \frac{n_k}{60} \quad (1)$$

There is always some slip between the wheel and the soil for vehicles moving in the field, which is reflected by the quantity slip ( $s$ ). Therefore, the actual speed of the machine group had to be measured. The actual speed was measured by a fifth wheel measuring system attached to the trailer. This calculates the actual speed  $v_H$  from the rolling radius and the revolution of the fifth wheel, in a similar manner to (1).

Slip percentage is calculated from the difference between these two speeds with equation (2).

$$s = \frac{V_k - V_H}{V_k} \cdot 100 \quad (2)$$

where  $s$  is slip,  $v_k$  is the peripheral speed of the driven wheel, and  $v_H$  is the actual speed.

The revolution of the tractor was measured indirectly by an impulse signal transmitter mounted on the PTO of the tractor. The revolution could be calculated from the fixed transmission rates.

Fuel consumption was recorded by an AVL PLU flow meter with a limit of measurement of 600 l/h, which was mounted on the braking attachment, but was inserted into the fuel system of the tractor. In order to determine fuel consumption precisely, measurement cycle times must be set. The difference between the measured flow in the forward and backward going branches of the system gives the quantity of consumed fuel in a unit of time. The accuracy of the fuel consumption meter, which is equipped with a temperature compensator, is  $\pm 1\%$ . The measured data was forwarded to the central data collector on the brake cart.

### 2.3 Data Processing

The signals transmitted by the different signal transmitters were received by a 16-channel measurer and data collector system (SPIDER Mobil). Sampling density was 10 Hz. The collected data were recorded by the CATMAN software, without preliminary filtering. The data were depicted in a chart that conformed to the sampling density, where data lines followed each other at 0.1 second resolution.

From the measurement data, correlation calculations were done by methods of mathematical statistics; while the mean value of dispersed data ( $x_i$ ) was determined automatically by the applied software.

Based on the mean values and the values of standard deviation the dataset was corrected: outliers were eliminated. With this method, the standard deviation of the mean value was reduced. In a second round of calculations, the mean value and the standard deviation was determined again, for the dataset without the outliers. The new values were used for further calculations. Thus, the filtered database represented the measured data properly, with a uniform standard deviation.

During the experiment, the number of test runs for each type of measurement was determined in the following way. If the variance of the population is unknown, the required sample size can be calculated by Chebyshev's inequality (3).

$$P\left(\bar{x} - k \cdot \frac{\sigma}{\sqrt{n}} < \mu < \bar{x} + k \cdot \frac{\sigma}{\sqrt{n}}\right) \geq 1 - \alpha \quad (3)$$

In the case of simple random choice, the formula in (3) is simplified to (4).

$$P(\bar{x} - \Delta < M(x) < \bar{x} + \Delta) = 1 - \alpha \quad (4)$$

If equation (4) is rearranged, the required sample size arises (5):

$$n = \frac{t^2 \cdot s_k^2}{\Delta^2} \quad (5)$$

where

n – required sample size;

t – probability constant;

s<sub>k</sub> – corrected empirical standard deviation;

Δ – accuracy range.

With the help of equation (5), the number of tests can be analyzed from the perspective of the proper range of standard deviation (i.e., accuracy range). The acceptable accuracy range for a given parameter at a given point at a given setup was determined based on the literature. In order to ensure uniform conditions and to minimize the number of influencing factors, the following measures were taken.

A test site with relatively homogenous surface and structure was selected within the larger test area (as far as this is possible in a ploughland). Test runs were repeated so that a new run would start on unaffected, untrodden ‘virgin’ soil.

Tests were carried out with the tractor’s accelerator being fixed.

At the first round of the tests, the brake cart was set to fixed speed mode (in order to keep the pre-set speed, traction force was modified). In the second round, traction force was fixed. We have no knowledge of other device that could ensure uniform traction force more accurately than this device.

More than 10 seconds were left between shifting gears so that the regulatory cycle of the braking cart could stabilize traction. Therefore, the following shifting took place from this balanced state.

A test cycle lasted for 350 s, i.e. owing to the 10 Hz sampling density, for each parameter 3500 pieces of data were produced. The following five parameters were tested: (i) TLT revolution; (ii) wheel speed; (iii) actual speed; (iv) fuel consumption per hour; (v) actual traction force. Two other operational values were calculated from the measured data: (vi) slip from the wheel speed (ii) and the actual speed (iii); and (vii) peripheral speed of the tractor’s driven wheel calculated from the

revolution (i) and the rolling radius. The five measured parameters (i)–(v) and the two calculated ones (vi)–(vii) amount to 24,500 pieces of data per test run.

As an illustration, the result data for the 3<sup>rd</sup> gear are given in Table 3.

Table 3  
Planned and actual number of measurements

		sexp.	scal.	t	$\Delta$	n [pc.]
Traction force	kN	0.5	0.45	1.96	0.05	312
Slip	%	0.2	0.14	1.96	0.05	30
Shifting duration	s	0.04	0.035	1.96	0.05	2
Fuel consumption	g/kWh	2	1.5	1.96	0.05	3500

$s_{exp}$  – experienced corrected empirical standard deviation;

$s_{calc}$  – calculated corrected empirical standard deviation;

t – probability constant;

$\Delta$  – accuracy range;

n – required sample size;

## 2.4 Measurement Process

The traction test was carried out in two scenarios: the brake cart was either in the fixed speed or in the fixed traction force mode of operation.

1) Fixed traction force Traction force was set to 30 kN on the brake cart. The accelerator was also fixed at the maximum position. The traction test started in gear B1. When the traction force was stabilized and traction became steady, the driver shifted to B2, then to B3, and finally to B4. In the second phase of this test, the driver changed down: B4–B3–B2–B1. The time between gear changes during which the traction force stabilized was 50 s. Data necessary for the distribution of the traction force during shifting was measured while changing up or down. Data were recorded by the measurer-collector system.

2) Fixed speed Speed was set to 1.4 m/s (5 km/h), with the accelerator being at the maximum position. Again, the traction test started in gear B1. After stabilization, the driver shifted to B2, then to B3, and finally to B4. In the second phase of this test, the driver changed down: B4–B3–B2–B1. Data were recorded at each shifting.

In one test cycle (changing up four gears and changing down four gears), approximately 50,000 pieces of data were recorded. Owing to the test circumstances (in a ploughland) and the high sensitivity of the measuring devices, the standard deviation of traction force and slip values were considerably high, with several outliers.

During processing, data series were cut up into sections. For the sections corresponding to steady traction phases, in the preprocessing phase methods of mathematical statistics were applied. Data that differed from the mean of the given section by more than  $\pm 5\%$  were replaced by the mean of the neighbouring 5-5 pieces of data (i.e., the average of 10 pieces of data). In order to analyze the shifting phases, the raw data series was analyzed to be able to follow the changes accurately.

An exact methodology had to be created to determine the limits of each section from the data series. In all cases, the need for traction force grew after shifting. Then, after the machine group accelerated back and the brake cart automatically regulated the speed, traction force started to approach the previous value. The starting point of a stable traction section was defined as the second when the actual traction force first gets under the pre-set value. The endpoint of the stable section was defined as the starting point of shifting.

### 3 Test Results

The frequent sampling during the tests allowed for the analysis of the transmission of the traction force during shifting. The changes in slip and traction force could be depicted. The high standard deviation of the data was due to the measurement circumstances, but trends could be detected and analysed.

Measured data were analysed in two phases. At first, characteristics of the stable traction phases were described. Secondly, the dynamic changes occurring during shifting were compared.

#### 3.1 Fixed Speed Scenario

Data recorded by the braking cart in the fixed speed scenario prove that traction parameters could be stabilized the fastest in the B3 gear. The traction force and slip values recorded during the test are shown in Figure 3.

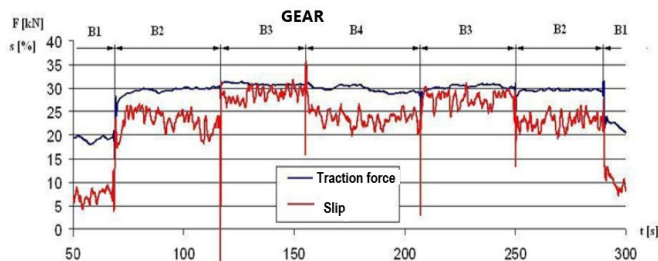


Figure 3

Changes of traction force and slip during shifting when loaded, fixed speed scenario

During the traction test, the value of the traction force could be kept in the range 25-30 kN, with the exception of the B1 gear. In the different gears, when traction force was stabilized, the standard deviation considerably diminished. Slip changes reflect the changes of the traction force, but with a different standard deviation. The speed was kept at the pre-set 5 km/h by the PLC in the brake cart. The standard deviation (SD) test proved that SD was the highest in the case of slip, out of all the parameters.

Table 3

Mean values of traction parameters and the corresponding standard deviation in the fixed speed scenario

Shiftin g	$\Delta s$ [%/s ]	$\Delta F$ [kN/s]	$t_k$ [s]	$t_0$ [s]
B1-2	38	26.8	0.15	0.6
B2-3	185	15.2	0.15	0.5
B3-4	80	29.3	0.15	0.4
B4-3	115	22.5	0.15	0.5
B3-2	23	7.5	0.15	0.6
B2-1	1.5	3.5	0.15	0.8

Table 4

Traction parameters during shifting

Gear	Stable traction parameters			
	$F_{mean}$ [kN]	$SD_F$ [kN]	$s_{mean}$ [%]	$SD_s$ [%]
B1	19.32	0.29	8.31	1.36
B2	29.46	0.69	23.08	2.1
B3	30.82	0.25	28.67	1.3
B4	29.71	0.66	23.71	1.52
B3	30.29	0.36	27.81	1.41
B2	29.55	0.18	23	1.5

$F_{mean}$  – mean traction force

$SD_F$  – standard deviation of traction force

$s_{mean}$  – mean slip

$SD_s$  – standard deviation of slip

$\Delta s$  – slip change per second

$\Delta F$  – traction force change per second

$t_d$  – clutch disengagement delay

$t_0$  – total shifting time

With respect to the data series, the starting point of shifting can be defined as the first point in time after stabilization, when the traction force gets lower than that of the stable section at least by 10%; and the peripheral speed of the wheel also drops. The endpoint of shifting is when the rise in the traction force after shifting reaches its maximum. This process is illustrated by Figure 4, where the time scale is stretched for better visibility.

In order to be able to analyse the dynamic changes of the measured parameters accurately, those parameters must be selected that allow for comparing all shift changes in a uniform manner. As the above figures show, the process always starts with the change of slip, which is followed with a certain delay by the corresponding change in the traction force.

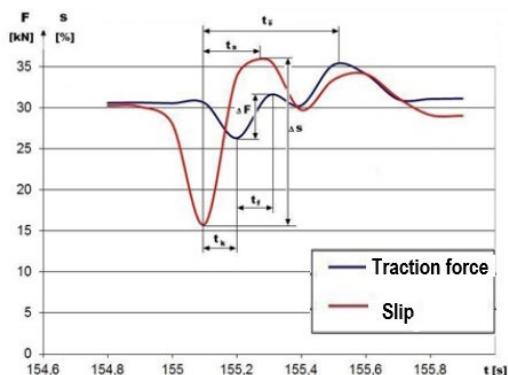


Figure 4

Changing of traction force and slip relative to time, at shifting from B3 to B4

The delay is marked as  $t_k$  in Figure 4 and Table 4. The delay can be explained by the characteristics of the forces arising at the soil-wheel interaction. As the driven wheel rolls over the surface, first the soil is deformed where the surfaces touch. This deformation requires time. Then, the tread of the wheel can adhere to this layer and exert traction force.

The size of the changes in traction parameters can be characterized by the change of traction force and the slip in a unit of time (1 s), i.e. the size of the change should be divided by the required time.

The total length of time needed for shifting ( $t_0$ ) is the time elapsed between the a starting point and the endpoint of shifting in seconds. The unit values of slip and traction force changes and the corresponding time required for shifting are given in Table 4 above.

### 3.2 Fixed Traction Force Scenario

For the fixed traction force scenario, the changes of the traction parameters relative to time are illustrated in Figure 5. In the stable periods after shifting, traction force stays around the pre-set 20 kN value. The slip changes compared to the mean value correspond to the changes in the track force. The standard deviation of the measured slip values are similar to that of traction values, but the standard deviation of slip is higher. After shifting, the traction force is increased so that the tractor could be accelerated back to the speed before shifting, which results in increased slip values.

To be able to compare the two scenarios objectively, the standard deviation of measured values had to be determined. The data presented in Table 5 below show that the standard deviation values of traction parameters are similar in the two scenarios: speed values have the lowest SD, while slip values have the highest SD.

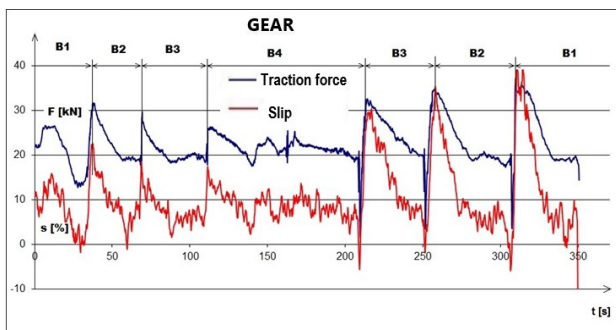


Figure 5

Changes of traction force and slip during shifting when loaded, fixed traction force scenario

Data in Table 5 prove that the parameter changes are different when changing up from those when changing down. SD values show that the most stable operational parameters were recorded in gear B3. Conforming to the expectations of operators and owing to the electro-hydraulic operation system, shifting underload happens in less than half a second. Despite the short time, traction parameters considerably change in this interval. In order to be able to analyze data thoroughly, it is worth enlarging the graph depicting the data for the shifting period.

Table 5

Standard deviation of traction parameter values in the fixed traction force scenario

Characteristics of stable traction				
Gear	$F_{mean}$ [kN]	SDF [kN]	$s_{mean}$ [%]	$SDs$ [%]
B2	18.99	0.43	6.51	4.02
B3	19.24	0.6	5.9	1.93
B4	21.52	1.3	9.23	1.98
B3	20.39	0.48	7.2	1.24
B2	19.08	0.95	4.76	2.72
B1	18.98	0.26	4.98	2.58

$F_{mean}$  – mean traction force

$SD_F$  – standard deviation of traction force

$s_{mean}$  – mean slip

$SDs$  – standard deviation of slip

Table 6

Traction parameters during shifting

Shifting	$\Delta s$ [%/s]	$\Delta F$ [kN/s]	$t_k$ [s]	$t_0$ [s]
B1–2	–	–	–	–
B2–3	6.73	6.25	1	3.2
B3–4	6.5	6.09	0.5	1.5
B4–3	8.2	14.22	0.7	1.8
B3–2	6.72	8.35	0.3	2.1
B2–1	12	15.81	0.9	2.1

$\Delta s$  – slip change per second

$\Delta F$  – traction force change per second

$t_k$  – clutch disengagement delay

$t_0$  – total shifting time

Figure 6 shows the data recorded during shifting from B4 to B3. In the shifting process, the traction force suddenly increases by 5 kN, and the corresponding increase in slip is 10%. In some seconds after shifting, traction force starts to

vacillate with a frequency around 2 Hz, in a similar manner to the vacillation of the engine's revolution.

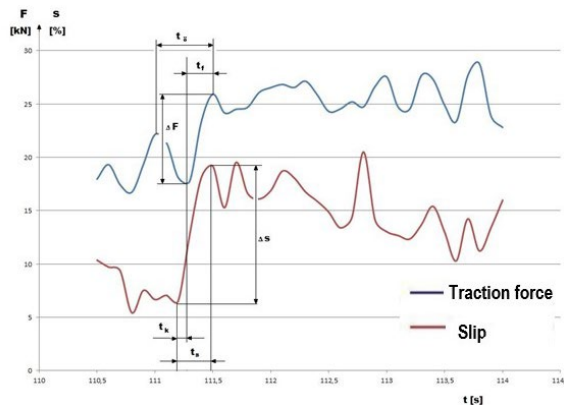


Figure 6

Changes of traction parameters relative to time when shifting from B4 to B3

The graph showing the parameter changes during the process of shifting proves that slip changes precede changes in the traction force. However, at the moment of shifting, for some milliseconds slip decreases, owing to the decreased torque and traction force transmission.

After shifting, slip values increase, but after some seconds, a decrease is witnessed. This shows the excess need for traction force after shifting in order to gain lost speed. The increased slip is the result of increased traction force. Similarly, to the other scenario, changes during shifting were compared. The relevant data are given in Table 6 above.

Processes during changing down are depicted using a stretched time scale. Data recorded during shifting from B4 to B3 are illustrated in Figure 7. In the case of changing down, the process starts with the decreasing of the slip, then after 0.15 s, traction force plummets by more than 15 kN at the beginning of shifting. At the same time, slip decreases. Due to the momentum of the brake cart, the minimum traction force is almost zero. As a result of, the tractor's inertia, the slip value becomes negative for the back wheels for a very short time during the slowing of the tractor.

As the data prove, the revolution of the engine cannot grow when the load is reduced. The load arising at the end of the shifting process causes a reduction of revolution by  $\Delta n = 3\text{-}5$  1/s (compared to the mean of the vacillating revolution). This fall in revolution does not exceed the revolution sensitivity of the engine, thus no reaction follows. The increase in traction force after shifting is due to the excess traction force exerted for accelerating back after “stopping short” during shifting.

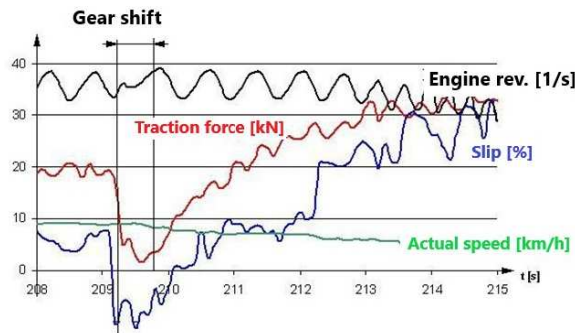


Figure 7

Traction parameters relative to time during shifting from B4 to B3

As the mapping curve for the traction force shows, the traction force gets back to the pre-set 30 kN within 3-5 seconds.

### Conclusions, suggestions

The measurement technique described in this article proved to be appropriate for testing the traction parameters during shifting process underload in tractors. The methods and devices applied in the field traction test make it possible to follow the changes of traction force, actual speed and slip in the course of time. The huge amount of data obtained owing to the high sampling frequency allows for the detailed analysis of the shifting process.

The measured data proves that information about shifting time and the changes in traction parameters is crucial for the operation of tractors and other vehicles with constant load. The analysis presented here shows that the slip, occasionally with changing signs, constantly causes considerable traction loss, although its amount is varied.

In order to decrease traction losses that arise during shifting under load, which are primarily caused by the increasing slip, the following recommendations can be made based on our traction test.

In the field of operation of machines with powershift transmission it is suggested to turn off the fixed engine revolution (hand accelerator) before shifting, so that the operator can make the following corrections with the accelerator pedal.

When changing up, in the moment of shifting the accelerator pedal should be retracted by 30-50% (depending on the actual load). After shifting, acceleration should be continuous in order to speed up the machine group with minimal slip.

When changing down, it is worth slowing down gradually so that the exerted traction force could slow down the machine group while maintaining useful work. Otherwise, the driven wheels slow down the machine group with vacillating, dynamic load, occasionally accompanied by negative slip values.

These actions require attention and experience on behalf of the operator. At the same time, they enhance the efficiency of operation and lengthen the lifespan of the parts of the clutch.

In the software development for powershift transmissions area compared to the simple electro-hydraulic control, more refined regulatory processes are required during shifting. The following should be taken into consideration.

- When changing down, the clutch disengagement delay should be prolonged in order to avoid negative slip. Based on the revolution of the engine and the chosen gear, the system calculates the corresponding speed. It only shifts into the chosen lower gear if the machine group has already slowed down appropriately. In ploughland circumstances, this delay only lasts for some deciseconds.
- When changing up, irrespective of the position of the accelerator pedal, the performance of the engine should be restricted if the slip were to exceed the pre-set limit (e.g. 25%), in order to avoid the sudden growth of slip.

The above suggestions are important not only from an energetic, but also from agrotechnical and environmental perspectives. If slip is high during agrotechnical operations, it leads to higher compacting of the soil, the formation of deep tracks, and thus the microstructure of the soil is damaged.

### Acknowledgements

We wish to express our gratitude to the experts conducting the measurements at the Institute of Agricultural Engineering, National Agricultural Research and Innovation Centre (NARIC MGI) and the colleagues participating in the test from the Vehicles and Agricultural Engineering Department at the Nyíregyháza University of Agricultural Sciences and Technology Institute (NYE MAI).

### References

- [1] Zöldy, M.: Improving heavy duty vehicles fuel consumption with density and friction modifier. *International Journal of Automotive Technology* 20(5) 971-978 (2019) DOI <https://doi.org/10.1007/s12239-018-y>
- [2] Todoruț, A., Molea, A., Barabás, I.: Predicting the Temperature and Composition – Dependent Density and Viscosity of Diesel Fuel – Ethanol Blends. *Per. Pol. Chem. Eng.* 64(2) 213-220, 10.3311/PPch.14757
- [3] Torok, A., Derenda, T., Zanne, M., Zoldy, M.: Automatization in road transport: a review. *Production Engineering Archives* 20(20) 3-7, doi: <https://doi.org/10.30657/pea.2018.20.01>
- [4] Zöldy, M.: Fuel Properties of Butanol – Hydrogenated Vegetable Oil Blends as a Diesel Extender Option for Internal Combustion Engines. *Per. Pol. Chem. Eng.* 64( 2), 205-212, 10.3311/PPch.14153

- [5] Lovarellia, D., Bacenetti, J.: Bridging the gap between reliable data collection and the environmental impact for mechanised field operations. *Biosystems Eng.* 160, 109-123, 10.1016/j.biosystemseng.2017.06.002
- [6] Zöldy, M. Vass, S. Detailed modelling of the internal processes of an injector for common rail systems. *Journal of KONES*, 25(2) 416-426
- [7] Vogt, H. H., de Melo, R. R., Daher, S., Schmuelling, B., Antunes, F., dos Santos, P., Albiero, D.: Electric tractor system for family farming: Increased autonomy and economic feasibility for an energy transition, *Journal of Energy Storage*, Volume 40, 2021, 102744, ISSN 2352-152X, <https://doi.org/10.1016/j.est.2021.102744>
- [8] Zöldy, M., Baranyi, P.: Cognitive Mobility–CogMob. In 12<sup>th</sup> IEEE International Conference on Cognitive Infocommunications (CogInfoCom 2021) *Proceedings IEEE* (pp. 921-925)
- [9] Xia Y, Sun D, Qin D, Hou W: Study on the design method of a new hydro-mechanical continuously variable transmission system, *IEEE AccessOpen Access* Volume 8, pp. 195411-195424, 2020, 10.1109/ACCESS.2020.3005915
- [10] Kilikevičius, A., Kilikevičienė, K., Fursenko, A., Matijošius, J.: The Analysis of Vibration Signals of Critical Points of the Bus Body Frame. *Periodica Polytechnica Transportation Engineering* 48(3) 296-304, <https://doi.org/10.3311/PPtr.12784>
- [11] Rádics, J. P., Jóri, J. I., Fenyvesi, L.: Intelligent tillage machines development to mitigate climate change effects. *Journal of International Scientific Publications: Agriculture and Food* 3(1) 1-11
- [12] Kerényi Gy., Farkas Zs.: Power flows an efficiency analysis of out- and inout coupled IVT. *Per. Pol. Mechanical Engineering* 53(2) 61-68, 10.3311/pp.me.2009-2.02
- [13] Linares, P., Mendez, V., Catalan, H.: Design parameters for continuously variable power-split transmissions using planetaries with 3 active shaft. *J. of Terramechanics* 47. 323-335, 10.1016/j.jterra.2010.04.004
- [14] Comellas, M., Pijuan, J., Potau, X., Nogués, M., Roca, J.: Analysis of a hydrostatic driveline for its use in off-road multiple axle vehicles. *Journal of Terramechanics* 49, 245-254, 10.1016/j.jterra.2012.07.003
- [15] Russini, A., Schlosser, J. F., de Farias, M. S.: Estimation of the traction power of agricultural tractors from dynamometric tests. *Rural Engineering* 48(4), 10.1590/0103-8478cr20170532
- [16] Molari, G., Sedoni, E.: Experimental evaluation of power losses in a power shift agricultural tractor transmission. *Biosystems Engineering* 100, 177-183, 10.1016/j.biosystemseng.2008.03.002

- [17] Szimandl, B., Németh, H.: Sliding Mode Position Control of an Electro-Pneumatic Clutch System. *IFAC Proceedings* 46(2), 707-712, 10.3182/20130204-3-FR-2033.00019
- [18] Zhu, Z., Chen, L., Xia, C., Cai, Y.: Test research on the adhesive and tractive performance of a wheeled tractor, *International Journal of Heavy Vehicle Systems*, 27 (1-2) pp. 65-82, 10.1504/IJHVS.2020.104425
- [19] Kiss P., Laib L. Questions on the energetics of off-road vehicles [In Hungarian] *MTA-AMB XXV. Gödöllői K+F Tan.*, 23–24 January 2001
- [20] Liu, M., Wang, X., Wang, J., Cui, B., Deng, B., & Shi, M.: Comprehensive Evaluation for Real-Time Compaction Quality Using i-AHP and i-GAM: Case Study of Earth-Rock Dam. *Applied Sciences* 9(8) 1543, 10.3390/app9081543
- [21] Chen, H., Cheng, X., Tian, G.: Modelling and analysis of gear shifting process of motor-transmission coupled drive system. *Journal of Nonlinear Computation Dynamics* 11(2) 021013-1–021013-15
- [22] Lengyel A., Szegedi A.: Analysis of gearing process under load [In Hungarian]. *Járművek és Mobil Gépek*, 139-145
- [23] Rövid, A., Palkovics, L., Várlaki, P.: Empirical White Noise Processes and the Subjective Probabilistic Approaches. *Per. Polytechnica Transportation Engineering* 48(1), 19-30, <https://doi.org/10.3311/PPtr.15165>
- [24] Szabó, Z., Török, Á.: Spatial Econometrics – Use in Transportation Sciences. *PP Tr. Eng.* 48(2), 143-149, <https://doi.org/10.3311/PPtr.12047>
- [25] Tanelli, M., Panzani, G., Savaresi, S. M., Pirola, C.: Transmission control for power-shift agricultural tractors: Design and end-of-line automatic tuning. *Mechatronics* 21.285-297, 10.1016/j.mechatronics.2010.11.006
- [26] Péter, T, Lakatos, I.: Hybrid model of vehicle and traffic for combined dynamic analysis. *I. J. of H. Veh. Sys.* 24(2), 10.1504/IJHVS.2017.083095
- [27] Biestrato M., Friso D., Sartori L.: Assessment of the efficiency of tractor transmissions using acceleration tests, *Biosys. Eng.* 112, 171180, DOI 10.1016/j.biosystemseng.2012.03.009
- [28] Siddique, M. A. A., Baek, S.-M., Baek, S.-Y.: Simulation of fuel consumption based on engine load level of a 95 kw partial power-shift transmission tractor. *Agriculture*, 11 (3), art. no. 276, 10.3390/agriculture11030276
- [29] Cutini, C., Bisaglia, C.: Development of dynamometric vehicle to assess the drawbar performance of high powered agricultural tractors. *Journal of Terramechanics* 65. 73-84, 10.1016/j.jterra.2016.03.005

# Integrated Torque Vectoring Control Using Vehicle Yaw Rate and Sideslip Angle for Improving Steering and Stability of All Off-Wheel-Motor Drive Electric Vehicles

**Mahmoud Said Jneid, Péter Harth**

Budapest University of Technologies and Economics, Department of Automotive Technologies, 1111 Budapest, Hungary  
E-mails: mah.jneid@edu.bme.hu, harth.peter@kjk.bme.hu

---

*Abstract: Recently electric vehicles with independent wheel-motor-drive showed great potential for advanced chassis active control integration leading to high driving performance, ensured safety, and compact packaging. Advanced motor drives and powerful power electronics enable highly sophisticated vehicle control systems to be applied and integrated using minimum hardware. This paper proposes an integrated torque vectoring control using vehicle yaw rate and sideslip angle to correct steering and improve stability of all off-wheel-motor drive electric vehicles. The control system is suggested with three control layers: the higher, medium, and lower. The main contribution of this work is implementing torque vectoring based on regenerative braking on the wheels allocated to develop braking force. The proposed torque vectoring control is implemented on a 7-DOF electric vehicle model in MATLAB/Simulink and verified by a double-lane change manoeuvre. Simulation results show explicit improvement in vehicle heading and stability.*

*Keywords: integrated torque vectoring; yaw rate; sideslip angle; electric vehicles; off-wheel-motor; regenerative braking; vehicle stability; steering correction*

---

## 1 Introduction

Electric vehicles (EVs) have many advantages compared to conventional internal combustion engine (ICE) vehicles such as being environment-friendly, high efficiency, having a simple layout, minimized drivetrain elements, easy maintenance, improved packaging, and compactness. The present trends in the transportation sector suggest that EVs replace ICE vehicles shortly [1]. In all-wheel-motor drive (AWM) EVs, the electric motor can be installed inside the wheel so known as in-wheel-motor (IWM) or offside the wheel as is convented in this paper by off-wheel-motor (OWM). With four electric motors, the wheels' torque can be

precisely controlled allowing for the application of a wide range of advanced chassis assistance systems (ACAS) and advanced driver assistance systems (ADAS) as holistic integrated systems [2].

Thanks to electric motors and their sophisticated control algorithms, these systems can be implemented as an electronic version of the e-system achieving real drive-by-wire (DBW) and brake-by-wire (BBW) control [3], [4]. The e-system list includes an e-anti-lock braking system (eABS), an e-electronic stability program (eESP), an e-limited slip differential (eLSD), and e-torque vectoring (eTV) [5], [6]. Currently, TV is a hot research topic and attracts many researchers' attention and companies' interests working in the domain of electrified vehicles.

The principal behind the TV is to generate a corrective yaw moment around the vehicle's vertical axis to correct the vehicle heading during turning and cornering manoeuvres leading to improved vehicle stability and steering [7]. The precise torque control of electric motors (EMs) over a wide range of speeds in both traction and braking directions allows the generation of unlimited combinations of driving and braking differential force couples which can handle vehicle heading and stability under various conditions.

With TV, the vehicle behaviour is ensured linear if the desired yaw rate reference is generated according to the bicycle vehicle model. At some critical safety conditions such as severe understeering and oversteering, TV becomes indispensable in maintaining either neutral or acceptable understeering vehicle behaviour and hence stability level.

In understeering, the vehicle's front wheels reach the minimum limit of friction, thus, TV is expected to correct the vehicle heading by generation more yaw moment on the rear wheels in the direction of turning. Similarly, in oversteering, the rear wheels lose friction with the ground requiring the TV to produce a yaw moment acting opposite to the direction of overturning [8], [9].

In this paper, an integrated torque vectoring control (ITV) based on vehicle yaw rate and sideslip angle is proposed using a hysteresis controller to correct steering and improve stability of all off-wheel-motor drive electric vehicles. The control structure includes three layers: the high-level layer, the intermediate layer, and the lower layer. In the higher layer, the vehicle's yaw rate and sideslip angle control occur based on tracking the desired reference generated according to the bicycle model. In the intermediate layer, a coordination layer, where the corrective yaw moments of both yaw rate and sideslip angle are allocated to the individual wheels according to static load-based front-to-rear axle and equal-opposite of traction-braking couples as left-to-right distributions. Finally, in the lower layer, EMs control is implemented based on field-oriented control (FOC) to provide individually allocated torques.

The remainder of the article is structured as follows: Sec. 2 presents vehicle layout and subsystem models, Sec. 3 spotlights the proposed wheel slip-based integrated

vehicle yaw rate and sideslip angle TV control, Sec. 4 introduces results demonstration and investigation, and Sec. 5 concludes the work.

## 2 Vehicle Layout and Subsystem Models

To validate the proposed ITV control, a vehicle dynamic model (VDM) is developed in MATLAB/Simulink. The EV layout includes 4x EMs, 4x drive controllers, 4x reduction gears, 7-DOF VDM, driver, and battery models. The vehicle structure with power flow directions and control lines is best described in Fig. 1, which is reprinted from [2].

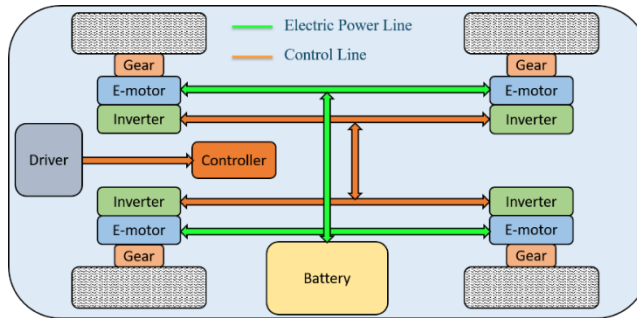


Figure 1

Schematic diagram of the suggested EV structure for the proposed ITV control

### 1.1 Vehicle Dynamic Model

For accurate validation of the proposed ITV control, the VDM is required to reflect the vehicle planar behaviour along with wheel dynamics precisely. Therefore, a 7-DOF EV VDM is suggested to describe the longitudinal, lateral and yaw dynamics as well as the wheel's rotational dynamics as shown in Fig. 2. The equation of motion that describe the chassis planar behaviour is given in (1)-(2) as follows:

$$ma_x = F_f^x + F_r^x \quad (1)$$

$$ma_y = F_f^y + F_r^y \quad (2)$$

Where:  $m$  is the vehicle mass,  $a_x$  ( $a_y$ ) vehicle's CoG longitudinal (lateral) acceleration,  $F_f^x$  ( $F_r^x$ ) front (rear) longitudinal forces,  $F_f^y$  ( $F_r^y$ ) front (rear) lateral forces. The vehicle yaw rate and sideslip angle are required for the ITV control integration and are given in (3)-(4) as follows:

$$I_z \dot{\gamma} = M_f^x + M_r^x + M_f^y + M_r^y \quad (3)$$

$$\beta = \tan^{-1} \left( \frac{v_y}{v_x} \right) \tag{4}$$

With:  $\dot{\gamma}$  vehicle's CoG yaw acceleration,  $I_z$  vehicle yaw moment of inertia,  $M_f^x (M_r^x)$  front (rear) yaw moments resulting from longitudinal forces,  $M_f^y (M_r^y)$  front (rear) yaw moments resulted from lateral forces,  $\beta$  vehicle sideslip angle,  $v_x$  ( $v_y$ ) vehicle CoG longitudinal (lateral) speeds. Vehicle parameters are provided in Table 1.

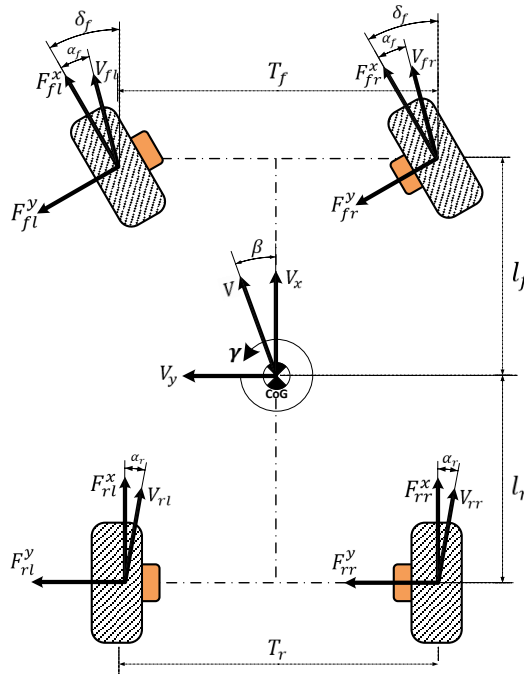


Figure 2

Schematic illustration of the 7-DoF VDM with wheels dynamic quantities

Table 1  
Vehicle parameters

Parameter	Description	Value	Parameter	Description	Value
m	vehicle mass	1181kg	Lr	front axle distance from the centre of gravity	1.504 m
Af	vehicle frontal area	2.11 m <sup>2</sup>	Tf (Tr)	vehicle front (rear) track width	1.922 m
Cd	drag coefficient	0.33	h <sub>CoG</sub>	vehicle centre of gravity height	0.134 m
Lf	rear axle distance from the centre of gravity	1.515 m	Iz	vehicle yaw inertia around the z-axis	2066 kg.m <sup>2</sup>

## 1.2 Tyre Model

Tires represent the interface of the vehicle to the external environment and are requested to be described with enough accuracy to reflect real vehicle behaviour. In literature, several tyre models are thoroughly investigated as describing real wheel dynamics for different purposes such as analysis, control, optimization, and simulation. The major models explored are the LuGre friction model [10], [11], the Dugoff model [12]-[14], the brush model [15]-[17], and Pacejka's magic formula (MF) model [18]-[20]. In this work, the MF model is chosen as it meets the performance requirements of combined dynamics and control of braking and traction forces under slip regulation at cornering necessary for performing the simulation of the double lane change (DLC) manoeuvre. MF model can be given according to (5), [21]:

$$y = D \sin[C \tan^{-1}\{Bx - E(Bx - \tan^{-1}(Bx))\}] \quad (5)$$

Where:  $y$  indicates the tyre output which can be either  $F_x$  or  $F_y$ ,  $x$  represents wheel longitudinal or lateral slip  $\kappa$  or  $\alpha$ .  $B$ ,  $C$ ,  $D$ , and  $E$  are empirical coefficients that denote the stiffness, shape, peak, and curvature of the MF solution, respectively. The tyre longitudinal slip  $\kappa$  under braking and traction conditions is given in (6):

$$\left. \begin{aligned} \kappa &= \frac{v_x - r_e \omega_w}{v_x} \\ \kappa &= \frac{r_e \omega_w - v_x}{r_e \omega_w} \end{aligned} \right\} \begin{array}{l} \text{at braking} \\ \text{at drivin} \end{array} \quad (6)$$

The lateral slip or sideslip angle of the front and rear wheels are given in (7) as follows:

$$\begin{aligned} \alpha_f &= \beta + \frac{\gamma l_f}{v_x} - \delta \\ \alpha_r &= \beta - \frac{\gamma l_r}{v_x} \end{aligned} \quad (7)$$

The electrodynamic behaviour of wheels can be described according to Newton's second law as given in (8):

$$I_w \dot{\omega}_w = T_d - T_b - r_e F_x \quad (8)$$

Where:  $\alpha_f$  ( $\alpha_r$ ) denotes the slip angle of the front (rear) wheels,  $\gamma$  the vehicle's yaw angle,  $\delta$  wheel's steering angle,  $l_f$  ( $l_r$ ) distance of the front (rear) axle to CoG,  $I_w$  the wheel's moment of inertia,  $\dot{\omega}_w$  the wheel's angular velocity,  $T_d$  the electric motor wheel's driving torque,  $T_b$  the total braking torque from the EM and brakes, and  $r_e$  the wheel's effective radius.

Finally, the normal load of wheels in terms of static and dynamic weights are given according to (9) as follows [22]:

$$\begin{aligned}
F_{fl}^z &= \frac{m}{2(l_r+l_f)} \left( gl_r - h_{cg} a_x - \frac{2l_r h_{cg}}{T_f} a_y \right) \\
F_{fr}^z &= \frac{m}{2(l_r+l_f)} \left( gl_r - h_{cg} a_x + \frac{2l_r h_{cg}}{T_f} a_y \right) \\
F_{rl}^z &= \frac{m}{2(l_r+l_f)} \left( gl_r + h_{cg} a_x - \frac{2l_f h_{cg}}{T_r} a_y \right) \\
F_{rr}^z &= \frac{m}{2(l_r+l_f)} \left( gl_r + h_{cg} a_x + \frac{2l_f h_{cg}}{T_r} a_y \right)
\end{aligned} \tag{9}$$

Where:  $F_{fl}^z$  ( $F_{fr}^z$ ),  $F_{rl}^z$  ( $F_{rr}^z$ ) indicate the weight on the front-left (front-right), and rear-left (rear-right) wheels respectively,  $g$  is the gravitational acceleration, and  $t_w$  is the vehicle's track width.

### 3 Integrated Torque Vectoring Control ITV

The main purpose of TV is to correct vehicle heading during cornering and maintain high stability through generating differential driving-braking forces which act at the vehicle's CoG to prevent undesired understeering and oversteering conditions. The differential forces from wheels result in a corrective yaw moment vector, which is generated by the main TV controller and has a direction the same as the vehicle turning.

Mainly, TV control consists of at least two control layers, the control and the distribution. The corrective yaw moment reference is generated in the control layer by tracking one or more parameters in terms of lateral stability. In-action states include the vehicle's yaw rate  $\dot{\gamma}$  [2], [22]-[26], yaw rate  $\gamma$  and sideslip angle  $\beta$  [29]-[35], yaw rate  $\dot{\gamma}$  and sideslip angle  $\beta$  with wheel slip  $\kappa$  [34]-[36]. Afterwards, the resulting yaw moment vector is broken into reference components based on allocation strategy and communicated to individual wheels' motor control. In literature, different TV control approaches investigated such as proportional-integral-differential (PID) [37], [38], neural network (NN) like PID [39], linear quadrature regulator (LQR) [40], [41], sliding mode control (SMC) [24], [42], [43], fuzzy logic control (FLC) [44], [45], FLC like PID [46], and model predictive control (MPC) [47]-[53].

In this work, a proposed integrated torque vectoring ITV control of the vehicle's yaw rate  $\dot{\gamma}$  and sideslip angle  $\beta$  is implemented. The corrective yaw moment vector is distributed into the four wheels based on front-rear and right-left equal-opposite pairs of driving/braking components. Fig. 3 shows a block diagram of the proposed ITV control.

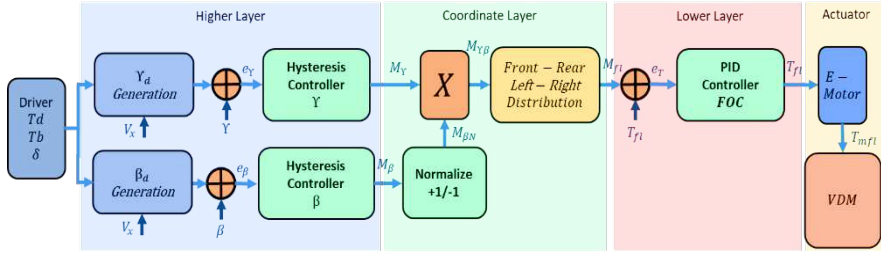


Figure 3

Block diagram of the proposed integrated torque vectoring control scheme ITV

### 3.1 Desired Control Reference

The ITV control is aimed at maintaining linear vehicle behaviour by tracking the vehicle's yaw rate  $\gamma$  and sideslip angle  $\beta$ . The desired reference values of  $\gamma$  and  $\beta$  can be derived based on the bicycle model with understeering behaviour  $k_u$  given in (10), (11) as follows [54]:

$$\gamma_d = \frac{v_x \delta}{(l_f + l_r) + k_u v_x^2} \quad (10)$$

$$\beta_d = \frac{l_r - l_f m v_x^2 / 2(l_f + l_r) C_f}{(l_f + l_r) + k_u v_x^2} \delta \quad (11)$$

With:

$$k_u = \frac{m}{(l_f + l_r)} \left( \frac{l_r}{C_f} - \frac{l_f}{C_r} \right) \quad (12)$$

Where:  $\gamma_d$  ( $\beta_d$ ) denotes the desired yaw rate (sideslip angle),  $k_u$  understeering characteristic factor,  $C_f$  ( $C_r$ ) the front (rear) wheel cornering stiffness according to [55].

### 3.2 Integrated Yaw Rate and Sideslip Angle Controller

In this work, the controller suggested for both  $\gamma$  and  $\beta$  is a hysteresis type. This controller meets the requirements of nonlinear control problems and is featured as a simple and model parameter-dependent controller. The output of  $\gamma$  controller is defined in (13) as follows:

$$M_\gamma = \begin{cases} +K_\gamma & \text{if } e_\gamma \geq 0 \\ -K_\gamma & \text{if } e_\gamma < 0 \end{cases} \quad (13)$$

With:

$$K_\gamma = \frac{1}{l_z}(l_f C_f - l_r C_r)\beta + \frac{1}{v_x}(l_f^2 C_f - l_r^2 C_r)\gamma - l_f C_f \delta \quad (14)$$

The output of the  $\beta$  controller can be designated as follows:

At steady state, the side slip angle is very small [28], thus, (4) is simplified into (15):

$$\beta = \frac{v_y}{v_x} \quad (15)$$

With  $v_x$  constant, the derivative of (15) is given in (16):

$$\dot{\beta} = \frac{\dot{v}_y}{v_x} = \frac{a_y}{v_x} \quad (16)$$

Compensate (2) into (16) and fix it, the output of the  $\beta$  controller is assumed the  $\dot{\beta}$  and defined in (17) as follows:

$$M_\beta = \begin{cases} +K_\beta & \text{if } e_\beta \geq 0 \\ -K_\beta & \text{if } e_\beta < 0 \end{cases} \quad (17)$$

With:

$$K_\beta = \frac{1}{mv_x}(C_f + C_r)\beta + \frac{1}{v_y}((l_f C_f - l_r C_r))\gamma - C_f \delta - m \quad (18)$$

Where:  $M_\gamma$  ( $M_\beta$ ) is the corrective yaw moment vector generated by the yaw rate (sideslip angle) controller,  $e_\gamma$  ( $e_\beta$ ) is the yaw rate (sideslip angle) error.

$M_\beta$  is normalized between  $\pm 1$  and used as a weight to bind the corrective yaw moment when the sideslip angle reaches the limit of stability that maintains vehicle safety. Eventually, the combined corrective yaw moment can be described in (19) as follows:

$$M_{\gamma\beta} = M_\gamma M_\beta \quad (19)$$

The resultant control law should be actuated by the four electric motors which represent an over-actuation control system. For optimal performance,  $M_{\gamma\beta}$  is allocated according to the front-to-rear and right-to-left equal-opposite strategy. First,  $M_{\gamma\beta}$  is distributed between the front and rear axles based on wheel static loads as in (20)-(22):

$$M_{\gamma\beta} = M_{\gamma\beta}^f + M_{\gamma\beta}^r \quad (20)$$

$$M_{\gamma\beta}^f = \frac{l_f}{l_f + l_r} M_{\gamma\beta}^f \quad (21)$$

$$M_{\gamma\beta}^r = \frac{l_r}{l_f + l_r} M_{\gamma\beta}^f \quad (22)$$

Afterwards, the front and rear yaw moment portions are distributed between the left and right wheels based on an equal-opposite combination according to (23)-(26):

$$M_{fl} = \left(\frac{1}{2}\right) M_{\gamma\beta}^f \text{sign}(\delta) \quad (23)$$

$$M_{fr} = -\left(\frac{1}{2}\right) M_{\gamma\beta}^f \text{sign}(\delta) \quad (24)$$

$$M_{rl} = \left(\frac{1}{2}\right) M_{\gamma\beta}^r \text{sign}(\delta) \quad (25)$$

$$M_{rr} = -\left(\frac{1}{2}\right) M_{\gamma\beta}^r \text{sign}(\delta) \quad (26)$$

Where:  $M_{\gamma\beta}^f$  ( $M_{\gamma\beta}^r$ ) is the front axle (rear axle) yaw moment portion,  $M_{fl}$  ( $M_{fr}$ ) the yaw moment portion of the front-left (front-right), and  $M_{rl}$  ( $M_{rr}$ ) the yaw moment portion of the rear-left (rear-right) wheels.

## 4 Simulation Results And Discussion

To validate the proposed ITV, a double lane change simulation manoeuvre (DLC) at  $50\text{kmh}^{-1}$  speed is performed in MATLAB/Simulink. Results of ITV based on hysteresis controller are presented and compared to classical TV with PID controller (only yaw rate control) and when TV-off. Results are introduced in terms of the vehicle's and wheels' behaviours. The results discussion covers the vehicle's planer position, controlled yaw rater, controlled sideslip angle, lateral acceleration response, wheels' longitudinal (lateral) slip, modulated torques, speed, and energy recovery.

Fig. 4 shows the vehicle lateral position under the proposed ITV control, compared with yaw rate-based TV, and TV-off. A stable trajectory is confined with left and right cone boundaries at a distance of around 1.2 m from the vehicle centerline. With ITV control, the vehicle enters and exits the track at stable behaviour maintaining enough margins inside the lane. With conventional TV, the trajectory is maintained inside the borders slightly approaching the left cones at the manoeuvre egress. The worst case is when TV-off, where the vehicle bypasses the track boundaries during both lane changes indicating unstable behaviour.

Fig. 5 shows the vehicle yaw rate under ITV against TV behaviour and TV-off in response to the desired yaw rate. It can be seen that the ITV performs quite fast-tracking of the reference yaw rate with almost full matching. TV also behaves similarly with a slight overshoot in both lane changes noticeably at the point when the vehicle returns to the lane. However, when TV-off, the vehicle behaves more aggressively changing both lanes at a high yaw rate (far from the desired reference value with understeering characteristics) with a potential tendency to lose stability, especially at the end of the DLC manoeuvre where the vehicle performs excessive lane departure.

Fig. 6 demonstrates the vehicle sideslip angle of the ITV control compared with those of TV and TV-off. The realisation of sideslip angle control appears clearly in this figure, where the vehicle sideslip angle follows a confined and uniform course. In addition, it can be noticed that the sideslip angle under ITV and TV approach zero more quickly than that without control. This indicates vehicle stability is maintained, and the effectiveness of the proposed ITV control in correcting the vehicle’s heading. However, with the TV-off, the vehicle is at the stability limit. In addition, the vehicle has no trajectory adjustment and is subject to loose controllability at severe manoeuvres, especially at the exit of the DLC test where the vehicle is assumed to return to its initial straight position more quickly.

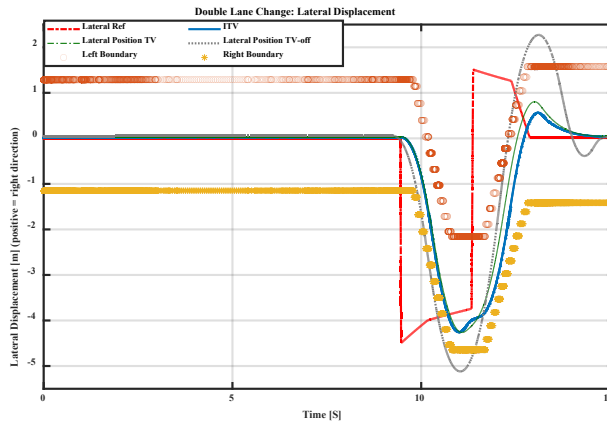


Figure 4

Vehicle lateral displacement under ITV control compared to TV and TV-off

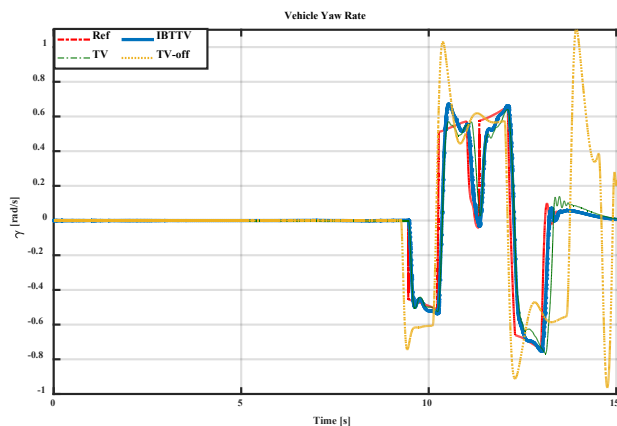


Figure 5

Vehicle yaw rate response under ITV control compared to TV and TV-off

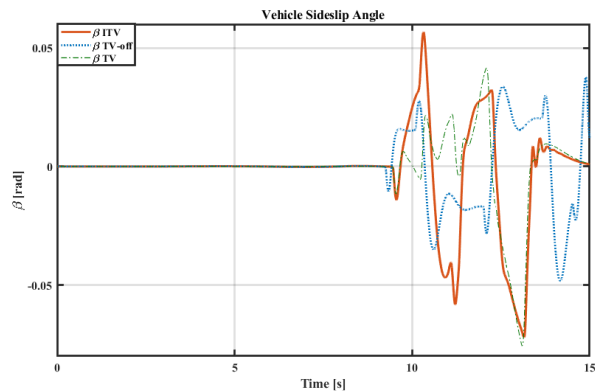


Figure 6

Vehicle sideslip angle under ITV control compared to TV and TV-off

Fig. 7 displays the vehicle lateral acceleration under ITV control, TV control, and TV-off. Again, stable vehicle behaviour can be the figure revealed with a max lateral acceleration of around 0.1 g, which is roughly lower than the max stability limit of 0.3 g. However, with TV-off, the vehicle quits the path at high acceleration with poor understeering characteristics.

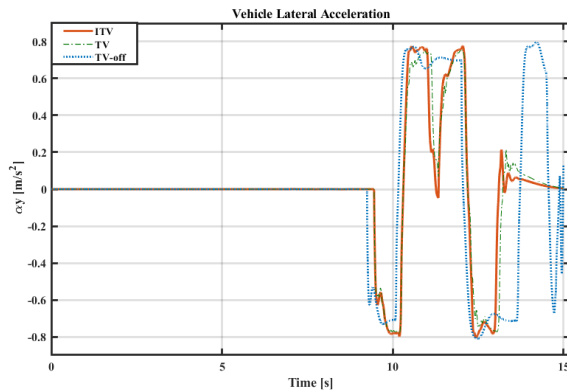


Figure 7

Vehicle lateral acceleration under ITV control compared to TV and TV-off

The potential performance of the ITV can be observed on the wheels' longitudinal slip as shown in Fig. 8. It is clear that the wheels' slip is maintained and limited within the optimal range  $[-0.2$  to  $0.2]$  for all front and rear wheels. This provides that the tyre-road friction is optimally utilised where wheels can generate max braking/traction forces. In contrast, wheels slip under both TV and TV-off exceeds the effective limit. To this end, the wheels under braking are subject to a locking-up case which may lead to vehicle stability issues, especially at lane change with high lateral acceleration.

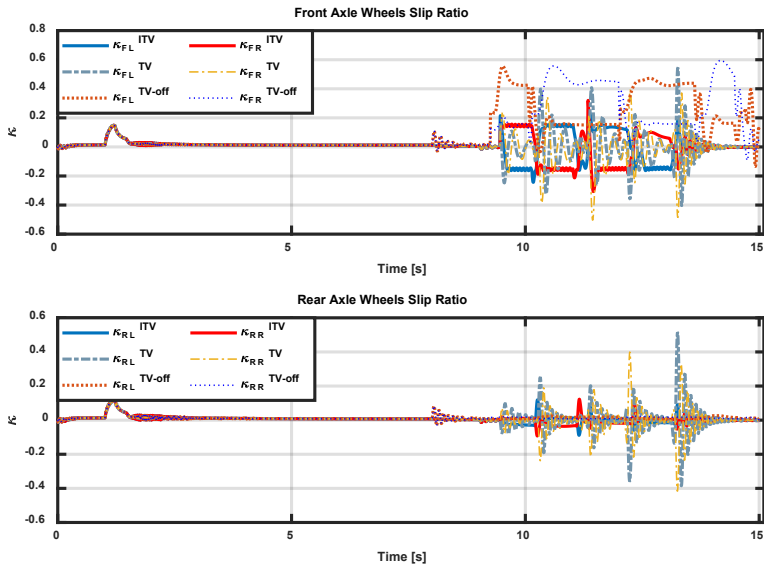


Figure 8

Wheels longitudinal slip under ITV control compared to TV and TV-off

Wheels slip angle regulation is a normal indirect consequence of the wheels' longitudinal slip regulation according to the fixed limit of the available friction circle. Fig. 9 demonstrates the slip angle of the front and rear wheels with stability control and without control. The slip angle of wheels under ITV and TV are confined within the range  $[-0.52$  to  $0.52]$ , while it exceeds the range with TV-off. This is how the wheels slip angles and hence lateral forces are controlled indirectly when ITV is in action leading to maintaining vehicle lateral stability.

In response to ITV control, the wheels' torque and speed are adjusted according to the reference value from ITV as depicted in Figs. 10 and 11. It is clear that the wheels' dynamics are faster under the ITV than those of TV and TV-off. However, the fast wheels' behaviour can be attributed to the reality of the high dynamic ITV hysteresis controller. In contrast, the wheels' torque and speed with TV modified slightly, while they remained unchanged with TV-off as shown in the given figures.

The last part of this discussion is dedicated to battery conditions powering the electric motors. Fig. 12 presents the battery state of charge (SOC) under ITV control, TV control, and TV-off. It can be observed that the battery is less discharged with ITV SOC=90.5% compared to that of TV and TV-off. This can be attributed to the energy recuperation due to the regenerative braking of wheels allocated to generate a brake torque where brake current is used to recharge the battery. However, with TV, the battery is more discharged and SOC decreased to 88.25% without regenerative braking, while the highest energy consumption

occurred with TV-off at SOC 84.9% was observed as there is no brake component and wheels' torque or speed unmodulated.

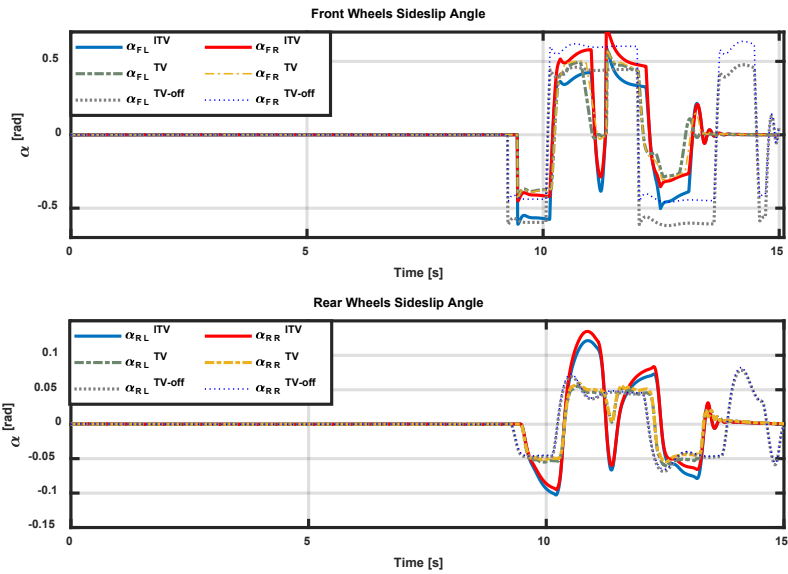


Figure 9  
Wheels slip angles under ITV control compared to TV and TV-off

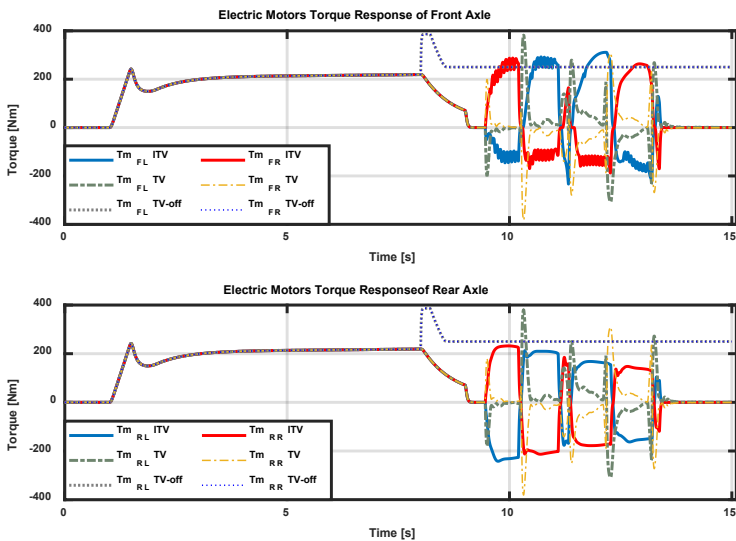


Figure 10  
Wheels adjusted torque under ITV control compared to TV and TV-off

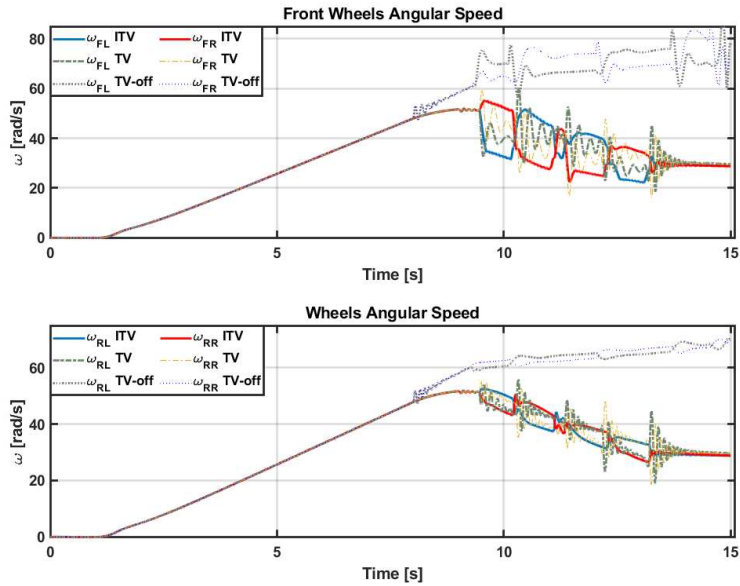


Figure 11  
Wheels adjusted velocity under ITV control compared to TV and TV-off

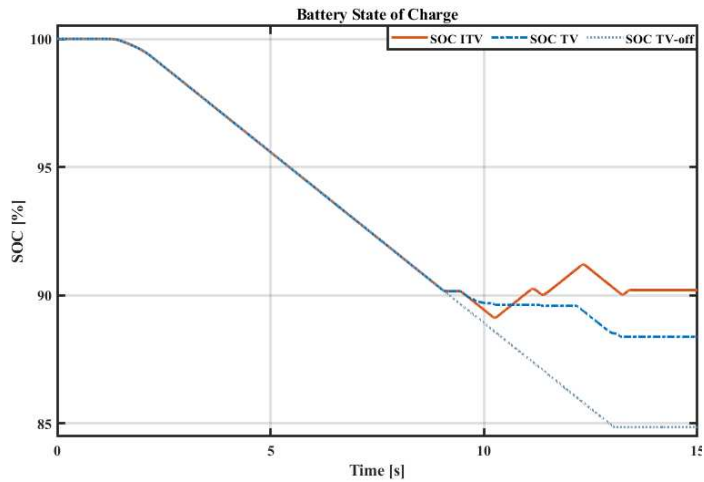


Figure 12  
Battery SOC under ITV control compared to TV and TV-off

### Conclusion

In this work, an integrated braking/driving torque vectoring (ITV) control is proposed based on yaw rate and sideslip angle tracking. The objective of the torque vectoring controller is to correct the vehicle heading during cornering by generating

two vectors of the corrective way moment and distributing the resultant yaw moment to the individual motors to maintain stability and improve vehicle handling. An axle load-based front-to-rear distribution and equal-opposite couples-based left-to-right distribution approaches are used for the yaw moment allocation.

A DLC simulation manoeuvre is performed on a 7-DOF electric vehicle model with AWD by OWM in MATLAB/Simulink to demonstrate the performance and effectiveness of the proposed IBTTV controller. Results reveal the effectiveness and the high performance of the proposed stability control in terms of vehicle stability, handling, and energy recovery.

The abbreviation list used in this work is provided in Table 2.

Table 2  
Abbreviation list

Abbreviation	Description	Abbreviation	Description
ABS	Anti-Lock Braking System	FLC	Fuzzy Logic Control
ACAS	Advanced Chassis Assistance Active Safety	ICE	Internal Combustion Engine
ADAS	Advanced Driver Assistance System	ITV	Integrated Torque Vectoring
AWM	All-Wheel-Motor	IWM	In-Wheel-Motor
BBW	Brake-By-Wire	LQR	Linear Quadrature Regulator
CoG	Centre of Gravity	MF	Magic Formula
DLC	Double Lane Change	MPC	Model Predictive Control
DBW	Drive-By-Wire	NN	Neural Network
DOF	Degree of Freedom	OWM	Off-Wheel-Motor
eABS	e-Anti-Lock Braking System	PID	Proportional Integral Differential
eESP	e-Electronic Stability Program	SOC	State Of Charge
eLSD	e-Limited Slip Differential	SMC	Sliding Mode Control
EM	Electric Motor	TV	Torque Vectoring
EV	Electric Vehicle	VDM	Vehicle Dynamic Model
FOC	Field Oriented Control	FLC	Fuzzy Logic Control

## References

- [1] M. Said Jneid, P. Harth, and P. Ficzero, "IN-WHEEL-MOTOR ELECTRIC VEHICLES AND THEIR ASSOCIATED DRIVETRAINS," *Int. J. TRAFFIC Transp. Eng.*, vol. 10, no. 4, Oct. 2020, doi: 10.7708/ijtte.2020.10(4).01
- [2] M. Said Jneid and P. Harth, "Integrated Braking and Traction Torque

- Vectoring Control Based on Vehicle Yaw Rate for Stability Improvement of All-Wheel-Drive Electric Vehicles,” *2023 IEEE Int. Conf. Electr. Syst. Aircraft, Railw. Sh. Propuls. Road Veh. Int. Transp. Electr. Conf. (ESARS-ITEC)*, Venice, Italy, no. Vdm, pp. 1–6, 2023, doi: 10.1109/ESARS-ITEC57127.2023.10114899
- [3] M. Said Jneid, M. Zöldy, and P. Harth, “Sensorless optimal control of electronic wedge brake based on dynamic model and Kalman filter state multiple-estimation,” *Proc. Inst. Mech. Eng. Part D J. Automob. Eng.*, 2023, doi: 10.1177/09544070231168168
- [4] M. Said Jneid and A. Joukhadar, “LQR-Based Control of a Single Motor Electronic Wedge Brake EWB for Automotive Brake-By-Wire System,” *Soft Comput. Electr. Eng.*, vol. 1, no. 1, pp. 12–35, 2019
- [5] M. Said Jneid and P. Harth, “Blended Regenerative Anti-Lock Braking System and Electronic Wedge Brake Coordinate Control Ensuring Maximal Energy Recovery and Stability of All-In-Wheel-Motor-Drive Electric Vehicles,” *J. Transp. Technol.*, pp. 1–27, 2023
- [6] S. Woo, H. Cha, K. Yi, and S. Jang, “ACTIVE DIFFERENTIAL CONTROL FOR IMPROVED HANDLING PERFORMANCE OF FRONT-WHEEL-DRIVE HIGH-PERFORMANCE VEHICLES,” *Int. J. Automot. Technol.*, vol. 22, no. 2, pp. 537–546, 2021, doi: 10.1007/s12239-021-0050-2
- [7] N. Ahmadian, A. Khosravi, and P. Sarhadi, “Integrated model reference adaptive control to coordinate active front steering and direct yaw moment control,” *ISA Trans.*, vol. 106, pp. 85–96, Nov. 2020, doi: 10.1016/j.isatra.2020.06.020
- [8] A. Medina Murua, G. Bistue, A. Rubio, and J. Gonzalez, “A Direct Yaw Moment Control logic for an electric 2WD FSAE using an error cube PD controller.”
- [9] L. De Novellis, A. Sorniotti, P. Gruber, and A. Pennycott, “Comparison of feedback control techniques for torque-vectoring control of fully electric vehicles,” *IEEE Trans. Veh. Technol.*, vol. 63, no. 8, pp. 3612–3623, 2014, doi: 10.1109/TVT.2014.2305475
- [10] Z. Li, P. Wang, H. Liu, Y. Hu, and H. Chen, “Coordinated longitudinal and lateral vehicle stability control based on the combined-slip tire model in the MPC framework,” *Mech. Syst. Signal Process.*, vol. 161, Dec. 2021, doi: 10.1016/j.ymsp.2021.107947
- [11] E. Hashemi, M. Pirani, A. Khajepour, and A. Kasaiezadeh, “A comprehensive study on the stability analysis of vehicle dynamics with pure/combined-slip tyre models,” *Veh. Syst. Dyn.*, vol. 54, no. 12, pp. 1736–1761, Dec. 2016, doi: 10.1080/00423114.2016.1232417
- [12] S. Rafatnia and M. Mirzaei, “Adaptive Estimation of Vehicle Velocity From Updated Dynamic Model for Control of Anti-Lock Braking System,” *IEEE*

- Trans. Intell. Transp. Syst.*, 2021, doi: 10.1109/TITS.2021.3060970
- [13] M. A. Saeedi, “Simultaneous improvement of handling and lateral stability via a new robust control system,” *Mech. Based Des. Struct. Mach.*, 2021, doi: 10.1080/15397734.2021.1888749
- [14] M. Bian, L. Chen, Y. Luo, and K. Li, “A dynamic model for tire/road friction estimation under combined longitudinal/lateral slip situation,” in *SAE Technical Papers*, 2014, vol. 1, doi: 10.4271/2014-01-0123
- [15] A. O’Neill, J. Prins, J. F. Watts, and P. Gruber, “Enhancing brush tyre model accuracy through friction measurements,” *Veh. Syst. Dyn.*, 2021, doi: 10.1080/00423114.2021.1893766
- [16] K. B. Singh, M. A. Arat, and S. Taheri, “An intelligent tire based tire-road friction estimation technique and adaptive wheel slip controller for antilock brake system,” *J. Dyn. Syst. Meas. Control. Trans. ASME*, vol. 135, no. 3, 2013, doi: 10.1115/1.4007704
- [17] C. Ahn, H. Peng, and H. E. Tseng, “Robust estimation of road friction coefficient using lateral and longitudinal vehicle dynamics,” in *Vehicle System Dynamics*, Jun. 2012, vol. 50, no. 6, pp. 961–985, doi: 10.1080/00423114.2012.659740
- [18] S. Santini, N. Albarella, V. M. Arricale, R. Brancati, and A. Sakhnevych, “On-Board Road Friction Estimation Technique for Autonomous Driving Vehicle-Following Maneuvers,” 2021, doi: 10.3390/app11052197
- [19] K. B. Singh, “Vehicle sideslip angle estimation based on tire model adaptation,” *Electron.*, vol. 8, no. 2, pp. 1–24, 2019, doi: 10.3390/electronics8020199
- [20] C. W. Barson and K. J. Hardy, “Tyre and vehicle dynamics laboratory,” *SAE Tech. Pap.*, 1989, doi: 10.4271/890107
- [21] H. Pacejka, *Tire and Vehicle Dynamics*. 2012
- [22] L. Su, Z. Wang, and C. Chen, “Torque vectoring control system for distributed drive electric bus under complicated driving conditions,” *Assem. Autom.*, vol. 42, no. 1, pp. 1–18, Jan. 2022, doi: 10.1108/AA-12-2020-0194
- [23] K. Y. J Y Park, S Na, H Cha, “Direct Yaw Moment Control With 4WD Torque-Vectoring For Vehicle Handling Stability And Agility,” *Int.J Automot. Technol.*, vol. 23, pp. 555–565, 2022, [Online]. Available: <https://link.springer.com/article/10.1007/s12239-022-0051-9>
- [24] G. Park, K. Han, K. Nam, H. Kim, and S. B. Choi, “Torque Vectoring Algorithm of Electronic-Four-Wheel Drive Vehicles for Enhancement of Cornering Performance,” *IEEE Trans. Veh. Technol.*, vol. 69, no. 4, pp. 3668–3679, Mar. 2020, doi: 10.1109/tvt.2020.2978099
- [25] Q. Lu, A. Sorniotti, P. Gruber, J. Theunissen, and J. De Smet, “H $\infty$  loop

- shaping for the torque-vectoring control of electric vehicles: Theoretical design and experimental assessment,” *Mechatronics*, vol. 35, pp. 32–43, May 2016, doi: 10.1016/j.mechatronics.2015.12.005
- [26] E. Morera-Torres, C. Ocampo-Martinez, and F. D. Bianchi, “Experimental Modelling and Optimal Torque Vectoring Control for 4WD Vehicles,” *IEEE Trans. Veh. Technol.*, vol. 71, no. 5, pp. 4922–4932, 2022, doi: 10.1109/TVT.2022.3158091
- [27] J. Liang *et al.*, “An Energy-oriented Torque-vector Control Framework for Distributed Drive Electric Vehicles,” *IEEE Trans. Transp. Electrification*, pp. 1–1, 2023, doi: 10.1109/tte.2022.3231933
- [28] H. Wang, J. Han, and H. Zhang, “Lateral Stability Analysis of 4WID Electric Vehicle Based on Sliding Mode Control and Optimal Distribution Torque Strategy,” *Actuators*, vol. 11, no. 9, 2022, doi: 10.3390/act11090244
- [29] M. Vignati and E. Sabbioni, “A cooperative control strategy for yaw rate and sideslip angle control combining torque vectoring with rear wheel steering,” *Veh. Syst. Dyn.*, vol. 60, no. 5, pp. 1668–1701, 2022, doi: 10.1080/00423114.2020.1869273
- [30] R. Hajiloo, “Multi-Actuated Vehicle Control and Path Planning/Tracking at Handling Limits,” 2021
- [31] L. De Novellis, A. Sornioti, P. Gruber, L. Shead, V. Ivanov, and K. Hoeping, “EVS26 International Battery, Hybrid and Fuel Cell Electric Vehicle Symposium Torque Vectoring for Electric Vehicles with Individually Controlled Motors: State-of-the-Art and Future Developments.”
- [32] M. Dalboni *et al.*, “Nonlinear Model Predictive Control for Integrated Energy-Efficient Torque-Vectoring and Anti-Roll Moment Distribution,” *IEEE/ASME Trans. Mechatronics*, vol. 26, no. 3, pp. 1212–1224, Jun. 2021, doi: 10.1109/TMECH.2021.3073476
- [33] E. Katsuyama, M. Yamakado, and M. Abe, “A state-of-the-art review: toward a novel vehicle dynamics control concept taking the driveline of electric vehicles into account as promising control actuators,” *Veh. Syst. Dyn.*, vol. 59, no. 7, pp. 976–1025, 2021, doi: 10.1080/00423114.2021.1916048
- [34] J. Wang, S. Lv, N. Sun, S. Gao, W. Sun, and Z. Zhou, “Torque vectoring control of rwid electric vehicle for reducing driving-wheel slippage energy dissipation in cornering,” *Energies*, vol. 14, no. 23, pp. 0–16, 2021, doi: 10.3390/en14238143
- [35] J. Kim and H. Kim, “Electric vehicle yaw rate control using independent in-wheel motor,” *Fourth Power Convers. Conf. PCC-NAGOYA 2007 - Conf. Proc.*, pp. 705–710, 2007, doi: 10.1109/PCCON.2007.373043
- [36] M. Said Jneid, P. Harth, and Á. Török, “Coordinate Torque Vectoring

- Control For Enhancing Handling and Stability of All-Wheel-Drive Electric Vehicles Through Wheel Slip Control Integration,” *2023 IEEE Cogn. Mobil. Conf. (CogMob), Budapest, Hungary. Forthcomming., 2023*
- [37] J. Antunes, C. Cardeira, and P. Oliveira, “Torque Vectoring for a Formula Student Prototype,” in *Advances in Intelligent Systems and Computing*, 2018, vol. 694, pp. 422–433, doi: 10.1007/978-3-319-70836-2\_35
- [38] B. Peng, H. Zhang, and P. Zhao, “Research on the Stability Control Strategy of Four-Wheel Independent Driving Electric Vehicle,” *Engineering*, vol. 09, no. 03, pp. 338–350, 2017, doi: 10.4236/eng.2017.93018
- [39] G. Cong, J. Biao, and Z. Xin, “Research on Torque Control Strategy for Electric Vehicle with In-wheel Motor,” in *IFAC-PapersOnLine*, Jan. 2018, vol. 51, no. 31, pp. 71–74, doi: 10.1016/j.ifacol.2018.10.014
- [40] J. Antunes, A. Antunes, P. Outeiro, C. Cardeira, and P. Oliveira, “Testing of a torque vectoring controller for a Formula Student prototype,” *Rob. Auton. Syst.*, vol. 113, pp. 56–62, Mar. 2019, doi: 10.1016/j.robot.2018.12.010
- [41] B. Zhao, N. Xu, H. Chen, K. Guo, and Y. Huang, “Stability control of electric vehicles with in-wheel motors by considering tire slip energy,” *Mech. Syst. Signal Process.*, vol. 118, pp. 340–359, Mar. 2019, doi: 10.1016/j.ymsp.2018.08.037
- [42] X. Li, N. Xu, K. Guo, and Y. Huang, “An adaptive SMC controller for EVs with four IWMs handling and stability enhancement based on a stability index,” *Veh. Syst. Dyn.*, vol. 59, no. 10, pp. 1509–1532, Oct. 2021, doi: 10.1080/00423114.2020.1767795
- [43] W. Cao, Z. Liu, Y. Chang, and A. Szumanowski, “Direct Yaw-Moment Control of All-Wheel-Independent-Drive Electric Vehicles with Network-Induced Delays through Parameter-Dependent Fuzzy SMC Approach,” *Math. Probl. Eng.*, vol. 2017, 2017, doi: 10.1155/2017/5170492
- [44] L. Chen *et al.*, “Lateral Stability Control of Four-Wheel-Drive Electric Vehicle Based on Coordinated Control of Torque Distribution and ESP Differential Braking,” 2021, doi: 10.3390/act10060135
- [45] L. S. Sawaqed and I. H. Rabbaa, “Fuzzy Yaw Rate and Sideslip Angle Direct Yaw Moment Control for Student Electric Racing Vehicle with Independent Motors,” *World Electr. Veh. J.*, vol. 13, no. 7, pp. 1–12, 2022, doi: 10.3390/wevj13070109
- [46] Y. Lu, J. Lu, J. W. Wu, and B. Guo, “Study on the stability of high-speed turning braking based on the hardware-in-the-loop test,” *Teh. Vjesn.*, vol. 25, no. 1, pp. 210–215, 2018, doi: 10.17559/TV-20170720161424
- [47] H. Deng, Y. Zhao, A.-T. Nguyen, and C. Huang, “Fault-Tolerant Predictive Control With Deep-Reinforcement-Learning-Based Torque Distribution for Four In-Wheel Motor Drive Electric Vehicles,” *IEEE/ASME Trans.*

- Mechatronics*, pp. 1–13, 2023, doi: 10.1109/tmech.2022.3233705
- [48] G. Wang, Y. Liu, S. Li, Y. Tian, N. Zhang, and G. Cui, “New Integrated Vehicle Stability Control of Active Front Steering and Electronic Stability Control Considering Tire Force Reserve Capability,” *IEEE Trans. Veh. Technol.*, vol. 70, no. 3, pp. 2181–2195, Mar. 2021, doi: 10.1109/TVT.2021.3056560
- [49] L. Wei, X. Wang, L. Li, Z. Fan, R. Dou, and J. Lin, “T-S Fuzzy Model Predictive Control for Vehicle Yaw Stability in Nonlinear Region,” *IEEE Trans. Veh. Technol.*, vol. 70, no. 8, pp. 7536–7546, Aug. 2021, doi: 10.1109/TVT.2021.3091809
- [50] C. Li, Y. Xie, G. Wang, X. Zeng, and H. Jing, “Lateral stability regulation of intelligent electric vehicle based on model predictive control,” doi: 10.1108/JICV-03-2021-0005
- [51] Q. Wang, Y. Zhao, F. Lin, C. Zhang, and H. Deng, “Integrated control for distributed in-wheel motor drive electric vehicle based on states estimation and nonlinear MPC,” *Proc. Inst. Mech. Eng. Part D J. Automob. Eng.*, 2021, doi: 10.1177/09544070211030444
- [52] M. Ataei, A. Khajepour, and S. Jeon, “Model Predictive Control for integrated lateral stability, traction/braking control, and rollover prevention of electric vehicles,” *Veh. Syst. Dyn.*, vol. 58, no. 1, pp. 49–73, Jan. 2020, doi: 10.1080/00423114.2019.1585557
- [53] B. Huang, S. Wu, S. Huang, and X. Fu, “Lateral Stability Control of Four-Wheel Independent Drive Electric Vehicles Based on Model Predictive Control,” *Math. Probl. Eng.*, vol. 2018, 2018, doi: 10.1155/2018/6080763
- [54] S. Ding, L. Liu, and W. X. Zheng, “Sliding Mode Direct Yaw-Moment Control Design for In-Wheel Electric Vehicles,” *IEEE Trans. Ind. Electron.*, vol. 64, no. 8, pp. 6752–6762, Aug. 2017, doi: 10.1109/TIE.2017.2682024
- [55] K. Nam, “Application of novel lateral tire force sensors to vehicle parameter estimation of electric vehicles,” *Sensors (Switzerland)*, Vol. 15, No. 11, pp. 28385–28401, Nov. 2015, doi: 10.3390/s151128385

# Who should Communicate to Make the World a Greener Place? Car Brand Loyalty as an Essential Attribute of Pro-Environmental Education

**Jana Majerova<sup>1</sup>; Lubica Gajanova<sup>2</sup>, Margareta Nadanyiova<sup>1</sup>, Tibor Sipos<sup>3</sup>**

<sup>1</sup> AMBIS University, Department of Economics and Management, Lindnerova 575/1, 180 00 Prague, Czech Republic  
jana.majerova@ambis.cz; margareta.nadanyiova@ambis.cz

<sup>2</sup> University of Zilina, Faculty of Operation and Economics of Transport and Communications, Department of Economics, Univerzitna 1, 010 26 Zilina, Slovak Republic; lubica.gajanova@fpedas.uniza.sk

<sup>3</sup> Budapest University of Technology and Economics, Department of Transport Technology and Economics, senior lecturer. Dr PhD. sipos.tibor@kjk.bme.hu

---

*Abstract: This article aims to investigate the socio-economic nature of car brand loyalty. The hypothesis is that brand loyalty is a complex structure with a complicated socio-economic background. Nowadays, massive research is focused mainly on the psychographic background of the brand loyalty phenomenon. However, a socio-economic aspect of consumers is also entering into brand loyalty creation. It is supposed that brands with loyal consumers have more educative strength than brands where brand loyalty is missing. As it is challenging to identify consumers with a psychographic profile suitable for loyal brands, the changes in consumer behaviour are hard to reach. However, if the socio-economic profile of loyal consumers is detected, environmental education can be focused precisely and with higher effectiveness. Some preliminary data have been collected in Slovakia to investigate the socio-economic background of car brand loyalty. To collect these data, a questionnaire survey has been used. It was realised in the last quarter of the year 2021 on the sample of 2035 Slovak inhabitants older than 15 years. Statistical analysis has been provided via a decision tree approach. It has been found that two relevant factors significantly influence brand loyalty - respondents' age and income. Based on these findings, it can be stated that, in general, brands with the higher pro-environmental communication potential in the case of the Slovak Republic are Škoda, Audi and BMW. An approach that includes the strength of pro-environmental orientation of consumers (focusing on age categories) confirms this order. However, in the case of the income perspective, Peugeot's list of car brands should be extended, which has been surprisingly identified as a car brand with the potential to be used widely in the scope of pro-environmental education in specific area's conditions in the Slovak Republic.*

*Keywords: brand loyalty; branding, car brand; green marketing; environmental education*

---

## 1 Introduction

The need for sustainable development should be the imperative of corporate existence in contemporary markets [1]. Corporate mature sustainable activity has a positive effect on resilience or financial performance and ensures protection against economic downturns caused by various types of crises [2]. Among other things, even future industry 6.0 focuses on sustainability [3]. Thus, even though many companies who own reputable brands across a variety of sectors invest much money to the socially responsible projects focused on changing the consumer behaviour in favour of green products and pro-environmentally oriented technologies, the situation worldwide remains without any significant change if the legislative stimulus for such behaviour is not applied [4].

Although the perspective of sustainable activity of enterprises is not as pessimistic it has used to be [5], the shift in pro-environmental orientation is still more formal than real [6]. It means that, despite the corporate effort (corporate social responsibility) and changes in consumer behaviour (personal social responsibility) the real effect is still low – or at least slower in progress than it would be required [7, 8].

One of the possible reasons for such a situation can be the absence of connection and relationship between sender and relevant receiver of the message. In detail, even if the message is well formulated, the communication with educational background is not effective if the receiver of the message is not perceptive to the message. One of the factors which can positively affect the perceptiveness of the receiver of the message is brand loyalty [9]. There are two fundamental dimensions of the relationship between the sender and the receiver of educational messages: 1) receivers are willing to be influenced by the brands to which they are loyal, and 2) only brands with loyal consumers are prospective efficient message senders. Thus, there is a close relationship between the brand and its loyal consumer in positions of educator and educated. Although contemporary scientific literature states this relationship, the more profound analysis of relevant brand educators with a significant impact on consumer buying behaviour in environmentally harmful sectors is missing [10]. Individual transport belongs to the category of environmentally most harmful sectors [11] due the fact that the transportation sector is one of the largest emitters of CO<sub>2</sub> [12] and is growing steadily [13].

There are two main ideological flows focused on the environmental harming effect of passenger car usage: 1) emissions and 2) urban factors. While the second focuses on excluding individual passenger cars from the city centres, the first one

has a less ambitious goal – if the left of car usage is impossible, then at least less harmful fuel technologies should be used [14].

Although consumers are aware of the pro-environmental benefits of abandoning traditional combustion fuels and preferring public transport, respectively, car-sharing, their real buying decisions still dominate existing patterns, and new fuel technologies are accepted with suspicion [15]. Sustainable buying behaviour is traditionally discussed in the scope of 1) food consumption and 2) package and recycling [16, 17].

The situation is that while many types of research focus on the psychological background of the buying behaviour (trying to analyse pro-environmental buying decisions ex-post) [18], the ex-ante analysis would be much highly appreciated to predict the buying behaviour and to create a more effective platform to influence it in the required way. As a consequence of this need, the profile of green consumers is analysed. Contemporary, mainly: 1) generational and 2) national approaches are used [19, 20]. However, the sector analysis is quite fragmented – luxury goods, services and physical products [21-24]. Surprisingly, such an approach is not massively used in the most polluting sectors [25].

Most of these analyses apply the psychographic approach [26]. On the one hand, such a fact is entirely understandable as the motivation to pro-environmental behaviour is more behavioural than cognitive, on the other hand, the strong potential of the socio-economic perspective is missing. Thus, the phenomenon of green persona is mainly connected with psychographic characteristics, which are problematic to be detected when any communication activity with educational potential is planned [27].

Many car brands focus their innovative activities on achieving sustainable goals and being environmentally oriented [28, 29]. Although many car producers are aware of the need to act pro-environmentally as a sign of their corporate citizenship, their effort is enormous, and their investments are not turning back. The reason is that consumers are sceptic, and they are still preferring traditional technological solutions. In this situation, car producers' intrinsic and extrinsic motivation decreases, and their effort is stimulated mainly by national governments and international pro-environmental legislation. Thus, a shift in buying behaviour patterns is required. It has been highlighted that a possible way to reach goals set on the platform of sustainable development is systematic education of consumers and legal stimulation of companies [30-32]. Thus, the only possible way to reach this status is to educate the consumers and act strategically. However, this education should not lie on the shoulders of the educational systems, and there should be an active, practical approach to the corporate sphere itself [33-35].

The strong educative potential of valuable brands has been already detected [36-37]. On the other hand, the educative potential of brands with loyal consumer platforms has been just slightly indicated [38]. Traditionally, brand loyalty is

discussed in the scope of its individual value sources – mainly relevant factors of brand attributes, attitudes, benefits and imageries [39]. The socio-economic analysis of the profile of loyal consumers is rather exceptional. Thus, it is not essential to identify brand loyalty sources (in the case of branding, yes, it is), but the socio-economic profile of loyal consumers. And not only this. Also, the status of the brand has loyal consumers. Unfortunately, not each brand considered valuable also has a reliable consumer platform. This explains shifts in brand value ranking and its sensitivity to changes in the macro-environment.

Therefore, the study presented in this paper aims to investigate the socio-economic nature of car brand loyalty. Thus, significant educators and educated can be determined to achieve higher environmental engagement of consumers. The article is structured as follows: the methodology is described after the introduction and literature review that forms the research question. In the methodology section, the detailed statistical tools of survey assessment are written. The results are being analysed and compared with contemporary scientific literature in the results and discussion part. Finally, the conclusion is drawn where the managerial implications, limits and barriers of the research and possible future research directions in this area are highlighted.

## 2 Methodology

The questionnaire survey, which is the elementary data source for the own analysis has been realised via the CAWI method in the last quarter of the year 2021 on the sample of 2035 respondents – Slovak inhabitants older than 15 years. Such an age limit has been set because the survey has been widely focused on four specific product categories, which represent quadratic concepts of buying behaviour patterns (complex buying behaviour, dissonance-reducing buying behaviour, habitual buying behaviour and variety-seeking behaviour). The basic presumption for statistic sample creation was the autonomous buying behaviour of respondents. This can be assumed from 15 years of age in the Slovak Republic as this is the legal limit for entering into labour law relations. Car brands have been chosen as adequate representatives for complex buying behaviour where the consumer's involvement is high and the differences between brands are low. For such a large sample size, sample distribution approximates a normal distribution, which a central limit theorem can prove. The questionnaire has been composed of two parts: (1) socio-demographic profile of respondents and (2) individual brand value sources perception in selected categories of representatives of buying behaviour patterns.

Statistical analysis has been provided via a decision tree approach. Decision trees are widely used machine learning methods that find their application in classification and regression tasks. In principle, it is a hierarchical, multi-stage

binary decision making system in which the fulfilment / non-fulfilment (if / else) of decision criteria or conditions is gradually evaluated until it is reached an accepted class or solution. The decision making process proceeds from the tree's root gradually through the individual nodes, which form branches with leaves. Although there are several different types of decision trees, the creation of tree structures is mainly governed by the fact that the decision criteria in the individual nodes are arranged according to information importance. The flag or criterion that has the most weight and allows you to best separate the input data into two binary classes (yes / no) becomes the root of the tree. The other nodes are gradually made up of the remaining criteria with less weight, with each node creating two binary descendants. The decision making process follows the individual branches of the tree until we reach the required class or solution (leaf).

The decision tree is a structure used to divide a large set of cases (cases are statistical units, in our consumer analysis) in a database into smaller sets of cases with the gradual application of simple decision rules. The decision tree consists of rules - rules (rules are relationships between variables) to divide a large heterogeneous population into smaller, more homogeneous groups (a group of cases is called a node) concerning the relevant output variable. When creating a decision tree, the criteria divided into individual nodes are critical. The criterion based on which the variable to be used at the appropriate branch level is selected depends on the nature of the output variable. The basic idea of tree growth is related to the theory of data purity. The criterion for selecting a branch is to increase the purity of the child nodes (a net node is considered to contain only cases of one class of output character).

Decision trees are used to identify groups discover relationships between them. It features visual classification to categorise the results and more clearly explain the analysis. Create classification models for segmentation, stratification, data reduction and variable screening. In this case, an ordinary top-down auto-scale decision tree was used, where the decision parameters were sex, age category, education level, size of the city, number of members of the household, and the dependent variable was car brand. A statistical multi-way tree algorithm was used to ensure that every combination of predictor variables was investigated and only the effective combination was visualised. The CHAID (Chi-Square Automatic Interaction Detection) algorithm checked the cross-correlation between predictor variables to examine all possible splits for each predictor (independent) variable category. CHAID creates all possible cross-tabulations for each categorical predictor until the best outcome is achieved, and no further splitting can be performed.

We used entropy as a branching criterion in the case of decision trees, which we created on data sets from market research. The entropy concept is often applied objective weighting method, which works based on recognising the best splitting attribute [40-42]. The entropy model is often used as a typical method of quantifying contamination while the randomness or impurity of data sets is

qualified by the decision tree [43]. When defining entropy, we consider a training set of  $n$  cases. The value of input character  $A$  describes each case, and the value output character  $Y$ . Let the input character take the values  $a_i$  ( $i=1,2,\dots,k$ ) and let the output character  $m$  have different values - classes  $y_j$  ( $j=1,2,\dots,m$ ). Let the probabilities of occurrence of the class  $y_j$  ( $j=1,2,\dots,m$ ) of the output character  $Y$  denote  $p_j$  ( $j=1,2,\dots,m$ ). The entropy of the output character  $Y$  can be expressed in the Equation (1):

$$H(Y) = - \sum_{j=1}^m (p_j \log_2 p_j) \quad (1)$$

where  $p_j$  is the probability of occurrence of class  $j$  of the output character.

The probabilities  $p_j$  can be estimated using relative abundances:  $\frac{n_j}{n}$ , where  $n_j$  is the absolute abundance of class  $y_j$  ( $j=1,2,\dots,m$ ) in a set of training cases. We then adjust Equation 1 to Equation (2):

$$H(Y) = - \sum_{j=1}^m \left( \frac{n_j}{n} \log_2 \frac{n_j}{n} \right) \quad (2)$$

Entropy is measured between 0 and 1. Entropy is a measure of disorder or uncertainty. When branching, the variable with the lowest entropy value (attribute information value rate) is used; therefore, finally, the combination of the lowest entropy variables leads to the lowest entropy model. Because if it is known how to measure disorder, it was evident that the reduction of disorder (RD) in our dependent variable due to the additional information (independent variable) can also be measured see Equation (3):

$$RD(Y) = H(Y) - H(Y|X) \quad (3)$$

This can be easily derived from Chi-Square Automatic Interaction Detection.

### 3 Results and Discussion

In the questionnaire, there were 2035 respondents country-wide. Of all the respondents, 49,9 % were male, and 50,1% were female. Their age distribution is shown in Figure 1.

Detailed analysis of the questionnaire showed a significant spatial difference in passenger car brand preference, but choosing no car was insignificant that strengthened the status symbol idea. The detailed systematic analysis showed that spatial-socio-economic parameters have a significant effect on the chosen brand of passenger cars (Figure 2).

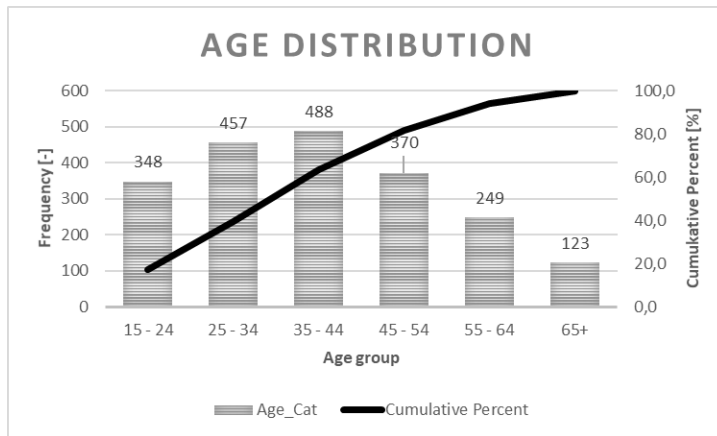


Figure 1

Age distribution in survey

Based on the decision tree analysis, two significant factors could be determined: the respondent's age and income could significantly influence brand loyalty. The Pareto solution of the decision tree can be seen in Figure 3.

Based on the research results, age and income are significant parameters of brand value recognition in the case of Slovak consumers. Thus, the educational activity of car brands should be realised following the finding that the brand loyalty phenomenon in the case of consumers under 35 years are influenced simply by this characteristic. In comparison, income is another relevant characteristic in the case of consumers above 35 years. In other words, in the case of younger consumers, their loyalty is not connected with their financial status. This fact is significant in the case of prospective pro-environmental orientation studying. As it has been already stated that typical green consumer is from Generation Z (those born since 1997) or from the generation of so-called Millennials (those born between 1981 and 1996), the future of pro-environmental orientation of passenger car consumers is green [36]. It declares the generational approach of Mosehpour et al. [19]. Consumers are not influenced by their income when considering brand loyalty. It means that: 1) their price sensitivity is less and 2) if there is no disposable income, the branded product would not be purchased, but the consumer would remain still loyal. From the point of view of the passenger car brands (and their sales goals), where higher prices manifest the pro-environmental innovations, the income parameter is still crucial, while from the point of view of general pro-environmental attitude, this situation is beneficiary. In this aspect, Silvestre & Tirca theory has been verified [28]. They have stated that many car brands focus their innovative activities on achieving sustainable goals and being environmentally oriented.

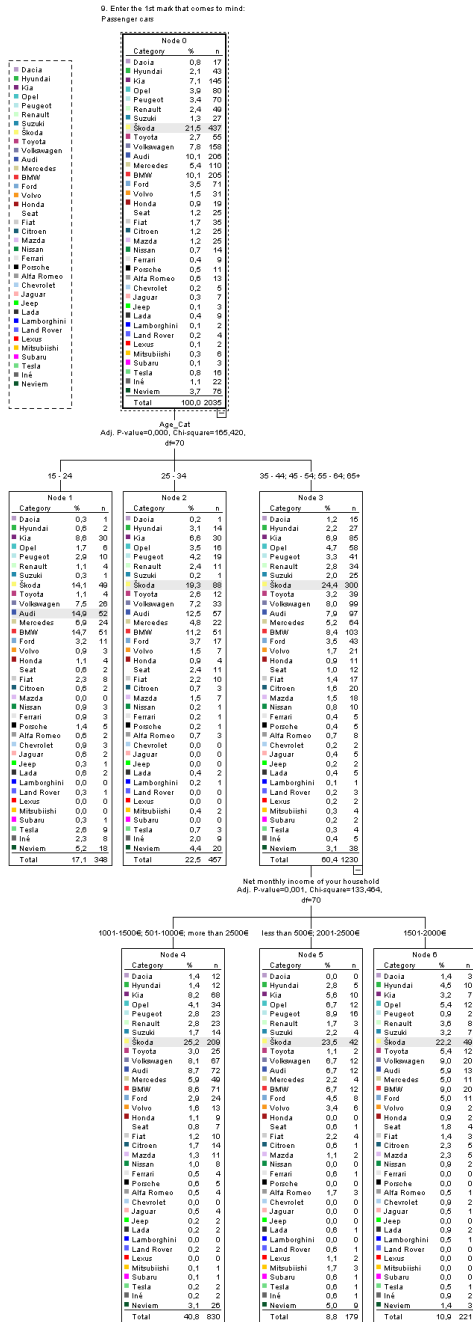


Figure 2  
Visualisation of decision tree

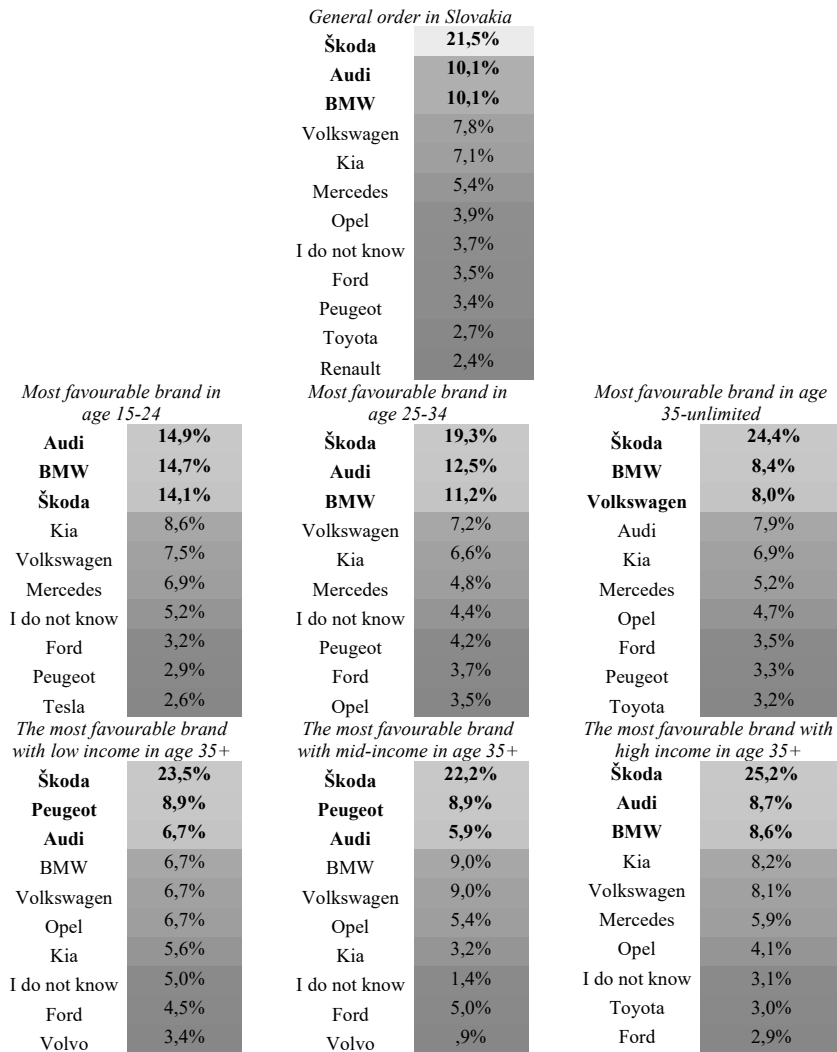


Figure 3

Node components of decision tree based on survey results

*\*Please note that as Pareto solution, only 80% of cumulative relative frequency were shown*

Consumers from younger generations (Generation Z and Millennials under 35 years) are surprisingly loyal to brands sold for prices above their disposable. It means that even though the purchasing experience of such consumers is missing in many cases, the brands are detected as highly valuable from the point of view of this category of consumers. Thus, a simultaneous special effect could be observed – as these consumers are not loyal based on their previous purchasing experience, a possible source of loyalty lies in the convergence of the pro-

environmental orientation of these brands and the generational green orientation. Such loyalty can be considered a special symbolic relationship between consumer and brand. From this point of view, Audi, BMW and Škoda are socially beneficial as they have solid educative potential towards consumers under 35 years and can be considered attitude makers in the broader perspective. That means that the trends they set are accepted by loyal consumers and transmitted to their consumer behaviour in the scope of other product categories. However, the environmental load of passenger car usage is not solved in such a case. At least not by switching to the usage of environmentally innovative cars produced by these brands.

On the other hand, possible side-effects can increase car sharing or public transport usage. While the situation in case of consumers under 35 years is quite clear – this category of consumers tends to pro-environmental purchasing behaviour and car brands with whose they are loyal to, strengthen this attitude generally (regardless of real purchasing decisions in favour of these brands), in case of age category above 35, the situation is different. Here, income is also a significant phenomenon of brand loyalty, and thus, the spectrum of car brands where consumer loyalty could be detected is broader. Therefore, if the consumer is above 35, also the income matters and instead of BMW, for this category of consumers from low or middle-income class, Peugeot is a car brand with a significant prospective impact on the pro-environmental purchasing and consumer attitudes. This potential has not been significantly recognised and used so far. Thus, the Peugeot car brand could solve environmental damages caused by traditional combustion engine passenger car usage by focusing more on eco-innovations and educating loyal consumers in favour of higher environmental engagement of their purchasing behaviour. Summarising the above-mentioned, for the consumers under 35 years, the most relevant car brands with educative potential are Audi, BMW and Škoda regardless of their income categories, while for the consumers above 35 years, the income category is relevant. Thus, the identified loyal car brands Audi, BMW and Škoda are capable of influencing the pro-environmental purchasing behaviour of a high-income category of consumers, while in the case of low and middle-income categories, BMW is replaced in the scope of loyalty ranking by Peugeot. In this aspect, the importance of Peugeot is even more remarkable because this category of consumers does not belong to the category of green consumers and thus, as Peugeot is considered a valuable brand, its loyal consumers are willing to buy it regardless of its eco orientation. Thus, it has been extended the theory of Xiao *et al.* has just slightly indicated the educative potential of brands with reliable consumer platforms [38].

While the managerial implications are apparent, some limitations should be accepted. Thus, the results are not generally applicable without reconsidering the specifics of the national environment. Even though it has been detected that psychographic specifics are not taken into account, instead of them, attention is paid to the socio-economic nature of brand loyalty, the psychographic nature of the market cannot be abandoned, primarily because of different levels of eco-

awareness and distribution of capital in the society. In other words, the research results should be revised before applying them in specific national market conditions. In this aspect, tradition and the brand's long-term image in society can be considered an essential pillar of brand loyalty. In the case of, the Slovak Republic, it is visible in the case of the Škoda car brand, which is still considered a former national brand due to the common socio-political development of the Czech and Slovak Republic during the 20<sup>th</sup> Century.

Similarly, from the psychographic point of view, this brand has a robust love brand status because of the very dominant position of this car brand in Slovak families in the past. However, this phenomenon is evident mainly in the case of older consumers (35 years and more). In the future, the aim of the study could be extended, and a deeper analysis of car brand innovation and educational activities should be realised. In such a case, it would be confirmed whether the innovative and educational activities are homogeneous across the age and impact categories as in the case of Audi, BMW and Škoda for consumers under 35 or Audi, Peugeot and Škoda for low and middle-income consumers above 35. If not, it would be helpful to be detected because of the theory and practice of eco-educational activities oriented to consumers. So far, it has been mainly stated the non-effectiveness of certain eco-education in general and not in a broader perspective that should explain the internal variability of eco-educational activities.

### **Conclusions**

This paper aimed to investigate the socio-economic nature of car brand loyalty. It has been supposed that brands with loyal consumers have more considerable educative strength than brands lacking brand loyalty. The data for the research has been collected in Slovakia to investigate the socio-economic background of car brand loyalty. To collect these data, a questionnaire survey has been used. It was realised in the last quarter of the year 2021 on the sample of 2035 Slovak inhabitants older than 15 years. Statistical analysis has been provided via a decision tree approach. It has been detected two significant parameters – age and income.

Based on these findings, it can be stated that for the consumers under 35 years, the most relevant car brands with educative potential are Audi, BMW and Škoda regardless of their income categories, while for the consumers above 35 years, the income category is relevant. Thus, the identified loyal car brands Audi, BMW and Škoda can influence only the pro-environmental purchasing behaviour of the high-income category of consumers. In contrast, in the case of low and middle-income categories, BMW is replaced in the scope of consumer loyalty ranking by Peugeot. In the scope of the above-mentioned, Audi, BMW, and Škoda are socially beneficial as they have solid educative potential towards consumers under 35 years and can be considered attitude makers in the broader perspective. That means that the trends they set are accepted by the platform of loyal consumers and transmitted by them to their consumer behaviour also in the scope of other product

categories. On the other hand, the importance of Peugeot is even more significant because consumers over 35 years do not belong to the category of green consumers, and thus, as Peugeot is considered a valuable brand, its loyal consumers are willing to buy it regardless of its eco orientation. Here, not only the educative but eco-innovative potential is equally important.

### Acknowledgement

The research was supported by OTKA - K21 - 138053- Life Cycle Sustainability Assessment of road transport technologies and interventions by Mária Szalmáné Dr. Csete.

### References

- [1] Friedman, A. (2019) Sustainable Development Past and Future. *Vitruvio-International Journal of Architectural Technology and Sustainability*, 4(1), VII–VIII. <https://doi.org/kgp6>
- [2] Lu, J., Rodenburg, K., Foti, L., & Pegoraro, A. (2022) Are firms with better sustainability performance more resilient during crises? *Business Strategy and the Environment*, 31(7), 3354-3370, <https://doi.org/kgp7>
- [3] Chourasia, S., Tyagi, A., Pandey, S., Walia, R. S., & Murtaza, Q. (2022) Sustainability of Industry 6.0 in Global Perspective: Benefits and Challenges. *Mapan-journal of Metrology Society of India*, 37(2), 443-452, <https://doi.org/kgp8>
- [4] Hanaysha, J. R., & Al-Shaikh, M. E. (2021) An examination of customer relationship management dimensions and employee-based brand equity: A study on ride-hailing industry in Saudi Arabia. *Research in Transportation Business & Management*, 43, 100719, <https://doi.org/grxj7v>
- [5] Haliscelik, E., & Soytaş, M. A. (2019) Sustainable development from millennium 2015 to Sustainable Development Goals 2030. *Sustainable Development*, 27(4), 545-572, <https://doi.org/gh2d3k>
- [6] Kiausiene, I. (2019) Sustainable Development: Theory and Practice. *Transformations in Business & Economics*, 18(2), 343-347
- [7] Majerova, J. (2022) Cognitive rationality and sustainable decision based on Maslow's theorem: A case study in Slovakia. *Cognitive Sustainability*, 1(1) <https://doi.org/jf2k>
- [8] Hamadneh, J., & Esztergár-Kiss, D. (2021) Potential travel time reduction with autonomous vehicles for different types of travellers. *Promet - Traffic & Transportation*, 33(1), 61-76, <https://doi.org/kgqb>
- [9] Huang, Y. C., & Liu, C. H. (2020) Buffering effects of brand perception to behavioural intention-Evidence of China airlines. *Research in Transportation Business & Management*, 37, 100468, <https://doi.org/kgqc>

- [10] Laming, C., & Mason, K. (2014) Customer experience—an analysis of the concept and its performance in airline brands. *Research in Transportation Business & Management*, 10, 15-25, <https://doi.org/kgqd>
- [11] Chlad, M. (2020) Elements of sustainable development in selected European Union countries. *Ekonomia I Prawo-Economics and Law*, 19(3), 435-447, <https://doi.org/kgqf>
- [12] Strömblad, E., Winslott Hiselius, L., Smidfelt Rosqvist, L., & Svensson, H. (2022) Characteristics of Everyday Leisure Trips by Car in Sweden – Implications for Sustainability Measures. *Promet – Traffic & Transportation*, 34(4), 657-672, <https://doi.org/grc28t>
- [13] Wu, N., & Liu, Y. (2023) Potential of Ecological Benefits for the Continuous Flow Intersection. *Promet – Traffic & Transportation*, 35(1), 106-118, <https://doi.org/kgqg>
- [14] Selzer, S., & Lanzendorf, M. (2019) On the Road to Sustainable Urban and Transport Development in the Automobile Society? Traced Narratives of Car-Reduced Neighborhoods. *Sustainability*, 11(16), 4375, <https://doi.org/gg22sn>
- [15] Aguilar, A., Twardowski, T., & Wohlgemuth, R. (2019) Bioeconomy for Sustainable Development. *Biotechnology Journal*, 14(8), 1800638, <https://doi.org/gmnn2b>
- [16] Nosi, C., Zollo, L., Rialti, R., & Ciappei, C. (2020) Sustainable consumption in organic food buying behavior: The case of quinoa. *British Food Journal*, 122(3), 976-994, <https://doi.org/kgqj>
- [17] Pinto, D. C., Herter, M. M., Rossi, P., Nique, W. M., & Borges, A. (2019) Recycling cooperation and buying status Effects of pure and competitive altruism on sustainable behaviors. *European Journal of Marketing*, 53(5), 944-971, <https://doi.org/kgqk>
- [18] Nica, E. (2020) Buying organic food as sustainable consumer decision-making behavior: Cognitive and affective attitudes as drivers of purchase intentions toward environmentally friendly products. In T. Kliestik (Ed.), *19th International Scientific Conference Globalization and Its Socio-Economic Consequences 2019—Sustainability in the Global-Knowledge Economy (Vol. 74, 04018)* EDP Sciences, <https://doi.org/kgqm>
- [19] Moslehpour, M., Chaiyapruk, P., Faez, S., & Wong, W.-K. (2021) Generation Y's Sustainable Purchasing Intention of Green Personal Care Products. *Sustainability*, 13(23), 13385, <https://doi.org/kgqn>
- [20] Zhao, L., Lee, S. H., & Copeland, L. R. (2019) Social media and Chinese consumers' environmentally sustainable apparel purchase intentions. *Asia Pacific Journal of Marketing and Logistics*, 31(4), 855-874, <https://doi.org/gkzf7m>

- [21] Jain, S. (2019) Factors Affecting Sustainable Luxury Purchase Behavior: A Conceptual Framework. *Journal of International Consumer Marketing*, 31(2), 130-146, <https://doi.org/gkct29>
- [22] Maesano, G., Carra, G., & Vindigni, G. (2019) Sustainable Dimensions of Seafood Consumer Purchasing Behaviour: A Review. *Quality-Access to Success*, 20, 358-364
- [23] Morales-Contreras, M.-F., Bilbao-Calabuig, P., Meneses-Falcon, C., & Labajo-Gonzalez, V. (2019) Evaluating Sustainable Purchasing Processes in the Hotel Industry. *Sustainability*, 11(16), 4262, <https://doi.org/ghrg7h>
- [24] Andrejszki, T., Torok, A., & Csete, M. (2015) Identifying the utility function of transport services from stated preferences. *Transport and Telecommunication Journal*, 16(2), 138-144, <https://doi.org/gm39>
- [25] Hoerler, R., van Dijk, J., Patt, A., & Del Duce, A. (2021) Car-sharing experience fostering sustainable car purchasing? Investigating car size and powertrain choice. *Transportation Research Part D-Transport and Environment*, 96, 102861, <https://doi.org/gjw2nb>
- [26] Mandliya, A., Varyani, V., Hassan, Y., Akhouri, A., & Pandey, J. (2020) What influences intention to purchase sustainable products? Impact of advertising and materialism. *International Journal of Productivity and Performance Management*, 69(8), 1647-1669, <https://doi.org/gg7xxm>
- [27] Hameed, I., Hyder, Z., Imran, M., & Shafiq, K. (2021) Greenwash and green purchase behavior: An environmentally sustainable perspective. *Environment Development and Sustainability*, 23(9), 13113-13134, <https://doi.org/kgqq>
- [28] Silvestre, B. S., & Tirca, D. M. (2019) Innovations for sustainable development: Moving toward a sustainable future. *Journal of Cleaner Production*, 208, 325-332, <https://doi.org/gf8t8r>
- [29] Niklas, U., von Behren, S., Eisenmann, C., Chlond, B., & Vortisch, P. (2019) Premium factor—Analyzing usage of premium cars compared to conventional cars. *Research in Transportation Business & Management*, 33, 100456, <https://doi.org/kgqr>
- [30] Tunçel, N. (2021) Intention to purchase electric vehicles: Evidence from an emerging market. *Research in Transportation Business & Management*, 43, 100764, <https://doi.org/gqnmjz>
- [31] Kostrzewski, M., Filina-Dawidowicz, L., & Walusiak, S. (2021) Modern technologies development in logistics centers: the case study of Poland. *Transportation Research Procedia*, 55, 268-275, <https://doi.org/kgqs>
- [32] Tare, M. (2020) Education for Sustainable Development. *Technology & Innovation*, 21(4), 1-3, <https://doi.org/kgqt>

- [33] Ekka, B. (2021) Book Review: Engaging Youth in Sustainable Development: Learning and Teaching Sustainable Development in Lower Secondary Schools. *Journal of Education*, 203(2), 489-490, <https://doi.org/kgqv>
- [34] Östman, L., Van Poeck, K., & Öhman, J. (2019) Principles for sustainable development teaching. In *Routledge eBooks* (pp. 40-55) <https://doi.org/kgqz>
- [35] Rezende, E. N. (2020) Environmental Law and Sustainable Development. *Veredas Do Direito*, 17(37), 7-10, <https://doi.org/kgq3>
- [36] Agbedahin, A. V. (2019) Sustainable development, Education for Sustainable Development, and the 2030 Agenda for Sustainable Development: Emergence, efficacy, eminence, and future. *Sustainable Development*, 27(4), 669-680, <https://doi.org/gjimpnv>
- [37] Headley, S. da S., & Sena de Souza, M. A. (2020) Do Label Information Influence the Choice of Sustainable Products? A Study of Buying Behavior Among University Students. *Revista Metropolitana De Sustentabilidade*, 10(2), 119-145
- [38] Xiao, Z., Wang, Y., Ji, X., & Cai, L. (2021). Greenwash, moral decoupling, and brand loyalty. *Social Behavior and Personality*, 49(4), e10038, <https://doi.org/kgq8>
- [39] Kliestikova, J., Kovacova, M., Krizanova, A., Durana, P., & Nica, E. (2019) Quo Vadis Brand Loyalty? Comparative Study of Perceived Brand Value Sources. *Polish Journal of Management Studies*, 19(1), 190-203, <https://doi.org/kgq9>
- [40] Gulati, P., Sharma, A., & Gupta, M. (2016) Theoretical Study of Decision Tree Algorithms to Identify Pivotal Factors for Performance Improvement: A Review. *International Journal of Computer Applications*, 141(14), 19-25, <https://doi.org/kgrb>
- [41] Li, M., Xu, H., & Deng, Y. (2019) Evidential Decision Tree Based on Belief Entropy. *Entropy*, 21(9), 897, <https://doi.org/kgrc>
- [42] Zhang, Y., & Yang, G. (2020) Application of Decision Tree Algorithm Based on Clustering and Entropy Method Level Division for Regional Economic Index Selection. In *Springer eBooks* (pp. 45-56) <https://doi.org/kgrd>
- [43] Kumar, S., Rajamanickam, N., Aparna, P., & Avanija, J. (2023) Concepts And Techniques Of Data Mining. AG PUBLISHING HOUSE (AGPH Books)

# Cost Efficient Training Method for Artificial Neural Networks based on Engine Measurements

**Márton Virt, Máté Zöldy**

Department of Automotive Technologies  
Budapest University of Technology and Economics  
Stoczek u. 6, H-1111 Budapest, Hungary  
e-mail: virt.marton@edu.bme.hu, zoldy.mate@kjk.bme.hu

---

*The artificial intelligence is an accurate predictive tool for different kinds of internal combustion engine (ICE) applications. However, the training process can be expensive due to the high computational and measurement costs. This work aims to describe a general methodology that can be applied to cost-efficiently train multilayer perceptron type artificial neural networks with measurement data from ICEs. The created methodology is based on analyses of a high-resolution dataset measured on a commercial diesel engine. Different methods and recommendations are presented for the model creation, evaluation, training method selection, input feature selection and architecture selection. In addition, a method is described in order to select the appropriate measurement resolution that provides proper information for training with minimal fuel consumption. The investigation showed that the presented workflow can reduce calculation time and fuel consumption, while maintaining good model accuracy. The method can be applied for any ICE related artificial neural network problems, but it can also be an aide for other research fields.*

*Keywords: Artificial Neural Networks; Internal Combustion Engines; Methodology; Cost Reducing*

---

## 1 Introduction

The ambitious goals of the Paris Agreement has a major effect on the climate policy of the European Union (EU). In order to keep the global warming well below 2°C, the EU is devoted to achieve climate neutrality by 2050 [1]. The Fit for 55 package is a set of proposals that is dedicated to cut greenhouse-gas emissions until 2030 by at least 55% compared to the 1990 level [2, 3, 4]. To meet these climate targets, tremendous efforts and investments are required in many sectors, including the transport sector. The first provisional agreement of the Fit for 55 package was made in 2022. This indicates carbon neutrality for the new

passenger cars and light commercial vehicles by 2035. The original proposal considers tailpipe CO<sub>2</sub> emissions only, thus this can be considered a ban for internal combustion engines (ICE) for these vehicle types [5]. This proposal set off many arguments, since a more holistic view is required to properly define carbon neutrality [6]. Besides the local CO<sub>2</sub> emission, the CO<sub>2</sub> emission of the full lifecycle and the Well-to-Wheel (WTW) CO<sub>2</sub> emission also has to be considered, which means that the internal combustion engines operated with e-fuels can also be climate neutral. Currently the political situation changes dynamically. At this point, the EU decided to permit the registration of new ICE cars after 2035 if they are operated with e-fuels.

From a technical point of view, the electrification is the best solution for applications, where the local pollutant emission has to be minimal. Therefore, the rapid electrification is a good solution for most of the passenger car use cases [7]. Since people have most of their personal experience with passenger cars, the simplest political message for campaigning is to provoke electrification in all segments of transportation. From engineering perspective this is an inadequate solution to achieve climate neutral transportation because there are many segments where the current maturity of the battery technology is insufficient [8]. Among other technologies, the sustainable advanced fuels are crucial to achieve true carbon neutral mobility. For applications, where the mass and volume of the energy storage system is critical, the low energy density of the batteries is problematic. This means that e-fuels can be the best short and medium-term solution for aviation, heavy-duty vehicles and road public transport. For applications where high amount of stored energy is required, such as sailing, the high demand for lithium and other expensive rare materials also limits the usability of batteries. The full elimination of ICE from passenger cars will also be a slow process, especially if the entire world's vehicle fleet is considered. The advanced fuels can help to achieve climate neutrality of passenger cars in this transition period, and they can also reduce the pollutant emission by realizing cleaner combustion.

The aspects described above support the urgent need to develop cheap and sustainable advanced fuels [9]. However, it is challenging to creating new advanced fuel compositions [10, 11]. Usually, time-consuming and complex simulations are necessary to model the fuels' effect on the combustion and emission. The applied tools are expensive and deep knowledge – therefore expensive labor is necessary to build and use the simulation models [9]. The artificial intelligence (AI) could provide an alternative approach to efficiently develop new climate neutral fuels. The AI does not require any knowledge on the real physical or chemical processes due to its empirical nature. Once a representative training dataset is available with the proper input and output features, the AI can learn the processes. Then, it can accurately predict the behavior of the investigated system.

The artificial neural networks (ANN) are among the most common AI methods. The structure of this algorithm is similar to the human brain. The inputs of the biological neurons are the dendrites and the output of them is the axon. Once the sum of the incoming electric signals from other neurons reach a certain threshold, the neuron discharges through its axon towards other neurons. The behavior of a neuron can be modelled with a weighted adder. Each connection between artificial neurons has a weight, and a neuron calculates the weighted sum of the incoming signals. Then, the output of a neuron will be modified by an activation function, and the next neuron will get this activation as its input. ANNs are trained with back propagation (BP) algorithms. These are iterative methods that modify the weights (and biases) of the network in order to reduce the error between the desired and actual output values. The most conventional ANN type for ICE related tasks is the multilayer perceptron (MLP) type neural network. This network has an input layer with the defined input features, and an output layer with neurons that calculate the final values of the output features. Between the input and output layer there is at least one hidden layer with a certain number of neurons. Every neuron of a layer is connected to all of the neurons of the next layer. An MLP network with at least one hidden layer is a universal approximator, thus it can be applied to nonlinear problems as well.

Many articles demonstrated the high accuracy of MLP networks for ICE parameter predictions. [12] successfully used an ANN model to accurately estimate soot concentrations in laminar diffusion flames. Authors of [13] trained a MLP network with steady-state  $\text{NO}_x$  emission measurements and then they validated it with transient data. The created model performed extremely well on the steady-state dataset with a correlation coefficient (R) above 0.99. The overall R values of the network with the transient  $\text{NO}_x$  data were 0.93 and 0.88 in two different operating points, which is a moderate accuracy. However, it is still a good result considering that the transient data lies far from the range of the steady state measurement points. In [14] ANN models were used to predict the ignition delay (ID) while different n-heptane, iso-octane and toluene mixtures were used. The ID could be predicted from the ambient conditions and the molar fraction of the components with a correlation coefficient above 0.99. The authors could also accurately predict the research octane number and motor octane number of the mixtures.

The development of a predictive tool that is able to estimate different engine parameters accurately in a wide range of operating points with different fuels requires a proper training dataset. However, the creation of high-resolution datasets is costly, especially with special fuels and expensive compounds. The ANN creation method also have to be effective in order to increase accuracy and reduce training time and computing costs. This means that a proper methodology is required to reduce costs and ensure high accuracy. As a first step of the methodology creation, a high-resolution dataset is needed that can be used in different analyses and optimization processes. In our previous study [15] we

created such a dataset with 6277 samples that covered most of the engine's useful operating range. We were able to accurately predict 10 different emission and combustion related parameters from the engine speed, torque and exhaust gas recirculation (EGR) valve position. Now this high-resolution dataset can be used to establish a methodology for cost efficient training of ANNs with ICE measurement data.

This paper presents a workflow that can be applied for the ANN model creation process of ICE related problems. Several investigation is presented to select good methods for the different ANN creation steps. A measurement grid resolution selection technique is also described to minimize fuel costs of measurements while maintaining good model accuracy. Section 3.2 – 3.6 presents the investigations related to efficient ANN creation. Section 3.7 describes the measurement resolution selection method. The full workflow is summarized in the conclusion section.

## **2 Experimental Apparatus and Methods**

### **2.1 Measurement System and Dataset Creation**

The high-resolution dataset was measured on a Cummins ISBe 170 30 turbocharged, medium-duty commercial diesel engine. This article builds on our previous work [15], therefore, the precise description of the measurement system, the calculation methods, and the process of high-resolution dataset creation can be found there. This section only describes methods related to the current study.

### **2.2 General Methodology of the Investigations**

The aim is to create a methodology that provides accurate models fast. The speed of the methods is described by the calculation times. The algorithms run in standardized conditions, where the only load of the computer is the investigated algorithm, thus the calculation times can be compared. To simplify the investigation, the model accuracy is only described with the determination coefficient ( $R^2$ ) of the models since this is one of the most illustrative indicators. A train (70%), a validation (20%) and a test (10%) dataset is used for the analyses. Usually, the validation  $R^2$  is used to describe the model performance. However, there are some analyses where the validation data also influence the created ANN models. An example for this is the architecture selection, where the final topology of the network is selected by investigating the validation  $R^2$ . In these cases, the validation  $R^2$  cannot be used for the final evaluation of the performance, so the test  $R^2$  is reported.

Most of the investigations use 3 ANN models that were created in our previous study [15]. The Indicated Mean Effective Pressure (IMEP) model had the highest accuracy in that work, so this is used as the representation of excellent models. The Particulate Matter (PM) emission had an average performance, so this represents models with average accuracy, and the Ignition Delay (ID) model was highly inaccurate, so this demonstrates models with bad performance. Therefore, the evaluation of the methods become more realistic. Most investigations use the same topology and input features that were used in [15]. If there is a difference, it is described in the given section.

### **3 Establishing Best Practices to Efficiently Train ANNs with ICE Measurement Data**

#### **3.1 Identifying Parameters of Interest for Optimizations**

Every problem that can be solved with an MLP network is different in many aspects, and there is a lot of ways to achieve a satisfying solution to each problem. The experience of the AI researchers shows that there is no general best practice for ANN model creation and the best possible solution can never be discovered. However, many good solutions can be found and researchers can create guidelines for specific problems to identify these easier. The goal of the presented work is to establish such a guideline to reduce computing efforts and measurement cost in case of ANN developments that focus on a wide ICE operation range.

The output of a MLP network depends on many parameters, such as the architecture and the used calculation methods. The necessary input features have to be selected to have the proper information to accurately calculate the output features. Then, this information has to go through the network that need to have the proper number of hidden layers and number of neurons inside the layers. The neurons need to have an appropriate activation function and initializing methods. Then, the created network has to be trained with one of the many existing training methods. Once the network is trained, its performance is needed to be evaluated with data that was not present in the training process. Although this is not a trivial task since the calculation depends on random factors as well.

In the following subsections, some general good practices will be presented on the selection of activation functions and initializing methods. Then, the 2 most common evaluation method will be analyzed. After this, the performance of 6 commonly used training algorithm will be compared. Thenceforth, the input feature selection and architecture selection methods will be discussed. Finally, a new method is described to identify the necessary resolution of a measurement

grid to achieve good accuracy with minimal fuel consumption during the measurement. The workflow is summarized in the conclusions section.

### **3.2 Activation Functions and Initialization**

The activation function is a vital element of neural networks since it brings nonlinearity in the equations. Without this nonlinearity, a single layer could represent the whole network, and the representation of more complex functions would not be possible. Originally the sigmoid function was the most common activation function for hidden layers. Later the tangent hyperbolic activation function also become common, as it provided easier training and better predictive ability. However, both of these functions have a problem: the saturation. When the weighted sum is too high, the gradient of these activation functions converge to zero, which leads to the so-called vanishing gradients problem. Nowadays, the rectified linear unit (ReLU) is the state-of-art activation function. The ReLU is a piecewise linear function that gives a constant gradient for positive weighted sums. This activation function solves the vanishing gradient problem, thus its usage in the hidden layers is a good practice for MLP networks. For the output layer, a pure linear activation function has to be used since the current mathematical problem is a regression. [16]

Besides the activation functions, the initial value of the network's weight also needs to be determined in order to start the calculations. The weights are initialized to small random numbers, and the initialization method depends on the used activation functions. For sigmoid, tangent hyperbolic and pure linear activation functions usually Xavier initialization is used [17]. This method is not ideal for ReLU activation function, so He initialization is used for that [18]. The networks not only have weights, but biases as well. These also have to be initialized, but usually it is a good practice to set their initial values to zero.

The training of the ANN can start after the initializations. During this process, a loss function that represent the network's error is minimized. For regression problems the mean squared error (MSE), mean squared logarithmic error (MSLE) and the mean absolute error (MAE) can be used as a loss function. The MSLE is usually used when the output values can be really high, and the MAE is usually used when extreme outliers are expected. Generally, the use of MSE is the best practice for scaled data, therefore, this is used in our methodology.

### **3.3 Performance Evaluation**

The performance of the ANNs have to be evaluated in order to demonstrate their predictive ability. The output features have a random nature due to the applied random factors during calculation. This randomness has to be treated for proper and consistent results. The 2 most common methods for this are the repeated

evaluation and the k-fold cross-validation. The repeatability of the results and the evaluation time highly depends on the used techniques. This step affects all later analyses of this work; hence the performance evaluation method is studied first.

During repeated training, the network is trained with the training dataset and evaluated with the validation dataset for multiple times. Then, the reported results are the average of each training-evaluation pairs. Here, the parameter of the method is the number of evaluations ( $n_{eval}$ ). The other method is the k-fold cross-validation. This technique divides the full dataset into  $k$  folds. The network is trained and evaluated for  $k$  times, and a different fold is chosen as a validation hold-out dataset for each training and evaluation pairs. Thus the network is always validated with a different fold, and the remaining  $k-1$  folds are used to train the network. The final result is the average of the  $k$  evaluation. The parameter of this method is the  $k$  number of folds. This section compares these methods with different settings.

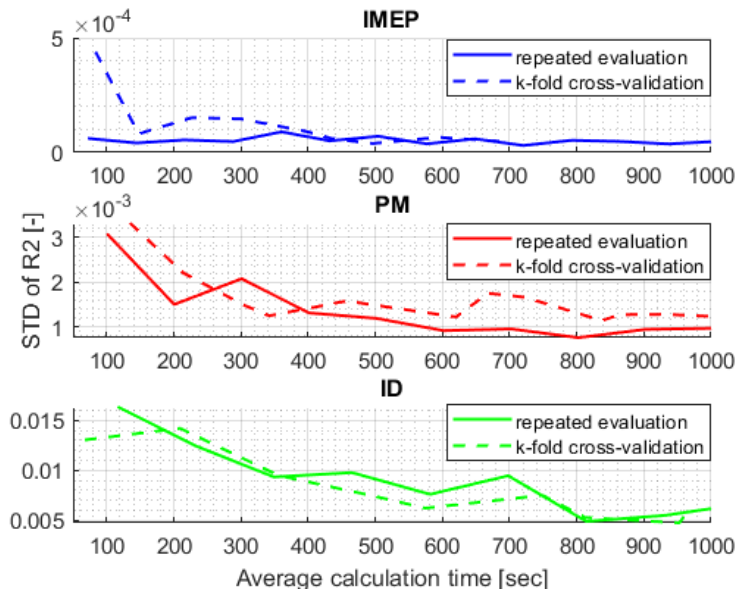


Figure 1

Standard deviations of R2's with repeated evaluation and k-fold cross-validation

The standard deviation (STD) of the R2 shows a decreasing tendency for increasing  $n_{eval}$  and  $k$  values, but the evaluation time increases. The goal is to identify the method that can achieve smaller STD (thus better repeatability) within the same calculation time. This analysis investigates the  $n_{eval}$  between 1 and 20 and the  $k$  between 2 and 10. The evaluation with each  $n_{eval}$  and  $k$  value is repeated 15 times to get the STD of the validation R2 and the mean evaluation time of them. The investigation is done with the IMEP, PM and ID models to investigate the effect of different accuracies.

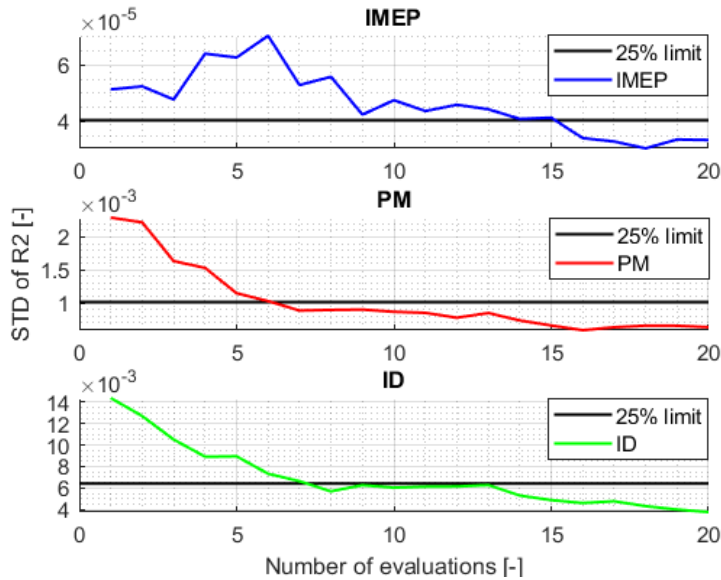


Figure 2

Comparing the standard deviations of R2's with the 25% limit

The results are presented on Figure 1. In case of the IMEP model, the repeated evaluation shows a nearly constant STD as a function of calculation time. The k-fold cross validation has a much higher STD until 400 seconds, then it has nearly the same STD. Therefore, in case of accurate models, the repeated evaluation is better, however, the magnitude of STD is really small for both methods. On the PM model, it is discernible that the STD with the k-fold cross-validation is higher for most of the calculation times. This means that the repeated evaluation is also the better method in case of average accuracy models, however, the difference is not marginable. For the ID model, the two methods have a similar performance. The cross-validation becomes slightly better between 400 and 750 seconds. Overall, there is not much difference between the two methods' performance at any model accuracy levels, although the repeated evaluation appears to be slightly better. The implementation of this method is also simpler, so this is selected for the workflow.

Next, the optimal number of evaluations have to be determined. On Figure 2, the STD of R2's are presented as a function of  $n_{eval}$ . A moving average was applied to the curves with a window of 3 to smooth their characteristics. The value of STD is accepted after it reaches the 25% of the difference between the maximal and minimal STD value. The STD reaches this limit after 15 evaluation repeats for the IMEP model, 6 in case of the PM model, and 7 in case of the ID model. The STD is really low in case of the highly accurate models, thus the 15 repeating is unnecessary. The results show that 8 repeating ensures a good repeatability even for inaccurate models, thus this value is chosen for  $n_{eval}$ .

### 3.4 Training Algorithm

As the next step of the general workflow creation, a training algorithm has to be selected. During training, the weights and biases of the network are modified in order to minimize the error between the desired and actual outputs. The most common training method is the stochastic gradient descent (SGD) [16]. This algorithm is used to find a set of input parameters that results in a minimum of a target function. In case of neural network trainings, the input variables of the SGD are the weights and biases, and the target function is the loss function that describes the average prediction error for a subset (batch) of the training dataset. The SGD iteration follows the negative gradients of the loss function in order to find the minimum. The gradients are calculated with the back propagation algorithm. The degree of the change in the direction of the gradient is described by the step size (or learning rate). However, the selection of this hyperparameter is difficult because too large values result oscillations and the minimum cannot be found, while too low values cause slow convergence. In addition, the learning rate should be modified during the optimization because the step size should decrease as the minimum is approached. Therefore, the best practice is to use adaptive techniques that automatically change this hyperparameter during training.

In this section, six different adaptive training methods are investigated: the AdaGrad, RMSprop, Adadelta, Adam, Adamax and Nadam algorithms. The Adaptive Gradients (AdaGrad) algorithm is a simple SGD based method that uses an adaptive learning rate with respect to previous gradients [19]. The AdaGrad needs an initial learning rate, and later it calculates a step size for each dimension in the search space. The method is not that sensitive to the initial learning rate, thus 0.001 is used in this paper, which is a common default value. The Root Mean Squared Propagation (RMSprop) algorithm is based on the AdaGrad algorithm [20]. The problem of AdaGrad is that it can result too small step sizes at the end of the training. The RMSprop also calculates the step size from the previous gradients, but it uses a decaying average in order to eliminate the effects of early gradients, so the learning rate is mostly influenced by recent gradients. A gradient moving average decay factor ( $\delta$ ) with a value between 0 and 1 is required to determine the extent of the decay. Experience of researchers shows that the RMSprop is very efficient, and this is one of the best training algorithms for deep neural networks [16]. The Adadelta algorithm is based on the AdaGrad and RMSprop algorithms [21]. It also uses a gradient moving average decay factor to improve the influence of the recent gradients compared to the early ones like the RMSprop, but the step size is calculated differently. Another difference is that this method does not require an initial learning rate. The Adaptive Movement Estimation (Adam) algorithm is also a successor of AdaGrad and RMSprop [22]. This method uses a second decay factor; thus it has three hyperparameters. The commonly used default values (initial learning rate: 0.001; decay factor for first momentum: 0.9; decay factor for infinity norm: 0.999)

usually provide good results, thus this work operates with these. The Adam is a widely used ANN training method due to its good performance. In Adam, the weights are updated with the squared norm of past gradients. The AdaMax algorithm which is based on Adam, provides a more generalized approach as it uses the infinite norm of past gradients. The Nesterov-accelerated Adaptive Moment Estimation (Nadam) is another method based on Adam [23]. The main difference between the two algorithms, is that Nadam uses Nesterov's Accelerated Gradient for the calculations. This means that the weight updates are performed with the gradient of the projected update instead of the actual gradient. The default hyperparameter values also provide good results for Adamax and Nadam.

Similarly, to the previous section, the performance of the training algorithms will be represented by the validation R2 of the IMEP, PM and ID models. A repeated evaluation is used with 8  $n_{eval}$  and the full evaluation time is recorded. Firstly, a good value for the  $\delta$  of RMSprop and Adadelta is selected. Figure 3 presents the validation R2 for RMSprop and Adadelta with 9 different  $\delta$  values. The decay factor of 0.95 shows a good compromise between the calculation time and the accuracy for both algorithms for all models, thus this is selected.

Now the performance of the six algorithms can be compared with each other at Figure 4. It is discernible that the fastest and most accurate methods are the Adam and the RMSprop for all models. The Nadam and Adamax models also have a good performance, but they are a bit slower. The investigated models have the same architecture for all six methods. The architecture can also have influences on the performance of the different methods thus this also has to be considered. However, this investigation demonstrated the superiority of Adam and RMSprop, hence only these methods are investigated next.

To study the performance of the Adam and RMSprop on different architectures, 90 models were analyzed with 1 and 2 hidden layers. The number of neurons in the layers was varied between 40 and 80, with a 5 neuron step, and each combination was evaluated with repeated evaluation. The average calculation time and validation R2 of both methods are presented at Table 1. The average calculation time decreased by 29.7% with the RMSprop method, while the accuracy remained the same. The PM model could be calculated 15.4% faster with the RMSprop, but the average validation R2 dropped by 0.6%. For the ID model, the achieved calculation time improvement with the RMSprop was 22.3%, and the accuracy decrease was 4.5%. Overall, the RMSprop can notably accelerate the training for the cost of a small drop in accuracy. Since multiple iterations are necessary to produce the final ANN model, the RMSprop is a better choice because it is also accurate enough. However, the Adam can also be used when the calculation time is not a limiting factor.

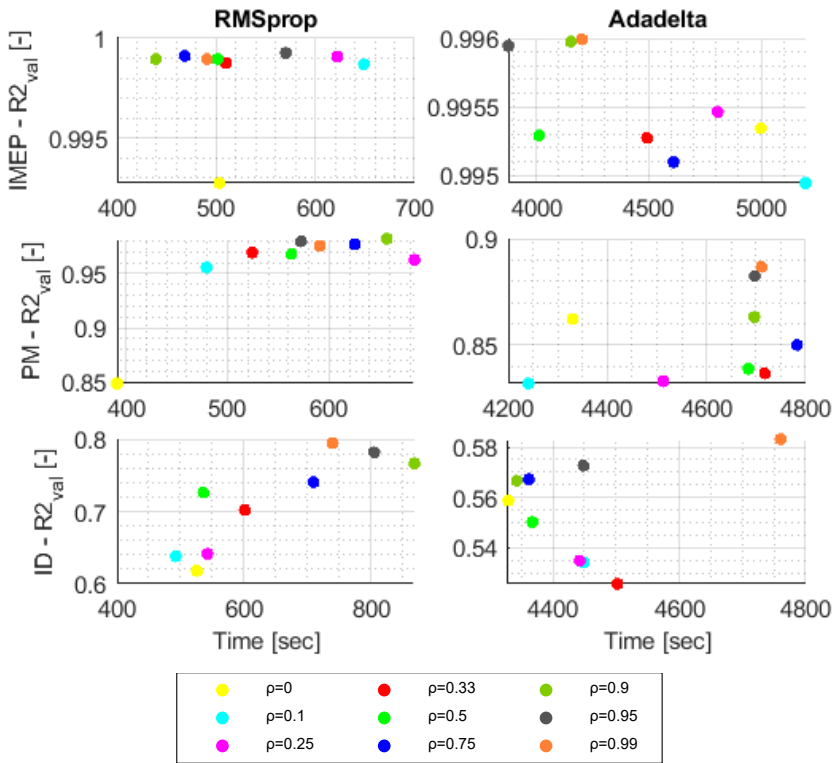


Figure 3

Performance of RMSprop and Adadelta with different moving average decay factors

Table 1

Average time and accuracy results for Adam and RMSprop algorithms

	<i>Adam</i> avg. calc. time [sec]	<i>RMSprop</i> avg. calc. time [sec]	<i>Adam</i> avg. val. R2 [-]	<i>RMSprop</i> avg. val. R2 [-]
<b>IMEP</b>	506.36	390.46	0.999	0.999
<b>PM</b>	690.20	598.13	0.980	0.974
<b>ID</b>	890.92	728.66	0.796	0.762

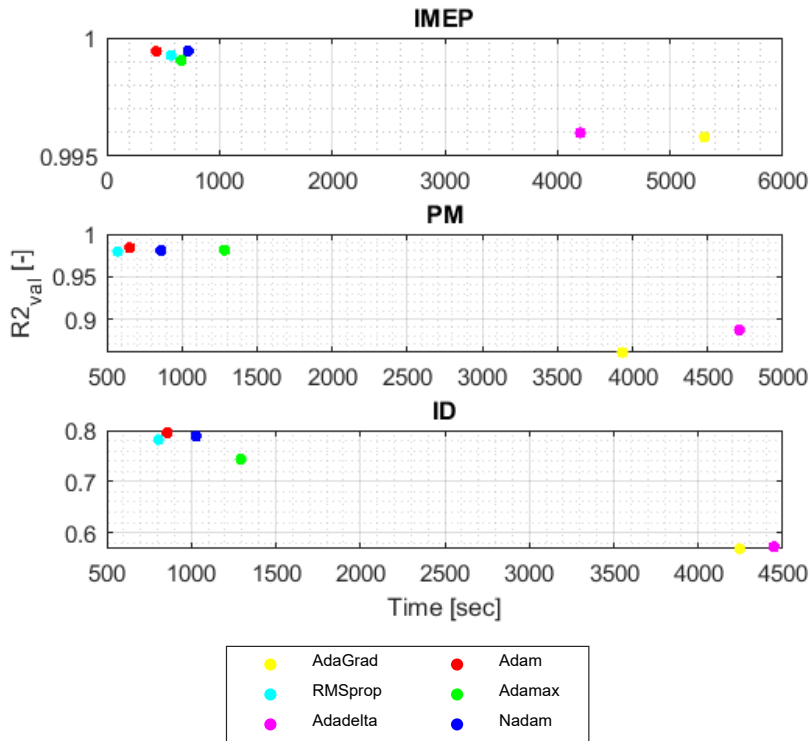


Figure 4

Comparison of the performance of six adaptive training methods

The training is an iterative method, where the samples of the training dataset are going through the network and the error of the result is used to update the weights of the model. The period when all samples participated in the weight update is called an epoch. Multiple epochs are necessary to create accurate ANN models, thus this is also a hyperparameter that has to be considered. If the number of epochs is small, the model will not be accurate enough (underfit). More epochs lead to more accurate models; however, overfitting can occur if this hyperparameter is too high. An overfitted model performs well in the training dataset, but it has a bad performance on the validation dataset. Moreover, the increased number of epochs leads to longer training time, so a good compromise has to be found. The early stopping method provides a good approach to use the proper number of epochs during training. A maximum epoch number is defined and when this is reached, the training stops. The training also stops if the validation MSE starts to increase. The stopping is not necessarily immediate: a patience parameter can be used, and the training only stops if the validation MSE increases continuously for a predefined number of epochs. This method avoids overfitting and reduces the training time. In this section, the optimal maximum number of epochs ( $\epsilon_{max}$ ) and the patience ( $p$ ) hyperparameter is also investigated.

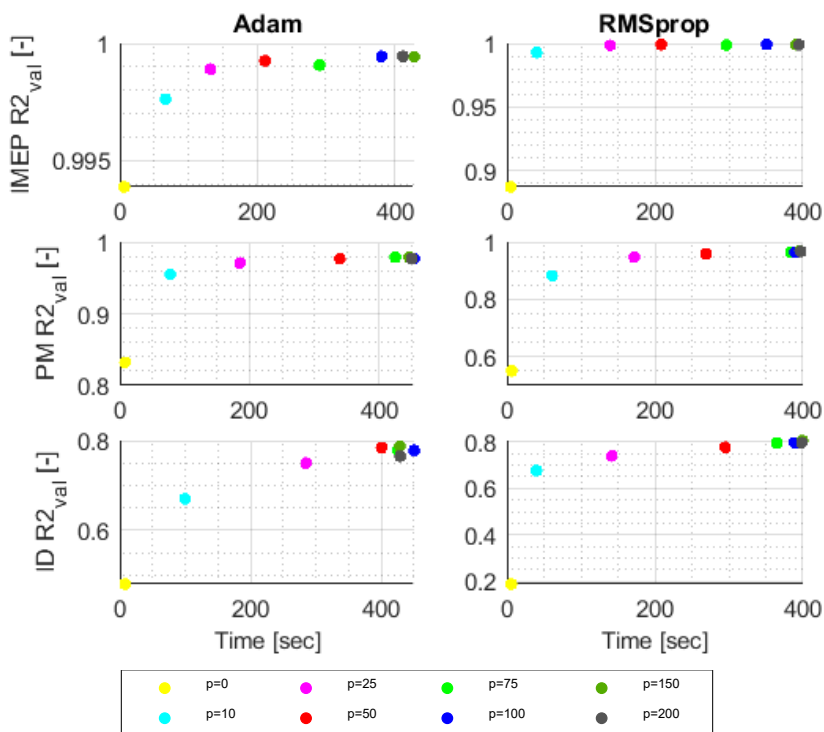


Figure 5

Performance of Adam and RMSprop with different patience values (max. number of epochs: 500)

The combination of 8 different  $p$  and 13  $\varepsilon_{max}$  hyperparameters are investigated. First, a good  $p$  is selected. Higher patience results longer calculation time. However, the increase of accuracy stops when the ANN reaches a good fit. Therefore, the validation R2 converges to a certain level at each diagram of Figure 5. This figure shows that  $p=50$  is a good choice for both Adam and RMSprop: this value usually provides the fastest training to reach the converged maximal accuracy level. There are some cases where lower  $p$  could be enough, but these lower values cannot provide good results for all models. Note that Figure 5 only presents the results with  $\varepsilon_{max}=500$ , which will be later chosen as the best  $\varepsilon_{max}$  value. All 13  $\varepsilon_{max}$  was investigated and the results were similar for each:  $p=50$  showed the best compromise, thus only one  $\varepsilon_{max}$  is presented here.

Next, the necessary  $\varepsilon_{max}$  is determined. The training can be stopped by two criteria: accuracy drop and reaching of  $\varepsilon_{max}$ . Usually, the best case if the training is stopped by the accuracy drop, because this means that a good fit was found and further training leads to overfitting. However, there can be some models that has too slow convergence, thus the training has to be stopped before reaching the best fit to reduce calculation time.

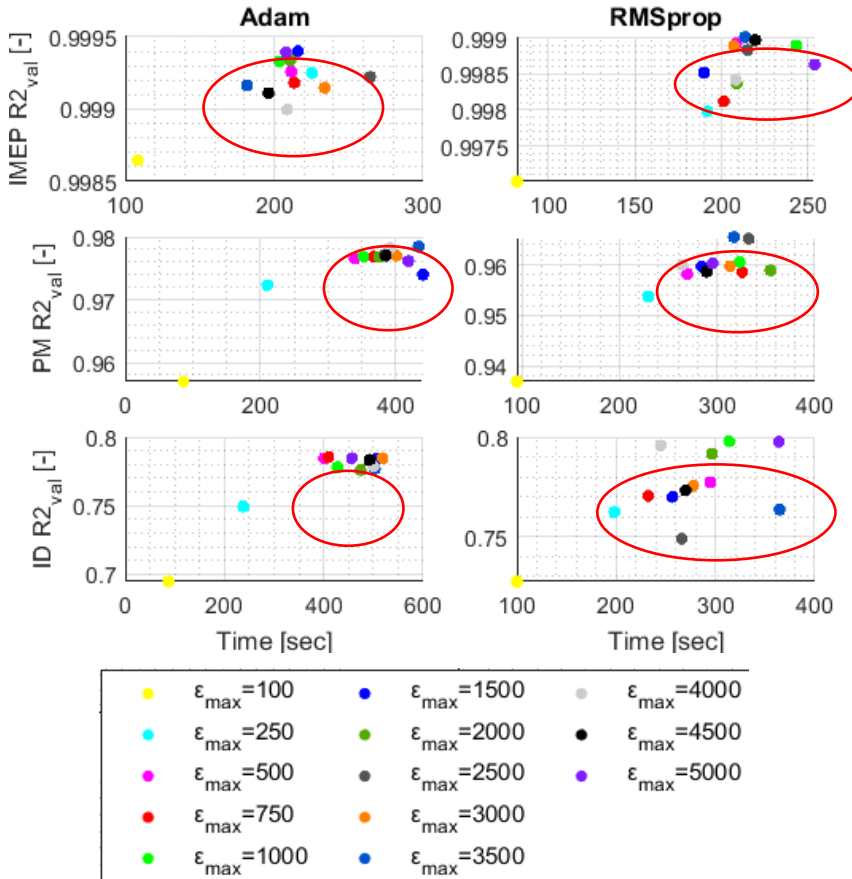


Figure 6

Performance of Adam and RMSprop with different maximum number of epochs (patience: 50 epochs)

Here, the aim is to find the lowest value for  $\epsilon_{max}$  that provides enough epochs to develop good fit models for most cases. Figure 6 investigates the validation accuracy of the IMEP, PM and ID models when the patience is set to 50 epochs. The result of each diagram shows separate clusters with similar accuracies and training times. In these clusters, a good fit model was reached and the training was stopped by the accuracy drop. From here on, the  $\epsilon_{max}$  has no influence on the calculation time and accuracy and the differences come from the randomness of the process. Note that the clusters of Adam algorithm are smaller, thus its results are more stable than the RMSprop. The best  $\epsilon_{max}$  value is 500 epochs because this is the lowest that is present in all clusters.

To sum up the outcomes of this section, the RMSprop algorithm is the best from the investigated methods, if the training time is the bottleneck. Adam algorithm can also be used, when a little longer calculation time is acceptable and further

increase in accuracy is required. It is recommended to set the Adam algorithm's hyperparameters to their default values, and the  $\delta$  of RMSprop to 0.95. Regarding early stopping, the 500 epoch  $\varepsilon_{max}$  and the 50 epoch  $p$  is suitable for both methods.

### 3.5 Input Feature Selection

Another important aspect of the ANN model creation is the selection of proper input features. Sufficient input information is needed to map a systems behavior. However, too much information can also worsen the accuracy since irrelevant data can lead the training into false paths. The two main approach for input feature selection are the supervised and unsupervised selection methods. The unsupervised methods ignore the outcome of the model, while the supervised methods use target variables to remove unnecessary features [24]. Supervised methods such as wrapper, filter or intrinsic methods usually provide better results. Wrapper methods create multiple models with different input features and select the useful ones. This provides really good results, but the computational costs can rise. Filter methods chose the important inputs with statistical scores between the input and output features. Intrinsic methods are built-in feature selection methods of some training algorithms. From these possibilities, the wrapper methods fit the best for our purpose, since high accuracy is required and the computational costs remain low due to the low number of available input features.

The recommended workflow is as follows. First, the possible influencing parameters have to be identified manually, based on the available information of the system. Then the quasi-constant features have to be removed, because these have no relevant data for the training. Then the redundant features also needed to be eliminated. Here, the priority of each feature can be predefined manually, and the higher priority can be held in the inputs. Next a wrapper method have to be performed. The recursive feature elimination (RFE) is such a method, where at first a machine learning algorithm creates models with all input features, and then the method starts to remove them. In this paper, such an RFE method is implemented to select the necessary input features from the preselected ones. The RFE also creates ANNs to select input features, thus the results include randomness. Therefore, the RFE process is also repeated 8 times, and the inputs that were among the results at least 50% of the repetitions are selected.

This workflow was implemented for the IMEP, PM and ID models. Since a new input feature set generates a modified behavior, a new architecture was selected using a grid search algorithm with the settings described in [15]. The investigated output features are combustion and emission relevant parameters. Therefore, the two main set of manually selected input features for the RFE are:

- the measured inlet properties: pressure, temperature, mass flow rate

- the measured mixture composition and formation relevant parameters: EGR valve position, engine speed, air-fuel equivalence ratio, inlet and outlet oxygen concentration, fuel dose, start of injection, number of injections, ratio of main injection compared to pre-injection

The RFE algorithm selected 4, 6, and 8 input features for the new IMEP, PM and ID models respectively. This behavior is logical because the harder the modelled problem, the more information is needed to properly map the system. Table 2 compares the test R2 and the test root mean square error (RMSE) of the new models with the original ones. The IMEP shows a decrease in accuracy, but it still has an excellent performance. The PM model has slightly better performance with the new input set. The ID model shows a drastic improvement. The original model was unacceptably inaccurate, but the new input features developed it into a well performing one. Overall, the used input feature selection method performed well, and can be included in our workflow.

Table 2

Comparing the performance of the IMEP, PM and ID models with the original and new input features

	<i>IMEP</i>		<i>PM</i>		<i>ID</i>	
	<b>Original inputs</b>	<b>New inputs</b>	<b>Original inputs</b>	<b>New inputs</b>	<b>Original inputs</b>	<b>New inputs</b>
<i>R2<sub>test</sub></i>	0.9995	0.9929	0.9874	0.9882	0.8303	0.9782
<i>RMSE<sub>test</sub></i>	0.078 bar	0.303 bar	0.130 g/kWh	0.120 g/kWh	1.103 °CA	0.413 °CA

### 3.6 Architecture Selection

The architecture of an ANN highly affects its performance. The capacity of a network describes the ability of learning complex problems. Generally, the more neurons and layers the network has, the higher its capacity. Too low capacities result underfit while too high capacities lead to overfit, hence a good architecture have to be identified. The grid-search algorithm is a common architecture selection method, where a lower and a higher boundary for the number of layers, and for the number of neurons in a layer is selected. Then all possible combinations are investigated between these boundaries with a certain step size and the architecture with the best accuracy is selected. This method is popular because of its simplicity and accuracy; however, the calculation time can be too high. We used this method in our previous research, but now faster have to be found due to its slow speed. The constructive architecture selection is a common technique to identify a good network topology [25]. This method uses an initial architecture that definitely provides too small capacity for the problem. Then, it adds new neurons and layers to the network to achieve a good fit. Such a simple constructive method was created in this work to replace the previous technique. First, it generates a model with a single layer that has an initial neuron number.

Then, it starts to increase this number with a defined step until it reaches an upper boundary. Next, it creates a new layer with an number of neurons corresponding to the step size, and it continues to increase this layer. The iteration stops when the defined maximal number of layers reached. However, the iteration usually does not last this long since it has an accuracy criterium that stops the process when fulfilled. This criterium investigates the validation  $R_2$ , and when it reaches 0.98, the model is considered accurate enough [26]. If this accuracy cannot be reached with the defined topological boundaries, then the most accurate model is selected.

Table 3

Comparing the performance of the constructive architecture selection and the grid-search algorithm

	<i>IMEP</i>		<i>PM</i>		<i>ID</i>	
	<b>Original method</b>	<b>New method</b>	<b>Original method</b>	<b>New method</b>	<b>Original method</b>	<b>New method</b>
$R_{2test} [-]$	0.998	0.998	0.977	0.980	0.759	0.740
$t_{archOpt} [h]$	6.66	0.12	8.50	2.49	7.71	2.26

Table 3 demonstrates the architecture selection's calculation times ( $t_{archOpt}$ ) and the achieved test  $R_2$  of the new constructive algorithm compared to the previous grid-search algorithm. The new test  $R_2$ s did not change notably compared to the old method, but the improvement in calculation times is immense. The excellent models can fit really fast, so the necessary time for architecture selection becomes small. The average and bad models also show about 70% improvement in the calculation time, thus the new method contributes to lower computing costs.

### 3.7 Measurement Grid Resolution Selection

The experimental investigation of new advanced fuels is a major cost of development due to the high price of special compounds. This can also raise the expenses of ANN development since the dataset is created by measurements. To reduce these costs, a measurement grid resolution selection method is also created in this paper. The measurement grid needs high enough resolution to provide sufficient data for the ANN training, but unnecessarily dense measurements have to be avoided to reduce fuel costs. More complex problems require a denser measurement to properly map the system's behavior. The correlation coefficient can describe the complexity of an input-output relationship. When  $R$  is close to 0 the two parameters are not related, when it's close to 1 the relationship is linear, while the intermediate values represent a nonlinear behavior. To identify the proper resolution, the  $R$  between the varied grid parameters and the target values of the investigation have to be determined and compared with the achievable accuracies of multiple models created with different resolution datasets.

To establish a best practice for resolution selection, the original high resolution dataset [15] is used that has 3 varied parameters in the measurement grid. This investigation examines the 10 target variable of [15] to identify optimal resolutions for different complexities. First, the complexity of the 30 input-output relationship is needed to be determined, and the correlation coefficient between these pairs will describe it ( $R_{\text{pair}}$ ). This can be done with a parameter sensitivity measurement that requires a small amount of fuel to measure at least 10 sample per varied grid parameter. This 10 sample is recorded for each varied parameter in the predefined measurement range. The other varied parameters need to have a fixed value during the measurement to guarantee that the only influencer of the investigated outputs will be the investigated input feature. These fixed values are selected as the middle values in the range of the given input parameters. Then, the  $R_{\text{pairs}}$  can be calculated from the samples. This study calculated 30  $R_{\text{pairs}}$  for the investigated 30 input-output relationships. Note, that the absolute values have to be used to describe the complexity of the relationships. Now, an optimal resolution has to be found for these  $|R_{\text{pair}}|$  values.

In the next step, 72 datasets with different resolutions were created from the original high-resolution dataset. An ANN model was created with the workflow described in this paper for the 10 output feature with each dataset. Then a prediction was made with the created 720 ANN models for the 6618 samples of the original high-resolution dataset, thereby the performance of the models was explored with the most detailed information available on the system. The reported accuracy measure is the determination coefficient for the full dataset ( $R2_{\text{full}}$ ). After the calculations, there are 72  $R2_{\text{full}}$  values for the 10 output features and the best model have to be selected for each output. A model is considered acceptable if its  $R2_{\text{full}}$  is at least 0.98. If there are multiple models for an output feature that satisfies this criterium, the one that was created with the smallest dataset is selected as the best, since this requires the least fuel. Now, the optimal resolution of the 3 varied parameter of the measurement grid is known for each output feature. However, only 6 models provided results with  $R2_{\text{full}}$  above 0.98, so only 18 data points can be used to describe the relationship between complexity and necessary resolution.

Figure 7 shows the 18 optimal resolution –  $|R_{\text{pair}}|$  data points. Here, the resolution means the number of grid points in the measurement range of a varied parameter. Three main parts can be separated. If  $|R_{\text{pair}}|$  is lower than 0.4, then the investigated input feature does not have a significant effect on the investigated target variable, therefore, a lower resolution is enough. The average resolution in this area is 6.5, thus 7 equidistant value is enough for the varied parameter.

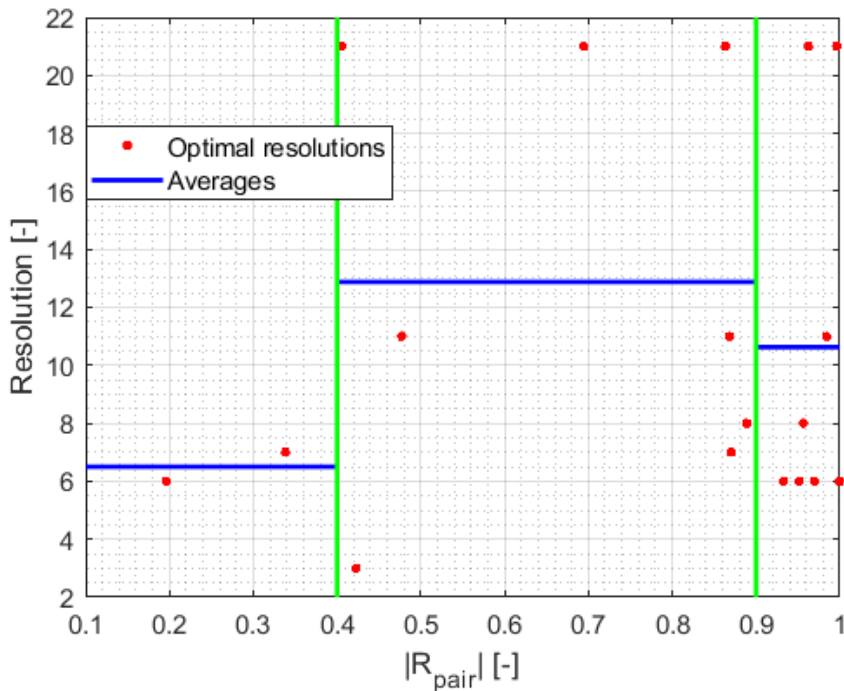


Figure 7

The optimal resolution of input-output pairs of different complexity

If  $|R_{pair}|$  is above 0.9, the correlation is strong between the varied parameter and the target variable, thus a higher resolution is needed to map the behaviour. The average is 10.625, so 11 variation is needed in this case. The in-between area needs an even higher resolution because here the relationship is highly nonlinear. The average resolution here is 12.87, so 13 equidistant value is necessary in the grid. This simple practice can create datasets with good resolutions to minimize fuel consumption while accurate models are provided. However, more investigation is needed to establish a more precise method for resolution selection.

### 3.8 Summary of the Created Methodology

The final workflow can be generated based on the previously presented investigations. Figure 8 summarizes the methods to efficiently create representative datasets from engine measurements, and to build accurate and fast ANN models from them. The upper part describes the methods related to the first goal. A proper measurement resolution can be designed that provides enough information to train the networks, while the fuel costs are minimized. This is based on a parameter sensitivity measurement, where the complexity of the

relationship between the varied grid parameters and the target variables are determined in order to select the proper measurement grid resolutions (Section 3.7). After the measurement, the created dataset is used to create a MLP type ANN. The lower part of Figure 8 demonstrates the workflow for this task with the steps and methods described previously (Section 3.2 – 3.6). The investigations proved that this workflow is able to reduce calculation time, fuel costs and provide accurate results.

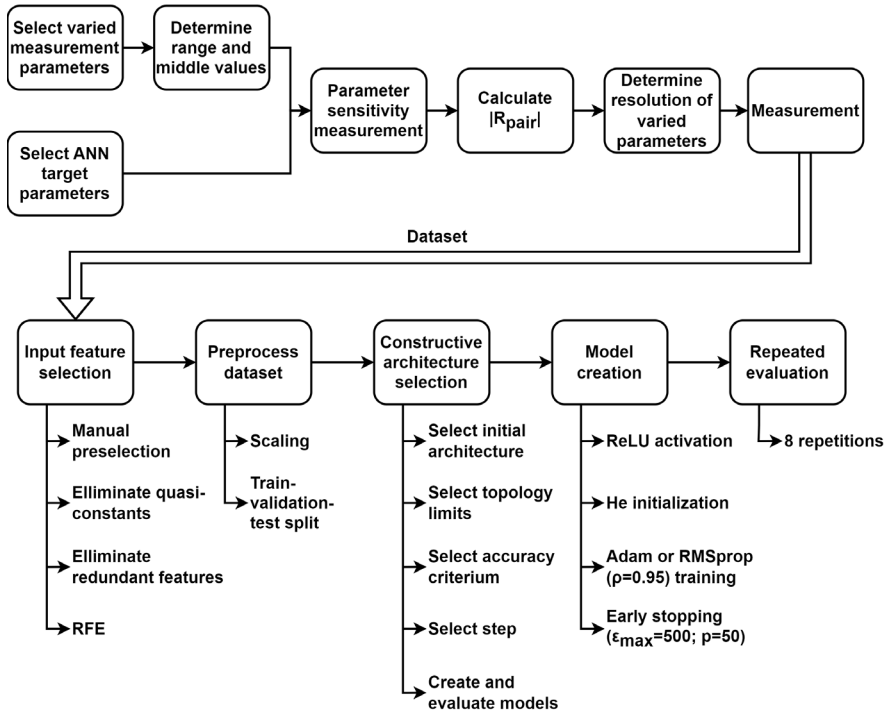


Figure 8

Final workflow to cost-efficiently create ANN models from engine measurements

## Conclusions

This paper presented the investigations that led to the creation of a workflow for cost efficient ANN creation from engine measurements. A high resolution dataset was used to test multiple methods for the different steps of model generation. The results showed that the RFE method can be applied to select the necessary input features from a dataset and the constructive architecture selection is an efficient method to determine proper network structure. Regarding the training algorithms, the Adam and the RMSprop had the best performance from the investigated 6 method. The RMSprop is the recommended algorithm if the calculation time is the bottleneck. However, the Adam algorithm generates more accurate models. Therefore, this has to be applied if the speed of the training

process is not important. The random nature of the results has to be treated with repeated evaluation. The methodology also aids the determination of the proper measurement grid resolution. After a simple parameter sensitivity measurement, the complexity of the input-output relationships can be determined. Then, the resolution of the varied parameters can be selected.

The methodology ensures the cost-efficient creation of representative datasets and accurate ANN models; therefore, it contributes to help the development of our AI based e-fuel designer tool. The achieved accurate results prove that the AI is an important tool to enhance sustainable mobility. Besides our purposes, it can be applied to similar mathematical problems of different research fields as well. However, note that there is no general best practice for ANN creation, thus other researchers should consider the specialties of their mathematical problems.

### **Acknowledgement**

The research leading to this result was funded by the KTI\_KVIG\_8-1\_2021.

This work was supported by AVL Hungary Kft.

### **Abbreviations**

AdaGrad, Adaptive Gradients; Adam, Adaptive Movement Estimation; AI, Artificial Intelligence; ANN, Artificial Neural Network; BP, Back Propagation; EGR, Exhaust Gas Recirculation; EU, European Union; ICE, Internal Combustion Engine; ID, Ignition Delay; IMEP, Indicated Mean Effective Pressure; MAE, Mean Absolute Error; MLP, Multilayer Perceptron; MSE, Mean Squared Error; MSLE, Mean Squared Logarithmic Error; Nadam, Nesterov-accelerated Adaptive Moment Estimation; PM, Particulate Matter; ReLU, Rectified Linear Unit; RFE, Recursive Feature Elimination; RMSE, Root Mean Square Error; RMSprop, Root Mean Squared Propagation; SGD, Stochastic Gradient Descent; STD, Standard Deviation; WTW, Well-to-wheel;

### **References**

- [1] P. Plötz, J. Wachsmuth, T. Gnann, F. Neuner, D. Speth, S. Link: Net-zero carbon transport in Europe until 2050 – targets, technologies and policies for a long-term EU strategy, Fraunhofer Institute for Systems and Innovation Research ISI, 2021
- [2] M. Ovaere, S. Proost: Cost-effective reduction of fossil energy use in the European transport sector: An assessment of the Fit for 55 Package, Energy Policy, 2022, Vol. 168, 113085
- [3] Zalacko, R., Zöldy M., and Simongáti Gy: "Comparative study of two simple marine engine BSFC estimation methods." *Brodogradnja: Teorija i praksa brodogradnje i pomorske tehnike* 71.3 (2020): 13-25

- [4] A. Vučetić, V. Sraga, B. Bućan, K. Ormuž, G. Šagi, P. Ilinčić, and Z. Lulić, “Real Driving Emissions from Vehicle Fuelled by Petrol and Liquefied Petroleum Gas (LPG)”, *CogSust*, Vol. 1, No. 4, Sep. 2022
- [5] T. Koller, C. Tóth-Nagy, and J. Perger, “Implementation of vehicle simulation model in a modern dynamometer test environment”, *CogSust*, Vol. 1, No. 4, Sep. 2022
- [6] eFuel Alliance: Press Release, 2022. Only available at: [https://www.efuel-alliance.eu/fileadmin/Downloads/E\\_PM\\_eFA\\_EU-Parlament\\_vor\\_Richtungsentscheidung\\_02062022.pdf](https://www.efuel-alliance.eu/fileadmin/Downloads/E_PM_eFA_EU-Parlament_vor_Richtungsentscheidung_02062022.pdf)
- [7] M. Zöldy, "The effect of bioethanol–biodiesel–diesel oil blends on cetane number and viscosity." 6<sup>th</sup> international colloquium, January. 2007
- [8] J. Matijošius, A. Juciūtė, A. Rimkus, and J. Zaranka, “Implementation of vehicle simulation model in a modern dynamometer test environment”, *CogSust*, Vol. 1, No. 4, Sep. 2022
- [9] E. Cipriano, T. C. F. da Silva Major, B. Pessela, A. A. Chivanga Barros: Production of Anhydrous Ethyl Alcohol from the Hydrolysis and Alcoholic Fermentation of Corn Starch, *Cognitive Sustainability*, 2022, 1(4) <https://doi.org/10.55343/cogsust.36>
- [10] M. Zöldy, P. Baranyi: The Cognitive Mobility Concept, *Infocommunications Journal*, 2023
- [11] M. Zöldy, "Improving heavy duty vehicles fuel consumption with density and friction modifier." *International Journal of Automotive Technology* 20 (2019): 971-978
- [12] M. Jadidi, S. Kostic, L. Zimmer, S. B. Dworkin: An Artificial Neural Network for the Low-Cost Prediction of Soot Emissions, *Energies*, 2020, Vol. 13, 4787, <https://doi.org/10.3390/en13184787>
- [13] X. H. Fang, F. Zhong, N. Papaioannou, M. H. Davy, F. C. P. Leach: Artificial neural network (ANN) assisted prediction of transient NOx emissions from a high-speed direct injection (HSDI) diesel engine, *International Journal of Engine Research*, 2022, Vol. 23(7), pp. 1201-1212
- [14] Y. Cui, H. Liu, Q. Wang, Z. Zheng, H. Wang, Z. Yue, Z. Ming, M. Wen, L. Feng, M. Yao: Investigation on the ignition delay prediction model of multi-component surrogates based on back propagation (BP) neural network, *Combustion and Flame*, 2022, Vol. 237, 111852
- [15] M. Virt, M. Zöldy: Artificial Neural Network Based Prediction of Engine Combustion and Emissions from a High Resolution Dataset, 1<sup>st</sup> IEEE International Conference on Cognitive Mobility, 2022
- [16] I. Goodfellow, Y. Bengio, A. Courville: *Deep Learning*, MIT Press, 2016

- 
- [17] X. Glorot, Y. Bengio: Understanding the difficulty of training deep feedforward neural networks, Proceedings of the Thirteenth International Conference on Artificial Intelligence and Statistics, PMLR 9:249-256, 2010
- [18] K. He, X. Zhang, S. Ren, J. Sun: Delving Deep into Rectifiers: Surpassing Human-Level Performance on ImageNet Classification, Proc. IEEE Int. Conf. Comput. Vis. (ICCV), pp. 1026-1034, 2015
- [19] J. Duchi, E. Hazan, Y. Singer: Adaptive Subgradient Methods for Online Learning and Stochastic Optimization, Journal of Machine Learning Research, Vol. 12, pp. 2121-2159, 2011
- [20] T. Tieleman, G. Hinton: Lecture 6.5-rmsprop: Divide the gradient by a running average of its recent magnitude, COURSERA: Neural Networks for Machine Learning, 2012
- [21] M. D. Zeiler: ADADELTA: An Adaptive Learning Rate Method, arXiv preprint arXiv:1212.5701, 2012
- [22] D. P. Kingma, J. L. Ba: ADAM: A Method for Stochastic Optimization. <https://arxiv.org/abs/1412.6980>, 2018
- [23] T. Dozat: Incorporating Nesterov Momentum into Adam, Proc. ICLR, pp. 1-4, 2016
- [24] M. Kuhn, J. Kjell: Applied predictive modelling, New York: Springer, vol. 26, 2013
- [25] S. Curteanua, H. Cartwright: Neural networks applied in chemistry. I. Determination of the optimal topology of multilayer perceptron neural networks, J. Chemometrics, Vol. 25, pp. 527-549, 2011
- [26] S. Dey, N. M. Reang, P. K. Das, M. Deb: Comparative study using RSM and ANN modelling for performance-emission prediction of CI engine fuelled with bio-diesohol blends: A fuzzy optimization approach, Fuel, Vol. 292, 2021

# Digitalization and Adaptation, from a Regional Perspective – a Hungarian Case Study

**Mária Szalmáné Csete**

Budapest University of Technology and Economics, Faculty of Economic and Social Sciences, Department of Environmental Economics and Sustainability, Műegyetem rkp. 3, H-1111 Budapest, Hungary, csete.maria@gtk.bme.hu

---

*Abstract: Currently, digital transition and innovation are significant dimensions of transition processes and development policies. These are becoming increasingly important as more diverse and complex social, economic and environmental problems and challenges emerge. The achievement of digital transition and the promotion of sustainable development are crucial elements of the European development policy. Digital transformation can bring new challenges and many new opportunities and solutions for individual stakeholders, companies, sectors, and regions. However, little is known about the interrelations between mobility, sustainability, digitalization and climate change, especially from a regional perspective. This research aims to explore ways to make the interrelations between sustainability, climate change and digitalization more tangible, measurable and traceable. To investigate this question, (i) the spatial interpretation of the interrelations between mobility, sustainability, digitalization and climate change was formulated, (ii) an indicator-based database was developed, and (iii) a methodology for assessing the digitalization and adaptation by the regional level was formulated. The analysis exploring the correlations between digitalization and adaptation was carried out in 2021 and focused on the level of districts (LAU 1 level in Hungary). Based on the digitalization and adaptation parameters, the Spatial Digitalization Index and the Spatial Adaptation Index were conceptualized. The dynamic regression analysis proved that digitalization is increasing at the LAU 1 in Hungary, and digitalization can support and strengthen adaptation to an increasing degree in different sectors such as transportation enhancing sustainability. The findings highlight the important role of different stakeholders and the challenge-based regional or local planning perspectives.*

*Keywords: digitalization; sustainability; adaptation; climate change; mobility*

---

## 1 Introduction

Research on the interrelations between sustainable regional development where mobility plays important role and climate change promotes holistic approaches and integrated solutions owing to their inter-, multi- and transdisciplinary

characteristics. Consequently, technical-technological and socio-economic aspects and natural-environmental factors have come to the forefront of studies. The results of analyses on connections and interrelations between sustainability and adaptation bridge a gap both at the regional and the sectoral level (transportation for instance), and they improve the plannability of relevant development processes, their implementation and general livability.

One of the most significant and complex global challenges of our time, is climate change, and our knowledge about its possible effects and consequences is widening daily [1]. In addition to international agreements and treaties, a growing number of professionals from the scientific, political and social circles draw our attention to the various preparatory and preventive measures that could mitigate the effects of this phenomenon. Climate change is also gaining focus in spatial and regional development. The arising challenges may be regarded as potentials for the European regions concerning employment and innovative capacities.

The future phenomena and effects of climate change are difficult to predict with high certainty [2] [3]. Thus, challenges concerning ecological, social, economic and transportation systems and their resilience and willingness to adapt are expected to be even more significant [4]. Preparation for and adaptation to the expected effects of climate change are not isolated tasks, but they constitute a plannable process that requires cooperation at the social, political, regional and sectorial levels. The primary aim of preparation is to increase the resilience to various expected effects and to enhance the sustainability of regions and characteristic sectors. This is achieved by shifting the focus from preventive measures and control to the ability to live together with the constantly changing and occasionally dangerous environment. Adaptation to climate change can be very versatile, and the different methods require different preparatory measures, tools and methods especially considering regional characteristics [5] [6]. Socio-economic processes take place in a given area and in a given time, which – when speaking about the practical implementation of sustainability – are complemented by the fact that these processes are embedded in the natural environment, i.e., the biosphere. The adaptation to and preparation for unavoidable effects are closely related to the concept of sustainability. Consequently, the compilation and realization of spatial and sectoral, local, regional and national economic strategies, irrespective of being sustainability, climate or adaptation strategies, can all help avoid expected effects and mitigate potential damage [7-10]. Concerning regional livability, research today tends to focus on measurability in addition to theoretical explanations. Therefore, it is shown how, primarily socio-economic processes and interventions lead to the deterioration of environmental quality; thus, the effects of these processes and climate change are revealed, together with the potential effects on the practical realization of sustainability and their effect on mobility and daily life [11-13]. In relation to cognitive mobility altogether five key areas can be identified [14] including cognitive sustainability, that can contribute to and foster the understanding of mobility and economic process-related interactions [15] [16].

From this perspective, it is worth examining whether digitalization and adaptation from a regional perspective can turn into an effective tool to promote sustainability. Societies have always had to respond to climate variability and extreme weather events. Climate has always existed, it exists, and it will exist. However, the expected effects of climate change and possible solutions for these challenges differ, and they influence the motivation for turning to sustainability to a variable degree. As the connections between sustainability and climate change prove, climate change itself is one of the most significant hindering factors on the way to sustainability. The present study discusses the possible local interpretations of the connections between present-day global processes, with a special focus on the triplet of sustainability–climate change–digitalization. Concerning the steps towards sustainable regional development, the investigations presented here aim to explore how the connections between adaptation and digital transformation can be realized at the local level.

## 1.1 Sustainable Regional Development and Adaptation

The effects of climate change can be directly experienced already today, and this trend will not change. Consequently, expected impacts will affect everyone from the most vulnerable social groups, sectors and regions to the most resilient ones [2], [3]. The European Union is preparing for the expected effects, especially for the growing frequency and intensity of extreme weather events, primarily interpreted at the local level. At this level, decision-makers should prepare to handle such problems, in which the subsidiarity principle also plays a role. When setting up mitigatory, preparatory, and adaptive measures, programs and strategies designed in harmony with the precautionary principle, it is also a challenge to determine the extent of intervention by those concerned, for which the experiences gained in the past years or decades should be used as guidelines. Today, it focuses on how the following questions may be answered [17] [18]: What changes are expected in a given region or sector? Will the planned level of intervention prove to be satisfactory in fighting off the expected challenges?

Sustainability and climate change are in a circular relationship, which is reflected in several research results [19-21]. The expected direction and characteristics of development can fundamentally influence the climate change process; however, climate change also affects the chances of moving towards sustainability, both from a mitigatory and adaptive perspective. Focusing on sustainable regional development, adaptation to climate change and sustainability have gained more focus, together with analyzing synergic effects among climate-friendly solutions, tools, methodologies and policies. The research area is a European inland territory located in the Carpathian basin. The examined Central European country is Hungary, where the ratio of rural areas is still beyond the EU average [22], which results in higher exposure and vulnerability. A related UN document implied Hungary, as one of the most vulnerable countries in Europe, considering the

possible effect of climate change on biodiversity [23]. The possible impacts of climate change on the environment are crucial especially when fostering digital transformation and sustainable transition on regional or local level and its cross-fertilization effect on mobility and transport. In Hungary, several research reports and studies have published prognoses on the expected effects of climate change [23] [24]. Such prognoses are becoming more accurate over time regarding the extent of the effect and the probability and risks of its occurrence. Preparation for and prevention of expected effects and the mitigation of the connected risks are the fundamental interest of all those concerned due to the facilitation of resilience and the fact that this resilience is profitable [25] [26]. According to the available knowledge and research results, climate change affects Hungary to an extreme degree, both on the global and the European scale; but the different parts of the country are to be affected differently. These impacts may strengthen existing socio-economic differences, and regional differentiation might also be enhanced, leading to significant novel social inequalities [23] [27]. Climate change might influence every dimension of sustainability, and it fundamentally affects regional living conditions, incomes, health status etc., which are considered the cornerstones of sustainable regional development [8]. In order to preserve or enhance the standard of living and livability, it is advisable to offer incentives. The best measures are cost-effective and environment-friendly; as further positive externalities, they might also help to enhance living standards, the health status of local people (e.g., due to better air quality), might provide jobs for local professionals, and act as a driver for the local economy. In order to create a solid basis for the preparation and adaptation of local communities, it is indispensable to explore the needs and expectations for forming a general concept. In Hungary, one of the main hindering factors, for local ambitions, remains the lack of financial sources. The cost-effective adaptation to climate changes should focus on realizing local initiatives, i.e., local preparatory adaptive measures should be economically profitable and serve livability, conservation or sustainability.

The regional or local perspective is of utmost importance in analyzing connections between climate change and sustainability, with special emphasis on the following facts:

- Climate change is generally ignored in the practical implementation of sustainability measures.
- The exploration of how local sustainability-related initiatives and models are connected to regional strategies is typically missing from earlier studies.
- Reaching sustainability while considering climate change is impossible without exploring local economic activities and sectors and considering local living conditions and interests.
- The primary income-generating sector must be analyzed, focusing on climate change and local adaptive possibilities. Such analyses are lacking both at the domestic and the international levels.

- The role of digitalization in sustainable regional development considering the possible impacts of climate change.

While exploring the interconnections between the concepts of sustainability and adaptation, it was proven that endogenous factors play a key role in forming the main motivating forces in the transition towards sustainability. It was also stated that the subsidiarity principle plays a role in the practical realization of this transition. It can be stated that climate change strategies, mitigation and adaptation policies and political decisions have complex (economic, social and ecological) effects with respect to sustainable mobility. In the “normal” business operation of the market economy of today and the near future, decisions are passed respecting sustainability values only to a limited degree, although natural and environmental interests can only be taken into consideration successfully if they are in line with strategic political goals [17], [28-31]. The ability to adapt should not only be interpreted as resistance to outer effects (resilience), but the ability of the system to adapt flexibly to the changing conditions, especially local conditions, should also be included in this concept. Moreover, based on the above claims, the transition towards sustainability and the adaptation to global, regional and local challenges can be most effectively facilitated by the best practices of sustainable regional development [32]. Available and future adaptive tools may be extremely versatile both within regions and sectors, depending on the stakeholders, the target group of adaptive measures, and the expected results. Several uncertainty factors should be considered when planning preparatory measures and adaptation strategies to climate change and its expected effects. Uncertainty may stem from various causes [33]:

- Available information – the lack of information or information asymmetry might be severe hindrances during the planning of adaptive measures and the management of challenges
- Limitations of predictions
- The impossibility of estimating the future effects of planned measures during the preparatory and adaptive processes
- The responses of the given society, and the uncertainty of predicting these responses

Adaptation means the reactions and processes of a system together with their outcomes, which aim to make the system ready to tackle changing circumstances more easily and effectively [35]. These include the mitigation of damage and reconstruction after present events, the preparation for and prevention of future events, and also the enhancement of resilience to various stress scenarios. In the adaptation process, the identification of two factors is of primary importance: (i) who wishes to adopt (e.g., the society, individuals, communities, institutions, sectors, regions, settlements); and (ii) what they wish to adapt to (e.g., warming, the increasing frequency and intensity of weather events, biodiversity loss), only after the identification of these two factors that is it worth examining the available skills, abilities, possibilities and the potential devices. Adaptation has many forms

depending on its duration, character or effects on those concerned or the pilot area. The adaptive capacity of a given region also depends on whether a given resource might be replaced by something else, and if yes, at what costs.

Environmental and socio-economic challenges of climate change can be regarded as primary threats to the realization of sustainability. The transition toward sustainability might also serve the mitigation of climate change. The circular relationship between sustainability and climate change is also related to the different development directions. Regional adaptive processes, actions and measures may not only serve the preparation for the expected effects of climate change or the mitigation of present damage, but by improving local living conditions, they might also facilitate the transition toward sustainability.

## **1.2 Spatial Aspects of Digitalization and Climate Innovation Initiatives**

The achievement of digital transition and the promotion of sustainable development are crucial elements of the European development policy. Innovation processes play a key role in enhancing the economy's efficiency, greenness and competitiveness. The European Commission incentivizes the realization of sustainable sectoral and regional development, which the European Green Deal also supports. There is a need for further research how can digitalization foster sustainable transition and what extent. Most of the studies published on this topic focus on the environmental [35-37] or social dimension of sustainability [38-40], there are limited examples for multidimensional and interdisciplinary research [41-44] which have shown an increasing trend only in recent years in the scientific literature. At the end of February 2021, the new European Adaptation Strategy [45] was published. This document focuses on the achievement of resilience to the effects of climate change in the European Union, which is in line with the EU's green economy and sustainability ambitions. The most important goal in the strategy is to make the EU a society resilient to the effects of climate change by 2050, in which achieving climate innovations in non-urban areas might play a significant role. In order to find local solutions to global challenges, applying a systematic and holistic approach is indispensable, with special focus on subsidiarity and the precautionary principle.

Today, in both sectoral and regional analyses, it is advisable to focus not only on the mitigation of climate change and the adaptation to the expected effects, but also on the challenges and effects of the digital transition. New challenges require novel solutions: novel problems call for non-traditional, often creative, inter- or multi-disciplinary perspectives and solutions. The key to solving the problems related to climate change lies, among other things, in the promotion of creative and innovative solutions and in implementing related proposals effectively. While technical and technological innovations may significantly contribute to the solution of social challenges, they may also bring about social externalities, which should be

considered both in the design phase and during implementation. Beyond problem-based planning the challenge-based planning can play a pivotal role from regional development perspective due to digitalization. The interrelations between sustainability, digitalization and innovation can be grouped into four categories, from a regional perspective:

- 1) SD: Digitalization processes and developments serving sustainability
- 2) SC: Sustainable and climate-oriented processes and developments
- 3) CD: Climate-oriented digitalization processes and developments
- 4) SCD: Climate-oriented digitalization processes and developments were serving sustainability

This research aims to explore ways to make the interrelations between sustainability, climate change and digitalization more tangible, measurable and traceable. Today it is widely accepted that intelligent and innovative solutions, digitalization are required to mitigate climate change, enabling us to offer adequate socio-economic, spatial and sectoral solutions for the complex challenges arising in the future [46-50]. The present national governments tend to regard climate change mitigation and adaptation more and more as a possibility rather than an obstacle to economic welfare [51]. The concept of innovation was introduced by Joseph Schumpeter, one of the founding fathers of modern economic theory, in his 1911 book entitled “The theory of economic development”. Compared to the five basic categories of innovation established by Schumpeter (i.e., new product, the introduction of new production technology or method, the discovery of a new market, a new resource on the input market, establishment of a new organization), today's innovation is a much broader concept [52]. Despite being widely researched, literature on the connection between innovation and answers to climate change is scarce. Currently, only two major organizations deal with climate innovation and the interpretation of the background concepts: the WWF and the EIT Climate-KIC (Knowledge and Innovation Community). Today Climate-KIC is one of the most significant innovation collaborations with both public and private goals in Europe, which focuses on climate innovation to mitigate climate change and adapt to it. There are other similar fields, such as sustainable innovation; however, climate innovation is a much narrower concept. Novel ideas related to climate innovation are typically connected to mitigatory activities, although they can also be adaptive actions [53]. The systematic approach followed by the EIT Climate-KIC [54] categorizes climate innovations according to whether they are incremental or disruptive. Moreover, it also differentiates different levels of change, from the level of products and processes to the level of changes in value systems. However, this approach lacks the recognition of spatial aspects, local circumstances and characteristics. As far as it can be seen, climate-oriented digitalization processes and developments serving sustainability (cf. SCD in Figure 2) are very often spatial climate innovation initiatives as well, at the same time. Climate innovation can also be interpreted as a unique kind of innovation – be it a technological solution, a

product, a process, a service etc. – which can mitigate the expected negative effects of climate change to some extent or can aid preparation for these changes [55]. The concept of climate innovation can be interpreted from several perspectives, including spatial and sectoral ones and emission reduction and adaptation viewpoints [56] [57].

In order to include the missing regional perspectives an indicator-based analysis was conducted to examine the spatial interdependencies between digital transition and climate change. Based on the introduction the research question is whether there is a correlation between digitalization and adaptation on regional level.

## 2 Methodology

For the statistical tests on digitalization, 22 parameters were identified from the available databases (Different databases of the Hungarian Central Statistical Office were used: TMER, TIMEA, TeIR) (Table 1). Various temporal and spatial distributions characterized parameters. In Hungary the LAU 1 (Local Administration Unit 1, previously NUTS 4 level) level is the so-called, district level (“járás” in Hungarian). The NUTS classification (nomenclature of territorial units for statistics) is a spatial hierarchical system of the European Union. The current Eurostat NUTS list, which is valid from 2021, contains 92 regions at NUTS 1 level, 242 regions for NUTS 2 level and 1166 regions in the NUTS 3 level.

One of the bottlenecks of the analysis was that district level data were not always available. Regarding the data on adaptation, 72 parameters were identified, with various spatial and temporal distributions (TMER, TIMEA, TeIR). Finally, the 2013-2018 period was considered for both district level digitalization and adaptation parameters. Concerning the district level digitalization data, the DESI index (Digital Economy and Society Index) served as a starting point, while for the collection of adaptation data, adaptation capacity models [58] [59] were considered as the methodological basis.

In the context of this research, it is necessary to assess Hungary’s digitalization and climate change adaptive capacity on LAU 1 level. No such coherent database exists until now on this spatial level for Hungary. Author has established database. Let us formulate a methodology for assessing the digitalization and adaptive capacity on LAU 1 spatial level. The purpose of this technique is to merge two complex estimates.

Table 1  
List of indicators

<b>Name of indicator on LAU-1 level</b>	<b>Dimension</b>	<b>Start and end year</b>
Internet access per capita	[pcs/1000 capita]	2013-2019
Number of official places with internet access per 1000 capita in public educational institutions	[pcs/1000 capita]	2001-2009
Number of internet access	[pcs]	2003-2010
Number of operating enterprises in the information and communication branch of the national economy	[pcs]	2008-2011
Number of operating enterprises per thousand inhabitants	[pcs]	2012-2018
Proportion of professional, scientific enterprises within the operating enterprises	[%]	2006-2018
Net income per capita,	[HUF/capita]	2006-2018
Unemployment rate	[%]	2006-2018
Population density, on 31 December	[capita/km <sup>2</sup> ]	2012-2019
Population	[capita]	2006-2018
Passenger cars	[pcs]	2006-2018
Average size of real estates	[m <sup>2</sup> /real estate]	2006-2018
Forest covered area	[km <sup>2</sup> ]	2012-2018
Urban green spaces	[km <sup>2</sup> ]	2012-2018
Electricity consumption	[1000 kWh/capita]	2006-2018
Volume of gas supplied to households per capita,	[1000 m <sup>3</sup> /capita]	2006-2018
Proportion of real estates connected to a public sewer network	[%]	2006-2018
Proportion of real estates connected to the public drinking water network	[%]	2006-2018
Amount of total municipal solid waste transported	[t]	2006-2018
Number of granted patents	[pcs]	2009-2016
Ratio of the extent of total protected natural areas to the area of settlements	[%]	2006-2018
Hospital beds per ten thousand capita	[pcs/10 000 capita]	2006-2018

Based on the above digitalization and adaptation parameters, the Spatial Digitalization Index and the Spatial Adaptation Index were conceptualized (Fig. 1):

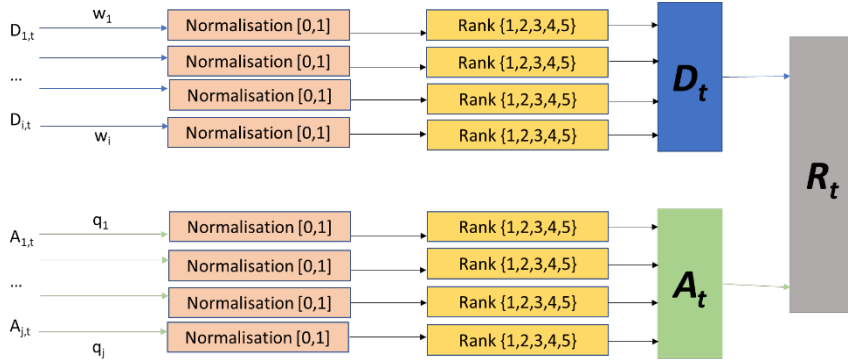


Figure 1  
Conceptual framework of assessment

Firstly, the index components needed to be defined therefore correlation analysis was made to filter out the multicollinear parameters (1), (2):

$$r_{k,t;k+1,t} = \frac{\sum_{k=1}^i (D_{k,t} - \bar{D}_t)(D_{k+1,t} - \bar{D}_t)}{\sqrt{\sum_{k=1}^i (D_{k,t} - \bar{D}_t)^2 (D_{k+1,t} - \bar{D}_t)^2}} \quad (1)$$

$$r_{l,t;l+1,t} = \frac{\sum_{l=1}^j (A_{l,t} - \bar{A}_t)(A_{l+1,t} - \bar{A}_t)}{\sqrt{\sum_{l=1}^j (A_{l,t} - \bar{A}_t)^2 (A_{l+1,t} - \bar{A}_t)^2}} \quad (2)$$

Where,

$r_{k,t;k+1,t}$  – the correlation coefficient of the linear relationship between the variables  $k^{th}$  and  $k+1^{th}$  at the year  $t$

$D_{k,t}$  – the  $k^{th}$  values of the digitalization parameter variable in a sample at year  $t$

$\bar{D}_t$  – the mean of the values of digitalization parameter variable

$D_{k-1,t}$  – the  $k-1^{th}$  values of the digitalization parameter variable in a sample at year  $t$

$A_{k,t}$  – the  $k^{th}$  values of the adoption parameter variable in a sample at year  $t$

$\bar{A}_t$  – the mean of the values of adoption parameter variable

$A_{k-1,t}$  – the  $k-1^{th}$  values of the adoption parameter variable in a sample at year  $t$

Multicollinearity is a phenomenon in which one predictor variable in a multiple regression model can be linearly predicted from the others. In this situation, the coefficient estimates of the multiple regression may change erratically in response to small changes. Ordinary least squares method requires the absence of multicollinearity. The remaining parameters were normalized to the 0–1 scale (3) and (4):

$$\widehat{D}_{i,t} = \frac{D_{i,t}}{\max \{D_{i,t}\}} \quad (3)$$

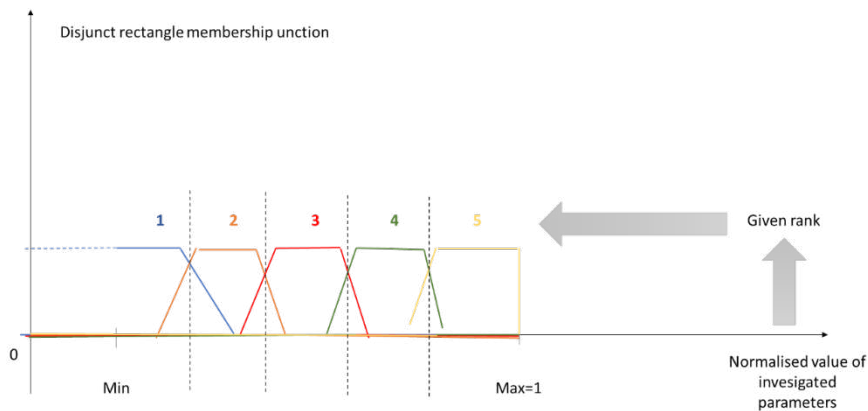
$$\widehat{A}_{i,t} = \frac{A_{i,t}}{\max\{(A_{i,t})\}} \quad (4)$$

Where,

$\max\{(D_{i,t})\}$  – maximum of  $D_i$  at year  $t$

$\max\{(A_{i,t})\}$  – maximum of  $A_i$  at year  $t$

The filtered parameters had different weights. Using this normalized scale, each district was assigned a rank from 1 to 5 for each year. For that author fuzzified the problem and established a membership function to be able to automatize the assignment. The membership function was based on the maximum and minimum value of parameters and automatically calculated five steps =Figure 2):



Visualization of membership functions

For faster calculation core of membership function were maximized and boundary of membership function were minimized (Figure 3). The weights for each parameter for each of the two indices were determined by the SPSS program, applying principal component analysis to the normalized, time-independent data.

### 3 Results – Local Adaptation in the Digital Era

The Sixth Assessment Report on impacts, adaptation and vulnerability of the IPCC (Intergovernmental Panel on Climate Change) was published at the end of February 2022 [3]. In addition to a wide range of adaptation possibilities, various risks, adaptation types and major hindering factors are also presented. Digital solutions as means for enhancing the efficiency of adaptation appear in this report several times, irrespective of the area of adaptation or the topic of discussion. One of the major objectives of the new Adaptation Strategy of the EU (2021) is that by 2050, the

Union should become a society resilient to the expected effects of climate change, i.e., a society which is capable of providing intelligent, dynamic and systematic answers and can carry out the required steps [45]. The question is how to interpret this objective in the era of the digital transition. The effects of climate change arise in different forms in various areas. Thus, it may be crucial to identify and utilize the potentials at various spatial levels in regions with different conditions. This section explores how the correlations between digitalization and adaptation can be considered at the local level to harmonize regional development initiatives with the digital transition.

The premise of the analysis is that digitalization and adaptation are correlated: more digitally developed regions adapt to the expected effects of climate change more quickly. If a given region has no sufficient adaptive ability, it becomes vulnerable, resulting in reduced livability and a diminished sustainable regional development potential. It is a fundamental question whether initiatives related to digital transition might influence this process, and if yes, to what extent. The adaptive ability of a given region is related to the level of living standards and development. Both adaptation and digitalization are characterized by versatility concerning their types and measurability. From an ecological economics perspective, digitalization can be interpreted as a tool for closing socio-economic chains and, thus, as a factor contributing to the transition towards sustainability. Finally, the district level results were visualized on maps (QGIS): *Figure 3.* shows the average values of the Spatial Digitalization Index for each district in Hungary, while *Figure 4.* depicts the average district level values of the Spatial Adaptation Index.

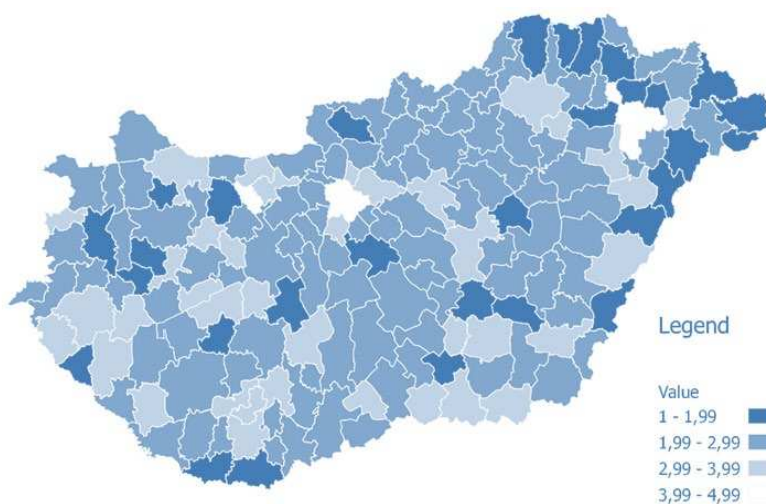


Figure 3

Visualization of digitalization parameters based on the average of 2013-2018

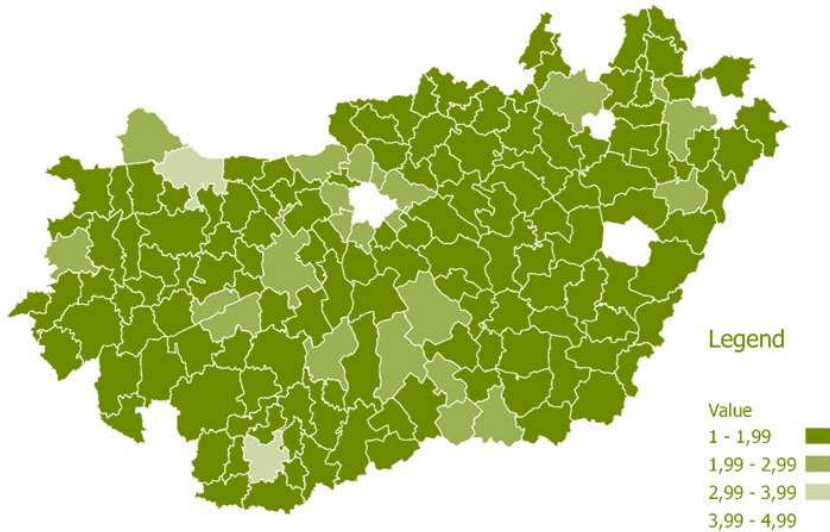


Figure 4

Visualization of adaptation parameters based on the average of 2013-2018

## 4 Analysis

The analysis exploring the correlations of digitalization and adaptation presented here was carried out in 2021 and focused on the level of districts (NUTS 3 level in Hungary). The dynamic regression analysis proves that digitalization is increasing at the district level in Hungary and digitalization can support and strengthen adaptation to an increasing degree:

$$\min\{\varepsilon_t\} \rightarrow A_t = \alpha \cdot D_t + \varepsilon_t \quad (5)$$

where,

$A_t$  is adoption rank at year  $t$

$D_t$  is digitalization rank at year  $t$

$\alpha$  is slope of linear regression

$\varepsilon_t$  is the error term in year  $t$

In the examined period, the level of digitalization increased and helped adaptation; thus, the excess of support also grew owing to the higher level of digitalization over time (Figure 5):

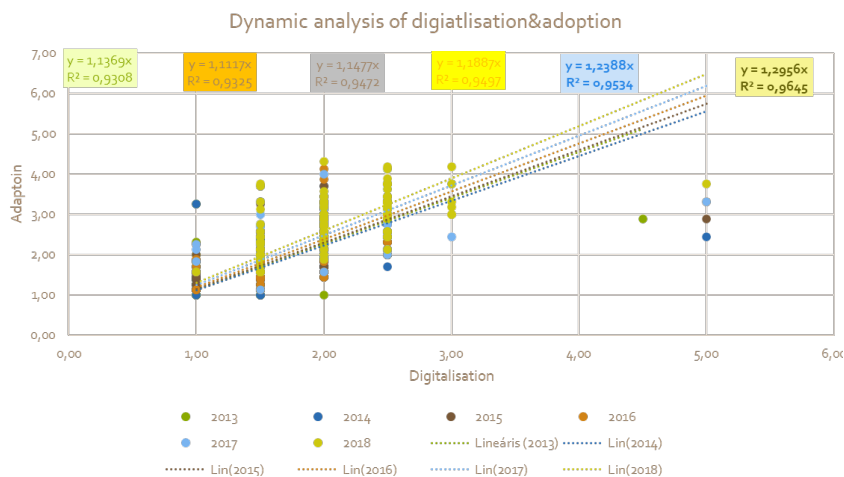


Figure 5

The change of the correlation between digitalization and adaptation of Hungarian districts between 2013 and 2018

The tests prove that the weight of certain digitalization and adaptation parameters is different. This analysis proves a correlation between the district-level values of the Digitalization Index and the Adaptation Index. Digitalization might play a role in the integrated approach to adaptation. The data prove that the level of the digital infrastructure of Hungarian districts is growing, which in turn aids the adaptation of districts to a higher extent, which can also contribute to the relevant region's transition to sustainability.

Sustainability is the development and a possibility at the same time, and development can be interpreted as an improvement in adaptation. From the perspective of regional development, it is crucial to determine the extent to which climate change affects endogenous and exogenous factors and how this can be interpreted in the era of digitalization.

The present study wishes to explore how the interpretation framework and spatial characteristics can be interpreted from a sustainability perspective, focusing on the challenges posed by climate change. Another research question is whether correlations can be found between digitalization and adaptation from a spatial perspective. Owing to the strong locality of the expected effects of climate change, local solutions will be required. The question is how innovative adaptation can be interpreted concerning sustainable regional development. Spatial aspects may influence the flexibility of adaptation to various degrees. The above analyses prove that the exploration of correlations between digital transition and adaptive capacity and the strengthening of potential synergic effects may contribute to enhancing livability at the local level and strengthening local sustainability.

## Conclusions

Sustainability and climate change are connected in several ways and exist in a circular relationship. The direction of climate change may fundamentally be affected by the direction and characteristics of regional development. Additionally, the occurrence of the expected effects of climate change may modify the chances of moving towards sustainability even at the local level, both from a mitigatory or an adaptive perspective. Moreover, the achievement of digital transition and the promotion of sustainable development are central elements in European development policies.

This study interpreted the interrelations of sustainability and digitalization with a special focus on the phenomenon and concept of climate innovation. Regional climate innovation ambitions might facilitate the movement of the region towards sustainability. One reason for this is that various innovative digital solutions, which might serve as effective tools to handle the challenges related to climate change, may also contribute to the change of adaptive capacity. This is especially true for the potential of digital transition, which is also supported by the correlation explored in this study between the district-level Digitalization Index and Adaptation Index and by the mutual strengthening effect of processes related to digitalization and adaptation.

The major focus of this study was on adaptation, which can be interpreted as a new dimension of sustainable regional or local development. In sum, the study's results on connections between digitalization and adaptation at the regional level direct attention to the interrelations of the transition towards digitalization and sustainability in the era of climate change.

Taking into account the challenge-based planning options can be pivotal in regional sustainable development perspectives. This also highlights those aspects of sustainable regional development which might provide useful information for experts, designers, policymakers and local decision-makers.

## Acknowledgement

This work was supported by the János Bolyai Research Scholarship of the Hungarian Academy of Sciences and supported by the ÚNKP-22-5 New National Excellence Program of the Ministry for Innovation and Technology from the source of the National Research, Development and Innovation Fund.

## References

- [1] Li, J., Li, W., & Lian, G. (2022) A Nonlinear Autoregressive Model with Exogenous Variables for Traffic Flow Forecasting in Smaller Urban Regions. *Promet*, 34(6), 943-957, DOI: <https://doi.org/kh9z>
- [2] IPCC (2021) Climate Change 2021: The Physical Science Basis. Contribution of Working Group I to the Sixth Assessment Report of the Intergovernmental Panel on Climate Change [Masson-Delmotte, V., P. Zhai,

- A. Pirani, S. L. Connors, C. Péan, S. Berger, N. Card, Y. Chen, L. Goldfarb, M. I. Gomis, M. Huang, K. Leitzell, E. Lonnoy, J. B. R. Matthews, T. K. Maycock, T. Waterfield, O. Yelekçi, R. Yu, and B. Zhou (eds.) Cambridge University Press
- [3] IPCC (2022) Climate Change 2022. Impacts, Adaptation and Vulnerability. Summary for Policymakers. Working Group II contribution to the Sixth Assessment Report of the Intergovernmental Panel on Climate Change
- [4] Isoard, S. (2011) Perspectives on adaptation to climate change in Europe. In Ford, J.-d. & Berrang-Ford, L. (Eds.), *Climate Change Adaptation in Developed Nations* (pp. 51-68) Springer. DOI: <https://doi.org/cqg7sq>
- [5] Biesbroek, G. R., Termeer, C. J. A. M., Klostermann, J. E. M. & Kabat, P. (2013) On the nature of barriers to climate change adaptation. *Regional Environmental Change*. 13, 1119-1129, DOI: <https://doi.org/f5b9bt>
- [6] Bosello, F. (2014) The role of economic modelling for climate change mitigation and adaptation strategies. In A. Markandya, I. Galarraga & E. S. de Murieta (Eds.), *Routledge Handbook of the Economics of Climate Change Adaptation*. Routledge: Abingdon, UK. DOI: <https://doi.org/kh92>
- [7] Dubois, C., Cloutier, G., Potvin, A., Adolphe, L., Joerin, F. (2015) Design support tools to sustain climate change adaptation at the local level: A review and reflection on their suitability. *Frontiers of Architectural Research* 4(1). 1-11, DOI: <https://doi.org/gd85pv>
- [8] Szalmáné Csete M. (2018) Prepare and adapt. In: Sági, Zs.; Pál, K. (eds.): *Temperate climate zone? Responsible actions for effective climate protection*. [in Hungarian: *Felkészülés és alkalmazkodás*. Sági Zs.; Pál, K. (szerk.): *Mérsékelt öv? Felelős cselekvési irányok a hatékony klímavédelemért*] Association of Climate Friendly Municipalities [in Hungarian: *Klímabarát Települések Szövetsége*] Budapest. ISBN 978-615-00-1120-2, pp. 61-74
- [9] Ledda, A., Di Cesare, E., Satta, G., Cocco, G., Calia, G., Arras, F., Congiu, A., et al. (2020) Adaptation to Climate Change and Regional Planning: A Scrutiny of Sectoral Instruments. *Sustainability*, 12(9), 3804. MDPI AG. DOI: <https://doi.org/kh93>
- [10] Szabó, Z., Török, Árpád, Sipos, T. (2021) Order of the Cities: Usage as a Transportation Economic Parameter. *Periodica Polytechnica Transportation Engineering*, 49(2), pp. 164-169, DOI: <https://doi.org/gt43>
- [11] Wilson, E. (2006) Adapting to Climate Change at the Local Level: The Spatial Planning Response. *Local Environment* 11(6) 609-625, DOI: <https://doi.org/djvnd9>
- [12] Granberg, M., Elander, I. (2007) Local Governance and Climate Change: Reflections on the Swedish Experience. *Local Environment* 12(5) 537-548, DOI: <https://doi.org/d68gq9>

- [13] Zöldy, M., & Baranyi, P. (2021) Cognitive Mobility–CogMob. In 12<sup>th</sup> IEEE International Conference on Cognitive Infocommunications (CogInfoCom 2021) Proceedings IEEE (pp. 921-925)
- [14] Biró, K., & Toldi, O. (2022) Hungarian agricultural pathways revealing climate-related challenges. *Cognitive Sustainability*, 1(4) DOI: <https://doi.org/gr2bdt>
- [15] Zoldy, M., Szalmane Csete, M., Kolozsi, P. P., Bordas, P., & Torok, A. (2022) Cognitive Sustainability. *Cognitive Sustainability*, 1(1) DOI: <https://doi.org/htfq>
- [16] Xu, L., Marinova, D., Guo, W. (2015) Resilience thinking: a renewed system approach for sustainability science. *Sustainability Science* 10(1). 123-138, DOI: <https://doi.org/f6tj8j>
- [17] SEG – Scientific Expert Group on Climate Change (2007) *Confronting Climate Change: Avoiding the Unmanageable and Managing the Unavoidable*. Report prepared for the United Nations Commission on Sustainable Development. Sigma Xi, Research Triangle Park, NC, and the United Nations Foundation, Washington, DC.
- [18] Berrang-Ford, L., Ford, J. D., Paterson, J. (2011) Are we adapting to climate change? *Global Environmental Change* 21(1) 25-33, DOI: <https://doi.org/dxcsvw>
- [19] Munasinghe, M, and Swart, R. (2000) *Climate change and its linkages with development, equity and sustainability*. Netherlands: N. p., 2000. Retrieved from URL: <https://www.osti.gov/etdeweb/biblio/20032653>
- [20] Munasinghe, M. (2001) Exploring the linkages between climate change and sustainable development: A challenge for transdisciplinary research. *Conservation Ecology* 5(1): 14. Retrieved from URL: <http://www.consecol.org/vol5/iss1/art14/>
- [21] Beg N., Morlot J. C., Davidson, O., Afrane-Okesse, Y., Tyani, L., Denton, F., Sokona, Y., Thomas, J. P., Lèbre La Rovere, E., Parikh, J. K., Parikh, K. & Rahman, A. (2002) Linkages between climate change and sustainable development, *Climate Policy*, 2:2-3, 129-144, DOI: <https://doi.org/dmf8f2>
- [22] OECD (2020) *Rural Well-being: Geography of opportunities*. Country Note: Hungary. Retrieved from URL: <https://www.oecd.org/regional/Rural-WellBeing-Hungary.pdf>
- [23] Láng I., Csete L., Jolánkai M. (2007) *Global climate change: domestic impacts and responses [in Hungarian: A globális klímaváltozás: hazai hatások és válaszok]*. The VAHAVA report [in Hungarian: A VAHAVA jelentés] Budapest, ISBN 0609001358167

- [24] NÉS-2 (2018): 23/2018 (X.31.) National Assembly Decision: Second National Climate Change Strategy [in Hungarian: 23/2018 (X.31.) OGY Határozat: Második Nemzeti Éghajlatváltozási Stratégia]
- [25] Takács-Sánta, A. (2008) International experience of municipal climate programmes - lessons for domestic action [in Hungarian: A települési klímprogramok nemzetközi tapasztalatai – tanulságok a hazai intézkedésekhez] *Klíma-21 Füzetek* 54, pp. 22-36
- [26] Buzási A., Csizovszky A. (2021) Sustainability and climate adaptation in urban development - lock-in analysis through the example of the XVII district of Budapest [in Hungarian: Fenntarthatóság és klímaadaptáció a városfejlesztésben – lock-in elemzés Budapest XVII. kerületének példáján keresztül] *Space and Society* [in Hungarian: Tér és Társadalom] 35(1) 72-91, DOI: <https://doi.org/kh94>
- [27] Szlávik J. (2018) Prepare and adapt. In: Sági, Zs.; Pál, K. (eds.): *Temperate climate zone? Responsible actions for effective climate protection.* [in Hungarian: Felkészülés és alkalmazkodás. Sági Zs.; Pál. K. (szerk.): Mérsékelt öv? Felelős cselekvési irányok a hatékony klímavédelemért] *Association of Climate Friendly Municipalities* [in Hungarian: Klímabarát Települések Szövetsége] Budapest, ISBN 978-615-00-1120-2, pp. 75-86
- [28] Du Pisani, J. (2007) Sustainable development – historical roots of the concept. *Environmental Sciences* 3(2). 83-96, DOI: <https://doi.org/b4bjwn>
- [29] Puppim de Oliveira, J. A. (2009) The implementation of climate change related policies at the subnational level: An analysis of three countries. *Habitat International* 33(3) 253-259, DOI: <https://doi.org/bskqkr>
- [30] Reckien, D., & Elisaveta P Petkova, P. E. (2019) Who is responsible for climate change adaptation? *Environmental Research Lettter* 14 014010 DOI: <https://doi.org/gq66x3>
- [31] Sipos, T., Szabó, Z., & Török, Á. (2021) Spatial econometric cross-border traffic analysis for passenger cars–Hungarian experience. *Promet-Traffic&Transportation*, 33(2), 233-246, DOI: <https://doi.org/gq66x3>
- [32] Szalmáné Csete M., Buzási A. (2020) Hungarian regions and cities towards an adaptive future - analysis of climate change strategies on different spatial levels. *Időjárás / Quarterly Journal of the Hungarian Meteorological Service* 124 : 2 pp. 253-276, DOI: <https://doi.org/hz9q>
- [33] Szalmáné Csete M., Taksz L. (2016) European and national trends in climate change adaptation. In: Pálvölgyi, T.; Selmeczi, P. (eds.): *Knowledge sharing, adaptation and climate change. Research and development results of the Hungarian Geological and Geophysical Institute for the establishment of the National Adaptation Geoinformatics System.* Hungarian Geological and Geophysical Institute [in Hungarian: A klímaváltozáshoz való alkalmazkodás európai és hazai irányzatai In: Pálvölgyi T., Selmeczi P.

- (szerk.): Tudásmegosztás, alkalmazkodás és éghajlatváltozás. A Magyar Földtani és Geofizikai Intézet kutatási-fejlesztési eredményei a Nemzeti Alkalmazkodási Térinformatikai Rendszer létrehozására. Magyar Földtani és Geofizikai Intézet], Budapest. ISBN 978-963-671-308-9, pp. 17-25
- [34] Smit, B., Wandel, J. (2006) Adaptation, adaptive capacity and vulnerability. *Global Environmental Change* 16(3). 282-292, DOI: <https://doi.org/b68fzw>
- [35] Gouvea, R., Kapelianis, D., & Kassicieh, S. (2018) Assessing the nexus of sustainability and information & communications technology. *Technological Forecasting and Social Change*, 130 (2018) pp. 39-44, DOI: <https://doi.org/kh95>
- [36] Isensee, C., Teuteberg, F., Griese, K.-M. & Topi C., (2020) The relationship between organizational culture, sustainability, and digitalization in SMEs: a systematic review. *Journal of Cleaner Production*, 275 p. 122944. DOI: <https://doi.org/gg7vvh>
- [37] Del Río Castro, D; M.C. González Fernández, M. C.; & Uruburu Colsa, Á. (2021) Unleashing the convergence amid digitalization and sustainability towards pursuing the Sustainable Development Goals (SDGs): a holistic review. *Journal of Cleaner Production*, 280, p. 122204. DOI: <https://doi.org/gk9nrq>
- [38] Axelsson, K., Melin, U., and Lindgren, I., (2010) Exploring the Importance of Citizen Participation and Involvement in E-government Projects—Practice, Incentives and Organization. *Transforming Government: People, Process and Policy*, (4:4): 299-321, DOI: <https://doi.org/bbmns>
- [39] Park, S. (2017) Digital inequalities in rural Australia: A double jeopardy of remoteness and social exclusion. *Journal of Rural Studies* 54: 399-407, DOI: <https://doi.org/ggt334>
- [40] Zavrtnik, V., Podjed, D., Trilar, J., Hlebec, N., Kos, A., & Stojmenova Duh, E. (2020) Sustainable and community-centred development of smart cities and villages. *Sustainability*, 12(10), 3961, DOI: <https://doi.org/kh96>
- [41] Brenner, B.; & Hartl, B. (2021) The perceived relationship between digitalization and ecological, economic, and social sustainability. *Journal of Cleaner Production*, (315) 128128, DOI: <https://doi.org/grsp47>
- [42] Esses, D., Csete, M. S., & Németh, B. (2021) Sustainability and Digital Transformation in the Visegrad Group of Central European Countries. *Sustainability*, 13(11), 5833, MDPI AG, DOI: <https://doi.org/hbkx>
- [43] Foronda-Robles, C., L. Galindo-Pérez-de-Azpillaga (2021) Territorial intelligence in rural areas: The digitization of non-profit associations through social media. *Technology in Society*, Volume 64, 2021, 101459, ISSN 0160-791X, DOI: <https://doi.org/kh97>

- [44] Mubarak, F., Suomi, R. and Kantola, S.-P. (2020) Confirming the links between socio-economic variables and digitalization worldwide: the unsettled debate on digital divide, *Journal of Information, Communication and Ethics in Society*, Vol. 18 No. 3, pp. 415-430, DOI: <https://doi.org/gq8mwj>
- [45] COM/2021/82 final: Communication from the Commission to the European Parliament, the Council, the European Economic and Social Committee and the Committee of the Regions, Forging a climate-resilient Europe - the new EU Strategy on Adaptation to Climate Change, Brussels, 24.2.2021, URL: <https://eur-lex.europa.eu/legal-content/EN/TXT/PDF/?uri=CELEX:52021DC0082&from=EN>
- [46] Schieferdecker, I., & Mattauch, W. (2014) ICT for Smart Cities: Innovative Solutions in the Public Space. *ICT for Smart Cities: Innovative Solutions in the Public Space* In: Zander, J.; Masterman, P.J. *Computation for Humanity: Information Technology to Advance Society 2014*, Taylor Francis Group, LLC p. 30
- [47] Bibri, S. E. (2019) On the sustainability of smart and smarter cities in the era of big data: an interdisciplinary and transdisciplinary literature review. *Journal of Big Data*, 6 (25) DOI: <https://doi.org/gf2ffj>
- [48] Trască, D. L., Stefan, G. N., Sahlian, D. N., Hoinaru, R., & Serban-Opreescu, G-L. (2019) Digitalization and Business Activity. The Struggle to Catch Up in CEE Countries. *Sustainability* 11, 2204, DOI: <https://doi.org/ggs2n6>
- [49] Shkarlet, S., Dubyna, M., Shtyrkhun, K., & Verbivska, L. (2020) Transformation of the Paradigm of the Economic Entities Development in Digital Economy. *WSEAS TRANSACTIONS on ENVIRONMENT and DEVELOPMENT*. 16, 413-422. DOI: <https://doi.org/gp66jz>
- [50] Matthess, M., & Kunkel, S. (2020) Structural change and digitalization in developing countries: Conceptually linking the two transformations. *Technology in society*, 63, 101428, DOI: <https://doi.org/gjwqw2>
- [51] OECD (2021). *OECD Economic Outlook, Volume 2021 Issue 1: Preliminary version*, No. 109, OECD Publishing, Paris. DOI: <https://doi.org/gpjwf9>
- [52] Schumpeter, J. A. (1939) *Business Cycles: A Theoretical, Historical and Statistical Analysis of the Capitalist Process*. McGraw-Hill Book Company, New York – Toronto – London
- [53] WWF (2011) *Enabling the Transition, Climate Innovation Systems for a Low Carbon Future*, WWF Report, WWF Sweden, Stockholm. ISBN 978-91 89272-19-4
- [54] EIT Climate-KIC (2016) *System Climate Innovation for a Transformative Impact. Climate Innovation Insights, Series 1.3, Climate-KIC UK*. URL: [https://www.climate-kic.org/wp-content/uploads/2017/03/Insight03\\_Proof4.pdf](https://www.climate-kic.org/wp-content/uploads/2017/03/Insight03_Proof4.pdf)

- 
- [55] Szalmáné Csete M., Barna O. (2021) Assessment of Regional Climate Innovation Potential in Hungary. *International Journal of Global Warming* 25(3-4) 378-389, Paper: IJGW\_306287. DOI: <https://doi.org/kh98>
- [56] Fűr, A., Csete, M. (2010) Modeling methodologies of synergic effects related to climate change and sustainable energy management. *Periodica Polytechnica Social and Management Sciences*, 18(1), pp. 11-19, DOI: <https://doi.org/hbkw>
- [57] Biró, K., Szalmáné Csete, M. Corporate social responsibility in agribusiness: climate-related empirical findings from Hungary. *Environ Dev Sustain* 23, 5674–5694 (2021) DOI: <https://doi.org/gjh974>
- [58] Juhola, S., Peltonen L., Niemi, P. (2012) The ability of Nordic countries to adapt to climate change: assessing adaptive capacity at the regional level. *Local Environment* 17(6-7) 717-734. DOI: <https://doi.org/gg32p5>
- [59] Juhola, S., Kruse, S. (2015) A framework for analysing regional adaptive capacity assessments: challenges for methodology and policy making. *Mitigation and Adaptation Strategies for Global Change* 20. 99-120, DOI: <https://doi.org/kh99>

# Competition vs. Cooperation: Do Subsidies with Government-Set Eligibility Threshold Values Produce Lower Battery Electric Vehicle Prices?

**Wengritzky Zsuzsánna**

Faculty of Economics and Business Administration, Babeş–Bolyai University,  
Teodor Mihali Street 58-60, RO-400591, Cluj-Napoca, Romania;  
zsuzsanna.wengritzky@econ.ubbcluj.ro

---

*Abstract: The present work is related to a subsidy program, with government-set eligibility threshold values, for Battery Electric Vehicles (BEVs), based on the tender of the Hungarian Ministry of Economics and Technology related to the Climate Action plan. After describing the program, the Hungarian BEV market in this period is presented using aggregate registration data available from 2016 to 2021. The paper has a methodological contribution by showing the relevant breakpoints of illustrated profit functions with imposed threshold values for subsidy eligibility in a monopolistic frame. On this basis, the program's effects on the prices' behavior for three selected BEV models is analyzed and the extent to which the threshold values impact the firms' cooperation in an oligopoly market is evaluated. Results show that the program was inefficient upon its launching since the threshold value was too high, and thus firms could partially capture benefits of the subsidy. On the other hand, it is shown in the third cycle of the program that a threshold value chosen from the optimal price interval gathers prices higher than the threshold to the focal point given by the threshold, and thus it has a price-decreasing effect. In the last cycle of the program, a lower threshold value could have been more effective; however, data on these models show that non-optimum thresholds create competition, and thus prices decrease until a certain level regardless.*

*Keywords: BEV; battery electric vehicles; government subsidy; focal point; price control; equilibrium price*

---

## 1 Introduction

The objective of the present work is to analyse a specific subsidy type on the Hungarian battery electric automotive market, where firms have to set their prices below a government-set threshold value in order to be eligible for the subsidy. The aim of the program was to spread the strictly electric vehicles in the country in the time period of 2016 and 2021. The most constraining criteria of product eligibility was a government-imposed threshold value (or values), which acts as a

price limitation, very similar to a price ceiling, except that, it is not compulsory for firms to price their products below the imposed value, only if they want them to gain eligibility. Thus, an expected effect of the threshold is the restructuring of the pricing system on the market, so sellers of models with prices exceeding the threshold by a small amount will tend to reduce their sales prices, while those under it will tend to increase them.

The first assumption has already been confirmed, as prices for several models were reduced upon the announcement of the subsidy program. For instance, according to the Portfolio.hu online Hungarian magazine, the price of Peugeot e-2008 was reduced slightly below the threshold from HUF 12.1 M to HUF 11.99 M. Furthermore, price reductions have been implemented for the Kia e-Niro and the Nissan Leaf models as well. Moreover, based on the data, it is obvious that the prices of several models, such as Hyundai Ioniq and Kia EV6, were set just below the threshold of eligibility. There are two interesting questions to be addressed. First, to what extent does the value of the threshold affect the prices of the analyzed models in order to meet the eligibility criteria? Second, will threshold values act as focal points, or will competition force firms to decrease their prices even more below the eligibility threshold?

The present paper uses aggregate data on new BEV registration in Hungary from 2016 to 2022 and adopts the equations included in the methodology suggested by Berry, Levinsohn, and Pakes (1995) [3] to provide a graphical illustration of the results. Expressions derived from the demand and supply theory are used to illustrate profit functions with government-set threshold and subsidy values, assuming the coordination of firms in order to analyse the behavior of these functions. The assumption on the coordination of firms is rather harsh, but it comes with a great advantage since this way a monopolistic frame can be illustrated, and thus the tools for approaching the firms' profit functions are given. The methodology will be presented in more detail in subsections 5.3 and 6.3. Graphical representations are used to show through that the profit functions are not continuous, as their breakpoint locations depend on the threshold values and the subsidy amounts. In the empirical analysis, three BEV models are selected, namely the Kia e-Niro, Hyundai Kona, and Honda-e. In order to represent their profit functions, a total cost value is assumed based on other papers' estimations [1] [8] [13], and further assumptions are made on the value of product characteristics and error terms.

Results show that the program was the most efficient in the third cycle, when analyzed firms priced their products at the focal point that was slightly below the threshold value. In the fourth cycle, due to the higher threshold, competition had more pulling power than cooperation, and thus the analyzed firms priced with roughly 5% below the threshold. This reveals two aspects regarding the fourth cycle: with a lower threshold, prices could have been pushed downwards, but also, in an oligopoly, when the threshold is slightly higher than the optimum, competition will decrease prices until a certain level regardless. This result contributes to the

literature on focal points by showing that the higher the threshold value, the lower the probability of tacit collusion [20] and the less likely is the focal point phenomena to happen. The second cycle was quite inefficient due to the very high threshold value, which probably had an undesired effect on firms' pricing strategy.

The present enriches the literature on fuel-efficient vehicles that has become very rich in the recent decades, mostly due to the increased popularity of green transportation and climate action programs. Gallagher and Muehlegger's (2008) [14] paper is one of the earliest works that studies the hybrid-electric automobile market in the US, and it concludes that the type of the tax incentive (sales tax, income tax, or non-tax incentive) has the same importance as its value. One year later, Diamond (2009) [6] analyses the impact of government incentives on the adoption of three selected HEV models. Chandra et al. (2010) [5] analyzed a sales tax rebate on HEVs in five provinces in Canada and found that a \$1,000 increased in the provincial sales tax rebate increases the market share of hybrid vehicles by 31-38%. Analyzing the incidence of existing subsidies for Toyota Prius, Sallee (2011) [23] determined the benefits from tax incentives for hybrids and concluded that consumers had captured the benefits of the subsidy even though they had had to face long queues because of the high demand. Later, Beresteanu and Li (2011) [2] made another contribution to the literature by adopting a structural method to estimate an equilibrium model for the entire US automobile market, with a focus on gasoline prices and HEV adoption. Jenn et al. (2013) [19] implement a model that is able to neglect the increase in sales as a result of technology adoption and not due to government incentives, and thus it obtains a more realistic result on the effectiveness of the programs. The present work aims to contribute to the presented literature, as it analyses the pricing strategies of three selected BEV models and finds that the value of the eligibility threshold is extremely important for the achievement of price decreases on the targeted BEV market.

Further, the literature on the implementation of focal point hypothesis and on firms' cooperation vs. competition pricing strategies when a price control of some nature is introduced by the government is elaborated. It is known from the theory of focal points that there exists some kind of gathering of prices around certain natural focal points (e.g., \$199.99), which may lead to tacit collusion [20]. Let us now introduce a government-set price ceiling. It is expected that prices will be set at the ceiling, and so it is realistic for ceiling values to act as focal points without necessarily involving tacit collusion [20]. Confirming this result, results of the paper at hand show that in certain cycles of the analyzed subsidy, firms decrease the price of their products to the focal point given by the threshold value, which acts like a price ceiling in this case. Another important aspect of the focal point is that, all else being equal, it becomes more difficult to sustain tacit collusion as the focal point rises [20]. The underlying logic is straightforward: the higher the gap between the focal point and the equilibrium point, the higher the place for competition and the more will profits rise with lower prices than with cooperation. Moreover, in this paper it is contended that the higher the threshold value, the lower the probability of the

focal point phenomena to occur. This affirms the expectations of Zhang et al. (2020) [25], who argue that a lower price ceiling would result in higher coordination, whilst a higher price ceiling would reduce the probability of reaching a common price at the focal point on the Chinese gasoline station market. Their paper presents an example of tacit collusion, analyzing a price ceiling on the Chinese gasoline station market and outlining some situations in which stations increase prices and coordinate to the focal point at the price ceiling, thus challenging the assumption that price ceilings serve the purpose of preventing firms from monopolizing consumer surplus [24].

The paper signed by Fan and Zhang (2020) [12] is crucial since, to my knowledge, it is the only work that analyses a subsidy program with some type of price control set by the government. The analyzed subsidy form has similar aspects to the one examined in this paper, except that once a firm had gained eligibility for a product, it was constrained to price it below the winning ceiling. Therefore, competition was required for eligibility, and the focal point theory could not hold either since the ceiling values differed both on the firm and product level. The paper at hand seeks to find answers to the same fundamental questions but in a slightly different scenario, using a different approach: will threshold values act as focal points and result in decreased prices? Is there an optimal threshold value that generates the lowest prices for the analyzed BEVs, thus increasing the consumer surplus and the spread of BEVs in the country?

## 2 Background and Data

The Hungarian Ministry of Economics and Technology announced a subsidy within the Climate Action program that aims to stimulate the purchase of fully electric vehicles. The program started in the year 2016 and the last application period was in 2021. Within this time frame, there were four different cycles of the program, all having their specific subsidy benefits and eligibility requirements shown in *Table 1*. The data comes from the private company DATAHOUSE, which collects and processes data on new car registration in Hungary. The provided database contains information on imported and sold automotive vehicles from 2014 to 2022 that covers a wide range of product characteristics and on new BEV registrations from October 2016 to October 2022. In this period a total of 14,112 BEVs were registered.

Unfortunately, we do not have price data on some high-end models such as Tesla, therefore these observations were removed from the database, and thus we end up with 13,676 sold BEVs in this period.

Table 1

Benefits and requirements of the government subsidy program between 2016 and 2021 (prices and values in HUF)

	I	II	III	IV
<b>Application Period</b>	09.2016 — 08.2018	10.2018 — 02.2020	15.06.2020	06.2021
<b>Value</b>	21% (max. 1.5 M)	21% (max. 1.5 M)	2.5 M / 0.5 M	2.5 M / 1.5 M
<b>Threshold</b>	15 M	20 M	11 M / 15 M	12 M / 15 M
<b>Budget</b>	2.3 B	3 B	2 B	3 B

*Table 2* presents the central tendency and variability measures of the gross prices of registered BEVs with dealer discounts other than the subsidy in each cycle of the program. Note that due to slow administrative procedures some of the BEVs subsidized in the first cycle were actually registered in 2019 and 2020. Similarly, registrations from the second cycle were dragged on at least until 2021. Having information on actual purchases in almost each year from official statements [9] [10] [11] [16-18], the data company delimited the cycle periods when BEVs were actually registered, accumulating linearly in time the subsidized registrations in each cycle. In this sense, the first cycle includes all BEV registrations from 2016 to 2018 and the remaining subsidized registrations from January 2019 and 2020 respectively. The second, the third, and the fourth cycle include all registrations from February 2019 to May 2020, from June 2020 to July 2021, and from August 2021 to October 2022 respectively.

Firstly, it is to be observed that contrary to the maximum values, the minimum values of BEVs did not increase remarkably; the most expensive electric vehicle in the last cycle being almost 5 times higher than in the first one. This increase in prices on the high-end comes along with the worldwide spread of BEVs and thus the appearance of luxury electric vehicles that are usually SUV models and are more expensive to produce. For instance, in *Table 2*, the maximum values for 2020 and 2021 correspond to the Audi E-tron GT and Mercedes EQS sports cars respectively, both having a kW power value greater than 400. It is interesting to note that in the first cycle even the price of the most expensive car was non-binding and more than that, it appears from import data that 100% of the list prices were non-binding in the second cycle until the end of the application period. This brings up an interesting question about the meaning of the threshold value in these years. In the third cycle, the mode value is HUF 10.99 M, which is slightly below the eligibility threshold. This suggests that there might be a gathering of prices around a focal point defined by the threshold value in the third cycle.

The median price is rising, however its value in the fourth cycle is only 1.43 times as high as in the first one, while the maximum price increased to a 4,83 times higher value in the same period.

Table 2

Descriptive statistics measures of gross prices with dealer discounts of BEVs registered in Hungary during the four cycles of the analyzed subsidy program (prices in million HUF)

	I. Cycle	II. Cycle	III. Cycle	IV. Cycle
<b>Total Obs.</b>	2119	2421	3129	5460
<b>Minimum</b>	6.91	6.55	6.50	6.57
<b>Maximum</b>	13.88	33.01	53.25	67.09
<b>Mean</b>	9.71	12.03	12.42	15.92
<b>Mode</b>	7.15	11.25	10.99	8.49
<b>Median</b>	9.89	11.29	11.97	14.19
<b>Std. dev.</b>	2.10	4.10	4.30	8.20

Further, the mean price increased by 64% during the four cycles, which is again higher than the increase of the median value (43%), showing that even though the BEVs' scale of diversity and price value has risen, the majority of the vehicles are priced lower than the average and probably target the low- and middle-class of consumers. Finally, the standard deviation measures of prices increased significantly, which was expected taking into account the above-mentioned widening of the price range.

### 3 Illustration of Profit Functions with Thresholds Required for Subsidy Eligibility Following a Cooperative Strategy

This paper makes use of the equations from the mentioned BLP approach that builds on a random-coefficients logit model. After shortly presenting the demand and supply sides of this model, several scenarios will be presented to show the potential equilibrium prices of cooperating firms considering a subsidy with government-imposed threshold values set for eligibility. As it is assumed that firms cooperate, we can implement a monopoly market that simplifies the model that implements several advantages to be presented later on. The assumption of a monopolistic market structure may seem harsh at first sight, but considering the subsidy eligibility as carrying a higher market power than competition, thus encouraging firms to set prices at the focal point, the monopolistic approach might be a realistic one.

#### 3.1 Demand

The utility that consumer  $i$  obtains from consuming product  $j$  is given by equation (1):

$$u_{ijm} = \alpha_i p_{jm} + x_{jm} \beta_i + \xi_{jm} + \varepsilon_{ijm} \quad (1)$$

where  $\alpha_i$  is the individual-specific coefficient of price,  $p_{jm}$  is the price of product  $j$  in market  $m$ ,  $x_{jm}$  is a vector of non-price attributes of product  $j$  in market  $m$ ,  $\beta_i$  is an individual-specific vector of the coefficients,  $\xi_{jm}$  is the product-specific utility in market  $m$  that is unobserved by the researcher and correlated with  $p_{jm}$ . The product- and individual-specific idiosyncratic error term,  $\varepsilon_{ijm}$ , is assumed to be an iid type I extreme value random variable.

We can decompose the term  $\alpha_i$  from equation (1) as  $\alpha_i = \alpha + \sigma v_{i\alpha_i}$  random variable, with the expected value of  $\alpha$  and variance  $\sigma$ ,  $v_i \sim N(0,1)$ . In this model specification, the probability that a randomly chosen consumer chooses product  $j$  in market  $m$  is given by equation (2):

$$S_{jm} = \int_{R^K} \frac{\exp((\alpha + \sigma v_{i\alpha_i})p_{jm} + x_{jm}(\beta + \Lambda v_i) + \xi_{jm})}{1 + \sum_{r=1}^J \exp((\alpha + \sigma v_{i\alpha_i})p_{rm} + x_{rm}(\beta + \Lambda v_i) + \xi_{rm})} \phi(v_{i\alpha_i} v_i) dv_{i\alpha_i} dv_i \quad (2)$$

The probability that a randomly chosen consumer chooses none of the products in market  $m$  is given by equation (3):

$$s_0 = \int_R \frac{1}{1 + \sum_{r=1}^J \exp((\alpha + \sigma v_{i\alpha_i})p_{rm} + x_{rm}(\beta + \Lambda v_i) + \xi_{rm})} \phi(v_{i\alpha_i} v_i) dv_{i\alpha_i} dv_i \quad (3)$$

Since the integral in equation (2) cannot be calculated exactly, it is usually approximated by the Monte Carlo simulation given by equation (4):

$$\widetilde{S}_{jm} = \frac{1}{N} \sum_{i=1}^N \frac{\exp((\alpha + \sigma v_{i\alpha_i})p_{jm} + x_{jm}(\beta + \Lambda v_i) + \xi_{jm})}{1 + \sum_{r=1}^J \exp((\alpha + \sigma v_{i\alpha_i})p_{rm} + x_{rm}(\beta + \Lambda v_i) + \xi_{rm})} \quad (4)$$

### 3.2 Supply

We assume that firms engage in a pricing game. There are  $F$  firms,  $f \in \{1, \dots, F\}$ , and we suppose they solve a standard Bertrand price competition – thus, one firm sets its prices given other firms' retail prices, so we denote the prices of competitor firms' products by  $p_{-fm}$  and the marginal cost of product  $j$  in market  $m$  by  $mc_{jm}$ . We denote the product set of firm  $f$  in market  $m$  by  $J_{fm}$ . The profit of firm  $f$  is defined as:

$$\Pi_f(p) = M \sum_{j \in J_{fm}} (p_{jm} - mc_{jm}) s_{jm}(p_{fm}, p_{-fm})$$

where  $p_{jm}$  is the vector of all prices in market  $m$  and  $M$  is the number of consumers in market  $m$ . For notation purposes, we denote the market share function in equation (2) as  $s_{jm}(p_{fm}, p_{-fm})$ . The Nash equilibrium is given by the solution of the non-linear system of equations:

$$\frac{\partial \Pi_{fm}}{\partial p_{jm}}(p) = 0, f = 1, \dots, F$$

which is equivalent to:

$$s_{jm}(p) + \sum(p_{rm} - mc_{rm}) \frac{\partial s_{rm}}{\partial p_{jm}}(p) = 0$$

This equation stands for the standard case where firms are not constrained by a threshold value for eligibility. However, not being free to set any price and also benefiting from the subsidy changes this equation. The case of threshold constraints will be elaborated in the next section by discussing several scenarios that lead to different equilibrium prices on the market.

### 3.3 Illustration of Equilibrium Prices with Government-Set Threshold Values for Subsidy Eligibility in Cooperation

Assuming that firms cooperate, we consider a market of monopoly for analyzing the behavior of the profit functions with imposed threshold values above which products are not eligible for the subsidy. The analysis is performed with the help of a graphical representation of the profit functions in four scenarios that have distinct profit-maximizing price outcomes due to the differently defined set-ups of threshold and subsidy amount values. For illustration purposes, we will use a simpler version of equation (4), where we define the market share as being dependent on price  $p$  and gather all other variables in a parameter  $d$ :

$$s(p) = \frac{\exp(-p+d)}{1+\exp(-p+d)}$$

In the standard case when there is no government-set subsidy available, the profit function takes the following form:

$$\pi(p) = (p - c)s(p)$$

and the firm wants to maximize its profit:

$$\max_p \left( (p - c) \frac{\exp(-p+d)}{1+\exp(-p+d)} \right)$$

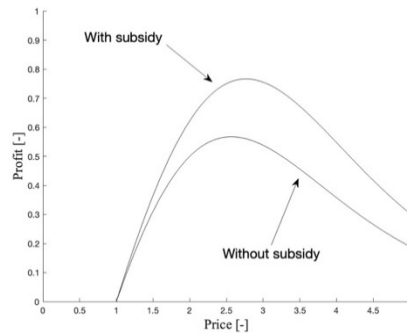
In order to illustrate the profit function, we have to assume the values of marginal cost, product characteristics, and error term, so let  $c = 1$  and  $d = 2$ . Further, we introduce a government subsidy,  $q = 0.5$ ; however, for now, we assume there is no threshold for eligibility. Thus, the profit function takes the following form:

$$\pi(p) = (p - c)s(p - q)$$

and the firm wants to maximize its profit:

$$\max_p \left( (p - c) \frac{\exp(-(p-q)+d)}{1+\exp(-(p-q)+d)} \right), \text{ such that } c = 1, d = 2, q = 0.5$$

*Figure 1* contains the graphical representation of the profit functions with and without subsidy, which, as expected, are concave and continuous respectively.



Profit functions for monopoly with and without subsidy ( $q = 0.5$ ) and without eligibility threshold

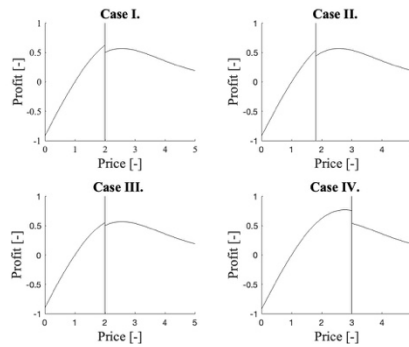
We can easily observe in *Figure 1* the pricing strategy mechanism when a subsidy without any price limitation is “freely” given by the government. For any price that generates a positive profit, the profit function with subsidy is above the one without subsidy, and thus we can see that the value of profit is higher for any price greater than one. Moreover, the profit function with subsidy reaches its maximum at a higher price, and thus the monopolist will raise the price of the product in order to increase the producer surplus and partially capture benefits of the subsidy. Obviously, the aim of such incentives is the spread of subsidized products, and thus producers increasing prices and benefiting from the subsidy is highly counterproductive.

A solution to this issue is the application of a threshold price above which products do not benefit from the subsidy. We denote the threshold by  $\bar{p}$  and let  $\bar{p} = 2$ , and thus the profit function takes the following form:

$$\begin{cases} (p - c)s(p - q) & \text{if } p < \bar{p} \\ (p - c)s(p) & \text{if } p \geq \bar{p} \end{cases}$$

Depending on the threshold value and the subsidy amount, there are four important scenarios that must be distinguished. *Figure 2* illustrates these four cases using different threshold values and subsidy amounts in order to analyse their effect on the profit-maximizing prices. Firstly, it is to be noted that the profit functions are not continuous, their breakpoints being at the threshold. Secondly, observe that there are cases in which the profit-maximizing price is higher than the threshold. Furthermore, in the last case, the profit-maximizing price is below the threshold, but note that this scenario generates the highest price.

The first case is the only one in which the profit-maximizing price is at the threshold. In the second case, the threshold value is lower,  $\bar{p} = 1.8$ , and thus the value of profit at the profit-maximizing price without subsidy is higher than any other value of profit with subsidy. The outcome of the third case is similar, but here the difference is in the subsidy amount, which is reduced to  $\bar{q} = 0.2$ .



Graphical illustration of monopolist profit functions facing different eligibility threshold values and subsidy amounts

Again, due to the low subsidy amount, the profit-maximizing price is higher than the threshold value. Lastly, in the fourth case, the threshold value is increased to  $\bar{p} = 3$ . In this case, there is no point using the threshold value as a limitation since the profit-maximizing point is below it. To conclude, the second and the third case is the same as if there had not been any subsidy available, while the fourth case is as if there had not been any price limitation for eligibility. In this sense, the most efficient scenario is the first one, where the price was reduced compared to the one without subsidy. This structure shows that if the price chosen by a monopolist is not equal to the threshold, then a better setting of the threshold value or subsidy amount probably exists. In addition, if the profit-maximizing price is below the threshold, the firm is partially benefiting from the subsidy, and a lower threshold would generate a lower price.

#### 4 Illustration of Profit Functions with Thresholds Required for Subsidy Eligibility following a Cooperative Strategy

Considering the illustrations presented in Section 4.3, I analyses three selected BEV models and observe if the data correspond to any of the cases in a monopolistic frame. Thus, we can confirm whether the assumption on pricing at the focal point is stronger than that of competition among firms. Three BEV models are selected, specifically Kia e-Niro, Hyundai Kona, and Honda-e. These models were selected for several reasons. First of all, these are among the few that directly indicated the price decreases made in the interest of subsidy eligibility for each vehicle sold. This is a crucial advantage since this way it is known that these models were indeed priced and sold in the framework of the program. Secondly, the selection was made

so that analyzed models belong to manufacturers from different countries. Lastly, by opting for this selection, examples of every program cycle and most threshold variations can be examined. In the following section, I will analyse the gross list prices of the mentioned BEVs with discounts other than the subsidy and then illustrate their profit functions based on the presented theory.

#### 4.1 Evolution of BEV Sales and Prices of the Analyzed Models

The first analyzed model is the Kia e-Niro with 100 kW power. It can be seen in *Table 3* that the highest price of this model was in the second cycle, when the threshold value was very high compared to the equilibrium price; thus, firms engaged in an unconstrained price competition and probably even monopolized part of the consumer surplus due to the subsidy.

Table 3

Price and number of Kia e-Niro (100 kW) BEVs registered in Hungary (prices in thousand HUF)

	II. Cycle		III. Cycle		IV. Cycle
<b>Sales Price</b>	11,799	12,499	10,999	10,899	11,499
<b>Sold no.</b>	2	29	150	3	151

In the third cycle, the highest number of sales was made with almost all of the Kia e-Niro models priced at the threshold. Then in the fourth cycle we can observe the second highest number of sales combined with the second lowest price, which is below the threshold value of HUF 12 M.

The second analyzed model is the Hyundai Kona with 100 kW power, which is very similar to the previous one considering its pricing strategy. We can calculate from *Table 4* that 92.18% of the total sales for this model were registered in the third cycle and priced slightly below the threshold of HUF 11 M.

Table 4

Price and number of Hyundai Kona (100 kW) BEVs registered in Hungary (prices in thousand HUF)

	II. Cycle	III. Cycle	IV. Cycle		
<b>Sales Price</b>	12,049	10,999	13,299	14,469	10,699
<b>Sold no.</b>	15	271	4	3	1

Also, we can see that within this cycle period 100% of the BEVs were priced at the threshold value. Note that in the second cycle the price of this model is approximately HUF 1 M (9.55%) higher than in the third cycle. Also, note that in the fourth cycle the sales of these models were relatively low and the prices were above the threshold value that increased to HUF 12 M. However, it is to be mentioned that these models were all registered in 2022, and thus probably this dramatic price increase is not only due to the fact that there was no subsidy in 2022 but also to increased production costs caused by the high inflation in the energy and raw material sectors. More than that, we know from the import data that the original

list price value for six of these models was HUF 11,650 K, but they were eventually sold for a higher price.

The third analyzed BEV model, the Honda-e, was not a very popular choice among consumers, as it can be seen in *Table 5* that the total number of registered models was 26.

Table 5  
Price and number of Honda-e (100 kW) BEVs registered in Hungary (prices in thousand HUF)

	II. Cycle	III. Cycle
Sales Price	10,999	11,555
Sold no.	16	10

However, regarding the pricing strategy, it follows the path of the Kia e-Niro, and Hyundai Kona models since 16 vehicles were priced exactly below the threshold value of HUF 11 M in the third cycle. Moreover, just like in the case of the previous models, the price is set with roughly HUF 500 K below the threshold of HUF 12 M in the fourth cycle.

## 4.2 Assumption of BEV Production Total Cost and Consumer Valuation of Product Characteristics

In order to implement the theory presented, the values for cost and product characteristics had to be assumed. The cost of producing a BEV is higher than for an internal combustion (IC) vehicle, mainly due to the high battery costs [7]. In order to become competitive with IC vehicles, the battery pack cost of a BEV must be less than roughly \$150 per kWh [13] [22]. In the same paper, the authors calculate with a cost of \$250 per kWh for the Li-ion batteries in the optimum scenario [13]; based on this paper, the estimated cost of a Li-ion battery weighting 451 kg is \$16,125 [8]. However, technology has advanced, and thus the cost of Li-ion battery production has decreased since the year 2000. Based on other publications of future cost estimations, the cost in 2020 is expected to reach \$200 per kWh. This is in line with the battery pack cost assumption of \$190–\$210 per kWh made in 2019 [1], but it is still higher than the competitive price estimated by [15]. Calculating with a price of \$200 per kWh, *Table 6* shows the estimated costs based on the battery types of the analyzed models in the year 2019. The costs are converted to HUF on the average exchange rate in 2019, which was HUF 290.6518/\$1.

Table 6  
Estimated battery costs of the analyzed BEVs in 2019

Model	Type	Capacity (kWh)	Cost (US\$)	Cost (HUF)
Kia e-Niro, Hyundai Kona	Li-Poly	42	8,400	2,441,475
Honda-e	Li-ion	35.5	7,100	2,063,628

Knowing that the total cost of a base IC automotive vehicle is about \$22.5 K, subtracting the IC-related content and adding the BEV-related content but the battery-pack, the total cost of a base BEV is \$24.5 K [1]. Adding the battery pack costs, we get a total cost of \$32.9 K for Kia e-Niro and Hyundai Kona, while for Honda-e the total cost is \$31.6 K. Converting USD to HUF, we get that in 2019 the estimated total cost of Kia e-Niro and Hyundai Kona is HUF 9,562,444 and for Honda-e is HUF 9,184,597. Thus, we assume the cost parameter  $c$  from equation (9) to be HUF 9.6 M and HUF 9.2 M respectively. The consumer valuation of BEVs is captured through the product characteristics and unobserved terms measured by parameter  $d$  from equation (8). For all analyzed models, except for Honda-e, this parameter is assumed to be HUF 12 M, so roughly the average between the amounts payable with and without subsidy. As Honda-e has a smaller battery capacity and a smaller size, the assumed consumer valuation of the product will also be lower.

### 4.3 Simulation of the Profit Functions for the Analyzed Models

In the second cycle of the subsidy, the profit functions of the Kia e-Niro and Hyundai Kona models are illustrated in *Figure 3* based on the monopolistic frame described in Section 4.3 and the assumption on cost and product valuation parameters. The two curves represent the profit functions with and without subsidy deduction, and the vertical line stands for the threshold value.

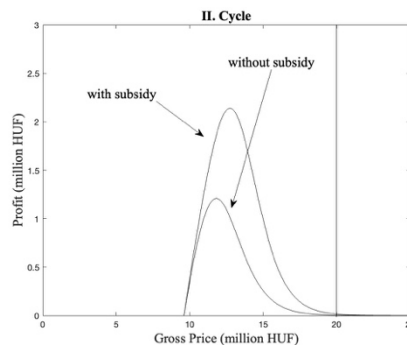


Figure 3

Illustration of the profit functions with and without subsidy of the Kia e-Niro and Hyundai Kona models in the second cycle

We can observe in *Figure 3* that in the second cycle the threshold value for eligibility was very high compared to the profit-maximizing point. Therefore, it

basically did not have any direct effect on the pricing strategy<sup>1</sup>. This scenario can be associated with the fourth case of the presented monopoly structure. As the threshold is very high, the firm increases the price and chooses the profit-maximizing point benefiting from the subsidy, thus transforming potential consumer surplus into producer surplus. This supports the first focal point hypothesis, as the gap between the focal point and the market equilibrium is too high and firms refuse to cooperate [20]. We can graphically observe that if the vertical line representing the threshold value would shift to the left to any point in the price interval of the profit-maximum values with and without subsidy, the price would be equal to the threshold. Also, note that the profit-maximizing point with subsidy is roughly at the true price value of the models presented in Tables 3 and 4.

As the production costs of BEVs have become cheaper over time, mainly due to reduction of battery production costs [4], we also gradually reduce the value of the total cost estimation. Whereas by mid-2020, the total base cost of a BEV had reached \$27.4 K – \$28.8 K, this is expected to decrease to \$21.2 K – \$22.6 K by 2025 due to improvements in battery efficiency, reduction in battery pack cost, increase in volume and material substitution [4] [21] [25]. This means a cost reduction of 18.55% on average, and thus parameter  $c$  is reduced from \$32.9 K to \$26.8 K for the Kia e-Niro, and Hyundai Kona models and from \$31.6 K to \$25.7 K for the Honda-e model. On the other hand, the exchange rate of Hungarian forint continued to decline compared to the US dollar, and thus the costs increased indirectly. Converted to HUF at the average 2020 exchange rate before the subsidy program was available (HUF 312.986/ \$1), the cost parameter  $c$  is HUF 8.4 M and HUF 8 M respectively. Moreover, there were minor improvements performed on the same models over the years (e.g., design), and consumers' valuation of BEVs grew as well due to high popularity and marketing effects. Thus, the parameter  $d$  is increased from HUF 12 M to HUF 12.5 M for the Kia e-Niro and Hyundai Kona models. However, Honda-e having lower battery capacity and a smaller size, it was necessary to assign a lower parameter value of product valuation, thus  $d$  being HUF 12 M for this model. The subsidy amount  $q$  takes the real value of HUF 2.5 M in the third cycle. In *Figure 4*, we can see the illustrations of the profit functions of the Kia e-Niro, Hyundai Kona, and Honda-e BEVs with and without the government subsidy.

---

<sup>1</sup> It may have had some psychological marketing effects on consumers, as they must have perceived the real price as a good deal being almost twice as low as the threshold.

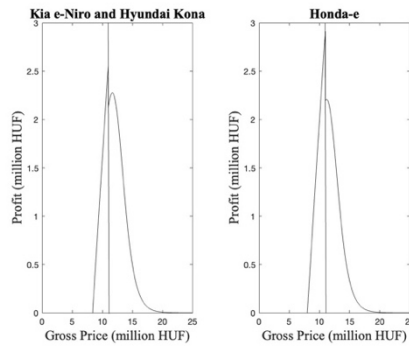


Figure 4

Illustration of profit functions of the analyzed BEVs with imposed eligibility thresholds in the third cycle

In the third cycle, the government lowered the eligibility threshold to HUF 11 M, and we can see in *Figure 4* that the profit-maximizing price for all models is at the threshold. Since Honda-e has a lower total cost and a lower assumed product characteristics value, when comparing the profit-maximizing points with and without subsidy, the absolute difference in the profit values is higher for Honda-e than for the other analyzed models. Perhaps, had it lowered the price, Honda could have sold more models but with a lower profit margin. However, in this period, 100% of the analyzed models were priced slightly below the threshold. This reflects the first case of the monopolistic frame and shows a gathering of these products' prices at the focal point that is at the threshold. This indicates that the threshold value was set to optimum for these models, as a higher value might have resulted in tacit collusion at a higher price [20], whereas a lower value would have been probably ignored by Kia and Hyundai, as the profit without subsidy almost equals that with subsidy for  $\bar{p} = \text{HUF } 11 \text{ M}$ .

The fourth cycle is the one in which the monopolistic frame partially contradicts the reality. In the illustration presented in *Figure 5*, we can see that the equilibrium price should be at the threshold, but in reality, it is by approx. HUF 500 K below it for all analyzed models<sup>2</sup>.

<sup>2</sup> Note that the cost parameter  $c$  was further reduced to \$23 K for the Kia e-Niro and Hyundai Kona models, while parameter  $d$  was increased to HUF 13.5 M. In 2021, the average USD/ HUF exchange rate was HUF 296.85/ \$1, so parameter  $c$  is HUF 6.8 M.

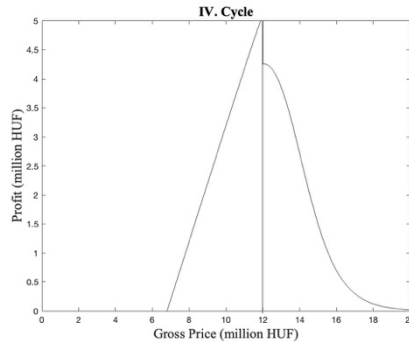


Figure 5

Illustration of the profit functions with and without subsidy of the Kia e-Niro and Hyundai Kona models

This result is consistent with the finding of Zhang et al. (2020) [25], showing that the higher the price ceiling, the lower the probability of coordination. A speculative reason in this typical case, supported by the large number of sales in the case of Kia e-Niro, would be a higher gap between the cooperation at the focal point and the initial market equilibrium with no subsidy, and thus the reduction of prices in hope of higher sales in an oligopoly market. We should also observe that Honda-e did not decrease its prices in the third cycle despite the large gap between the focal point and the initial equilibrium and thus ended up with a low number of sales. In addition, note that, as a rule, profit values show an upward tendency year by year for all BEVs, an observation that might justify the competitive strategy.

In *Figure 6*, we can observe a counterfactual simulation of the fourth cycle, where all values remain unchanged except for the threshold value, which is reduced to HUF 11 M. We can see that in this situation the new equilibrium price might be the original one due to the lower threshold value, representing the second case in the monopolistic frame. According to this counterfactual illustration, it is probable that in reality the threshold would be the equilibrium since the profit values are almost the same for the two functions, and the lower price would attract more consumers in an oligopoly. However, it was rational from the government to increase the threshold value and avoid a scenario in which firms refuse to take the subsidy eligibility into account. More than that, we find that even though the threshold value was slightly higher than the optimum, tacit collusion did not occur at the higher threshold since prices were reduced in the hope of higher profits in an oligopoly market.

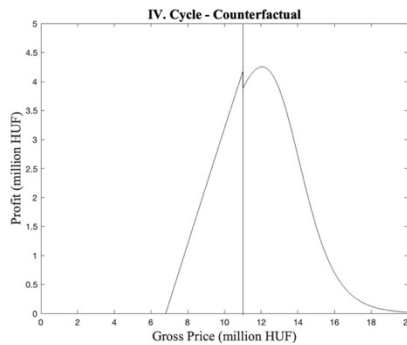


Figure 6

Counterfactual illustration of the profit functions with and without subsidy, when  $\bar{p} = 11$

## Conclusions

We can conclude that the analyzed subsidy program for BEVs, launched by the Hungarian Ministry of Economics and Technology, was overall effective, considering both the increase in sales and decrease in prices of BEVs, during the program period. The sales of the Kia e-Niro model were 5.76 times higher in 2020 compared to 2019, and the price of the model decreased by 12%, reaching the threshold, in the same period. Furthermore, the sales of the same model increased from January 2021, when no subsidy was available, to May 2021, when the fourth cycle was announced, by 61.97%, while the price decreased by 9.45%. Moreover, 91.03% of all Hyundai Kona models were sold in the third subsidy cycle (in the period of 2019–2022) and at the lowest price. On top of that, all models sold in the third cycle, were priced at the threshold for eligibility, and an increase in prices could be observed subsequently. Also, the highest prices and the lowest sales of the analyzed models were in periods when no subsidy cycle was available.

In the second cycle, the program was inefficient, as the threshold value was too high considering the profit-maximizing prices of the BEVs on the market. This resulted in increased MSRPs and producer surplus. However, it could have had a positive marketing effect on the perception of sales prices by consumers. On the other hand, the choice of the threshold value was highly appropriate in the third cycle, confirmed by both the raw data and the similarity to the theoretical monopolistic frame. Concerning this cycle, it can be concluded that cooperation at the focal point was stronger than competition, and thus the monopolistic pricing strategy could be applied. In the fourth cycle, the increase of the threshold value was rational, as – according to the graphical counter-simulation – without this decision there would have been a risk of firms opting for the profit-maximizing price without the subsidy.

Although here the monopolistic frame could not be applied, we have come to understand that whenever the threshold value is slightly higher than the optimum, firms will engage in a competition and still lower their prices until reaching a new equilibrium point.

## Acknowledgements

Firstly, I wish to thank the Hungarian Academy of Sciences for contributing to the budget of the project via the DOMUS scholarship. I am very grateful to my supervisor, Prof. Zsolt Sándor, for his thorough review of the present work and his useful comments. Also special thanks to the entire DATAHOUSE team, who gathered, processed and transferred the raw data, and especially the Managing Director, Mr. István Bisztriánszky, who helped to structure the data to fit the purpose of this paper.

## References

- [1] Baik, Y. – Hensley, R. – Knupfer, S. (2019): Making electric vehicles profitable. *McKinsey & Company*. Available online: <https://www.mckinsey.com/industries/automotive-and-assembly/our-insights/making-electric-vehicles-profitable> (accessed on 22 Mar 2023)
- [2] Beresteanu, A. – Li, S. (2011): Gasoline Prices, Government Support, and the Demand for Hybrid Vehicles in the United States. *International Economic Review*, 52(1):161-182
- [3] Berry, S. – Levinsohn, J. – Pakes, A. (1995): Automobile Prices in Market Equilibrium. *Econometrica: Journal of the Econometric Society*, 63(4): 841-890
- [4] Burd, J. T. J. – Moore, E. A. – Ezzat, H. – Kirchain, R. – Roth, R. (2021): Improvements in Electric Vehicle Battery Technology Influence Vehicle Lightweighting and Material Substitution Decisions. *Applied Energy*, 283: 116269
- [5] Chandra, A. – Gulati, S. – Kandlikar, M. (2010): Green Drivers or Free Riders? An Analysis of Tax Rebates for Hybrid Vehicles. *Journal of Environmental Economics and Management*, 60(2): 78-93
- [6] Diamond, D. (2009): The Impact of Government Incentives for Hybrid-Electric Vehicles: Evidence from US States. *Energy Policy*, 37(3): 972-983
- [7] Duffner, F. – Wentker, M. – Greenwood, M. – Leker, J. (2020): Battery Cost Modeling: A Review and Directions for Future Research. *Renewable and Sustainable Energy Reviews*, 127: 109872
- [8] Eaves, S. – Eaves, J. (2004): A Cost Comparison of Fuel-Cell and Battery Electric Vehicles. *Journal of Power Sources*, 130(1–2): 208-212
- [9] Elektromobility (e-mobi) (2016): Tender and Guide *GZR-D-Ö-2016*. (Elektromobilitás (e-mobi): *Pályázati kiírás és útmutató GZR-D-Ö-2016*.) Available at: [https://palyazat.e-mobi.hu/palyazati\\_kiiras.pdf](https://palyazat.e-mobi.hu/palyazati_kiiras.pdf). Last accessed: 01.02.2023
- [10] Elektromobility (e-mobi) (2018): Amended calling for tender *GZR-D-Ö-2016* (Elektromobilitás (e-mobi): *Módosított pályázati kiírás GZR-D-Ö-*

- 2016) Available at: [https://elektromobilitas.humda.hu/2016/modositott\\_palyazati\\_kiiras.pdf](https://elektromobilitas.humda.hu/2016/modositott_palyazati_kiiras.pdf). Last accessed: 01.02.2023
- [11] Elektromobility – IFKA (2018): Calling for tender and Guide *GZR-D-Ö-2018*. (Elektromobilitás – IFKA: *Pályázati kiírás és útmutató GZR-D-Ö-2018*.) Available at: [https://elektromobilitas.humda.hu/2018/medias/4/palyazati\\_kiiras\\_gzr\\_d\\_o\\_2018\\_20200114.pdf](https://elektromobilitas.humda.hu/2018/medias/4/palyazati_kiiras_gzr_d_o_2018_20200114.pdf). Last accessed: 01.02.2023
- [12] Fan, Y. – Zhang, G. (2021): *The Welfare Effect of a Consumer Subsidy with Price Ceilings: The Case of Chinese Cell Phones*. Technical report. National Bureau of Economic Research
- [13] Gaines, L. – Cuenca, R. (2000): *Costs of Lithium-Ion Batteries for Vehicles*. Technical report. Argonne National Lab., IL (US)
- [14] Gallagher, K. S. – Muehlegger, E. (2011): Giving Green to Get Green? Incentives and Consumer Adoption of Hybrid Vehicle Technology. *Journal of Environmental Economics and management*, 61(1): 1-15
- [15] Hardman, S. – Fleming, K. L. – Khare, E. – Ramadan, M. M. (2021): A Perspective on Equity in the Transition to Electric Vehicle. *MIT Sci. Policy Rev.*, 2: 46-54
- [16] IFKA (2020): Calling for tender *ZFR-D-Ö-2020* (*Pályázati kiírás ZFR-D-Ö-2020*) Available at: [https://elektromobilitas.humda.hu/2020/medias/4/zfr-d-a-2020\\_1sz\\_mad\\_20200610.pdf](https://elektromobilitas.humda.hu/2020/medias/4/zfr-d-a-2020_1sz_mad_20200610.pdf). Last accessed: 01.02.2023
- [17] IFKA (HUMDA) (2021\_a): Calling for tender E-CAR-2021/ residential. (*Pályázati kiírás E-AUTO-2021/ lakossági*.) Available at: [https://msz.elektromobilitas.humda.hu/medias/1/e\\_auto\\_2021\\_lakossag\\_palyazatikiaras\\_elektromosgjmbeszerz\\_1.sz.\\_mad.pdf](https://msz.elektromobilitas.humda.hu/medias/1/e_auto_2021_lakossag_palyazatikiaras_elektromosgjmbeszerz_1.sz._mad.pdf). Last accessed: 01.02.2023
- [18] IFKA (HUMDA) (2021\_b): Calling for tender E-CAR-2021/ business organizations. (*Pályázati kiírás E-AUTO-2021/ gazdasági társaságok*.) Available at: [https://gt.elektromobilitas.humda.hu/medias/4/e-auto\\_2021\\_gt\\_palyazatikiaras\\_elektromosgjmbeszerz\\_friss.pdf](https://gt.elektromobilitas.humda.hu/medias/4/e-auto_2021_gt_palyazatikiaras_elektromosgjmbeszerz_friss.pdf). Last accessed: 01.02.2023
- [19] Jenn, A. – Azevedo, I. L. – Ferreira, P. (2013): The Impact of Federal Incentives on the Adoption of Hybrid Electric Vehicles in the United States. *Energy Economics*, 40: 936-942
- [20] Knittel, C. R. – Stango, V. (2003): Price Ceilings as Focal Points for Tacit Collusion: Evidence from Credit Cards. *American Economic Review*, 93(5): 1703-1729
- [21] Lutsey, N. – Grant, M. – Wapperlhorst, S. – Zhou, H. (2018): *Power Play: How Governments Are Spurring the Electric Vehicle Industry*. Washington, DC: ICCT

- [22] Nykvist, B. – Nilsson, M. (2015): Rapidly Falling Costs of Battery Packs for Electric Vehicles. *Nature Climate Change*, 5(4): 329-332
- [23] Sallee, J. M. (2011): The Surprising Incidence of Tax Credits for Toyota Prius. *American Economic Journal: Economic Policy*, 3(2): 189-219
- [24] Shajarizadeh, A. – Aidan, H. (2015): Price-Cap Regulation, Uncertainty and the Price Evolution of New Pharmaceuticals. *Health Economics*, 24(8): 966-977
- [25] Zhang, X-B. – Fei, Y. – Zheng, Y. – Zhang, L. (2020): Price Ceilings as Focal Points to Reach Price Uniformity: Evidence from a Chinese Gasoline Market. *Energy Economics*, 92: 104950

# Trends in Cognitive Mobility in 2022

## Máté Zöldy

BME, Innovative Vehicle Technologies Research Center, H-1111 Stoczek str.6.,  
Budapest, Hungary, zoldy.mate@kjk.bme.hu

## Péter Baranyi

University of Pannonia, H-8200 Veszprém Egyetem Str. 10.  
baranyi.peter@mik.uni-pannon.hu

## Ádám Török

BME, Advanced Fuels Research Group, H-1111 Műegyetem rkp 3, Budapest,  
Hungary, torok.adam@kjk.bme.hu

---

*Abstract: Cognitive mobility framework has developed in the year 2022. The first international scientific congress (1st IEEE Cognitive Mobility at Bosch Budapest Innovation Center – CogMob Conference) was organised to create a space for sharing thoughts and starting conversations about the topic. This paper aims to summarise and evaluate the main tendencies of cognitive mobility. After reviewing the presented papers, there were evaluated according to essential elements of cognitive mobility, and statistical analysis was carried out to evaluate the papers. In our work, the five core topics of cognitive mobility in 2022 were defined and evaluated according to the essential elements. The similarity measure and proximity index-based evaluation of the abstracts and the keywords show that sustainability-related topics, energy sources, and their utilisation area are the most frequented. The tendency is expected to continue, but the international military situation could influence the weight of the topics.*

*Keywords: cognitive mobility; elements of cogmob; statistical evaluation*

---

## 1 Introduction

This paper aims to provide an overview of the actual focal points of cognitive mobility based on the CogMob Conference 2022 key topics and evaluate the interdependence scientifically. The conference's papers covered broad research

areas of mobility, from intelligent and sustainable mobility systems to the safety and security of ITS-related (ITS-Intelligent Transportation Systems) cognitive systems and advanced fuels and drivetrains.

Mobility is a crucial dimension of our society. The efficiency and sustainability of our life are heavily dependent on mobility and similar factors. *"Cognitive Mobility (CogMob) investigates the entangled combination of the research areas such as mobility, transportation, vehicle engineering, social sciences, artificial intelligence, and cognitive infocommunications. The key aim of CogMob is to provide a holistic view of how mobility, in a broader aspect, can be understood, described, and optimised as the blended combination of artificial and natural/human cognitive systems. It considers the whole combination as one inseparable CogMob system and investigates what kind of new cognitive capabilities of this CogMob system are emerging"* [1]. Mobility as one of the most important pillars of our society has several dimensions. Developing transportation sectors are merging with the increasing cognitivity level [2, 3] and cognitive mobility can be an enabler to make our cities more sustainable [4, 5, 6]. Deeper understanding of mobility with the help of cognitive approach [7] is the way to reduce the overall impact of mobility on the environment [8, 9, 10].

Based on its nature, one of the CogMob focus areas is engineering applications in the mobility domain.

This paper firstly summarises the relevant areas of cognitive mobility by analysing the papers presented at the conference. In the second part, these areas are related to the essential domains. The third chapter evaluates the fields of CogMob2022 in the elements of cognitive mobility and in the fourth part presents a statistical analysis to examine the interdependencies.

## **2 Trends in CogMob Area Analysis**

The trends of cognitive mobility cover the connected cognitive vehicles, safety and security of ITS-relevant cognitive systems, cognitive aspects of orientation and navigation, advanced electric vehicles, and augmented conventional drives.

### **2.1 Cognitive Connected Vehicles**

Raising the cognitive level of vehicles is one of the critical drivers of cognitive mobility. One direction is the development of methods to provide objective indicators for the complex tasks of road transport. One of the keys is to define an evaluation framework that can be applied in developing and evaluating new AI-based models. The aim is to define the metrics used in the development process and to facilitate the qualitative evaluation and comparison of algorithms. One of

the proposed methods aims at broad applicability by choosing only metrics obtained from sensors already installed in vehicles [11].

With the proliferation of self-driving vehicles, motorcyclists, representing a vulnerable group of road users, require specific solutions. Their risk of severe injuries and fatalities is higher than the average and therefore requires the development of assistive systems to improve driving safety. Two promising methods are also being introduced, called sub-area and dynamic frame rate evaluation, to reduce the computational effort from raw video data to driver posture information [12].

One of the keys to the Traffic Sign Recognition and Detection System (TSDR) is its high-speed operation, which can be derived from the high-speed of vehicles. Through computer vision and human-machine communication, these systems help vehicles navigate. Improving and speeding up traffic sign recognition is one of the areas of development that will continue to drive future developments [13].

Demand Responsive Transport (DRT) services are gaining ground with the ability to configure mobility to individual needs. Alternatives to public transport systems and the increasingly popular shared mobility systems. Their development aims to improve their service quality further. One innovative form is the implementation of autonomous fleet systems. Research is investigating the challenges of deploying low-speed self-driving minibuses (tracking) in DRT and the primary tasks that must be carried out to prepare for the future introduction of such a service. A systematic process-oriented approach will be used to investigate the specific parameters, conditions and options for the vehicle and the operational options (for DRT). As a result, system interfaces will be identified, and the conditions for establishing such a service will be analysed [14].

Cognitive measures are increasingly necessary for all mobility modes, from motorbikes to urban buses. Different vehicle categories have different challenges, but using AI for prediction, environment perception data acquisition, improved human-machine interfaces, and system-level vehicle control offers cognitive mobility solutions [15].

## **2.2 Safety and Security of ITS-related Cognitive Systems**

The mobility system's growing autonomy increasingly requires system security and cybersecurity improvements. Software development for modern vehicles is increasingly based on a service-oriented approach. Building software systems from software components add specific capabilities to the system and allow fine-tuning details. Methods are being developed to implement flexible software vehicle architectures based on adopting out-of-the-box software. One development direction follows the dynamic changes of the set parameters and provides easily extensible interfaces to new parameters or requirements. The concept further

introduces a priority metric that describes the impact of services in the system and models how this metric is inherited through dependencies [16].

One area of understanding vehicle behaviour is accident investigation, where vehicle data is downloaded using target hardware and expert forensic software. Research is investigating the process of analysing the extracted data and the conclusions drawn based on a growing database of modern cognitive vehicles [17].

The relationship between vehicles and infrastructure is also at the forefront of cognitive mobility security research. Its impact on vehicle safety has implications for the further development of V2X-based (vehicle-to-everything) design processes. The research presents a novel methodological background for characterising the safety impact of network performance metrics on V2X-based automotive applications. The results are used to identify the safe operating range of a given V2X-based application [18].

Cognitive mobility system components are also increasingly becoming victims of cyberattacks. The application and implementation of Attack Graph, a commonly used IT security tool, is under way in vehicles. Cognitive mobility systems are based on autonomous decision making by the participants. To trust vehicles to make the right decisions, we need to make them immune to failures and malicious manipulation. A general model is proposed to automate the generation and analysis of attack paths in TARA. Several use cases of the model are discussed, including the enumeration of possible attack paths, the automatic assessment of the feasibility and risk of each path, and the construction of a protection diagram to ensure system security [19].

The fusional handling of safety and security aspects is a typical example of emerging cognitive mobility. An increasing number of sensors and activators is followed by intensive communication that, on the one side, is an opportunity to increase safety but, on the other hand, is a threat to security risks.

### **2.3 Cognitive Aspects of Orientation and Navigation**

In the area of human-machine communication, CogMob co-manages human and machine capabilities in mobility, and in this regard, it should aim to help humans to preserve their spatial ability even when providing navigational aid [20].

GPS is a key element of current mobility systems. It is a human-machine interface that is mainly used to provide turn-by-turn navigational aid to human drivers. From one perspective, the user could save cognitive capacity by relying on this turn-by-turn navigational assist. Thus, they can pay more attention to the driving itself. On the other hand, frequent use of GPS (Global Positioning System) can erode human navigational abilities [21]. That is an often overlooked but crucial human skill in everyday life and special areas. Researchers provide design

principles to support and not replace human cognitive skills. Such a method can raise awareness of the phenomenon [22], [23]. Another is to initiate active encoding as if the user has to deal with spatial information actively, it can achieve better knowledge [24]. A third possible way is to modify GPS software to encourage users to pay more attention to the environment by referring to landmarks in the instructions [25]. For more details, please be referred to [20].

## 2.4 Advanced Electric Vehicles

Electric vehicles are characterised by excellent energy efficiency and local zero CO<sub>2</sub> (carbon-dioxide) emissions, but overall it is necessary to assess production and reuse together with use. The growing amount of data that can be collected on vehicles will allow a more accurate understanding of the whole life cycle. A detailed analysis of these issues has been conducted to propose solutions to accelerate the path toward climate neutrality. Based on this extensive analysis, a forecast of future trends in electric vehicle technologies and beyond for other CO<sub>2</sub>-neutral solutions will be made [26].

One of the electric vehicle powertrain's fundamental dynamics and sustainability aspects is the analysis of inverters and their power transistors. There is an exciting transition in the type of circuit breakers used in inverters. In addition to technical and safety aspects, including lifetime, reliability and possible failure modes, other aspects, such as cost, market needs and availability, are also considered. [27]

Accurate battery temperature prediction in electric vehicles is critical for efficient thermal management of the battery system. The research uses a nonlinear autoregressive exogenous network to model the complex thermal behaviour of the battery cell. Using conventional driving data, the model is trained, and its accuracy is proven over a wide temperature range, demonstrating the approach's simple, general and robust applicability. [28]

Synchronous reluctance motors are becoming an increasingly important player in electric mobility due to the growing need to reduce the amount of rare-earth metals in electric vehicle components. Novel post-processing methods are being developed based on differential inductances of finite element analysis inductance tensor maps. A force method based on the number of rotor displacement rises coupled with the coefficient of coercivity determines the required inductance map resolution. Reduction of nonlinear effects by modifying the current profiles through motor control can only be achieved with a well-defined tensor mapping method. An adequately defined motor model, together with an appropriate control compensation method, can further improve the efficiency of synchronous reluctance motors and provide the required performance in the low speed and part load range where the real operating points of an average used vehicle are found [29].

A critical dimension of e-mobility is the battery and its degradation during use. Considering the typical use of electric vehicles, a test track has been designed from which detailed data can be collected from highly sensorised vehicles. Results showed that batteries lose 4% of their capacity over 10 000 km and almost 14% over 45 000 km [30].

Hybrid propulsion technology is one of the most critical research areas today, as these technologies can improve fuel consumption through energy recovery. Laboratory measurements of the drives are carried out on test benches in the first development phase to keep the parameters constant. In addition to the conventional combustion engine-electric drive hybrid systems, other combined systems are also being developed, such as an electric motor and a hydraulic pump/motor unit (HPM). The experimental hybrid power source is designed to achieve the highest efficiency during vehicle starting, acceleration and regenerative braking [31].

Electric vehicles have different noise, vibration and harshness (NVH) characteristics than conventional powertrain vehicles. Increasingly accurate data collection and evaluation requiring high computational power allow complex tests. In a comparative study of electric drive cars, vibration and noise have been measured at different speeds at several locations on the driveline and in the passenger compartment. The results show that vibration intensity and noise primarily depend on vehicle speed [32]. During the acceleration phase, the gear shift commands dominating the vehicle exterior were almost inaudible [33].

The market launch of electric vehicles is one of the answers to the improved demand for sustainable mobility. Electric drives standalone, multiplied or used with a combination of internal combustion engines are more accessible to control and could enable a more complex optimisation field during the control. Its elements, such as the battery, inverters, and electric motors, are the developments' focus. Connected to this, the noise and vibration questions are also heavily investigated.

## **2.5 Augmented Conventional Vehicle Drives**

The electrification of mobility is one of the significant trends, but the technological and supply constraints mean that conventional powertrains have a long future ahead of them. Extended conventional powertrains are and will be part of mobility in the coming decades. On the one hand, diesel powertrains are branded as the enemy of the environment, and on the other hand, there is still no alternative in some application areas.

One of the main objectives of diesel engine development is to keep overall emissions and fuel consumption low. The complexity of turbocharged diesel engines with low and high-pressure exhaust gas recirculation poses a technical

control challenge, requiring multiple determinations of the recirculated exhaust gas mass flow. This is only possible through complex system monitoring, data collection and a complex control system. Experimental methods are being developed to estimate the recirculated exhaust mass flow in high and low-pressure systems [34].

Other research included a numerical study on integrating a gas-air mixer into the heating mantle housing to reduce fuel consumption. In this method, a heating mantle was fixed to the outer wall of the gas-air mixer. The gas-air mixture and the heating medium used a reverse flow method. Water at constant temperature and with different flow rates depending on the engine speed was used as the heating fluid. The results of the CFD analysis confirm a significant increase in the temperature of the gas-air mixture at the outlet of the mixer. Therefore, the new integrated preheater-mixer design can be used in internal combustion engines for gas-air mixture and temperature control [35].

The development of new advanced fuels requires more efficient cost-reduction methods. Artificial neural networks can be used in fuel design, but creating data sets can be costly. A new line of research aims to create high-precision, multi-layer, perceptron-like artificial neural network models for predicting the combustion and emission characteristics of a medium-performance commercial diesel engine. It was found that the high-resolution dataset resulted in truly accurate models that can be used to pursue cost optimisation research [36].

Lubricants play a crucial role in the energy loss of an engine. Several technical solutions exist to reduce friction and wear losses caused by lubricants. With the proliferation of low-friction engine oils such as 0W-20 and below, the importance of tribological lubricant additives is increasing. This research investigates the tribological potential of selected nano-scale ceramic particles (zirconia, copper oxide and yttria) as lubricant additives and compares them in terms of their financial impact. The results show that additives with the best tribological properties are not always the best for mass-produced lubricants [37].

The physical and chemical condition of the lubricant also plays a crucial role in the long-term performance of engineering systems. Knowledge of the lubricant condition allows optimisation of condition-based oil changes, which can help reduce wastage by extending the life of engine oils. A study presents a methodology for processing FT-IR data that simplifies decision making on the extended shelf life of used engine oil. The presented methodology can be implemented as a planned maintenance step during scheduled service in the workshop and during regular inspections by fleet operators [38].

The cognitive mobility approach enables traditional drive developments, finer control, and more efficient utilisation. Developments like EGR control solutions or alternative fuels could support further diesel technology in areas where the current battery electric technology cannot offer real advantages. Research in the lubricant domain helps to decrease fuel consumption, i.e., overall energy demand.

### 3 Evaluation according to Cogmob's Basic Elements

Basic elements of cognitive mobility were first described with the following five dimensions [15]: triggering necessity, decision, tool/vehicle/quality, infrastructure/resources and human-machine interface. This chapter evaluates the five CogMob areas according to these five dimensions.

The "Cognitive connected vehicles" area involves nearly all the areas. Triggering the necessity of mobility is not a heavy aspect here, but the other four play a role with a centre of gravity in decision assistance and human-machine interfaces.

Safety and security of ITS-related cognitive systems affect the tool/vehicle/quality dimension as the safety and security demand higher complexity of the systems. It is closely connected with triggering necessity, as safety aspects could increase entry limits, thus postponing or even canceling mobility.

Cognitive aspects of orientation and navigation are heavily connected with decision and HMI, as they improve the environment perception capabilities.

Advanced electric vehicles and augmented conventional vehicle drives focus on the vehicle itself, but secondarily, they affect the resources through fuel economy and alternative energy sources.

Table 1  
Evaluation of 2022 key areas according to Cogmob basic elements

	triggering necessity	decision	tool/vehicle/quality	infrastructure/resources	human-machine interface
cognitive connected vehicles		focal area	linked	linked	focal area
Safety and security of ITS-related cognitive systems	focal area		focal area		
cognitive aspects of orientation and navigation		focal area			focal area
advanced electric vehicles			focal area	linked	
augmented conventional vehicle drives			focal area	linked	

## 4 Statistical Evaluation

The aim of the statistical evaluation of the presented papers of Cogmob2022 was to understand deeper the interdependencies between the domains. The analysis was carried out with the WosViewer software. VOSviewer uses a similarity measure known as association strength [39, 40]. This similarity measure is sometimes referred to as the proximity index [41] or the probabilistic affinity index [42]. Using the association strength, the similarity  $s_{ij}$  is calculated between two words  $i$  and  $j$  as (1):

$$s_{i,j} = c_{ij}(w_i, w_j)^{-1} \quad (1)$$

where  $c_{ij}$  denotes the number of co-occurrences of items  $i$  and  $j$  and where  $w_i$  and  $w_j$  denote either the total number of occurrences of items  $i$  and  $j$  or the total number of co-occurrences of these items. It can be shown that the similarity between items  $i$  and  $j$  calculated using (1) is proportional to the ratio between, on the one hand, the observed number of co-occurrences of words  $i$  and  $j$  and, on the other hand, the expected number of co-occurrences of words  $i$  and  $j$  under the assumption that occurrences of items  $i$  and  $j$  are statistically independent.

The abstract analysis results are presented in Fig 1. It shows that energy sources, environmental effects, artificial intelligence, and ADAS elements are the primary nodes, and further peripheral areas are also linked.

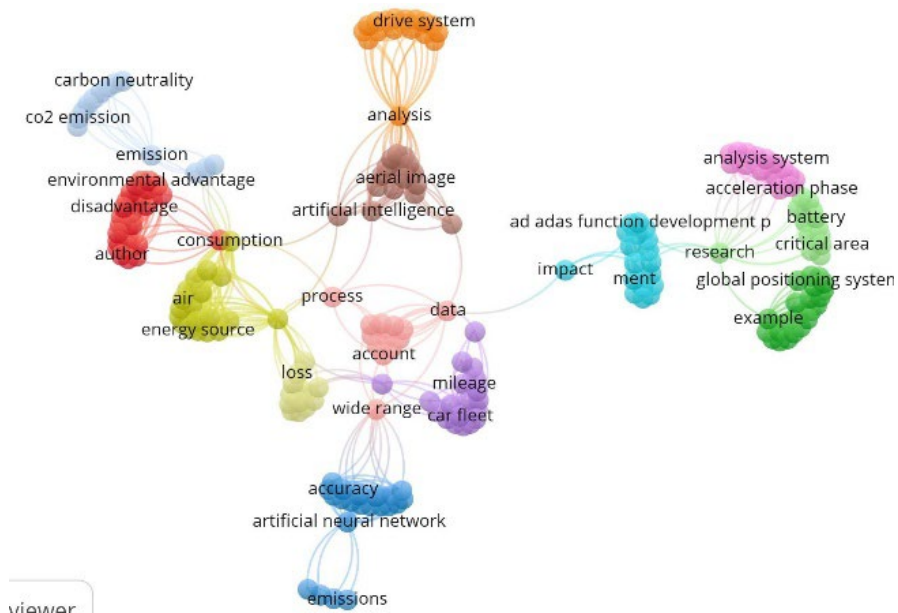


Figure 1  
Analysis of the abstracts of CogMob2022

Keywords analysis is presented in Fig. 2. According to this ecological footprint, electric vehicles, electric mobility, NVH, and e-drives are the most important intersection points.

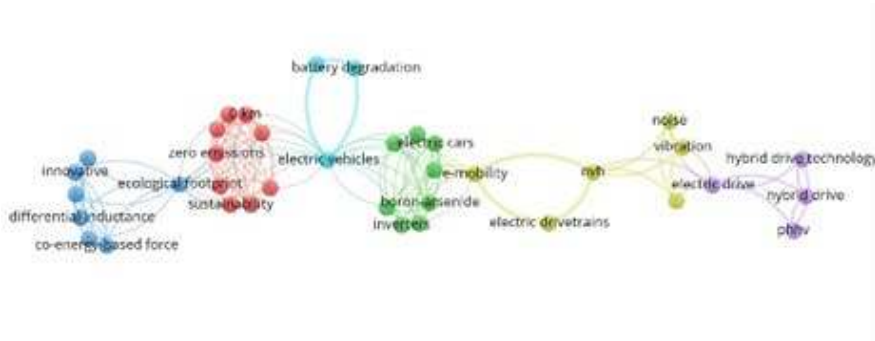


Figure 2  
Analysis of the keywords of CogMob2022

If the two analysis results are compared, the outcomes are the following: sustainability aspects of mobility appear in both evaluations (environmental effects and ecological footprint). As this is one of the strongest driving force of mobility development nowadays, its shortage would have been unexpected. The elements of Fig 2. mainly could be incorporated into the energy sources node. The other nodes related to autonomous mobility do not appear within the keyword analysis's focal points.

## Conclusions

Cognitive mobility is one of the emerging domains of the 21<sup>st</sup> Century. Analysing the themes, the following can be summarised: The topics of the papers cover five domains: connected cognitive vehicles, safety and security of ITS-related cognitive systems, cognitive aspects of orientation and navigation, advanced electric vehicles, and augmented conventional vehicle drives. Four elements of cognitive mobility are in the focal area, and the fifth is linked, as presented in Table 1. The similarity measure and proximity index-based evaluation of the abstracts and the keywords show that sustainability-related topics, energy sources, and their utilisation area are the most frequented. It is expected that it will be continued, and as a function of the military situation, the defence-related domain's role increase is expected.

## Acknowledgement

The CogMob conference aims to help achieve these goals by bringing together researchers and practitioners from relevant domains of science and industry. We thank the session organisers and the many contributors for making the conference lively with their work. We thank Robert Bosch Ltd for their co-organisation, hosting and support, especially for Janka Patkó.

We would especially like to acknowledge the enthusiastic support of the CogMob Technical Program Committee members and the work and effort of all members of the organisation team, without whom this conference would not have been possible. We hope that all participants of CogMob 2022 will find the conference to be an intellectually stimulating and enjoyable event.

## References

- [1] Zöldy, M., & Baranyi P. (2023) "The Cognitive Mobility Concept", *Infocommunications Journal*, Special Issue: Internet of Digital & Cognitive realities, 2023, pp. 35-40, <https://doi.org/10.36244/ICJ.2023.SI-IODCR.6>
- [2] Rybicka I, Drożdziel P, Stopka O, Lupták V. Methodology to Propose a Regional Transport Organization within Specific Integrated Transport System: a Case Study. *Transport Problems*, 13(4), 115-125. DOI: 10.20858/tp.2018.13.4.11
- [3] Stopka, O., Šimková, I., & Konečný, V. (2015) The quality of service in the public transport and shipping industry. *NAŠE MORE: znanstveni časopis za more i pomorstvo*, 62(3 Special Issue), 126-130.. DOI: 10.17818/NM/2015/SI7
- [4] Bundza, O. Z., Sakhno, V. P., Poliakov, V. M., & Yashchenko, D. M. (2020) Mobility of the metrobus. Ways of improvement. *Archiwum Motoryzacji*, 89(3), 61-73. DOI: 10.14669/AM.VOL89.ART5
- [5] Hazarie, S., Soriano-Paños, D., Arenas, A., Gómez-Gardeñes, J., & Ghoshal, G. (2021) Interplay between population density and mobility in determining the spread of epidemics in cities. *Communications Physics*, 4(1), 191. doi:10.1038/s42005-021-00679-0
- [6] Šulyová, D., Vodák, J., & Koman, G. (2020) Implementation smart city concepts for mobility, case study of world logistic models on the smart principles. *LOGI-Scientific Journal on Transport and Logistics*, 11(2), 110-119. DOI: 10.2478/logi-2020-0020
- [7] Strömlad, E., Winslott Hiselius, L., Smidfelt Rosqvist, L., & Svensson, H. (2022) Characteristics of Everyday Leisure Trips by Car in Sweden – Implications for Sustainability Measures. *Promet - Traffic&Transportation*, 34(4), 657–672. <https://doi.org/10.7307/ptt.v34i4.4039>
- [8] Impact of the Electric Mobility Implementation on the Greenhouse Gases Production in Central European Countries. *Sustainability*, 11(18), Article no. 4948. DOI: 10.3390/su1118494
- [9] Zoldy, M., Csete, M. S., Kolozsi, P. P., Bordas, P., & Torok, A. (2022) Cognitive sustainability. *Cognitive Sustainability*, 1(1).
- [10] Matijošius, J. (2022) Cognitive evolution of transport spatiality. *Cognitive Sustainability*, 1(3)

- 
- [11] Farkas P., Szoke L., Aradi Sz.: Defining metrics for scenario-based evaluation of autonomous vehicle models, Proceedings of 1<sup>st</sup> IEEE CogMob Conference, pp 155-160
- [12] Stolle K.A., Wahl A., Schmidt S: Motorcycle rider posture measurement for on-road experiments on rider intention detection, Proceedings of 1<sup>st</sup> IEEE CogMob Conference, pp 51-56
- [13] Lebumfacil, A. J., Abu, P. A. Traffic Sign Detection and Recognition Using YOLOv5 and Its Versions, Proceedings of 1<sup>st</sup> IEEE CogMob Conference, pp 11.18
- [14] Toth B., Lakatos A., Toth J., Turoń K.: Innovative complex-system-based cooperation between demand responsive transport services, shared mobility and autonomous bus services, Proceedings of 1<sup>st</sup> IEEE CogMob Conference, pp 127-134
- [15] Zöldy, M., Baranyi, P. (2021). Cognitive Mobility–CogMob. In 12th IEEE International Conference on Cognitive Infocommunications (CogInfoCom 2021). Proceedings IEEE pp. 921-925
- [16] Schindewolf M., Grimm D., Lingor C., Sax E.: Toward a Resilient Automotive Service-Oriented Architecture by using Dynamic Orchestration, Proceedings of 1<sup>st</sup> IEEE CogMob Conference, pp 147-154
- [17] Répás J., Schmidt M., Berek L: Downloading modern vehicles data for Forensics examination – A case study, Proceedings of 1<sup>st</sup> IEEE CogMob Conference, pp 29-30
- [18] Pethó Zs., Kazár T. M., Kraudy R., Szalay Zs., Török Á.: Considering the impact of PKI security on network performance in V2X-based AD/ADAS service development, Proceedings of 1<sup>st</sup> IEEE CogMob Conference, pp 135-140
- [19] Saulaiman M., Csilling Á., Kozlovsky M., Bánáti A.: Use Cases of Attack Graph in Threat Analysis And Risk Assessment for The Automotive Domain, Proceedings of 1<sup>st</sup> IEEE CogMob Conference, pp. 85-92
- [20] Berki B.: Overview of the relationship between human spatial abilities and GPS usage, in 1st IEEE International Conference on Cognitive Mobility, 2022, pp. 21–24
- [21] McKinlay R.: Technology: Use or lose our navigation skills, Nature, vol. 531, no. 7596, pp. 573–575, mar 2016
- [22] Leshed G., Velden T., Rieger O., Kot B., Sengers P.: In-car GPS navigation: Engagement with and disengagement from the environment, in Proceeding of the Twenty-sixth Annual CHI Conference on Human Factors in Computing Systems - CHI '08. ACM Press, 2008
- [23] Hejtmanek L, Oravcova I, Motyl J., Horacek J., Fajnerova I.: Spatial knowledge impairment after GPS guided navigation: Eye-tracking study in

- a virtual town, *International Journal of Human-Computer Studies*, vol. 116, pp. 15–24, aug 2018
- [24] Munzer S., Zimmer H. D., Schwalm M., Baus J., Aslan I.: “Computer-assisted navigation and the acquisition of route and survey knowledge, *Journal of Environmental Psychology*, vol. 26, no. 4, pp. 300–308, dec 2006
- [25] Ruginski I. T., Creem-Regehr S. H., Stefanucci J. K., Cashdan E.: “GPS use negatively affects environmental learning through spatial transformation abilities,” *Journal of Environmental Psychology*, vol. 64, pp. 12–20, aug 2019
- [26] Vajsz T., Horváth Cs., Geleta A., Wendler V., Bálint R., P., Neumayer M., Varga D., Z.: An investigation of sustainable technologies in the field of electric mobility, *Proceedings of 1<sup>st</sup> IEEE CogMob Conference*, pp. 57-66
- [27] Geleta A., Vajsz T., Horváth Cs.: An analysis of the power transistors of electric vehicle inverters: present and the future trends, *Proceedings of 1<sup>st</sup> IEEE CogMob Conference*, pp. 105-118
- [28] Liebertseder J., Wunsch S., Sonner C., Berg L-F., Doppelbauer M., Tübke J.: Temperature Prediction of Automotive Battery Systems under Realistic Driving Conditions using, *Proceedings of 1<sup>st</sup> IEEE CogMob Conference*, pp 167-172
- [29] Paiss V., Kovács R. C.: Inductance tensor calculation method for characterizing synchronous reluctance machines, *Proceedings of 1<sup>st</sup> IEEE CogMob Conference*, pp 173-178
- [30] Tollner D., Zöldy M.: Long term utilisation effect on vehicle battery performance, *Proceedings of 1<sup>st</sup> IEEE CogMob Conference*, pp 79-84
- [31] Harth P.: Examination of hydraulic hybrid drive unit for PHHV, *Proceedings of 1<sup>st</sup> IEEE CogMob Conference*, pp 141-146
- [32] Zöldy Mar., Dömötör F.: Noise and vibration test of electric drive cars, *Proceedings of 1<sup>st</sup> IEEE CogMob Conference*, pp 121-124
- [33] Zöldy M., Pathy-Nagy Z.: Evaluating of E-Vehicle Gear Noise, *Proceedings of 1<sup>st</sup> IEEE CogMob Conference*, pp 93-96
- [34] Nyerges Á.: Dual loop EGR mass flow rate estimation, *Proceedings of 1<sup>st</sup> IEEE CogMob Conference*, pp 23-28
- [35] Muhssen H., Khalaf K.: Thermal investigation of gas-air mixture inside the compound of mixer and shell heating method using CFD, *Proceedings of 1<sup>st</sup> IEEE CogMob Conference*, pp 37-46
- [36] Virt M., Zöldy M.: Artificial Neural Network Based Prediction of Engine Combustion and Emissions from a High-Resolution Dataset, *Proceedings of 1<sup>st</sup> IEEE CogMob Conference*, pp 97-104

- 
- [37] Tóth Á.D., Szabó Á. I.: Applicability of nanoscale ceramic particles as tribological lubricant additives, Proceedings of 1<sup>st</sup> IEEE CogMob Conference, pp 31-36
- [38] Nagy A. L., Agocs A.: Processing FT-IR data for facilitated oil condition monitoring, Proceedings of 1<sup>st</sup> IEEE CogMob Conference, pp 47-50
- [39] Van Eck, N. J., & Waltman, L. (2007) Bibliometric mapping of the computational intelligence field. *International Journal of Uncertainty, Fuzziness and Knowledge-Based Systems*, 15(05), 625-645
- [40] Van Eck, R. (2006) Digital game-based learning: It's not just the digital natives who are restless. *EDUCAUSE review*, 41(2), 16
- [41] Peters, H. P., & Van Raan, A. F. (1993) Co-word-based science maps of chemical engineering. Part I: Representations by direct multidimensional scaling. *Research Policy*, 22(1), 23-45
- [42] Zitt, M., Bassecoulard, E., & Okubo, Y. (2000) Shadows of the past in international cooperation: Collaboration profiles of the top five producers of science. *Scientometrics*, 47(3), 627-657

# Neural Network-based Multi-Class Traffic-Sign Classification with the German Traffic Sign Recognition Benchmark

Csanád Ferencz, Máté Zöldy

Department of Automotive Technologies, Faculty of Transportation and Vehicle Engineering, Budapest University of Technology and Economics, Stoczek 6, 1111 Budapest, Hungary; E-mail: csanadferencz@edu.bme.hu, zoldy.mate@kjk.bme.hu

---

*Abstract: Traffic-sign detection has an essential role in the field of computer vision, having many real-world applications more and more object recognition and classification task is being solved by using Convolutional Neural Networks (CNNs or ConvNets), especially in the field of intelligent transportation. In the present article, we offer an implementation chosen from several CNN-based traffic-sign recognition and classification algorithm architectures, using a ConvNet classifying 43 different types of road traffic signs in the TensorFlow framework, as part of the German Traffic Sign Recognition Benchmark (GTSRB) competition. A Deep ConvNet was trained end-to-end, aiming to improve the prediction performance of a DCNN-based autonomous driving system equipped with a front-facing digital camera, with as input a sequence of images, as output directly the prediction results. The results obtained on held-out data demonstrated the high accuracy of the model, matching the state-of-the-art multi-class recognition and classification accuracies, as well as related human-level recognition performances.*

*Keywords: convolutional neural networks; end-to-end classification model; German traffic-sign recognition benchmark (GTSRB); traffic-sign recognition; cognitive mobility*

---

## 1 Introduction

As a result of, their fast execution and high recognition rate, Deep Convolutional Neural Networks (DCNN-s) have been pointed out in recent years to offer state-of-the-art traffic sign classification performance, beyond what could be accomplished by former state-of-the-art methods.

The emergence of modern discoveries and developments in deep learning gave rise to positive state-of-the-art results for traffic sign classification and recognition, with most of the research focusing on designing and developing cognitive techniques, such as DCNN-s for enhanced recognition accuracy. In the realm of mobility, cognitive methods can aid in making immediate decision. At the moment, nearly all

of the state-of-art network architectures for traffic-sign classification are based on Convolutional Neural Networks (or ConvNets) [14], [18], [19].

In the present article, the authors introduce a revised end-to-end traffic sign detection and recognition system, while thoroughly describing the design and development processes of the ConvNet through which the real-time processing of images, as well as classification of localized objects are implemented [20].

The presented end-to-end cognitive approach revealed a substantial efficiency decrease during testing and development for the recognition and classification of road signs in real conditions, a simple template matching classification algorithm was not able to achieve high-quality recognition results due to limited set of predefined templates, angle of rotation, contrast in images of localized traffic signs or too intense variations in the illumination. To improve the system's recognition performance, a possible solution might be that these widely applied convolutional neural networks could be combined with the localization algorithm that has shown good results [14], [18], [19].

The experiments conducted demonstrate that the perception module shows promising performance results, and the classifier is capable of detecting and sorting the various signs properly enough regardless of quality, orientation or size. The work shows promising results that push the complexity boundaries regarding navigating self-driving cars with a cognitive toolbox through towns [18], [19].

The final model was more than capable of a smooth detection and classification of a significant number of traffic signs on the German Traffic Sign Recognition Benchmark (GTSRB) dataset, with an accuracy as high as 97.98%, even approaching the related human-level recognition performance of 98.81%. It is interesting to note that the best 13 networks submitted for the GTSRB competition all use CNNs with a classification performance of at least 98.10%. Human-level accuracy is outperformed by 5 of these, indicating once again why it is the most commonly used state-of-the-art traffic-sign classification method [25].

In the following parts of the study beginning with *Section 2*, a detailed description will be given regarding the classification task and dataset pre-processing, in *Section 3* the layer architecture definition, building and training of the model provided in *Section 4*, and last but not least *Section 5* concluding with result validation and discussion.

## 2 Traffic Sign Classification Task, Dataset Pre-Processing and Loading

CNN-s are frequently used for different purposes in image processing, such as segmentation, classification, or detection [25]. The traffic-sign classification problem has been addressed with various well-known methods, including neural

networks (NNs), Support-vector machine model architecture (SVM), or Naive Bayes classification. Many approaches used for traffic-sign recognition are based on sliding window methods, which resolve the classification and recognition problems simultaneously, but require unfeasible computational resources. However, several recent literature state-of-the-art systems separate recognition from classification. Firstly, we would deal with the recognition with custom-built computationally inexpensive methods, e.g. color thresholding. After that, the classification will be conducted on the detected samples with algorithms having higher accuracy.

Traffic-sign recognition is a rather constrained problem, it has many direct real-world applications, road signs being unique with little variability in appearance, fixed, and intended to be displayed for the drivers. Even though the current task is exclusively classification, when designing a classifier the ultimate objective of detection is to optimize both efficiency and accuracy. With color thresholding and various heuristics, for instance, we first detect sign shapes, followed by multi-layer NN classification for each type of traffic sign outer shape. The method has the advantage of fast training, reduced chance of overfitting, needs fewer samples, and it is great for local information capturing and reducing the complexity of a given model [6].

The German traffic sign detection dataset consists of 39 209 image samples corresponding to 43 different classes (ranging from 0 to 42), each one of the signs having its folder of different image sizes and resolutions. The training dataset is made up of 34 799 images, the validation dataset of 4 410 images, and respectively the test set of 12 630 images. Because samples are divided unevenly between the related classes, our model could predict some of the classes with higher accuracy than others. The samples are composed of video sequence frames of 1 [s], and as the camera approaches a given sign each real-world sample produces 30 samples increasing in resolution [23], [24], [25]. The total number of samples present in our dataset exceeds 50 000 images.

Thus, we will categorize  $40 \times 40$  RGB pixel space input images into 43 possible traffic sign categories:  $h: \mathbb{R}^{4800} \mapsto \{0, 1, \dots, 42\}$ . Note that due to the three-color channels, we have a  $40 \times 40 \times 3 = 4800$  - dimensional input. In this task, convolutional neural networks (CNN-s) usually perform at around 90-95% accuracy [8], [24], [25]. We will try to train a network that performs better than humans — 98.9% on the original German Traffic Sign Recognition Benchmark (GTSRB).

Many images from the sample set given by the GTSRB competition present several difficult challenges, some of these are very hard to distinguish and classify even for a human (low-contrast, viewpoint variations, motion-blur, physical damage, occlusions, colors fading or input resolution as low as  $15 \times 15$ ). However, we can assume that the ground truth that we have is exact.

Because the image samples present in the dataset dynamically varies between a wide range of dimensions from  $15 \times 15 \times 3$  to  $250 \times 250 \times 3$ , it is not possible to pass them directly to the CNN model, hence this cannot be trained on different image dimensions, but we also need to avoid stretching the images too much when compressing them to a single dimension. All things considered, we will use an already pre-processed version of the images re-sized to  $40 \times 40 \times 3$ .

Furthermore, because the present project's objective is to build a robust recognizer excluding temporal evidence accumulation, road signs in the training dataset will be available as video sequences, and temporal information will not be in the test dataset [6], [23], [24], [25]. Moreover, we will populate and diversify the original set of data as well with various image modifying techniques such as rotations, color distortions and blurring techniques. Therefore, at this stage we are performing data augmentation (see *Figure 1*).



Figure 1

Data augmentation creating modified input sample versions [5]

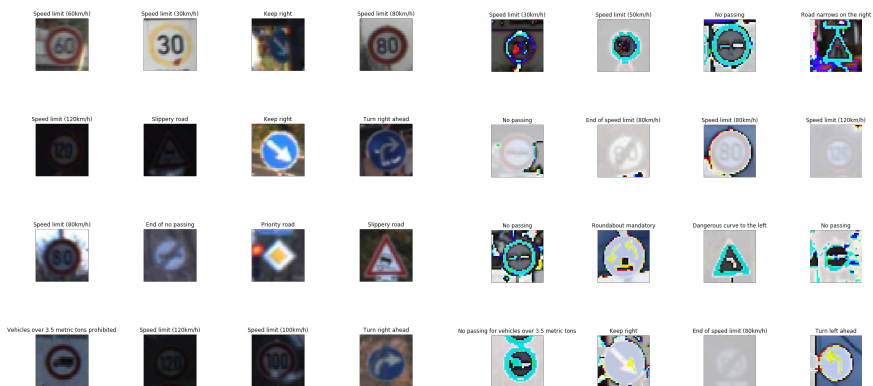


Figure 2

Labeled input dataset before and after augmentation, pre-processing and normalization [5]

With this solution basically we are adding more sample to our dataset, but without collecting any new one. The samples following data augmentation, pre-processing

and normalization will look like as presented in *Figure 2*. All of the dataset image samples were normalized, in order to help the model converge faster, the data having a mean of zero and equal variance.

After finding out the model's actual accuracy by training on the original dataset, in the next step by adding even more data and evening out the classes we will check the accuracy again [6]. The purpose of the test set would be to detect, during training, that the model has overfitted and to implement, e.g. early stopping, dropout or some other method to compensate. Once the model is completely trained, the validation set needs to be simply run through the model and the results reported. In order to have diverse datasets and higher prediction performance on unseen data, we will extract randomly one sample per class for validation, instead of mixing all images randomly and separating into similar training and validation datasets [16].

### 3 Network Layer Architecture

Generally speaking, similarly to regular NN, convolutional neural networks also consists of neurons having learnable biases and weights, organized in layers. Contrary to regular neural networks, however, CNNs make the most of the fact that they constrain the input architecture composed of images in a more sensible way, in particular having layers with neurons arranged in three dimensions [11], [16].

However, a ConvNet will take a two-dimensional image and progressively will process it with the convolutional layer. In the case of this classification task, the input volume samples of activations having the size of  $40 \times 40 \times 3$  (40 - width, 40 - height, 3 color channels), in the first hidden layer a single fully connected neuron would have  $40 \times 40 \times 3 = 4\ 800$  weights. This volume still looks computable, however, this structure certainly will not scale to larger images, e.g. size of  $250 \times 250 \times 3$ , in the case of regular neural networks, because that would lead to neurons that have 187 500 weights, and because we generally want to have more than one of these neurons the parameters would add up quickly [11]. It is clear that full connectivity would not be particularly efficient, and these considerable amounts of parameters would swiftly give rise to overfitting.

As *Figure 3* illustrates, each of the ConvNet's layers will transform the three-dimensional input volume to a three-dimensional output volume with neuron activations. In the case of the left example, the red input layer's height and width will be the image dimensions, while the depth will correspond to the red, green, and blue channels. The right figure illustrates an example input volume of a  $32 \times 32 \times 3$  image and the volume of neurons in the first convolutional layer. In this case, there are 5 neurons along the depth, connected to or looking at the same region of the input volume. These 5 neurons do not represent the same weights, they are only associated with 5 different filters, sharing the same receptive field [25].

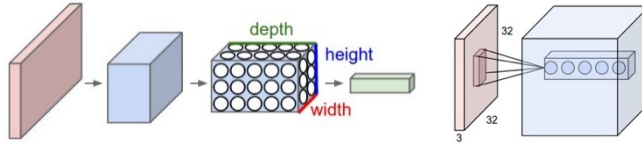


Figure 3

3-layer network vs CNN organizing neurons in three dimensions [25]

When dealing with deep CNN, normal CNNs generally have two or three layers, but deep CNNs will have multiple hidden layers usually more than 5, which are used to extract more features and increase the accuracy of the recognition. Therefore, the depth of the network shall correlate with the amount of data, a deep network with insufficient data will produce an overfitted model, while a shallow network with a lot of data will not have a high accuracy [11]. Moving from layer to layer, the low-level input feature vector is put into the first layer and transformed into a high-level feature vector. The neuron number in the output layer is equal to the classifying class number, while the vector of probability output is showing the possibility of the input vector belonging to a corresponding class. The output of a weighted adder is described by (1):

$$a_j^i = \sigma(\sum_k a_k^{i-1} w^i_{jk}) \quad (1)$$

where  $a_j^i$  -  $j^{th}$  neuron,  $i^{th}$  layer and  $w^i_{jk}$  - weight of synapse, connecting  $j^{th}$  neuron in the layer  $i^{th}$ , with the  $k^{th}$  neuron in the  $i - 1$  layer. As activation function the logistic function will be applied, frequently used in regression problems [2], [25].

In classification problems during training process the goal is to minimize the cost function by gradient decent with minimization methods. In this case, cross entropy is the most widely used cost function,  $H(p, q)$  being the cross-entropy of the distribution  $q$  relative to a distribution  $p$  over a given set, presented in (2):

$$H(p, q) = - \sum_i Y(i) \log y(i) \quad (2)$$

Because in computer vision CNN classification is the state-of-the-art method for pattern recognition, our implemented network layer structure, illustrated in *Figure 4*, is also mostly based on convolutional layers, following the architecture Input — Convolutional Layer — ReLU — Pooling Layer — Fully Connected (FC) Layer. Image convolution is the simple sum of element-by-element matrix multiplication between weights and the input volume region they are connected to, followed by a summing of the elements together [25]. These layers operate in the form of sliding windows, and do not require a fixed image size, while the output of these will be the spatial arrangement of activations, or so-called feature maps of any size, which allow us to detect the same features in different locations [1], [2], [24].

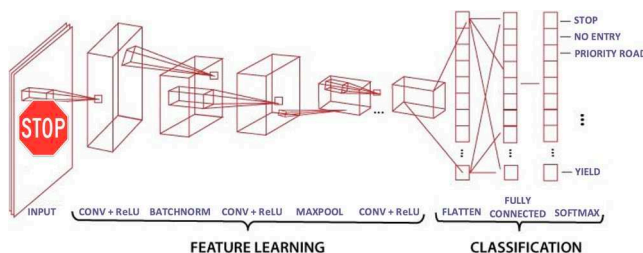


Figure 4

Applied classification layer structure (Own work, 2021)

In substance, the convolutional layer requires four hyperparameters ( $S$  - stride,  $K$  - number of filters,  $F$  - spatial extent,  $P$  - the amount of zero padding) and accepts a  $W1 \times H1 \times D1$  volume size. A common setting of the hyperparameters is  $F = 3$ ,  $S = 1$ , and  $P = 1$ . It produces a volume of size  $W2 \times H2 \times D2$ , where heights and widths are equally computed by symmetry, described by (3), (4), and (5):

$$W2 = \frac{(W1 - F + 2 \cdot P)}{S} + 1 \quad (3)$$

$$H2 = \frac{(H1 - F + 2 \cdot P)}{S} + 1 \quad (4)$$

$$D2 = K \quad (5)$$

Using sharing of parameters, for  $(F \times F \times D1) \times K$  weights and  $K$  biases,  $F \times F \times D1$  weights per filter will be introduced. Regarding the output volume, a  $W2 \times H2$  sized  $d^{th}$  depth slice will result after performing a convolution of the  $d^{th}$  filter with a stride of  $S$  over the input volume, offset then by the  $d^{th}$  bias.

As a next layer, we implement batch normalization to stabilize training and facilitate a smoother hyperparameter tuning process, while substantially increasing the classification performance [1], [25]. This normalization operation normalizes the elements of  $x_i$  inputs by calculating the mean  $\mu_B$  and variance  $\sigma_B^2$  over the time, spatial and observation dimensions independently in the case of every channel, respectively also calculating the so-called normalized activations as in (6) [2]:

$$\hat{x}_i = \frac{x_i - \mu_B}{\sqrt{\sigma_B^2 + \epsilon}}, \quad (6)$$

where  $\epsilon$  — constant, improving numerical stability when variance is small.

This operation additionally scales and shifts the activations, allowing those inputs with unit variance as well as zero mean to not be optimal for operations following batch normalization, using the transformation presented in (7) [1]:

$$y_i = \gamma \hat{x}_i + \beta, \quad (7)$$

where  $\hat{x}_i$  - the resulting normalized activation having zero mean and unit variance,  $\beta$  — offset and  $\gamma$  — scale factor. These parameters are learnable and updated during

the training of the network. In order to make predictions after training, batch normalization assumes a fixed mean and variance, calculated from training data after or during training, to normalize data [2].

Between consecutive convolutional layers we can insert periodically an intermediate pooling layer, with the intention of operating independently on the input's each depth slice and successively reducing the spatial size, number of parameters, and network computation, leading also to controlling the overfitting. The most frequently used form of this is a  $2 \times 2$  filter size pooling layer downsampling every input depth slice with a stride of 2 across both height and width, discarding two-thirds of the activations, but leaving unchanged the depth dimension, described by (8), (9) and (10). This pooling layer requires two hyperparameters, the  $S$  - stride and  $F$  - spatial extent, while accepting a  $W1 \times H1 \times D1$  sized volume, and producing a  $W2 \times H2 \times D2$  sized volume, where:

$$W2 = \frac{(W1-F)}{S} + 1 \quad (8)$$

$$H2 = \frac{(H1-F)}{S} + 1 \quad (9)$$

$$D2 = D1 \quad (10)$$

It should be also emphasized that only two predominantly used max pooling layer variation is found in practice, the more common one with  $S = 2$  and  $F = 2$ , but also a configuration of  $S = 2$  and  $F = 3$ , or the so-called overlapping pooling. Pooling sizes with bigger receptive fields could be too detrimental [1], [2]. *Figure 5* illustrates the most widely used max-pooling downsampling operation with a stride of 2. The  $224 \times 224 \times 64$  sized input volume is pooled with stride 2 and filter size 2 into a  $112 \times 112 \times 64$  sized output volume, while the volume depth is preserved [9], [10].

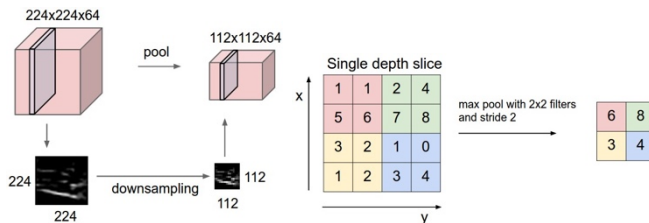


Figure 5

Illustration of pooling layer downsampling the input volume [25]

In the final four layers, we will perform a flatten operation on the last convolutional layer's output, a final batch normalization, as well as a dropout operation while entering into the last output dense layer — this will be the same as the number of classes that we have. The purpose of using dropout is to avoid overfitting and to generalize while also improving reliability. Neurons with probability  $p$  of the current layer will disconnect randomly from the next layer's neurons, going through the depth of the network, learning more filters as the network deepens.

Training deep networks using several layers with a sigmoid activation function will be complicated because of the vanishing gradient issue [9], [10], [13]. To resolve this difficulty, we will specifically use the activation *Rectified Linear Unit (ReLU)*, which applies  $\max(0, x)$  elementwise non-linearity activation function thresholding at zero,  $x$  being the input to a neuron, presented in (11):

$$f(x) = x^+ = \max(0, x) \quad (11)$$

Using ReLU, compared with other similar activation functions such as the sigmoid function, enables a more efficient, but also faster training process of complex and large datasets attributed to deep neural architectures, leaving the volume size unchanged [12]. A *SoftMax* classifier is also added to the network to normalize the output of the previous layer, so the output of this will contain the probability values of belonging to a recognizable class (the layer's output basically will be the prediction values). The standard (unit) SoftMax function  $\sigma: \mathbb{R}^K \rightarrow [0,1]^K$  for  $i = 1, \dots, K$  respectively  $z = (z_1, \dots, z_k) \in \mathbb{R}^K$  is defined by (12):

$$\sigma(z)_i = \frac{e^{z_i}}{\sum_{j=1}^K e^{z_j}} \quad (12)$$

where  $\sigma$  - softmax,  $z$  input vector,  $e^{z_i}$  - standard exponential function for input vector,  $K$  - number of classes in the multi-class classifier,  $e^{z_j}$  - standard exponential function for output vector. Essentially what this does is that it takes a vector  $z$  as input with  $K$  real numbers and normalizes it. The probability distribution containing  $K$  probabilities will be proportional to the input numbers' exponentials.

At the end of the network, we add a fully connected layer as well, thus realizing class score computing, leading to volumes of a  $1 \times 1 \times 43$  size, where numbers will be matched to one of the 43 class category scores of the GTSRB dataset. The network will learn filters that activate when some type of visual feature can be seen on the first layer (e.g. edge of some orientation) and ultimately entire patterns on the network's higher layers [29].

## 4 Building and Training the Model

An illustration of the classifying process is presented in *Figure 6*. At this point, the built network processed from the training dataset a 50-image batch over one iteration. The so-called intermediate accuracy was calculated every 100 iterations, with a batch of 50 images from the test set to report progress. After successful training, the accuracy is calculated again, using all samples from the test set.

The input image of  $40 \times 40 \times 3$  is a multi-dimensional matrix, holding raw pixel values, having, just like a traditional matrix, a width of 40 (number of columns), a height of 40 (number of rows), as well as a depth of 3 for a standard RGB image,

representing the image channel number. Plotting the histogram for the sample images in our dataset for different road traffic signs will result in *Figure 7*.

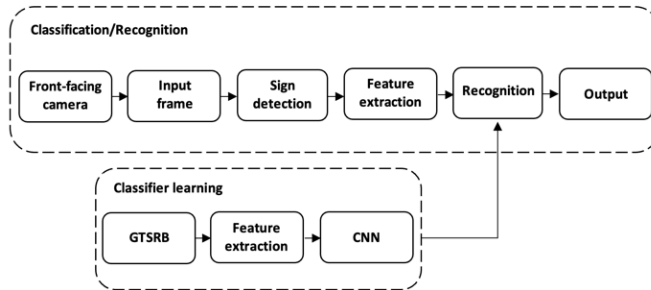


Figure 6

Simplified functional diagram of the classifying process (Own work, 2021)

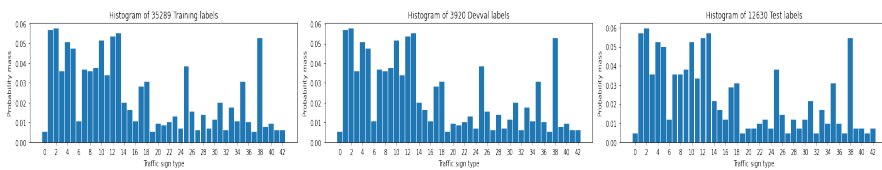


Figure 7

Histogram distribution of the augmented training image categories (Own work, 2021)

The sample numbers for each road sign are unevenly distributed between classes, not having the same number of samples for every class (also shown in the histogram distribution), leading to a biased model that recognizes and classifies some of the traffic signs more accurately than others. Thus, sample images had to be augmented for some of the classes to reach a minimum of 250 images in each class, while avoiding replicates in the input dataset [3], [26].

All coding of data arguments along with the training model is created in the *Jupyter Notebook* environment. The detailed CNN layer architecture and specification used, built with [21] and [22], is summed up in *Table 1*, respectively shown in *Figure 8* and *Figure 9* [8]. Among the types of layers used are two-dimensional convolution layers (Conv2D), batch normalization, two-dimensional max pooling, flatten, dropout, and dense - with detailed descriptions in the previous section [4].

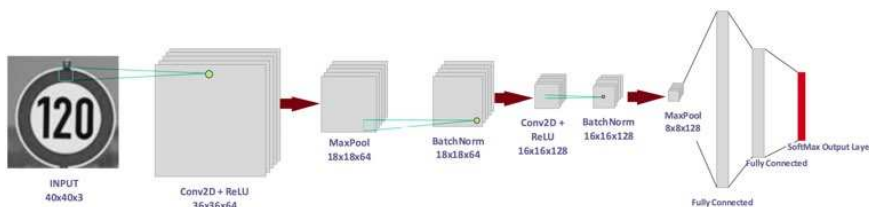


Figure 8

Implemented deep convolutional neural network layer architecture (Own work, 2021)

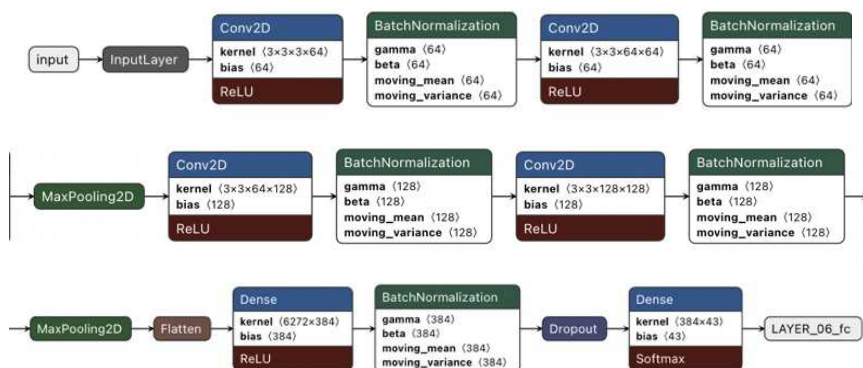


Figure 9

Deep convolutional neural network architecture specifications layer-by-layer (Own work, 2021)

The entire procedure for model training requires about two hours over a single GPU, the total number of parameters is 2 688 619 (from which 2 687 083 are trainable and 1 536 non-trainable), the training process is carried out with an Intel Core i7-4790K - 32 GB RAM, 4.00 GHz processor and Ubuntu-64 bit operating system [1], [2]. We will be using *Python 3.x* with *TensorFlow*, the scripts only reference standard libraries available over the 'pip' package manager, such as *os*, *time*, *numpy*, *zipfile*, or *matplotlib* backend.

To maximize likelihood (MLE) we have to minimize the sum/mean/root-mean-squared error (SSE/MSE/RMSE) [3], [4], [6]. Consequently, for result evaluation we adopt this MSE, the default loss for regression problems used to predict continuous target values, calculated as the average of the squared differences between the predicted ( $\hat{y}_i$ ) and actual ( $y_i$ ) values, shown in (13):

$$MSE = \frac{1}{m} \sum_{i=1}^m (\hat{y}_i - y_i)^2 \quad (13)$$

A supervised training gradient-based method is updating each one of the filters in each layer, in each filter bank in such a way that it minimizes the loss function, while the last stage's output is fed to a classifier. In the case of classification problems, we approximate  $p(Y|X)$   $k$ -class discrete conditional distribution with  $q(\hat{Y}|X)$  modeling distribution  $\mathbb{R}^n \rightarrow [0,1]^k$  [8], [15].

Table 1  
Network layer architecture, parameters and sizes

Layer type	Filter nr.	Kernel size	Activ. fc.	Output shape	Param. nr.
Conv1	64	3x3	RELU	(None, 38, 38, 64)	1 792
BatchNorm	-	-	-	(None, 38, 38, 64)	256
Conv2	64	3x3	RELU	(None, 36, 36, 64)	36 928

Layer type	Filter nr.	Kernel size	Activ. fc.	Output shape	Param. nr.
BatchNorm1	-	-	-	(None, 36, 36, 64)	256
MaxPool	-	2x2	-	(None, 18, 18, 64)	0
Conv3	128	3x3	RELU	(None, 16, 16, 128)	73 856
BatchNorm2	-	-	-	(None, 16, 16, 128)	512
Conv4	128	3x3	RELU	(None, 14, 14, 128)	147 584
BatchNorm3	-	-	-	(None, 14, 14, 128)	512
MaxPool1	-	2x2	-	(None, 7, 7, 128)	0
Flatten	-	-	-	(None, 62 72)	0
Dense	384	-	RELU	(None, 384)	2 408 832
BatchNorm4	-	-	-	(None, 384)	1 536
Dropout	-	-	-	(None, 384)	0
Dense	-	-	Softmax	(None, 43)	16 555

To maximize likelihood, we have to minimize cross-entropy  $H(p, q)$  or Kullback-Leibler (KL) divergence  $D_{KL}(p||q)$ . The entropy formula is given in (14), while the cross-entropy formula is given in (15),  $H(p, q) \geq H(p)$ , asymmetric [15], [25], [28]. KL Divergence is also known as relative entropy or information gain, given in (16),  $D_{KL}(p||q) \geq 0$ , asymmetric.

$$H(p) = -\sum_k p_k \ln p_k \quad (14)$$

$$H(p, q) = -\sum_k p_k \ln q_k \quad (15)$$

$$D_{KL}(p||q) = H(p, q) - H(p) \quad (16)$$

Cross-entropy loss function is given in (17) and (18), where we minimize the amount of surprise suffered between our expectation ( $q$ ) and reality ( $p$ ) [15]:

$$L_{xH} = -\frac{1}{m} \sum_i \sum_k p_{ik} \ln q_{ik} \quad (17)$$

$$p_{ik} = p(Y_i = k|X_i) \quad (18)$$

Our first hyperparameter (see *Table 2*), the number of epochs, indicates how many times should the network go through a full training process. In this case, the network will go over all the 50 000 images, as well as validate itself with 12 000 test images exactly 20 times. The number of batches in epoch is the training set size over the batch size. In case of setting this batch size to a larger value, the quality of our model could deteriorate, eventually leading to a point where the model is unable to generalize well on previously unseen data [4].

The hyperparameters controlling the output volume's size are the stride, zero-padding and depth. Stride is wherewith we slide the filter, if it is equal to 1, we are moving one pixel at a time for every filter. The zero-padding has a role in controlling spatial sizes of output volumes, and the output volume depth will correspond to the number of filters we are planning to use [25]. Another aspect

worth noting is the impracticality of connecting neurons to all previous volume neurons, rather connecting each neuron to only a local region, leading to the spatial extent called the receptive field — or otherwise called the filter size, summarized for each specific layer in *Table 1*.

The learning rate, defined between 0 and 1, in this case 0.001, describes our weights' update rate. Because cycling through all of the 50 000 samples at the same time would not be computationally feasible, the batch size will express the number of image samples our neural network will cycle through at once. Our optimizer will be created as the Adam optimizer for the stochastic gradient solver, while the weight decaying parameter is also set to 0.001 — this reduces overfitting [25], [26].

Table 2  
Training the network - hyperparameters

Parameter	Value [-]
Learning rate	0.001
Decay	0.001
Batch size (Training)	256
Batch size (Validation)	256
Epochs	2
Verbose	1

Regarding batch sizes, each batch size is composed of 256 frame inputs for the training, as well as in the case of the validation phase. Each batch trains the network in successive order, taking into account the updated weights coming from the appliance of the previous batch, each sample passed through to the network at one time. In the case of the hyperparameter batch size, we have to test and adjust it as per how our specific model performs during training. This hyperparameter also must be tested concerning how our machine is operating in respect of resource utilization [5]. Setting the verbose to 1 will mean that the progress of the model being trained will be shown during development time.

## 5 Validation Results and Optimization

The result validation phase during development gives us the improvement directions on how the precision accuracy could be increased. *Figure 10* presents some results during optimization with erroneous sample predictions, as well as the accuracy/loss variation of the model.

In the case of running the network without image augmentation, there are indications that the model's validation accuracy was rather high compared to the training accuracy, as *Figure 11* illustrates. At this point, we additionally defined two levels of dropout, one for convolutional layers with a rate of 0.75 and one for

fully connected layers with 0.5. The initial convolutional depth of 32 was also modified due to obtain better results with 64 [25]. Additionally, the right image in *Figure 11* presents the convolutional working process over some sample traffic signs, visually revealing the network's recognition principle.

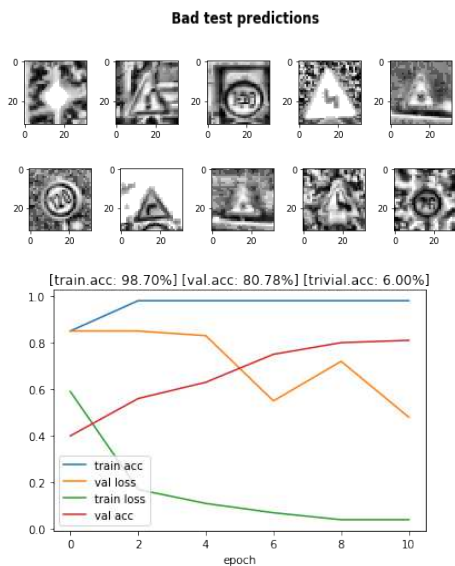


Figure 10

Samples with erroneous predictions and development accuracy/loss of the model (Own work, 2021)

The values of both loss function and precision accuracy variation for our model for 10 epochs are illustrated graphically in *Figure 12*. We can observe that the adopted CNN reduces smoothly the values of these performance metrics over the epochs, there is an apparent efficiency in the learning process, and these values tend to be flat and convergent, ultimately approaching the human-level recognition performance goal of 98.81% set in the first place, with a final recognition performance of 97.98%.

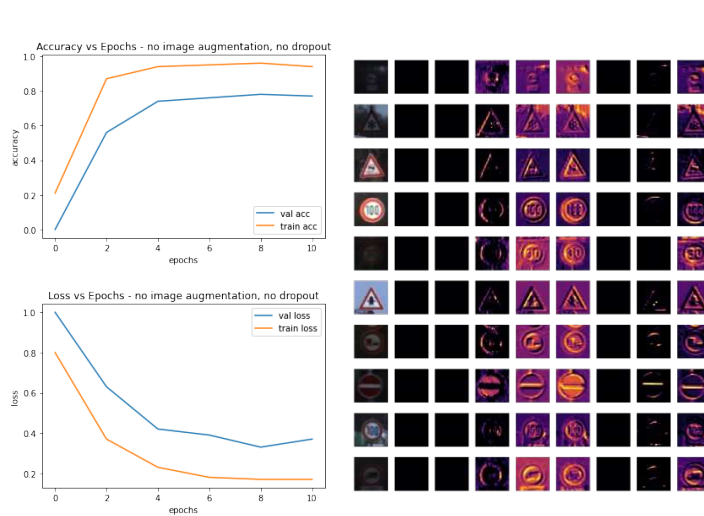


Figure 11

Accuracy and loss before optimization, and convolution visualization (Own work, 2021)

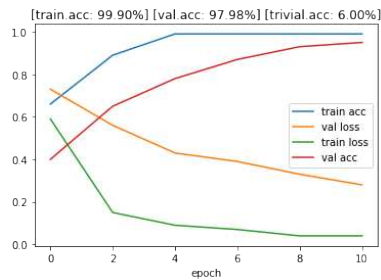


Figure 12

Final training and validation accuracy of the model (Own work, 2021)

## Conclusions

In this paper the authors presented a ConvNet system and its architecture with state-of-the-art results on the GTSRB dataset, investigated a real-world traffic-sign recognition and classification problem, built a highly configurable network, as well as developed a flexible method to assess multiple architectures. The research provides evidence of practicality of the presented applications, highlighting the enhanced efficiency brought by the cognitive methods [18], [19], [27].

The validation of the network showed promising and smooth results that hold up against existing literature findings and outcomes in the field of ML-based classification problems. The network is working effectively with the preprocessed images and produces good results. The remaining errors are due to either too low-resolution inputs or physically degraded road signs for which classification is not possible with just a single image instance.

Concerning possible future development directions, one could be the problem of perception input, the traditional ConvNet architecture could be modified by feeding features to the classifier of 1st stage besides features of 2nd stage, as well as by using greyscale driving images having strong correlation features among continuous frames instead of color and by increasing the network capacity [17]. Regarding the color image samples, by visualizing the erroneous predictions we can assume that normalized color channels could be more informative than raw color.

Future studies should examine the effect of input resolution to enhance processing speed and classification accuracy, in addition to processing with multiple networks, which might further improve accuracy [16]. Finally, the influence and effect of unsupervised pre-training of feature-extracting stages should be investigated as well, which could be more easily learned than with a strictly supervised method, explicitly with an increased number of features at each stage.

### Acknowledgement

Within the framework of the New Széchenyi Plan, the project “Development of talent management and researcher supply in the field of autonomous vehicle control technologies (EFOP-3.6.3-VEKOP-16-2017-00001)” provided funding for the study. The research was supported by the European Union and co-financed by the European Social Fund.

### References

- [1] A. Rosebrock, “Convolutions with OpenCV and Python,” 2016 (Online) Available at: <https://www.pyimagesearch.com/2016/07/25/convolutions-with-opencv-and-python/>
- [2] A. Rosebrock, “Keras Conv2D and Convolutional Layers,” 2018 (Online) Available at: <https://www.pyimagesearch.com/2018/12/31/keras-conv2d-and-convolutional-layers/>
- [3] A. Shustanov and P. Yakimov, “CNN Design for Real-Time Traffic Sign Recognition,” *Procedia Engineering*, Vol. 201, pp. 718-725, 2017, ISSN 1877-7058, DOI: <https://doi.org/10.1016/j.proeng.2017.09.594>
- [4] A. Wong, M. J. Shafiee and M. St. Jules, “MicronNet: A Highly Compact Deep Convolutional Neural Network Architecture for Real-Time Embedded Traffic Sign Classification,” *IEEE Access*, Vol. 6, pp. 59803-59810, 2018, DOI: <https://doi.org/10.1109/ACCESS.2018.2873948>
- [5] Benchmark - Institut für Neuroinformatik (INI), “Dataset - German Traffic Sign Recognition Benchmark,” 2021 (Online) Available at: [https://benchmark.ini.rub.de/gtsrb\\_dataset.html](https://benchmark.ini.rub.de/gtsrb_dataset.html)
- [6] L. Kovacs, L. Lindenmaier, H. Nemeth, V. Tihanyi and A. Zarandy, “Performance Evaluation of a Track to Track Sensor Fusion Algorithm,” *CNNA 2018: The 16<sup>th</sup> International Workshop on Cellular Nanoscale Networks and their Applications*, Budapest, Hungary, 2018, pp. 1-2

- [7] C. Ferencz and M. Zöldy, “End-to-end autonomous vehicle lateral control with deep learning,” 12<sup>th</sup> International Conference on Cognitive Infocommunications (CogInfoCom), IEEE Xplore, September 23-25, 2021, Budapest, ISBN 978-1-6654-2495-0
- [8] J. Credi, “Traffic sign classification with deep convolutional neural networks,” Master’s thesis in Complex Adaptive Systems, Department of Applied Mechanics, Chalmers University of Technology, 2016, Gothenburg, Sweden. Available at: <https://publications.lib.chalmers.se/records/fulltext/238914/238914.pdf>
- [9] D. Sanket, “Convolutional Neural Network: Learn And Apply,” 2019 (Online) Available at: <https://medium.com/@sdoshi579/convolutional-neural-network-learn-and-apply-3dac9acfe2b6>
- [10] D. Sanket, “Traffic Sign Detection using Convolutional Neural Network,” 2019 (Online) Available at: <https://towardsdatascience.com/traffic-sign-detection-using-convolutional-neural-network-660fb32fe90e>
- [11] E. Forson, “Recognising Traffic Signs With 98% Accuracy Using Deep Learning,” 2017 (Online) Available at: <https://towardsdatascience.com/recognizing-traffic-signs-with-over-98-accuracy-using-deep-learning-86737aadc2ab>
- [12] F. Nushaine, “Building a Road Sign Classifier in Keras,” 2020 (Online) Available at: <https://towardsdatascience.com/building-a-road-sign-classifier-in-keras-764df99fdd6a>
- [13] Google Colaboratory, “Welcome to Colaboratory,” 2021 (Online) Available at: <https://research.google.com/colaboratory/> (Accessed 10 08 2021)
- [14] G. E. Hinton and R. R. Salakhutdinov, “Reducing the dimensionality of data with neural networks,” *Science*, Vol. 313, No. 5786, pp. 504-507, 2006.
- [15] I. Sergey, and C. Szegedy “Batch Normalization: Accelerating eep Network Training by Reducing Internal Covariate Shift,” Preprint, 2015, <https://arxiv.org/abs/1502.03167>
- [16] J. Stallkamp, M. Schlipsing, J. Salmen, C. Igel, “Man vs. computer: Benchmarking machine learning algorithms for traffic sign recognition,” *Neural Networks*, Vol. 32, pp. 323-332, 2012, ISSN 0893-6080, DOI: <https://doi.org/10.1016/j.neunet.2012.02.016>
- [17] Keras - Simple. Flexible. Powerful, “API docs,” 2021 (Online) Available at: <https://keras.io/> (Accessed: 01 08 2021)
- [18] M. Zöldy and P. Baranyi, “Cognitive Mobility – CogMob,” 12<sup>th</sup> IEEE International Conference on Cognitive Infocommunications (CogInfoCom) pp. 915-919, 2021
- [19] M. Zöldy and P. Baranyi, “The Cognitive Mobility Concept,” *Infocommunications Journal*, Vol. 2023/01, pp. 35-40, 2022

- 
- [20] Netron App, “Lutz Roeder's Netron,” 2021 (Online) Available at: <https://netron.app> (Accessed: 05 08 2021)
- [21] NN-SVG, “Publication-ready NN-architecture schematics,” 2021 (Online) Available at: <https://alexlenail.me/NN-SVG/LeNet.html> (Accessed: 05 08 2021)
- [22] P. Baranyi and Y. Yam, “Singular value-based approximation with Takagi-Sugeno type fuzzy rule base,” Proceedings of 6<sup>th</sup> International Fuzzy Systems Conference, Vol. 1, pp. 265-270, 1997, DOI: <https://doi.org/10.1109/FUZZY.1997.616379>
- [23] P. Sermanet and Y. LeCun, “Traffic sign recognition with multi-scale Convolutional Networks,” The 2011 International Joint Conference on Neural Networks (IJCNN), 2011, pp. 2809-2813, DOI: <https://doi.org/10.1109/IJCNN.2011.6033589>
- [24] R. Uppala, “Traffic Signs Classification with a Convolutional Neural Network,” 2017 (Online) Available at: <https://medium.com/@techreigns/traffic-signs-classification-with-a-convolutional-neural-network-75911a1904>
- [25] Stanford University CS231n, “Convolutional Neural Networks for Visual Recognition,” 2021 (Online) Available at: <https://cs231n.github.io/convolutional-networks/>
- [26] S. Saha, S. Amit Kamran and A. Shihab Sabbir, “Total Recall: Understanding Traffic Signs Using Deep Convolutional Neural Network,” 2018 21<sup>st</sup> International Conference of Computer and Information Technology (ICCIT), 2018, pp. 1-6, DOI: <https://doi.org/10.1109/ICCITECHN.2018.8631925>
- [27] T. Péter, A. Hary, F. Szauter, K. Szabó, T. Vadvári, I. Lakatos, “Analysis of Network Traversal and Qualification of the Testing Values of Trajectories,” Acta Polytechnica Hungarica, Vol. 18, pp. 151-171, 2021, <https://doi.org/10.12700/APH.18.10.2021.10.8>
- [28] Wikipedia - The Free Encyclopedia, “Kullback–Leibler divergence,” 2021 (Online) Available at: [https://en.wikipedia.org/wiki/Kullback-Leibler\\_divergence](https://en.wikipedia.org/wiki/Kullback-Leibler_divergence) = shaded area
- [29] Z. Zhu, D. Liang, S. Zhang, X. Huang, B. Li, S. Hu, “Traffic-Sign Detection and Classification in the Wild,” Proceedings of CVPR, 2016, pp. 2110-2118

# Investigating Safety Effects of PKI Authentication, in Automotive Systems

Zsombor Pethó<sup>1</sup>, Tamás Márton Kazár<sup>1</sup>, Roland Kraudy<sup>2</sup>,  
Zsolt Szalay<sup>1</sup> and Árpád Török<sup>1</sup>

<sup>1</sup> Department of Automotive Technologies, Budapest University of Technology and Economics, Műegyetem rkp. 3, 1111 Budapest, Hungary; E-mail: zsombor.petho@edu.bme.hu, kazar.tamas@kjk.bme.hu, szalay.zsolt@kjk.bme.hu, torok.arpad@kjk.bme.hu

<sup>2</sup> Microsec Software Management and Consulting Ltd., Ángel Sanz Briz út 13, 1033 Budapest, Hungary; E-mail: roland.kraudy@microsec.com

---

*Abstract: Our study analyses the safety effects of Public Key Infrastructure (PKI), based authentication mated, related to certain wireless communication based automotive functions. The first part of the article focuses on quantifying the safety effect of quality of service (QoS) parameters in the case of wireless communication based automotive functions. Based on this concept, the paper discusses two scenarios: in the first case, there is no authentication process applied during the communication, and in the second case, the communication is secured by PKI authentication. This concept allows us to evaluate the safety effect of the security overhead caused by the additional computation demand related to the authentication process. Considering the results of our research, it becomes possible to define the requirements and expected conditions, regarding the operational circumstances.*

*Keywords: automotive safety; public key infrastructure; safety risk; V2X; network performance*

---

## 1 Introduction

Our paper aims to evaluate how Public Key Infrastructure-based security solutions (PKI) affect communication service quality and, thus, traffic safety. The reason why we need to analyze the PKI authentication process in detail is the fact that the available computational resources of the automotive systems are limited. Therefore, we need to find an acceptable trade-off between allocating our resources to improve the functionality and safety of the coordinated automotive applications or increasing the security of our system [1] [2]. Wireless communication between the components of the transportation system (e.g., vehicles, pedestrians, central management system, etc.) can significantly contribute to improving safety [3] [4] since the actors

of the cooperative intelligent transportation systems (C-ITS) will be able to exchange real-time information on their positions, velocities, accelerations, and planned trajectories. In certain cases, this information can be available sooner than the data collected by an environment perception module, especially in the case of some non-line-of-sight scenarios, where other sensor systems cannot detect the other actors in time.

Different types of messages exist in cooperative, connected and automated mobility (CCAM) systems that contain data used by safety-related applications. Cooperative Awareness Message (CAM) is a widely used message type that contains information on the vehicle's position and dynamics parameters by default. Therefore, it is well applicable for safety-related purposes [5].

To prevent malicious actors from joining the communication related to CCAM processes, the system must be capable of checking the authorization of the participants. CCAM systems use the PKI security solution to ensure authenticated, reliable communication, especially considering non-repudiation, integrity, and the freshness of the messages. X.509 PKI frameworks apply digital signatures, timestamps, hash functions and pseudonym certificates to sign messages. This provides both authenticity for CAMs and privacy for the users since the end-user identities do not contain any identifying data. Furthermore, the different authorization levels of CCAM system actors (such as police or normal driver) must also be handled. This results in further computational tasks that need to be performed beyond the processes of the classical automotive functions.

If it is not possible to assign additional computational capacity, the PKI authentication process can increase the delay / latency of the message transfer process. In everyday traffic scenarios, the extra computational demand needed for the authentication does not cause any difficulties since efficient algorithms (such as ECC – Elliptic Curve Cryptography) and application-specific hardware components support the procedure.

However, for example in case of sub-optimal network performance even the slight overhead introduced by PKI authentication can affect the system's ability to appropriately assess a safety-critical situation and react to it in time.

Therefore, the trade-off must be considered during the automotive development processes to find an optimal balance between safety and security [6] [7], especially considering automotive functions influencing high-risk processes such as braking, steering, etc.

Network performance can be affected by several external and internal factors (such as buildings, the weather, speed conditions, the number of actors participating in the communication process, or the applied security solutions). On the other hand, it must be emphasized that a malicious attack [8] or an unintentional error can considerably decrease network service quality.

Note that Public Key Infrastructure frameworks are also widely applied in other domains to provide an acceptable security level of the systems (e.g., the energy or the financial sector) [9] [10]. Many other research papers focused on the impact of authentication on communication delay [11], the effectiveness of Credential Management Systems related to CCAM solutions [12-15], and the security overhead of different coding algorithms [16]. Following the studied related works, we found that PKI authentication's safety effect in automotive systems has not yet been investigated in detail and needs further research.

To define the limits and boundaries where specific CCAM systems can be applied in a safe way, developers should pay attention to identify the expected risk level of the system related to particular combinations of the influencing factors. In that case, the system can be operated in the safe interval of the influencing factors, staying on the safe side. Accordingly, if the quality of service (QoS) decreases significantly, either because of an attack or an error, the controllable influencing factors can be modified to drive the system in a safe state [17-19].

## 2 Methods

This article investigates the expected effects of specific malicious interventions or random errors related to wireless communication based automotive functions taking into account the severity and probability of the considered unexpected event. Based on this, the applied risk estimation concept is introduced in the first part of the section, and in the next step, the probability estimation model is described [19].

### 2.1 Investigation Concept

During the evaluation, we investigated six cases focusing on intersecting vehicle movements [20]. All investigated cases included two cars (Target Vehicle – TV, Subject Vehicle – SV) where the neighboring legs of the junction meet at a 90-degree angle. Table 1 includes the velocities of the vehicles.

Table 1  
Investigated cases and the applied velocities

Test case	TC1	TC2	TC3	TC4	TC5	TC6
$v_{TV}$ [km/h]	20	50	20	50	20	50
$v_{SV}$ [km/h]	40	70	70	100	100	130

In order to guarantee that the two vehicles are on a collision course, the starting position of both vehicles are chosen accordingly. The test scenarios were built using the Cohda VSIM simulation framework. In the test setup two Cohda MK5 On-Board Units (OBUs) are used to facilitate wireless communication between the two vehicles using CAM messages. The VSIM software simulates the vehicles following their respective paths and generates a GNSS (Global Navigation Satellite System) data stream for both. This data stream is then fed to their respective OBUs via TCP/IP (Transmission Control Protocol/Internet Protocol) connection. The architecture of the test system is shown on Figure 1.

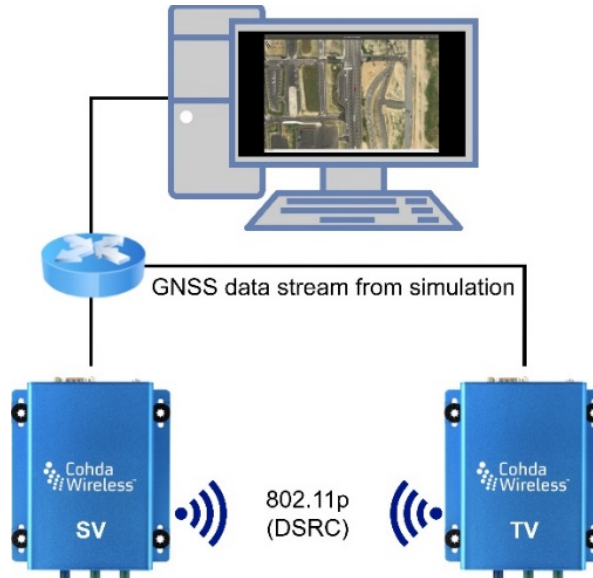


Figure 1  
Test system architecture

The test cases were implemented in the virtual model of the ZalaZONE test field to provide the possibility for the real test-based verification of the experimental results [21]. The below presented laboratory setup was used to carry out the measurements.



Figure 2  
Measurement laboratory setup

## 2.2 Representing Safety Risk

The below-presented part of the article describes the indicator applied to characterize safety risk. Beyond the vehicle generally applied dynamics parameters, the developed Safety Risk Index (SRI) considers the relevant QoS parameters, such as packet delivery ratio (PDR) or end-to-end latency (E2E). During the analysis, the stopping distance (denoted by  $d_{crit}$ ) was evaluated to characterize the safety level of a specific scenario.

When CAMs do not arrive before the following vehicle approaches the front vehicle to the stopping distance ( $d_{crit}$ ), the following car will not have enough distance to decelerate to a safe speed and avoid the accident.

In light of the above, if a CAM arrives to the following vehicle before the critical point, the car can prevent the collision. However, we also need to emphasize that it is not advantageous if the CAM arrives too early since the situation will not be classified as a hazardous event. Following this, we can identify a warning period ( $t_{warn}$ ) in which the CAM should arrive. If the speeds of the cars are higher, the warning period has to be longer.

Accordingly, in the development procedure of ADAS/ADS (Advanced Driver-Assistance System/Automated Driving System) applications, we must consider the proportion of the warning and the critical period. If the proportion is smaller, the application will become more effective, but the risk related to the application will also be larger.

The indicator describing safety risk is defined by multiplying the estimated occurrence and severity values in the case of specific scenarios due to the delayed arrival of cooperative awareness messages.

The occurrence value related to the delayed arrival of cooperative awareness messages in a specific scenario is calculated by subtracting the arrival timestamp ( $t_{TS}$ ) from the center point of the warning period ( $t_{TS\_CENT}$ ).

According to our concept, we estimate severity based on the collision energy. In light of this, it can be derived from the kinetic energy of the colliding vehicles. Following these assumptions, in the case of a longitudinal scenario, severity is proportional to the difference between the squares of velocities. In that case, risk can be represented by the following formula:

$$SRI = (t_{TS} - t_{TS\_CENT}) \cdot d_{crit} \quad (1)$$

Based on Eq. 1. we calculated the risk values related to the implemented test scenarios. Following this, it became possible to identify the polynomial regression function (Eq. 2.) capable of estimating the risks in the case of specific combinations of the considered input variables, such as the values of the investigated vehicle dynamics and QoS parameters:

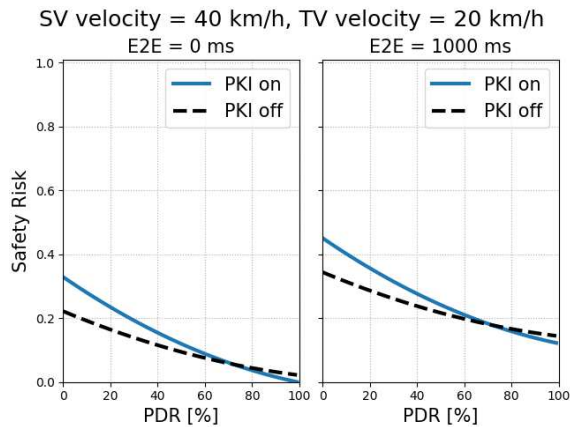
$$\hat{y} = \beta_0 + \beta_1 x_1 + \beta_2 x_2 + \dots + \beta_{12} x_1 x_2 + \beta_{13} x_1 x_3 + \dots \quad (2)$$

### 3 Results

This section focuses on the outcomes of the executed measurements. The safety risk of the V2V test cases is analyzed by applying the presented safety risk index. The below-presented figure pairs compare the risk functions. The left side of the figures show a low-latency scenario with minimal (~0 ms) E2E latency, the right side shows a high-latency (1000 ms) scenario. Each figure contains the results of two measurements, one with PKI authentication turned on (blue continuous line) and one with PKI turned off (black dashed line). Due to applying polynomial regression to the calculated SRI values the resultant safety risk values are normalized.

#### 3.1 Test Case TC1

In the first test case, the subject vehicle moves at 40 km/h while the target vehicle moves at 20 km/h. Due to the relatively low velocities, the expected risk level is relatively low. In both low- and high-latency cases the risk function is steeper when the PKI authentication is switched on.



Safety Risk function for TC1 test case

Table 2  
Safety Risk values for TC1 test case

PDR	E2E	Without PKI	With PKI
10%	0 ms	0.193	0.281
	500 ms	0.254	0.342
	1000 ms	0.315	0.403
50%	0 ms	0.095	0.121
	500 ms	0.156	0.182
	1000 ms	0.218	0.243
100%	0 ms	0.022	0
	500 ms	0.083	0.061
	1000 ms	0.145	0.122

### 3.2 Test Case TC2

In the following test case, the subject vehicle moves at 70 km/h, while the target vehicle moves at 50 km/h. We can recognize that the safety impact of the PKI authentication process is not emphatic, only a small difference can be observed at extremely low PDR levels (under 20%).

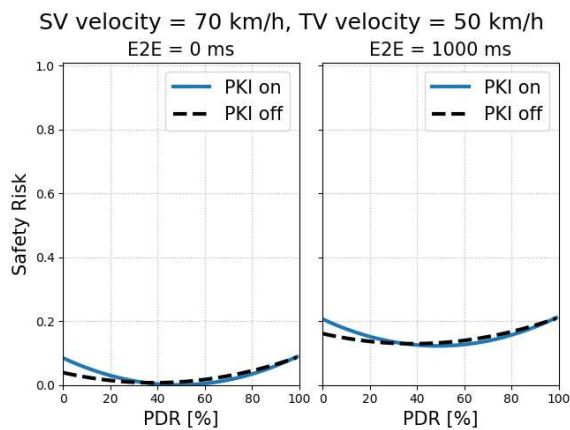


Figure 4  
Safety Risk function for TC2 test case

Table 3  
Safety Risk values for TC2 test case

PDR	E2E	Without PKI	With PKI
10%	0 ms	0.066	0.095
	500 ms	0.127	0.156
	1000 ms	0.188	0.217
50%	0 ms	0.051	0.042
	500 ms	0.113	0.103
	1000 ms	0.174	0.164
100%	0 ms	0.131	0.134
	500 ms	0.192	0.195
	1000 ms	0.253	0.256

### 3.3 Test Case TC3

In the third test case, the target vehicle moves at 20 km/h while the subject vehicle moves at 70 km/h. Due to the more considerable difference in velocities, the safety risk takes larger values when the quality of service becomes lower. On the other hand, we have to emphasize that the packet delivery ratio has a more significant influence on the safety risk. Comparing the safety risk of the systems with and without PKI authentication, the maximum value of the system with PKI is  $\sim 0.1$  larger than that of the system without PKI.

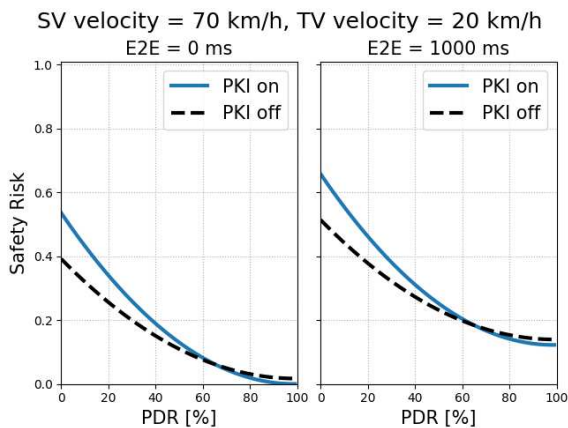


Figure 5  
Safety Risk function for TC3 test case

Table 4  
Safety Risk values for TC3 test case

PDR	E2E	Without PKI	With PKI
10%	0 ms	0.389	0.501
	500 ms	0.45	0.562
	1000 ms	0.511	0.623
50%	0 ms	0.178	0.198
	500 ms	0.239	0.26
	1000 ms	0.3	0.321
100%	0 ms	0.086	0.069
	500 ms	0.147	0.13
	1000 ms	0.208	0.191

### 3.4 Test Case TC4

Regarding the fourth test case, the target vehicle moves at 50 km/h while the subject moves at 100 km/h. Similar to the previous test case, the more significant difference in the velocities results in larger safety risk values in the case of lower quality of service levels. Besides this, we can also observe that the packet delivery ratio considerably impacts the safety risk. Comparing the safety risk of the systems with and without PKI authentication, the maximum value of the system with PKI is about the same as the system without PKI.

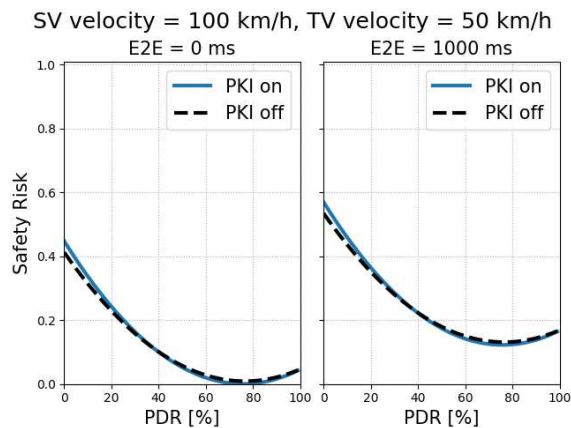


Figure 6  
Safety Risk function for TC4 test case

Table 5  
Safety Risk values for TC4 test case

PDR	E2E	Without PKI	With PKI
10%	0 ms	0.372	0.396
	500 ms	0.433	0.457
	1000 ms	0.495	0.518
50%	0 ms	0.116	0.11
	500 ms	0.177	0.172
	1000 ms	0.238	0.233
100%	0 ms	0.105	0.104
	500 ms	0.166	0.165
	1000 ms	0.228	0.227

### 3.5 Test Case TC5

Analyzing the TC5 test case, the target vehicle moves at 20 km/h while the subject vehicle moves at 100 km/h. In this test case, the large difference between the vehicles' velocity increases the safety risk significantly, especially when PDR is under ~30%. Besides, we can also observe that the packet delivery ratio considerably impacts the safety risk. The maximum safety risk in the case of the system with PKI approaches the value of 0.8 when the latency is relatively high.

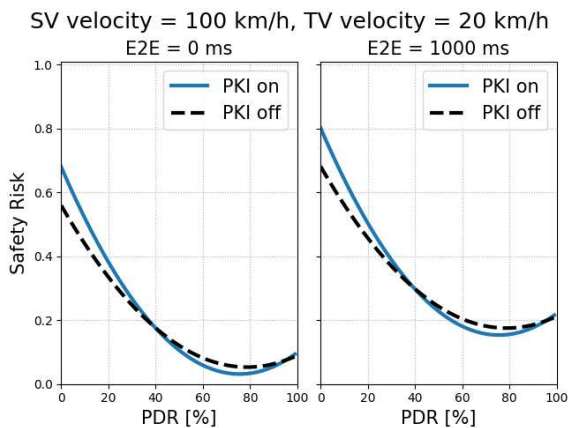


Figure 7

Safety Risk function for TC5 test case

Table 6  
Safety Risk values for TC5 test case

PDR	E2E	Without PKI	With PKI
10%	0 ms	0.513	0.593
	500 ms	0.574	0.654
	1000 ms	0.635	0.716
50%	0 ms	0.194	0.179
	500 ms	0.255	0.24
	1000 ms	0.317	0.301
100%	0 ms	0.163	0.173
	500 ms	0.225	0.234
	1000 ms	0.286	0.295

### 3.6 Test Case TC6

Regarding the most dangerous test case, the vehicles travel with 50 km/h and 130 km/h. In accordance with the above, we can observe the highest safety risk values among the examined scenarios in this test case. We can also conclude that the safety risk function changes steepest in this test case as a function of the packet delivery ratio.

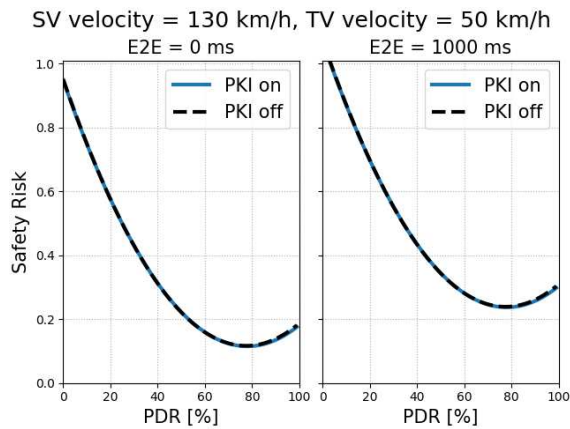


Figure 8  
Safety Risk function for TC6 test case

Table 7  
Safety Risk values for TC6 test case

PDR	E2E	Without PKI	With PKI
10%	0 ms	0.824	0.822
	500 ms	0.885	0.883
	1000 ms	0.946	0.945
50%	0 ms	0.295	0.296
	500 ms	0.356	0.357
	1000 ms	0.418	0.418
100%	0 ms	0.261	0.255
	500 ms	0.322	0.316
	1000 ms	0.383	0.377

## Conclusions

Our article investigates the impact of Public Key Infrastructure (PKI) based authentication processes, on the safety risk caused by the increased processing time in the case of different QoS parameter levels.

To evaluate the quantified risk values of the investigated test cases and to analyze the behavior of the system depending on different vehicle dynamics, we investigate the relationship between the change in the analyzed QoS parameters and the risk level related to the test cases.

When the packet delivery ratio is low, the value of the safety risk becomes outstandingly high, above 0.9. If we focus on the test cases with PKI switched on, we can observe that when the PDR is low, the risk values are generally larger than without the PKI. Though the differences vary the maximum difference is  $\sim 0.11$ .

When the packet delivery ratio gets higher, the risk levels related to the test cases with and without PKI get closer. Accordingly, if the packet delivery ratio is close to 100%, the overhead of the PKI process becomes negligible.

Based on our outcomes, the safety impact of Public Key Infrastructure based authentication is insignificant. The increased processing time can only result in unsafe cases if the quality-of-service decreases below an unacceptable level.

To solve this difficulty, we need to consider case-dependent resource allocation and make further computational resources available to our automotive systems in the case of critical situations when the QoS parameters make it necessary to reduce the processing time of the authentication process.

To reduce the mentioned risks, adaptive security-related solutions or detailed system limitations can be applied. System limitations must be validated to approve if the investigated applications can be operated safely by controlling system parameters between the pre-defined limits.

Based on the concluded outcomes of the research, we can formulate the following key messages:

- Packet loss has stronger effect on safety risk than latency.
- In the case of normal QoS levels, PKI has negligible effect on safety risk.
- If QoS reduces, PKI's negative effect on safety risk becomes more pronounced. In this case, adaptive, risk-reducing measures should be implemented and applied.

### Acknowledgements

The research was supported by the Ministry of Innovation and Technology NRDI Office within the framework of the Autonomous Systems National Laboratory Program.

This work was supported by the ÚNKP-22-3-II-BME-53 and ÚNKP-21-5 new national excellence program of the Ministry for Innovation and Technology from the source of the National Research, Development and Innovation Fund.

### References

- [1] M. Zöldy, "Legal barriers of utilization of autonomous vehicles as part of green mobility," in *International Congress of Automotive and Transport Engineering*. Springer, 2018
- [2] H. Tschürtz and A. Gerstinger, "The safety dilemmas of autonomous driving," in *2021 Zooming Innovation in Consumer Technologies Conference (ZINC) IEEE*, 2021
- [3] Z. Szalay, D. Ficzer, V. Tihanyi, F. Magyar, G. Soós, and P. Varga, "5g-enabled autonomous driving demonstration with a v2x scenario-in-the-loop approach," *Sensors*, Vol. 20, No. 24, 2020
- [4] D. Grimm, M. Stang, and E. Sax, "Context-aware security for vehicles and fleets: A survey," *IEEE Access*, 2021
- [5] T. Sipos, A. Afework Mekonnen, and Z. Szabó, "Spatial econometric analysis of road traffic crashes," *Sustainability*, Vol. 13, No. 5, 2021
- [6] T. Bécsi, Á. Szabó, B. Kővári, S. Aradi, and P. Gáspár, "Reinforcement learning based control design for a floating piston pneumatic gearbox actuator," *IEEE Access*, Vol. 8, 2020
- [7] C. Csiszár and D. Földes, "System model for autonomous road freight transportation," *Promet-Traffic&Transportation*, Vol. 30, No. 1, 2018
- [8] B. Nagy, P. Orosz, T. Tóthfalusi, L. Kovács, and P. Varga, "Detecting ddos attacks within milliseconds by using fpga-based hardware acceleration," in *NOMS 2018-2018 IEEE/IFIP Network Operations and Management Symposium*. IEEE, 2018

- [9] J. Csátár and A. Dán, “Novel load flow method for networks with multipoint-grounded-neutral and phase-to-neutral connected equipment,” *International Journal of Electrical Power & Energy Systems*, Vol. 107, 2019
- [10] C. Krasznay and G. Gyebnár, “Possibilities and limitations of cyber threat intelligence in energy systems,” in *2021 13<sup>th</sup> International Conference on Cyber Conflict (CyCon) IEEE*, 2021
- [11] B. Fernandes, J. Rufino, M. Alam, and J. Ferreira, “Implementation and analysis of iecce and etsi security standards for vehicular communications,” *Mobile Networks and Applications*, Vol. 23, No. 3, 2018
- [12] B. Brecht and T. Hehn, “A security credential management system for v2x communications,” in *Connected Vehicles*. Springer, 2019
- [13] H. Qiu, M. Qiu, and R. Lu, “Secure v2x communication network based on intelligent pki and edge computing,” *IEEE Network*, Vol. 34, No. 2, 2019
- [14] I. Agudo, M. Montenegro-Gómez, and J. Lopez, “A blockchain approach for decentralized v2x (d-v2x),” *IEEE Transactions on Vehicular Technology*, Vol. 70, No. 5, 2020
- [15] M. Rumez, D. Grimm, R. Kriesten, and E. Sax, “An overview of automotive service-oriented architectures and implications for security countermeasures,” *IEEE access*, Vol. 8, 2020
- [16] A. Fazzat, R. Khatoun, H. Labiod, and R. Dubois, “A comparative performance study of cryptographic algorithms for connected vehicles,” in *2020 4<sup>th</sup> Cyber Security in Networking Conference (CSNet) IEEE*, 2020
- [17] Torok, A., & Pauer, G. (2022) Safety aspects of critical scenario identification for autonomous transport. *Cognitive Sustainability*, 1(3)
- [18] Török, Á. (2020) A novel methodological framework for testing automated vehicle functions. *European Transport Research Review*, 12(1), 1-9
- [19] Nyerges, L. Á., & Zöldy, M. (2023) Ranking of four dual loop EGR modes. *Cognitive Sustainability*, 2(1), 51-72

# Investigating the Energetics of Electric Vehicles, based on Real Measurements

**Dávid Tollner and Máté Zöldy**

Department of Automotive Technologies, Budapest University of Technology and Economics, Stoczek József u. 6, H-1111 Budapest, Hungary;  
tollner.david@kjk.bme.hu; zoldy.mate@kjk.bme.hu

---

*Abstract: Electric vehicles can offer a real alternative for mobility in the 21<sup>st</sup> Century, but the extent of their long-term wear and degradation is unknown. Obviously, both traffic and users have to adapt to the new types of drivetrains, as these cars can be driven optimally in a completely different style. A new measurement and evaluation methodology has been developed, and various tests have been defined to investigate the key questions of electric cars. We showed that energy consumption can be reduced by more than 1/3 at optimum ambient temperatures, compared to 0 °C. We examined the correlation between speed and energy consumption on highway, and found that reducing the average speed from 105 km/h to 85 km/h can increase the range by up to 40%. Finally, we calculated that at 50,000 km of mileage, the battery only degrades by 11%.*

*Keywords: sustainable mobility; electric vehicles; range; consumption; battery degradation*

---

## 1 Introduction

Modern mobility is not sustainable in its current form [1], therefore, alternative solutions need to be explored. Increasing recognition of a long-term perspective [2], can be an essential tool for mobility. The international community made several commitments related to transport, but most focus only on road safety or carbon emissions specifically.

Research for alternative solutions has been a popular topic over the past decades, but the global goal has not been achieved. First attempts were made to develop more environment-friendly fuels by reducing the sulfur and lead content [3] [3.1]. Further studies have been done on the possibility of fossil fuel blending with different alcohols [4-8], vegetable oil-based products [9-12], or with rare special blending materials [13-15]. On the technical side, the downsizing of petrol engines has started [16] [17], and for diesel engines, combustion and exhaust gas technologies have been improved [18-20]. At the same time, hybridization was also developed, which had promising results, for further fuel consumption reductions [21] [22].

Regardless of the powertrain type, the role of electricity has increased in vehicles, a modern car including up to 300 electric motors and sensors [24]. This is necessary because of the complexity of drivetrains and the requirement to comply with standards. With the development of safety systems, the vehicle acquires more and more data about its environment [25], which requires high-level data processing [26], artificial intelligence, and fuzzy structures [27] based decision-making in cognitive mobility.

Electric vehicles (EVs) have been a real alternative since the start of motorization. However, the early versions were powered by non-rechargeable primary cells. Over the last 100 years, the evolution of eDrives has been overshadowed by the development of internal combustion engines [23]. The diesel gate and the innovations in battery technology helped start a new era of e-mobility. The electric drivetrain has three main components: the battery, the electric motor, and the inverter.

The high-voltage battery (and its associated auxiliaries) is one of the components of EVs that is much more complex than in internal combustion engine (ICE) cars. The critical dimensions of batteries are: cathode materials (layered compounds, spinel and olivine), anode materials (graphite and lithium titanate), electrolytes, lithium salts, and separators [28]. During the lifetime of a battery, chemical reactions occur that cause it to age; this is the battery degradation. Degradation is a major area of research in lithium-polymer batteries [29].

Several types of electric motors are used in EVs. The proper e-motor selection has a significant influence on the vehicle's efficiency and stability [30]. One of the most preferred options is the Interior Permanent Magnet Synchronous Motor (IPMSM). The researchers focus on the effects of the size and placement of magnets [31].

For the development of inverters, the Hardware-In-the-Loop (HIL) concept is mainly used. This helps speed up the testing process to select the right performance and durability. New research uses the Power-HIL simulation, which can emulate PMSM machines [32].

Summarized the literature review, electric vehicles can be real alternatives for future mobility, which are already part of the transformation nowadays. As e-mobility is a relatively new research area, there are many open points and research orientations. With batteries and charging equipment more reliable and accessible than ever, adoption still depends on tax incentives and infrastructure deployment. Modern, first-generation electric cars are now reaching the average age of vehicles in Hungary, which is approximately 15 years. Utilization point of view, it is essential to be able to predict battery degradation. Our research focuses on the predictability of the degradation of electric vehicle batteries based on field data.

The Test and methods section contains a report on the tests performed, a description of the test vehicle, and the data logging process. The Results and discussion section shows the background calculations for energy consumption, range, and battery

degradation. Also, this chapter includes the final outcome of the calculations and possibilities for further improvements. The results are summarized in the conclusion section.

## 2 Tests and Methods

This article summarizes the results of 3 measurements (Table 1), which are consistently referred to as follows: Normafa winter, Normafa summer, and Balaton challenge. The 2 Normafa measurements compare winter and summer energy consumption on the same route, while the focus is on the range for the Balaton challenge. Furthermore, the battery degradation was determined from the average of the three measurements.

Table 1  
The tests performed and the specifications

Test	Date	Road type	Temperature	Repetition	Focus
Normafa winter	2022.03.10	City/Rural	-5 – 0 °C	3	Consumption
Balaton challenge	2022.07.25	Highway-	30 – 35 °C	1	Range
Normafa summer	2022.07.26	City/Rural	25 – 30 °C	3	Consumption

### 2.1 Test Vehicles

Six electric vehicles were used for the battery degradation test over lifetime. Therefore, vehicles were chosen with lower (~10,000 km) and higher (45,000 km) mileage, which were 4 and 2 years old (these values refer to the first test). There was a 4-month gap between the winter and summer tests, so the mileage in the summer test was already around 5,000 km higher for all cars. These vehicles were rented from a car-sharing company, driven by people with different experiences and driving habits, and often charged on a fast charger. The condition of the batteries was not measured previously; therefore, it was important to test with more vehicles.

First generation Volkswagen e-up! were used in the tests. These cars are not specifically designed with electric platforms, as there are also versions with internal combustion engines. The main details of the vehicles are given in Table 2.

For the e-up!, there are two drive modes: “D” and “B”, where the difference between the two modes is the regenerative braking power. In mode “D”, the recuperation is manually adjustable from level 0 to level 3, in level 0 there is no energy recuperation. In “B”, the strength of recuperation is fixed at level 4, corresponding to ~70 Nm of deceleration torque based on measurements.

Table 2  
Test vehicle specifications [33], [34]

Parameter	Value
Curb weight	1,139 kg
Power / Torque	60 kW / 210 Nm
Nominal energy	18.7 kWh
Nominal voltage	374 V
Battery capacity	50 Ah
Battery cell chemistry	Lithium nickel manganese cobalt oxides
Combined Energy Consumption	12 kWh/100 km
Range (WLTP)	133 km

The vehicle has three manually switchable driving profiles: Normal, ECO, and ECO+. In these modes, functions are limited in addition to performance to ensure optimal energy use (Table 3).

Table 3  
The impact of e-up! operating modes on performance and functions [34]

System/Driving profile	Normal	ECO	ECO+
Speed limit	130 km/h	120 km/h	95 km/h
Max torque	210 Nm	167 Nm	133 Nm
Peak power	60 kW	50 kW	40 kW
Acceleration (0-100km/h)	12.4 s	14.3 s	-
Accelerator pedal characteristic	Normal	Reduced	Flat
Air conditioning	Normal	Reduced	Deactivated

## 2.2 Data Logging

There are two options for data logging: use the built-in sensors in the vehicles or install sensors. Modern vehicles are equipped with complex on-board electronics for comfort, safety, and optimal operation. For this reason, we chose the first option, as it avoids disassembling the vehicle and calibrating the sensors.

Electric vehicles are completely different from internal combustion engine vehicles in their powertrains, but their low-voltage systems are nearly the same. There are several CAN buses in EVs for different functions, which are usually connected in a Gateway. Diagnostic CAN, may be used to access the Gateway via the OBD II connector.

The Unified Diagnostic Services (UDS) [35] communication protocol has been implemented for data extraction. The protocol standardizes the communication and the message formats, but the content of the messages is different for each vehicle.

We tested several types of hardware, but finally, Inventure's self-made data loggers were chosen because of their stable operation.

The parameters we have analyzed are shown in Table 4. To investigate the vehicle's energetics, it would be sufficient to monitor only the energy consumption (eConsumption) parameters, but the energy consumption depends on the driving style. The consumption also depends on the route (e.g., road surface, slope), but these are indirectly included in the driving style parameters. The purpose of collecting longitudinal dynamic data is to validate that the drives were done in the same styles. Other data were also examined for future evaluations and to identify potential problems, but the analysis of these data is outside of the scope of this article.

Table 4  
List of parameters collected from the CAN bus

Group	Parameter	Unit
eConsumption	Battery voltage	[V]
	Battery current	[A]
	State-of-charge	[%]
Driving style	Speed	[km/h]
	Motor rotation	[RPM]
	Torque	[Nm]
	Brake system pressure	[Bar]
	Accelerator Pedal Position	[%]
Others	Ambient temperature	[°C]
	Adaptive Cruise Control (ACC)	[Off / On]
	Air conditioning (A/C)	[Off / On]

## 2.3 Test Routes, Measurement Setup

In vehicle life cycle analysis, driving cycles are usually divided into three main groups: city, rural, and highway. Each type has different typical speed and torque values, and in addition, different specific use cases can be defined, e.g., parking in city, overtaking in rural, and emergency stopping on highways.

The energetics of electric cars are most influenced by two important factors related to the route: the slope and the maximum speed allowed. Therefore, an urban section with varied topography and a high-speed highway section were selected.

### 2.3.1 Normafa Winter and Summer

The city route was selected in Budapest from Móricz Zsigmond square to Normafa hill and back to Móricz Zsigmond square. The total length of the route is 15.4 km, with an elevation gain of 350 meters between the lowest and highest points (Fig. 1).

As the entire route was inside the city, the maximum speed limit was 50 km/h (in some places, it was limited to 30 km/h).

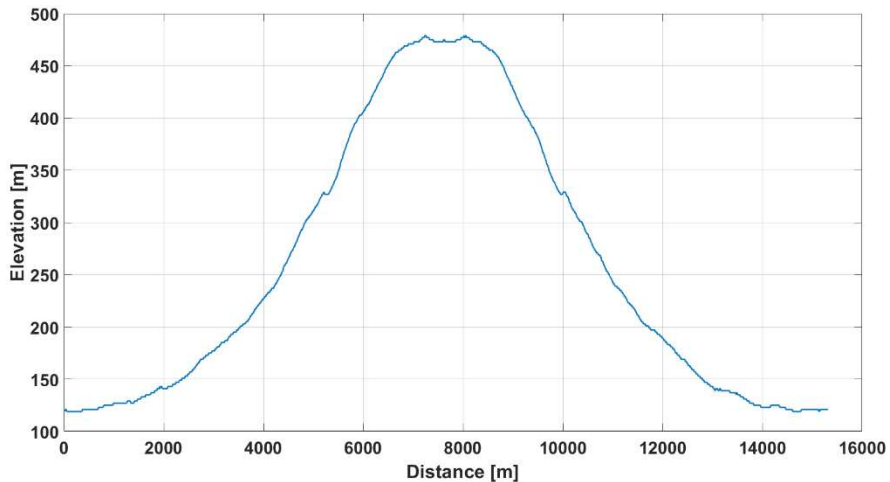


Figure 1

Elevation profile of the Normafa rest route

The tests were done on the same route in winter and summer to investigate the effect of temperature on energy consumption. In the Normafa winter test, the outside temperature was 0 °C, while in summer, it was 30 °C, which is the optimal temperature for the battery (Table 1). The vehicles were stored in an outdoor car park before the tests, so the initial temperatures of each component were nearly the same as the ambient temperature.

We drove in a convoy during the tests to ensure similar driving profiles. The tests were performed in real traffic, so there were differences in driving. To minimize this effect, the tests were done at night, and both tests were repeated three times in a row.

Drive mode “B” was used for the measurements to maximize energy recovery. We chose the Normal operating mode because we needed full power due to the high gradient. The Air Conditioning (AC) was not used, and the Positive Temperature Coefficient (PTC) battery heater is not manually adjustable.

### 2.3.2 Balaton Challenge

The M7 highway was chosen to test the range, as we thought that an important aspect of testing electric cars would be whether they could get from Budapest to Lake Balaton without charging. The test route is not completely flat due to the environmental conditions, but the slope is negligible (the maximum difference in altitude was 120 meters on the 110 km section). The first 15 km of the route was in

the city, with speed limits of 50 km/h, 80 km/h, and 100 km/h. The focus was on comparing different operating modes.

In the measurement, we varied several parameters between vehicles that have an effect on consumption, such as speed and AC (Table 5). The target speeds were chosen to be the highest speeds achievable in the given operating modes. This was complemented by activating Adaptive Cruise Control (ACC) in every second vehicle.

Table 5  
The settings used in the test vehicles

	Mode	Speed limit	AC	ACC
<b>Vehicle 1</b>	ECO	120 km/h	Off	Off
<b>Vehicle 2</b>	Normal	130 km/h	Off	On
<b>Vehicle 3</b>	ECO+	95 km/h	Off	On
<b>Vehicle 4</b>	Normal	130 km/h	On	Off
<b>Vehicle 5</b>	ECO+	95 km/h	On	Off
<b>Vehicle 6</b>	ECO	120 km/h	On	On

The measurement was performed only once in this test at an outside temperature of 35 °C. AC was manually set to automatic control and 22 °C in every second car, but the vehicle can override the AC compressor power based on Table 3. The windows were rolled up in all vehicles, as this has a significant effect on air resistance. During the measurement, drive mode “D” with level 0 recuperation was used in all cars to maintain the target speeds more uniformly.

Vehicle batteries could not be discharged to 0% for the following two reasons. In the first place, a vehicle pulling over on the highway can create a dangerous traffic situation. Second, the vehicle automatically switches to another mode to increase the range. At 20% State of Charge (SoC), the vehicle switches to ECO mode, which can be manually switched back to Nominal mode. At 12% SoC, it switches to ECO mode in a non-overrideable way, and at 8% to ECO+ mode.

### 3 Results and Discussion

In the measurements, vehicles with low mileage were consistently marked with Vehicles 1-3, while vehicles with high mileage were marked with Vehicles 4-6. These numbers also indicate the position in traffic. This is relevant for the Normafa measurements, as we were driving in a convoy there. Therefore, the further back a vehicle was in the convoy, the longer its driving time was. This may slightly increase the consumption.

### 3.1 Driving Profiles

The comparison of drivers is only relevant for the Normafa measurements, where the same driving style had to be used. Due to the similar route, only the longitudinal dynamics were investigated, which is well characterized by speed, motor torque, and throttle position. The driver can also control his speed with the brake pedal, but this is not included in the evaluation due to drive mode “B”. Because of the high recuperation level, the brake pedal had to be used only for stops, which were only 5-7 per measurement. When calculating averages, only values where the speed was greater than 0 were considered.

Figure 2 shows the comparison of drivers for Normafa winter and Normafa summer. It can be seen that the average speeds were approximately the same for both measurements, with a maximum difference of 0.5 km/h.

In the case of Normafa winter, the average torque of Vehicle 4 is slightly higher, but it is only 3 Nm higher than the torque of Vehicle 1. For the Normafa summer, a marginally larger variance is seen for the average accelerator pedal positions, but this may be due to different deceleration strategies. As no outliers were observed for any of the parameters, the drives were considered similar.

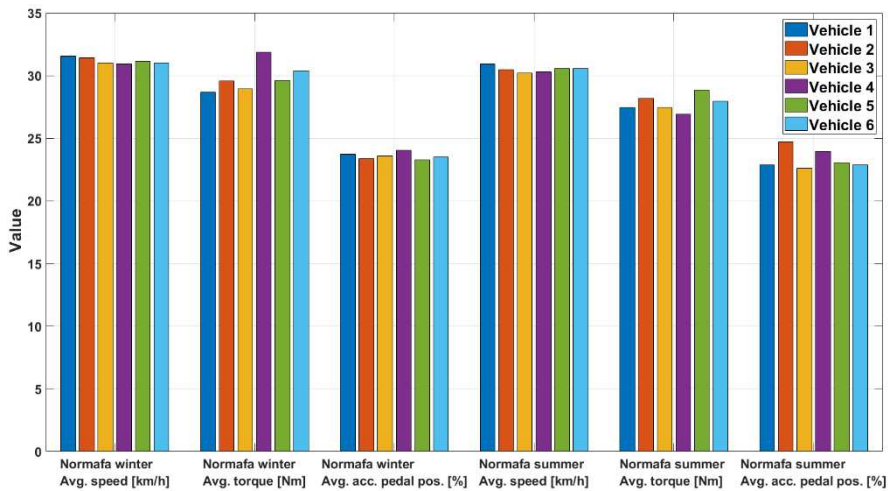


Figure 2

Comparison of driving styles in Normafa summer and winter tests

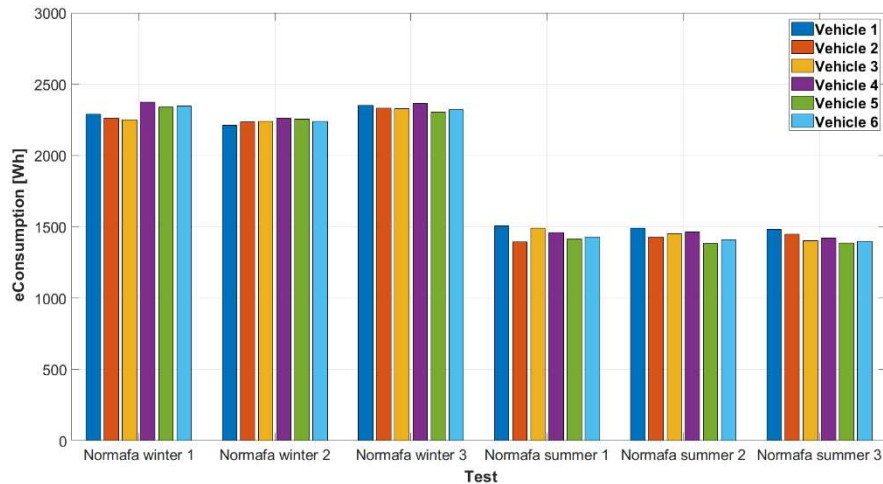
### 3.2 Energy Consumption

The vehicle's energy consumption is the amount of energy extracted from the battery. Some energy is used for the drive, and some for the power of other consumers. The amount of energy consumed with the measured values can be given by the following equation (Eq. 1):

$$eConsumption = \int W(t) dt = \int I(t) * U(t) dt \quad (1)$$

Where,  $W$  is the instantaneous delivered power,  $I$  is the current,  $U$  is the battery voltage, and  $t$  is the time.

The amount of energy used per test calculated from equation (1) is shown in Fig. 3. The graph clearly shows that while eConsumption was approximately similar in the same tests, consumption decreased significantly in the summer.



The amount of energy used in the tests per vehicle.

It can be seen that there is no significant difference in energy consumption between cars with low and high mileage. There is a minimal difference in the measurement of Normafa winter 1, but this may be due to calculation inaccuracies.

For the analysis of the results, it is important to note that the voltage and current values were recorded with different time stamps due to the CAN bus serial message transmission. Linear interpolation was applied to avoid this, which may result in some inaccuracy.

The averages of the three measurements for winter and summer are shown in Table 6. During the winter test, the average energy consumption was 2294 Wh, compared to 1435 Wh for the same route in summer. This results in a difference of 858 Wh, a 37.5% decrease in consumption in summer when temperatures are optimal.

In Normafa winter, cars with low mileage consumed on average 35 Wh less energy. In the case of the Normafa summer, cars with more mileage consumed 37 Wh less energy. These results imply that mileage does not affect the consumption of vehicles.

Table 6

Average eConsumption and differences between the Normafa winter and summer tests

	<b>Normafa winter</b>	<b>Normafa summer</b>	<b>Difference</b>
<b>Vehicle 1</b>	2,282 Wh	1,493 Wh	789 Wh
<b>Vehicle 2</b>	2,276 Wh	1,423 Wh	853 Wh
<b>Vehicle 3</b>	2,272 Wh	1,447 Wh	825 Wh
<b>Vehicle 4</b>	2,333 Wh	1,446 Wh	887 Wh
<b>Vehicle 5</b>	2,298 Wh	1,393 Wh	905 Wh
<b>Vehicle 6</b>	2,303 Wh	1,412 Wh	891 Wh
<b>Average</b>	2,294 Wh	1,435 Wh	858 Wh

The total length of the route was 15.3 km, from which the average city/rural consumption of the vehicles can be calculated, 15 kWh/100 km in winter and 9.4 kWh/100 km in summer. The manufacturer's specified combined energy consumption is 12 kWh/100 km, which includes highway driving. The air resistance is proportional to the square of the speed, the required power equals the speed multiplied by the drag force, so the energy consumption is proportional to the third power of the vehicle speed; therefore, highway sections increase consumption significantly. The conditions of the manufacturer's measurement are unknown, but it is within our measurement values and is therefore considered acceptable.

### 3.3 Range

During the Balaton challenge test, we ran into traffic jams on both the 10-15 km and the 21-31 km sections, which made it impossible to keep the target speeds (Figure 4). The real highway speed was only possible on the 32-92 km section. There is also a drop in speed around the 60 km point, but this is an absolutely realistic traffic situation, so we did not want to remove it from the results.

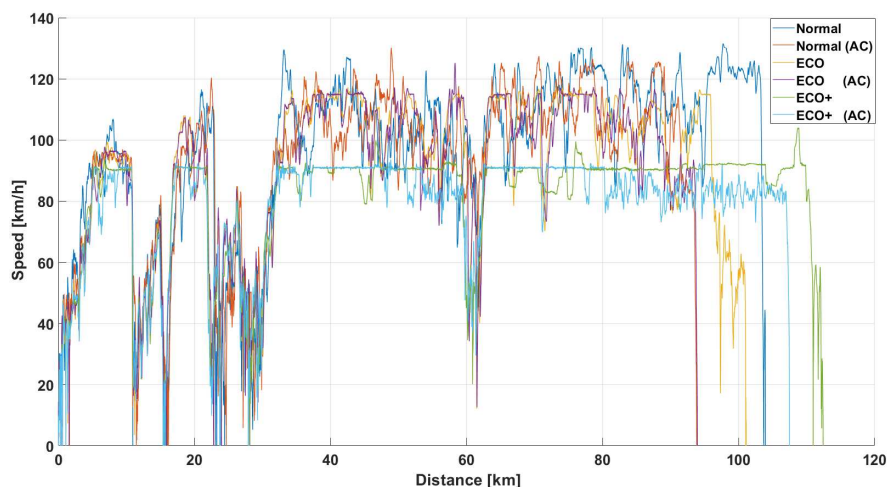


Figure 4

Speed profiles at the Balaton challenge measurement.

Columns 2 and 3 of Table 6 show the average speeds for the total route and the high-speed section, respectively. For both Normal and ECO+ modes, it is visible that the average speed is higher with AC on the total route, while the average speed is higher without AC on the high-speed section. From the perspective of energy consumption and range, the second was relevant for this measurement, so in the further evaluation we limit the route to this 60 km section.

Table 6

The result of speed and consumption in different modes

	<b>Avg. speed</b>	<b>Avg. speed (high-speed)</b>	<b>Standard deviation of speed (high-speed)</b>	<b>eConsumption (high-speed)</b>
<b>Normal</b>	66.4 km/h	106.3 km/h	13.8 km/h	8,151 Wh
<b>Normal (AC)</b>	66.9 km/h	105 km/h	11 km/h	7,980 Wh
<b>ECO</b>	59.8 km/h	101.4 km/h	17.2 km/h	7,967 Wh
<b>ECO (AC)</b>	59.5 km/h	100.6 km/h	17.4 km/h	8,010 Wh
<b>ECO+</b>	59 km/h	86.6 km/h	11.2 km/h	6,251 Wh
<b>ECO+ (AC)</b>	59.1 km/h	85.2 km/h	9.6 km/h	5,838 Wh

Figure 5 shows the consumption trend on the high-speed section. The results indicate that the consumption of 2 vehicles in ECO+ mode is significantly lower than the other four vehicles. Consumption is lower with air conditioning due to lower average speed and lower deviation (Table 6).

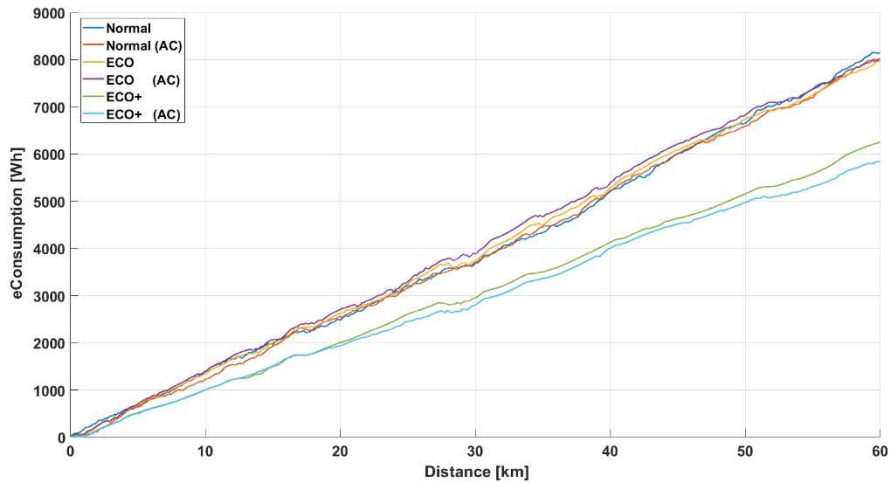


Figure 5

Consumption trends as a function of distance travelled

The consumption of Normal and ECO mode vehicles was approximately the same, although the average speed difference was  $\sim 5$  km/h. Vehicles in ECO mode had significantly greater deviation in speed, so they slowed down and accelerated more frequently, which increased energy consumption.

The results show that the average speed and deviation of speed have a large effect on eConsumption, while the use of air conditioning is almost negligible. During the test, it was not possible to produce the same values due to traffic. The range on the high-speed section can be calculated from the decrease in charge, assuming that the remaining charge would decrease at the same rate (Table 7).

Table 7

The relationship between calculated ranges and the odometer

	Odometer	$\Delta$ SoC	Calculated range
<b>Normal</b>	18,072 km	52.6 %	114 km
<b>Normal (AC)</b>	50,139 km	58.3 %	103 km
<b>ECO</b>	17,620 km	50.41 %	119 km
<b>ECO (AC)</b>	51,253 km	57.86 %	104 km
<b>ECO+</b>	13,106 km	39.02 %	154 km
<b>ECO+ (AC)</b>	51,057 km	41.64 %	144 km

In all three modes, we obtained significantly longer ranges for vehicles with low mileage than for those with high mileage, by an average of 12 km. This may indicate the degradation of the batteries. Furthermore, if the average speed of 105 km/h is reduced to 85 km/h, the range can be increased by 35-40%.

### 3.4 Battery Degradation

To investigate the degradation of the battery, the current capacity of the battery can be calculated from the measured consumption and the change in State-of-Charge using the following formula (Eq. 2):

$$Capacity = \frac{100}{\Delta SoC} * eConsumption \quad (2)$$

The average consumption and average  $\Delta SoC$  were used for the Normafa measurements. The vehicles were not stopped between the measurements, but the current values were close to 0 A, which would distort the consumption. For the Balaton Challenge test, the results were limited to the high-speed section.

Figure 6 shows the values of the calculated capacities for the three tests and the average of these values, with a black dashed line. The results of the Balaton Challenge measurement are the closest to the average capacities, as expected, as we could discharge the batteries almost completely. It can be observed that while the average for the first three cars with low mileage is about the same as the Balaton Challenge results, the average for the cars with high mileage is slightly lower for all three cars. One of the reasons for this could be the air-conditioning, as it was switched on for these three vehicles. The e-up!s have a high-voltage AC compressor, and its electrical management is not known. Another interesting result is that we got higher battery capacities in summer for five cars. In this measurement, the energy consumption was much lower, and the SoC value decreased less, but not at the same rate.

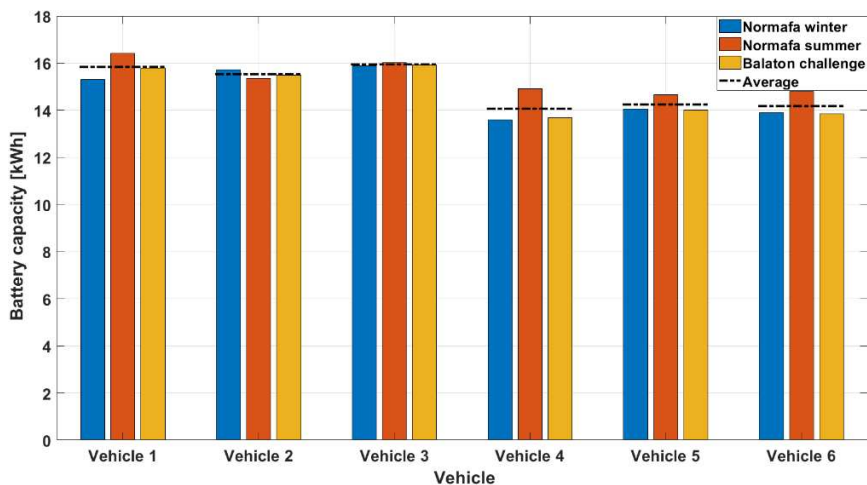


Figure 6  
Calculated battery capacities from measurements

Column 2 of Table 8 shows the average battery capacity values, column 3 shows the Odometer values after the third measurement. For e-up!, the usable capacity of the battery is not known, which is usually ~90% of the nominal capacity. An approximate value can be calculated from Table 2, the Combined Energy Consumption is 12 kWh/100 km, while the WLTP range is 133 km, giving a usable capacity of 15.96 kWh. The degradation is the ratio of the average battery capacity to the previous value expressed as percentages.

Table 8  
The calculated degradation values for the test vehicles

	<b>Average</b>	<b>Odometer</b>	<b>Degradation</b>
<b>Vehicle 1</b>	15.84 kWh	17,838 km	0.75 %
<b>Vehicle 2</b>	15.53 kWh	18,304 km	2.69 %
<b>Vehicle 3</b>	15.94 kWh	13,346 km	0.13 %
<b>Vehicle 4</b>	14.06 kWh	50,367 km	11.90 %
<b>Vehicle 5</b>	14.24 kWh	51,301 km	10.78%
<b>Vehicle 6</b>	14.17 kWh	51,471 km	11.22 %

A significant difference in the degradation can be observed as a function of mileage. The average degradation for vehicles with ~16,000 km is 1.19%, while for vehicles with 51,000 km it is 11.3%. For the first, the battery degradation calculated for the second vehicle highly increases the average. Due to the small number of cars, it is not possible to either interpolate or extrapolate the degradation, as the shape of the function is unknown, which would require measuring several vehicles with different mileages.

It is important to underline that although the results show higher degradation, the results are only approximations. The main reasons for this are: measurement accuracy, it is not possible to get more data with the same timestamp in serial communication, the current value can change rapidly with high amplitude, the SoC value is a calculated value, the battery discharge is not linear, driving style/traffic affects the results.

## Conclusions

We achieved the following results in this work. We developed a measurement and evaluation methodology for testing the energetics of electric cars, which was tested with six vehicles. In future research, this can be extended with additional vehicles to improve the results. Two measurements were done on the same route, one in winter at 0°C and the other in summer at 35°C. The results showed a 37.5% consumption decrease in summer, under optimal temperature conditions. The third measurement was performed on a highway, where the effect of speed on the range was investigated. If the speed is reduced to 85 km/h, instead of 105 km/h, the range can be increased by 35-40%. Summarizing the results of the three measurements, a battery degradation of 1.2% was calculated for cars with 16,000 km and 11.3% for cars with 51,000 km.

## Acknowledgements

Prepared with the professional support of the Doctoral Student Scholarship Program of the Co-operative Doctoral Program of the Ministry for Innovation and Technology from the source of the National Research, Development and Innovation Fund.

Project no. 2019-1.3.1-KK-2019-00004 has been implemented with the support provided from the National Research, Development and Innovation Fund of Hungary, financed under the 2019-1.3.1-KK funding scheme.

## References

- [1] M. Zöldy, M. Szalmane Csete, P. P. Kolozsi, P. Bordas, A. Torok, “Cognitive Sustainability”. *CogSust*, Vol. 1 (2022)
- [2] M. Zöldy, P. Baranyi, “Cognitive Mobility – CogMob”, *12<sup>th</sup> IEEE International Conference on Cognitive Infocommunications (CogInfoCom 2021)* Proceedings IEEE. 921-925, (2021)
- [3] J. Hancsók, Z. Eller, G. Pölczmán, Z. Varga, A. Holló, G. Varga, “Sustainable production of bioparaffins in a crude oil refinery”. *Clean Techn Environ Policy* 16, 1445-1454, (2014) <https://doi.org/10.1007/s10098-014-0743-6>
- [3.1] European Parliament and Council. “Directive 98/70/EC of the European Parliament and of the Council of 13 October 1998 relating to the quality of petrol and diesel fuels and amending Council Directive 93/12/EEC”. Brussels (1998)
- [4] I. Emőd, M. Füle, K. Tanczos, M. Zöldy, “Technical, economic and environmental conditions for the introduction of bioethanol in Hungary.” (In hungarian: A bioetanol magyarországi bevezetésének műszaki, gazdasági és környezetvédelmi feltételei). *MAGYAR TUDOMÁNY* 50., 278-286 (2004) <http://epa.oszk.hu/00600/00691/00015/03.html>
- [5] M. Virt, J. Sauer, “Investigating the Effects of Oxymethylene Ether in a Commercial Diesel Engine”. *Cognitive Sustainability*, online first, <https://doi.org/10.55343/cogsust.20>
- [6] W. Tutak, K. Lukacs, S. Szwaja, A. Bereczky, “Alcohol–diesel fuel combustion in the compression ignition engine”. *Fuel* 154, 196-206 (2015)
- [7] Z. Lulić, I. Mavrin, I. Mahalec, “Aspects of Using Biological Regenerative Fuels in Internal Combustion Engines”. *Promet-Traffic&Transportation* 10 (1-2) 75-80 (1998)
- [8] M. Zöldy, “Bioethanol-biodiesel-diesel oil blends effect on cetane number and viscosity”. *Bartz, WJ 6<sup>th</sup> International Colloquim: Fuels* 235 (2007)
- [9] A. Alahmer, H. Rezk, W. Aladayleh, A. O. Mostafa, M. Abu-Zaid, H. Alahmer, R. M. Ghoniem, “Modeling and Optimization of a Compression

- Ignition Engine Fueled with Biodiesel Blends for Performance Improvement”. *Mathematics* 10(3) 420.8 (2022)
- [10] N. Jeyakumar, Z. Huang, D. Balasubramanian, A. T. Le, X. P. Nguyen, P. L. Pandian, A. T. Hoang, “Experimental evaluation over the effects of natural antioxidants on oxidation stability of binary biodiesel blend”. *International Journal of Energy Research* (2022)
- [11] R: Longwic, P. Sander, W. Lotko, K. Gorski, B. Janczuk, A. Zdziennicka, K. Szymczyk, “Self-ignition of rapeseed and n-hexane mixtures in diesel engine”. *Przemysł Chemiczny* 99(2) 206-210 (2020)
- [12] J. Matijošius, A. Juciūtė, A. Rimkus, J. Zaranka, “Investigation of the concentration of particles generated by public transport gas (CNG) buses”. *CogSust*, Vol. 1 (2022)
- [13] P. V. Elumalai, S. K. Dash, M. Parthasarathy, N. R. Dhineshababu, D. Balasubramanian, D. N. Cao, A. T. Hoang, “Combustion and emission behaviors of dual-fuel premixed charge compression ignition engine powered with n-pentanol and blend of diesel/waste tire oil included nanoparticles”. *Fuel* 324, 124603 (2022)
- [14] K. Górski, R. Smigins, J. Matijošius, A. Rimkus, R. Longwic, “Physicochemical Properties of Diethyl Ether—Sunflower Oil Blends and Their Impact on Diesel Engine Emissions”. *Energies* 15(11) 4133 (2022)
- [15] I. Barabás, A. Molea, R. Suciú, “Fuel Properties of Diesel-Ethanol-Tetrahydrofuran Blends: Experimental and Theoretical Approaches”. *International Congress of Automotive and Transport Engineering* 197-208 (2018)
- [16] M. M. Namar, O. Jahanian, R. Shafaghat, K. Nikzadfar, “Engine Downsizing; Global Approach to Reduce Emissions: A World-Wide Review”. *HighTech and Innovation Journal* 2(4), 384-399 (2021)
- [17] D. K. Nguyen, T. Van Craeynest, T. Pillu, J. Coulier, S. Verhelst, “Downsizing potential of methanol fueled DISI engine with variable valve timing and boost control”. *WCX™ 18: SAE World Congress Experience*, SAE International (2018)
- [18] M. Virt, G. Granovitter, M. Zöldy, Á. Bárdos, Á. Nyerges, “Multipulse Ballistic Injection: A Novel Method for Improving Low Temperature Combustion with Early Injection Timings”. *Energies* 14(13), 3727 (2021)
- [19] Á. Nyerges, M. Zöldy, “Verification and comparison of nine exhaust gas recirculation mass flow rate estimation methods”. *Sensors* 20(24) 7291, (2020)
- [20] S. Vass, M. Zöldy, “Detailed model of a common rail injector”. *Acta Universitatis Sapientiae, Electrical and Mechanical Engineering*, 11(1) 22-33 (2019)

- [21] M. Zöldy, I. Zsombók, “Modelling fuel consumption and refuelling of autonomous vehicles”. *MATEC Web of Conferences* 235, 00037 (2018)
- [22] I. Zsombok, “Development vehicle test procedure for proving ground measurements”. (In hungarian: Fogyasztásmérések fejlesztése tesztpályás mérésekhez). *Műszaki Szemle* 40-47 (2019)
- [23] E. V. Belousov, M. A. Grigor’Ev, A. A. Gryzlov, “An electric traction drive for electric vehicles”. *Russian Electrical Engineering* 88(4), 185-188 (2017)
- [24] F. Rosique, P. J. Navarro, C. Fernández, A. Padilla, “A systematic review of perception system and simulators for autonomous vehicles research”. *Sensors* 19(3) 648 (2019)
- [25] M. Martínez-Díaz, F. Soriguera, “Autonomous vehicles: theoretical and practical challenges”. *Transportation Research Procedia* 33, 275-282 (2018)
- [26] A. Rövid, V. Remeli, N. Paufler, H. Lengyel, M. Zöldy, Zs. Szalay, “Towards Reliable Multisensory Perception and Its Automotive Applications”. *Periodica Polytechnica Transportation Engineering* 48(4), 334-340 (2020)
- [27] P. Baranyi, T. D. Gedeon, L. T. Kóczy, “A general interpolation technique in fuzzy rule bases with arbitrary membership functions”. *1996 IEEE international conference on systems, man and cybernetics*, Vol. 1, 510-515 (1996)
- [28] A. Mauger, C. M. Julien, “Critical review on lithium-ion batteries: are they safe? Sustainable?” *Ionics* 23, 1933-1947 (2017) <https://doi.org/10.1007/s11581-017-2177-8>
- [29] S. Kocsis Szürke, A. Dineva, S. Szalai, I. Lakatos, “Determination of Critical Deformation Regions of a Lithium Polymer Battery by DIC Measurement and WOWA Filter”. *Acta Polytechnica Hungarica* 19(2) 113-134 (2022)
- [30] Z. Cao, A. Mahmoudi, S. Kahourzade, W. L. Soong, “An Overview of Electric Motors for Electric Vehicles”. *2021 31st Australasian Universities Power Engineering Conference (AUPEC)*, 1-6 (2021) doi: 10.1109/AUPEC52110.2021.9597739
- [31] P. Horvath, Á. Nyerges, “Design aspects for in-vehicle IPM motors for sustainable mobility”. *Cognitive Sustainability* 1(1) (2022) <https://doi.org/10.55343/cogsust.5>
- [32] D. Kiss, I. Varjasi, “Power-HIL Application Analysis of a 3-level Inverter for PMSM Machine”. *Period. Polytech. Elec. Eng. Comp. Sci.* 65(1) 62-68 (2021)
- [33] D. Tollner M. Zöldy, “Long term utilisation effect on vehicle battery performance”. *CogMob.* 22 (2022)

- [34] Volkswagen AG, „Der e-up!“: *Selbststudienprogramm 527 Service Training*, Wolfsburg (2014)
- [35] International Organization for Standardization, “ISO 14229-1: Road vehicles - Unified diagnostic services (UDS) - Part 1: Application layer” (2020)